

Optimal Scheduling and Control of Uncertain Coupled Power-Water Distribution Networks

by

Anna Stuhlmacher

A dissertation submitted in partial fulfillment
of the requirements for the degree of
Doctor of Philosophy
(Electrical and Computer Engineering)
in the University of Michigan
2023

Doctoral Committee:

Associate Professor Johanna L. Mathieu, Chair
Professor Seth D. Guikema
Professor Ian A. Hiskens
Assistant Professor Line A. Roald, University of Wisconsin-Madison

Anna Stuhlmacher
akstuhl@umich.edu
ORCID iD: 0000-0002-5277-0600

© Anna Stuhlmacher 2023

Dedication

To Gabriel, who was a source of constant support during my Ph.D. journey. And to my cats Kiki and Sammie, who were sources of frequent distraction.

Acknowledgments

I would first like to thank my Ph.D. advisor, Professor Johanna Mathieu, for her advise and support throughout my Ph.D. program. Professor Mathieu is an amazing advocate for her students—I am grateful for her insights and guidance on publishing, conferences, and making academic connections as well as supporting internship and teaching opportunities. I would also like to thank my committee members—Professor Line Roald, Professor Seth Guikema, and Professor Ian Hiskens—for their invaluable discussions and suggestions for my dissertation. And last, this work was made possible by funding from the National Science Foundation (NSF) and the University of Michigan’s Rackham Graduate School.

Table of Contents

Dedication	ii
Acknowledgments	iii
List of Figures	viii
List of Tables	xii
List of Acronyms	xiii
Abstract	xiv
Chapter 1. Introduction	1
1.1. Integrated Optimization of Critical Infrastructure Systems	2
1.2. Background on Coupled Power and Water Networks	3
1.2.1. Power Networks	4
1.2.2. Water Networks	5
1.2.3. Literature Review on Coupled Water-Power Optimization	5
1.3. Organization of the Dissertation	6
Chapter 2. Estimating the Flexibility Potential of Water Distribution Networks	9
2.1. Wisconsin's Water Distribution Network Flexibility Potential	9
2.2. Estimating the Water Distribution Network Flexibility Potential in the U.S.	12
2.3. Chapter Conclusion	13
Chapter 3. Incorporating Water Demand Uncertainty Sources in a Chance-Constrained Water Distribution Network Voltage Support Problem	14
3.1. Notation	14
3.2. Chapter Introduction	16
3.3. Problem Description and Assumptions	17
3.4. Problem Formulation	18
3.4.1. Water Constraints	18
3.4.2. Power Constraints	20
3.4.3. Objective	21

3.4.4. Chance Constraints	21
3.4.5. Scenario Approach	22
3.5. Case Study	23
3.5.1. Set Up	23
3.5.2. Impact of Power Network Parameters On Pumping	24
3.5.3. Control Policy Parameters	26
3.5.4. Feasibility Range	27
3.6. Chapter Conclusion	28
Chapter 4. Incorporating Power Demand Uncertainty Sources in a Chance-Constrained Water Distribution Network Voltage Support Problem	29
4.1. Notation	29
4.2. Chapter Introduction	31
4.3. Problem Description	32
4.3.1. Schedule and Real-time Control of WDN Pumps	32
4.3.2. Power Distribution Network Model	33
4.3.3. Water Distribution Network Model	34
4.3.4. Deterministic Problem	37
4.3.5. Convex Relaxations	37
4.3.6. Compensating Power Demand Uncertainty	38
4.3.7. Chance-Constrained Optimization Problem	39
4.4. Solution Approach	40
4.5. Case Study	40
4.5.1. Set Up	40
4.5.2. Results	42
4.6. Chapter Conclusion	50
Chapter 5. Incorporating Multiple Uncertainty Sources in a Chance-Constrained Water Distribution Network Voltage Support Problem	51
5.1. Notation	51
5.2. Chapter Introduction	54
5.3. Problem Description	55
5.3.1. Power Distribution Network Model	56
5.3.2. Water Distribution Network Model	57
5.3.3. Deterministic Problem: Nonconvex Formulation	60
5.3.4. Approximations and Relaxations	61
5.3.5. Deterministic Problem: Convex Formulation	63
5.3.6. Incorporating Uncertainty	63
5.3.7. Flexibility Costs	65
5.3.8. Chance-constrained Optimization	67
5.4. Case Studies	69
5.4.1. Set Up	70

5.4.2. Illustrative Results	71
5.4.3. Impact of Convex Approximations and Relaxations	77
5.4.4. Simplifying the Power Control Policy	81
5.4.5. Comparison of Flexibility Cost Formulations	83
5.5. Chapter Conclusion	85
Chapter 6. Tractable Uncertainty-Aware Methods for Leveraging Water Pumping Flexibility for Power Networks	86
6.1. Notation	86
6.2. Chapter Introduction	89
6.3. Adjustable Robust Voltage Support Problem	91
6.3.1. Power Distribution Network Modeling	92
6.3.2. Real-Time Pump Adjustments Responding to Uncertainty	93
6.3.3. Basic Form of the AARC	94
6.4. Incorporating WDN Constraints	95
6.4.1. Water Distribution Network Modeling	95
6.4.2. Monotonicity of WDNs	99
6.4.3. Full AARC	104
6.5. WDN Approximations	105
6.6. Deterministic Problem	106
6.7. Robust Case Study	106
6.7.1. Set Up	106
6.7.2. Results	107
6.8. Probabilistic Problem Formulation	110
6.8.1. Power Distribution Network Constraints, $\mathcal{W}_p(\mathbf{x}, \Delta\rho)$	111
6.8.2. Water Distribution Network Constraints, $\mathcal{W}_w(\mathbf{x}, \Delta\rho)$	111
6.8.3. Full Probabilistic Problem	112
6.9. Probabilistic Case Study	113
6.9.1. Set Up	113
6.9.2. Results	116
6.10. Chapter Conclusion	122
Chapter 7. Coordination of Multiple Services	124
7.1. Notation	124
7.2. Chapter Introduction	127
7.3. Problem Description	127
7.3.1. Voltage Support, $\Psi_1(\cdot)$	129
7.3.2. Frequency Regulation, $\Psi_2(\cdot)$	130
7.3.3. Power Distribution Network Modeling, $\Psi_3(\cdot)$	131
7.3.4. Water Distribution Network Modeling, $\Psi_4(\cdot)$	132
7.3.5. Providing Both Voltage Support and Frequency Regulation	134

7.4.	Sequential Reformulation	135
7.4.1.	Step 1: Voltage Support Problem	136
7.4.2.	Step 2: Frequency Regulation Preprocessing	137
7.4.3.	Step 3: Frequency Regulation	137
7.5.	Case Study	138
7.5.1.	Set Up	139
7.5.2.	Results	139
7.6.	Chapter Conclusion	142
Chapter 8. Assessing the Resilience of an Optimal Water Pumping Control Strategy to Provide Frequency Regulation		144
8.1.	Notation	144
8.2.	Chapter Introduction	147
8.3.	Problem Description	147
8.3.1.	Problem Approach	148
8.3.2.	WDN Operational Control Strategies	149
8.4.	Hazard Event Modeling and Simulation	150
8.4.1.	Hazard Simulation and Outage States	150
8.4.2.	Hydraulic Simulation	152
8.4.3.	Evaluating Operational Resilience	152
8.5.	Optimal Coupled Power-Water Frameworks	154
8.5.1.	Modeling Water Flow Constraints	154
8.5.2.	Optimal Water Flow Pumping Control (OWF)	157
8.5.3.	Optimal Water Pumping Control + Frequency Regulation (OWF+FR)	158
8.6.	Case Study	160
8.6.1.	Set Up	161
8.6.2.	Results	163
8.7.	Chapter Conclusion	170
Chapter 9. Conclusion		171
9.1.	Summary of Key Results	171
9.2.	Synthesis of Approaches	173
9.3.	Barriers to Implementation	175
9.4.	Future Research	176
Appendix		178
Bibliography		181

List of Figures

5.1. WDN visualization including elevation and hydraulic head with respect to an elevation reference, flow rate, and head loss. Example equations of conservation of hydraulic head (5.15) and conservation of water (5.11) are included.	58
5.2. Convex hull for the pump power consumption (left) and pipe head loss (right).	62
5.3. Coupled power (left) and water (right) distribution network. The dashed lines show where the water supply pumps are connected to the PDN. The water tank is passive. We show the single-phase equivalent PDN but we used a three-phase unbalanced network model. The pumps are modeled as balanced three-phase loads.	69
5.4. Pump and tank schedules for Case B, $\epsilon = 5\%$ (left) and Case C, $\epsilon = 5\%$ (right). Dark and light blue shading show the flexibility bands around the scheduled flow rate associated with the water and power control policy, respectively. The schedule obtained from solving the deterministic problem is also shown.	72
5.5. Feasible and infeasible pump flow rate adjustments given water and power demand uncertainty for Case A, $\epsilon = 3\%$.	74
5.6. Three-phase PDN voltage profile for the schedule in Case A, $\epsilon = 3\%$. The square markers at each bus and phase are scaled according to the magnitude of the power control policy parameters. The dark squares represent pump 1's control policy parameters. The overlaying light squares correspond to pump 2's control policy parameters.	76
5.7. Water control policy pump and tank contribution given (i) only water demand uncertainty and (ii) water and power demand uncertainty for Case A, $\epsilon = 3\%$.	76
5.8. Comparison of the three-phase PDN voltage profile corresponding to the approximate, convex power flow model and the original, nonconvex power flow model for a scenario in Case A, $\epsilon = 5\%$.	80
5.9. Grouping of buses associated with power control policy parameters for simplification 1 (S1) and simplification 2 (S2).	81
5.10. Sensitivity analysis showing how the scheduled energy cost, $G_{w,1}^t$, and $G_{p,1}^t$ change when varying the weighting coefficients g_w^t [\\$] and g_p^t [\\$·kW ² /CMH ²] for Case A, $\epsilon = 5\%$, and flexibility cost Option 1.	84
6.1. Water storage tank diagram.	98
6.2. The feasible water flow solutions for tank formulation 1 (Left) and tank formulation 2 (Right) are shown in blue with an overlaid orange area indicating the feasible water flow solutions when enforcing monotonicity.	102
6.3. Coupled PDN (left) and WDN (right). The blue dashed line indicates where the water supply pump is connected to the PDN.	107

6.4. Pump flow rates and tank levels in the multi-period convex robust problem ($\sigma = 4\%$) for the robust schedule (solid blue lines) and the deterministic schedule based on forecasted demands (red dotted lines). The bounds on the robust pump flow rate and tank levels are shown with blue shading around the schedule. The black dashed lines are the minimum and maximum pump flow rates and tank levels.	109
6.5. Topology of the case study's coupled three-phase unbalanced PDN (left) and WDN (right). The blue dashed line indicates where the three-phase balanced water supply pump is located in the PDN.	114
6.6. Time-varying water and power demand multipliers (top) and electricity price (bottom) over the scheduling horizon.	115
6.7. Example probability density functions of the actual distributions (solid lines) for bus 8, phase c , and $t = 1$ compared with the estimated normal distribution (dashed lines) fitted using maximum likelihood estimation with 500 samples. The actual distributions are Case A (left) and Case C (right). . .	118
6.8. Comparison of pump power schedules for the probabilistic (solid blue line), deterministic (dotted red lines), and robust (dashed green lines) solutions for (top) Case A ($\epsilon_p = 3 \times 10^{-3}\%$ and $\epsilon_w = 1 \times 10^{-4}\%$) and (bottom) Case C ($\epsilon_p = 1 \times 10^{-9}\%$ and $\epsilon_w = 1 \times 10^{-9}\%$). The blue and green bands indicate the range of real-time voltage support adjustments of the pump around the probabilistic and robust schedule, respectively. The black dashed lines indicate the pump power limits.	120
7.1. Coupled power (left) and water (right) distribution networks. Pumps 1 and 2 are connected to buses 10 and 5, respectively.	138
7.2. Three-phase pump power consumption in the sequential problem ($\sigma = 7.5\%$). The solid black lines indicates the schedule, blue and green bands indicate the range of pump power adjustments allocated for voltage support and frequency regulation.	140
8.1. Topology of the coupled power distribution network (Left) and water distribution network (Right). Blue nodes in the power distribution network are used to indicate where the pumps are connected.	160
8.2. (a) Electricity prices over scheduling horizon and (b) Nominal three-second wind gust speed during the hazard event.	162
8.3. Probability of wooden utility pole failure as a function of the three-second gust wind speed. Fragility curves are depicted given the pole parameters used in the case study for varying θ values.	162
8.4. Power distribution network performance indicator functions for the percentage of distribution lines online (Left) and percentage of loads connected (Right) for varying wind speed intensities (each row). The solid black line is the average performance over the 50 scenarios.	164

8.5. (Left) Tank water levels—as percentage of total tank volume—and (Right) pump power consumption in the (Top) Rule-based, (Middle) OWF, and (Bottom) OWF+FR control strategies under normal operating conditions.	166
8.6. Pump power consumption in the OWF+FR problem. The blue solid line is the expected pump power consumption given the frequency regulation signal. The orange dashed line is actual pump power consumption simulated in WNTR.	167
8.7. Time-varying tank levels (as a percentage of available tank volume) simulated in WNTR with a 175% wind intensity for a) the rule-based control, b) OWF, and c) OWF+FR control strategies. The blue lines are the tank levels for each scenario. The solid black lines are the average tank levels over all scenarios.	169
A.1. Convex relaxation (shaded blue area) of a generic pipe head loss formula (black line). The quasi-convex hull is made from a set of linear functions (A.2)-(A.5), shown with blue lines.	179

List of Tables

2.1. Estimated Energy and Power Capacities in Wisconsin's Water Utilities (Case 1 - Distribution)	11
2.2. Estimated Energy and Power Capacities in Wisconsin's Water Utilities (Case 2 - Treatment and Distribution)	11
2.3. Estimated Energy and Power Capacities for Water Utilities in the U.S. (Case 1 - Distribution)	12
2.4. Estimated Energy and Power Capacities for Water Utilities in the U.S. (Case 2 - Treatment and Distribution)	12
3.1. Pump Parameters	23
3.2. Pump 1's Average Control Policy Parameter (%)	27
3.3. Violation Probability (%), Mean μ and Standard Deviation σ	27
4.1. Case Studies	41
4.2. Number of Scenarios Needed for Scenario Approach	42
4.3. Comparison of MICP and CP solver solutions	42
4.4. Scenario Approach Results	43
5.1. Case Studies	71
5.2. Relaxation and Approximation Comparison	78
5.3. Empirical Violation Probabilities for Convex and Nonconvex Constraints	80
5.4. Power Control Policy Simplification Results	82
5.5. Flexibility Cost Comparison	83
6.1. Single-Period Results	108
6.2. Case Studies	115
6.3. Probabilistic and Robust Results	117
6.4. Empirical Joint Violation Probabilities (%)	121
7.1. Average Three-Phase Results over 12-hour Scheduling Horizon	141
7.2. Comparison of Sequential and Co-optimized Solutions ($\sigma = 4.5\%$)	142
8.1. Power Distribution Network Resilience Metrics	165
8.2. Operational Costs	165
8.3. Water Distribution Network Resilience Metrics	168

List of Acronyms

AARC	Affinely Adjustable Robust Counterpart
ARO	Adjustable Robust Optimization
CAISO	California Independent System Operator
CDF	Cumulative Distribution Function
CMH	Cubic Meters per Hour
CP	Convex Problem
DER	Distributed Energy Resource
EPANET	Environmental Protection Agency Network Evaluation Tool
FR	Frequency Regulation
MICP	Mixed-Integer Convex Problem
MILP	Mixed-Integer Linear Problem
MGD	Million Gallons per Day
OWF	Optimal Water Flow
OWF+FR	Optimal Water Flow and Frequency Regulation
PDN	Power Distribution Network
SCADA	Supervisory Control and Data Acquisition
SDWIS	Safe Drinking Water Information System
VS	Voltage Support
WDN	Water Distribution Network
WNTR	Water Network Tool for Resilience

Abstract

Large amounts of renewable energy resources are being added to the electric power grid in a push to mitigate the effects of climate change. Due to the intermittent and uncertain nature of these resources, more flexibility is needed to ensure safe operating conditions of the power grid. A growing body of research has shown that real-time control of flexible electric loads can provide flexibility to the power grid. For instance, drinking water distribution networks can be treated as flexible, controllable assets to the power grid by leveraging the power consumption of water supply pumps and storage capabilities of water tanks. Initial research has explored optimizing the operation of water distribution networks to support the power grid; however, the impact of uncertainty on network performance and value has not been considered.

In this dissertation, an integrated power-water optimization problem is developed subject to the water and power network constraints and multiple sources of uncertainty. The operation of water distribution networks is optimized to provide multiple local and system services—such as voltage and frequency regulation—to power networks. The integrated optimization of the water distribution network and power network is challenging because both networks have nonconvex models and experience uncertainty (e.g., water and power demands). Additionally, changes in network operation need to clearly provide value to both system operators as well as maintain or improve upon network resilience. The associated benefits and drawbacks of the integrated water-power optimization framework are investigated, with a particular focus on performance, conservativeness, and computational tractability. First, state and country-wide estimates of the power and energy capacity of water distribution networks as flexible loads are calculated using publicly available water distribution network utility information, indicating that water distribution networks can provide a sizable flexible resource. Second, stochastic and robust optimization frameworks are developed to optimally schedule and control the water distribution network to provide power system services while ensuring the safe operation of the power and water distribution networks given power and water demand uncertainties. Third, to address challenges surrounding problem

complexity and scalability, this work develops proofs that the monotonicity properties apply to the water flow constraints under certain assumptions, uses approximation and relaxation techniques to reformulate the power-water problem as a convex program, and proposes an analytically reformulated probabilistic framework that manages uncertainty differently in the power and water network. Fourth, the flexibility of the water distribution network may be underutilized if any one power system service is considered. To prevent this, a formulation is developed where the water network provides multiple services simultaneously. This maximizes the overall benefit to the power grid and increases the value proposition to the water distribution network operator. And fifth, optimal pump operation strategies are evaluated to ensure that the power and water networks can respond and adapt to natural hazard events when the water distribution network is providing grid services.

Case studies demonstrate the capability of the water distribution network pumps to provide services to the power grid. By co-optimizing the power grid and the drinking water distribution network, improvement in costs, reliability, and resiliency can be realized across these two critical infrastructure systems. Additionally, leveraging the water distribution network to provide flexibility to the power grid can allow for greater quantities of renewable energy resources to be incorporated into the grid and reduce carbon emissions.

Chapter 1.

Introduction

Large amounts of renewable energy sources (e.g., solar photovoltaics and wind power) and new electric loads (e.g., plug-in electric vehicles) are being added to the electric grid in a push to mitigate the effects of climate change. Unlike traditional energy generation sources, renewable energy sources are intermittent and distributed, which causes the net power demand to be more variable and uncertain. Net demand deviations can cause frequency and voltage deviations outside of safe operating levels in the power transmission and distribution networks. To prevent unsafe operating conditions, more flexibility is needed in the power network to compensate for larger and more frequent net demand deviations. Traditional methods for regulating frequency and voltage in the transmission and distribution networks will become over-strained and more costly. In the power transmission network, fast-ramping power plants (e.g., natural gas units) are contracted to provide reserves. More reserves will need to be scheduled to handle fluctuations. In the power distribution network (PDN), voltage regulation is traditionally handled by step-voltage regulators, tap-changing transformers, and switched capacitors. With larger and more frequent voltage fluctuations, the wear-and-tear on voltage control devices increases, shortening the device lifespan and increasing maintenance costs.

Alternatively, research has shown that controlling the operation of flexible loads and storage devices can provide the same power system services as traditional flexibility methods [1, 15, 66, 68]. Flexible loads are able to shift their power consumption in time without impacting their quality of service (up to an extent). By shifting when they consume power, flexible loads can reduce or replace the need for conventional flexible generation sources and control mechanisms. There is a significant body of research on the control of thermostatically controlled loads (e.g., refrigerators, air conditioners, and water heaters) [57], industrial

and commercial buildings [78], plug-in electric vehicles [67], and energy storage units [73]. In this dissertation, we leverage the water distribution network (WDN) as a flexible load to provide multiple services for the power network given network uncertainty. We also work on identifying the associated benefits and drawbacks of the integrated power-water optimization framework. Particularly, we focus on performance, conservativeness, and computational tractability. This work is situated within a growing research area of co-optimizing coupled critical infrastructure systems. In the following sections, a brief background and literature review is presented on integrated optimization of coupled systems and the potential of using coupled power-water networks as flexible loads.

1.1. Integrated Optimization of Critical Infrastructure Systems

There is increasing interest in integrated optimization of critical infrastructure systems, such as water, power, natural gas, and district heating networks [25]. While these critical infrastructure systems are traditionally planned and operated independently, these systems are inherently interconnected and interdependent. For example, in a coupled gas and power network, the power network requires gas for electricity production in flexible gas-powered generators and the gas network uses electricity when distributing natural gas to customers (e.g., for the operation of compressors). Typically, the demands of one network on another can be shifted either spatially or temporally. For instance, in the coupled gas and power network, gas can effectively be stored in pipelines for use in later time periods by compressing it, which is known as ‘linepack’. Controlling the operation of multiple networks together can help relieve the new and growing burdens that these networks are experiencing. Potential benefits of co-optimizing coupled systems include being able to incorporate greater quantities of renewable energy resources, reducing carbon emissions, reducing operational and capital costs, and improving system resiliency [1]. We refer the reader to [44, 70] for a comprehensive review on the motivation, requirements, and best practices when modeling interdependent systems. Examples of research in this area include work on interconnected gas-power networks [84, 97, 132], power-district heating-natural gas networks [35, 105, 106], and islanded energy hubs for power-heat-gas-hydrogen networks [36].

There are four challenges associated with the integrated optimization of multiple critical infrastructure systems.

- First, the problem complexity and dimension significantly increases when considering multiple networks since we need to ensure that all networks are operating safely, i.e., the network variables are within acceptable ranges. Due to the underlying physics of multi-energy systems, the network constraints are nonlinear and nonconvex. Consequently, there is a trade-off in performance between computational tractability and optimality (or even feasibility) of the solution.
- Second, critical infrastructure systems experience uncertainty. These uncertainties can propagate through interdependent networks intensifying system vulnerabilities. Additionally, considering uncertainty in the optimization problem makes solving the problem more complicated.
- Third, new operational control strategies need to maintain or improve upon network performance, reliability, and resiliency. Additionally, the value proposition of new operational strategies needs to be demonstrated.
- Fourth, coordinated operation of multiple systems typically relies on sharing system data between system operators that are traditionally independent. This can cause privacy issues as well as a need for additional communication and/or measurement infrastructures.

In this work, we primarily focus on the first three challenges.

1.2. Background on Coupled Power and Water Networks

In this dissertation, we focus on coupled power networks and water networks. Water networks and power networks are critical infrastructure systems that are spatially and temporally coupled. Water pumps in the WDN are loads in the PDN and are capable of shifting their power consumption in time by storing water in elevated water storage tanks. Therefore, the water and power distribution networks are interconnected. Additionally, the water and power networks are experiencing similar challenges. Water and power system operators are both dealing with aging infrastructures and increasing consumer demands due to growing populations [47].

Utilizing the WDN as a flexible load can be beneficial to both networks. From the power network's perspective, around 4% of the electricity use in the United States goes to drinking

and waste water networks and a majority of this electricity (around 90% to 99%) is used for pumping [28]. Regionally, the energy consumption of water networks can be significantly larger. For example, in California, 19% of the state’s energy consumption goes to water-related uses [54]. From the water utility’s perspective, aging infrastructures are reaching the end of their planned lifespans, which causes systems to become less efficient, have greater water leakage, and higher maintenance costs [18, 88]. Electricity costs is one of the largest operating costs (around 80%) for water system operators [38]. By providing additional services, water utilities could offset this cost and help pay for new equipment investments. Most large water network utilities are capable of fast operational control (within seconds or minutes) via already present supervisory control and data acquisition (SCADA) systems [28, 63]. Below, the water and power networks are described in the context of integrated optimization.

1.2.1. Power Networks

The purpose of electric power networks is to produce and transport electrical energy to consumers. To reliably provide power, the supply and demand must always be balanced. As discussed earlier, increasing levels of renewable energy sources and new loads in the network can cause more frequent and larger net demand deviations which can have ill effects on the system frequency and voltage. Flexibility is traditionally provided by flexible generation units (e.g., natural gas plants). However, real-time control of flexible loads, like WDNs, can provide flexibility to the power network through demand response or grid services, such as frequency regulation and voltage support. Using these electricity-consuming water network assets to reduce the cost and/or increase the reliability of power systems in turn reduces the cost of water networks (via cheaper electricity) and improves their reliability (via fewer pumping/treatment outages that results from power outages).

Optimal operation of power networks is a very active research area. We refer the reader to [77] for a comprehensive review. There is also work on formulating and solving chance-constrained optimization programs for power networks [26, 94] with control policies used to approximate optimal real-time control actions [96, 124]. Additionally, there is a growing interest in quantifying and enhancing the reliability and resiliency of the power grid (e.g., [19, 48, 89]).

1.2.2. Water Networks

The purpose of water networks is to extract, treat, and distribute safe, reliable drinking water. In this work, our focus is on public supply¹ water distribution networks. Water distribution networks deliver drinking water to consumers (primarily serving residential, commercial, and industrial sectors but also delivering treated water to irrigation and thermoelectric sectors). Water distribution networks rely on gravity and water pumps to move water through the network. Most water networks have elevated storage tanks or standpipes to hedge against demand uncertainty and periods of high demand as well as provide pressure regulation [109]. System pressure heads must be maintained in order to supply water and meet emergency fire flow requirements.

Water network pumps (in conjunction with storage tanks) are capable of providing local and global services to the power network [109, 123]. While rule-based operation is traditionally employed, the water network infrastructure is capable of optimal day-ahead and real-time control. Water flow modeling is a very established research area, with algorithms such as the gradient method [102, 103], Newton-Raphson [55], and the (co)content method [22]. There is also research on the optimization of water distribution network operation, where the objective is typically either minimizing operational costs or improving water quality (or a combination of both). Solution approaches include linear approximations and relaxations [11, 32, 37, 49, 108, 128] and genetic algorithms [136]. A literature review of optimal control methodologies is given in [69, 85]. In [56], resiliency measures in WDNs are assessed.

1.2.3. Literature Review on Coupled Water-Power Optimization

While WDNs are physically capable of providing services to the power network, this research area is small. Other types of water networks have been studied more extensively as demand response resources, such as agricultural irrigation pumping [83] and wastewater treatment plants [88, 123].

Recently, there have been papers that explore the integrated optimization of WDN and PDN operation. A distributed solution approach is presented for a water-power flow optimization problem in [130]. In [61], relaxations and approximations are applied to a demand response operation problem for an agricultural irrigation system [61]. Ref. [31] develops of a framework for WDNs to consume surplus energy based of a signal from the PDN. In [81,

¹A public supply is defined as a public or private water network utility that serves a minimum of 25 people or has at least 15 connections [29].

82], the authors solve for the electricity-consumption flexibility from multiple WDNs to the power transmission network. Ref. [134] evaluates the interdependence of the WDN and PDN after simulating the optimal operations of the water network and power network. In [63], the authors create an optimization framework to determine the WDN’s possible demand response participation. In [4], the WDN and PDN are co-optimized to minimize power loss with an iterative convex program. While there are existing stochastic approaches to optimize the water network operation [5, 39, 40, 50, 53, 58] and power network operation [60, 90], there is no work optimizing the coupled WDN-PDN operation subject to uncertainty.

Additionally, there are a few papers that look at the resilience across a coupled power-water system, e.g., [101, 133, 135]. These works have helped define coupled power-water network resilience metrics. However, to the best of our knowledge, no other work considers the impact of optimal WDN control on the resilience of power and water distribution networks.

1.3. Organization of the Dissertation

This dissertation consists of seven main chapters. Chapters 3-5 focus on formulating the integrated water-power problem as a chance-constrained optimization problem subject to network uncertainty. They explore formulating the chance-constrained optimization problem, different sources of uncertainty, scenario-based solution approaches, the impact of approximations and relaxations, and ways to reduce network measurements. We chose a chance-constrained optimization framework because it gives a way to quantify risk and allows for the constraints to be satisfied almost all of the time but occasional violations are acceptable so that the solution is less conservative. Chapters 6-8 address the limitations and additional considerations arising from Chapters 3-5, such as conservativeness, computational tractability, maximizing the value added by providing grid services, and maintaining network resiliency of new operation strategies. The main content of each chapter is described below.

In **Chapter 2**, we estimate the WDN flexibility potential within the United States. We characterize the energy and power capacities of Wisconsin municipal water utilities and extrapolate the data to get a rough measure of the WDN potential within the United States. We use these calculations to motivate the potential impact of the following work.

In **Chapter 3**, we present a chance-constrained optimization problem to schedule WDN pumping subject to WDN and PDN constraints while managing water demand uncertainty. We selected this framework because it gives a way to quantify risk and allows for the constraints to be satisfied for almost all scenarios. We solve for a pump operation schedule and

parameters in a balancing real-time control policy that updates the pump operation based on the water demand forecast error. We apply a heuristic scenario-based approach to gain insight into the performance and evaluate the impact of the PDN constraints and parameters on WDN operation.

In **Chapter 4**, we consider power demand uncertainty when formulating a chance-constrained optimization problem to schedule WDN pumping subject to WDN and PDN constraints. Unlike Chapter 3, we develop a control policy that determines corrective control actions based on power demand uncertainty (as opposed to a balancing control policy to match water demand and supply) to prevent voltage limit violations. We apply convex relaxations and approximations and use a scenario-based approach that provides performance guarantees for the convexified problem.

In **Chapter 5**, we build off the work in Chapters 3 and 4 to formulate and solve the chance-constrained voltage support problem given both water and power demand uncertainty. We evaluate the relative importance of the water and power control policies, the impact of the approximations, and the implications of how we define the cost of real-time control actions on the optimal solution. Additionally, we explore the trade-offs in conservativeness, computational tractability, and measurement requirements given the formulation and solution approach.

In **Chapter 6**, we investigate solution approaches and formulations to improve the computational tractability and performance of the uncertainty-aware voltage support problem. We do this by proving that the monotonicity properties for dissipative flow networks apply to the WDN under several assumptions. With the use of monotonicity properties, affine control policies, and approximations, we reformulate the problem as a computationally tractable robust counterpart. We evaluate the implications of the monotonicity property assumptions on the problem. We propose an analytically reformulated probabilistic approach that manages uncertainty differently in the water and power network. We compare the performance of the robust and probabilistic approaches in terms of computation time, cost, and empirical violation probabilities.

In **Chapter 7**, we present a robust water pumping optimization problem to provide local and grid level services concurrently to the power grid. By considering multiple grid services simultaneously, we can fully utilize the flexibility provided to the power grid and generate additional revenue for the WDN. We formulate a robust water pumping problem to determine the amount of voltage support and frequency regulation that can be provided subject to network constraints while managing power demand uncertainty. We evaluate the benefits

and challenges of providing multiple services together and how these services complement or compete with each other.

In **Chapter 8**, we evaluate the impact of optimal control strategies on the operational resiliency of the WDN. We consider an optimal water pumping problem that minimizes the electricity costs as well as an optimal water pumping problem that also provides frequency regulation. The optimal control strategies are compared with a conventional rule-based operation. Through hydraulic simulations, we assess the performance of these control strategies given a wind-based hazard that causes pump outages.

Note that the mathematical notation is defined separately in every chapter.

Chapter 2.

Estimating the Flexibility Potential of Water Distribution Networks

In this chapter, we estimate the flexibility potential of WDNs to determine the viability of leveraging water distribution networks (WDNs) as flexible assets. The goal of this chapter is to evaluate the potential impact WDNs could have on the power network which motivates the work presented in this dissertation.

2.1. Wisconsin's Water Distribution Network Flexibility Potential

Because there are no published reports that have estimated the WDN's flexibility potential in the United States, we derive our own estimate. We use Wisconsin's publicly available data on municipal and investor-owned water utilities to estimate flexibility potential in Wisconsin and extrapolate the data to give a very rough estimate of flexibility potential in the United States. The presented calculations show the order of magnitude of the entire nation's WDN flexibility potential.

Our data is drawn from Wisconsin's Public Service Commission; specifically, we use the Annual Report Data e-portal for the year 2019². Our estimate covers both municipal and investor-owned water utilities. It should be noted that very few water utilities are private [23]; for example, there is only one investor-owned water utility in Wisconsin.

We estimate WDN flexibility using the terms 'power capacity' and 'energy capacity',

²2019 is the most recent reporting year where all utilities had filed their reports.

analogous to a battery. We define power capacity P_{cap} as the maximum power consumption of the WDN's supply pumps, i.e., the difference in power if all the pumps were switched on or off given a signal. We define energy capacity E_{cap} as the product of the power capacity and the duration d . The duration d calculates how long the water demand could be met by the elevated storage tanks if the pumps were forced off, i.e., the sum of the usable volumes of the storage tanks divided by the sum of the volumetric water demands. We estimate P_{cap} and E_{cap} for every water network utility in Wisconsin.

It can be challenging to distinguish between water network treatment and distribution processes when estimating the flexibility potential. This is due to a lack of standardized terminology in utility reports [88]. How each utility reports their pumps' primary purpose (i.e., primary, booster, or standby) and primary destination (i.e., treatment or distribution) impacts the flexibility potential estimate. Additionally, the treatment and distribution processes complement each other. Especially in smaller networks, pumps in the treatment process can also support the distribution process [88]. Consequently, we present two cases when estimating the potential in order to provide a more comprehensive estimate.

- Case 1: Considers only the electric supply pumps reported in the WDN.
- Case 2: Considers the electric supply pumps reported in the WDN *and* the electric primary pumps in the drinking water treatment plant.

In both cases, we only consider pumps with electric motors. We collect the following data from each utility's 2019 annual report [93].

- *Horsepower of pumps with electric motors.* We only consider active pumps (i.e., not standby pumps) and include pumps whose primary destination is either distribution (Case 1) or distribution *and* treatment (Case 2). We use this metric to estimate the power consumption of the pumps. Therefore, the power capacity P_{cap} is calculated from the sum of the pumps' horsepower. We assume a pump efficiency of 75% which is the pump efficiency default in EPANET, the U.S. Environmental Protection Agency's free WDN modeling and simulation software [102].
- *Monthly totals of water entering the distribution system.* This is used to calculate the average hourly water demand, i.e., the sum of the monthly water demands divided by 8760 hours/year.
- *Total capacity of the elevated storage tanks, standpipes, and reservoirs that have a positive elevation difference.* The duration d is calculated from the total capacity of

available storage divided by the average hourly water demand. The energy capacity E_{cap} is then calculated as $P_{\text{cap}} \times d$.

We collect data on the population served for each water utility from the Safe Drinking Water Information System (SDWIS) Federal Reporting database [118], which reports basic information and water quality violations for every water utility in the United States. With this data, we classify the Wisconsin water utilities by size³. We report the total power capacity and energy capacity in Wisconsin for water utilities' distribution supply pumps (Case 1) in Table 2.1 and for primary treatment pumps and distribution supply pumps (Case 2) in Table 2.2.

Table 2.1: Estimated Energy and Power Capacities in Wisconsin's Water Utilities (Case 1 - Distribution)

Utility Size	Number of Utilities	Total Power Capacity (GW)	Total Energy Capacity (GWh)
Very Small	87	0.004	0.308
Small	259	0.029	1.671
Medium	88	0.033	1.359
Large	73	0.089	2.440
Very Large	4	0.049	0.862
Total	511	0.203	6.640

Table 2.2: Estimated Energy and Power Capacities in Wisconsin's Water Utilities (Case 2 - Treatment and Distribution)

Utility Size	Number of Utilities	Total Power Capacity (GW)	Total Energy Capacity (GWh)
Very Small	87	0.004	0.324
Small	259	0.031	1.742
Medium	88	0.037	1.516
Large	73	0.104	2.757
Very Large	4	0.083	1.343
Total	511	0.259	7.682

³Utility size is determined by population served. We follow the definitions used in [88], where very small is 25-500 people, small is 501-3,300 people, medium is 3,301-10,000 people, large is 10,001-100,000 people, and very large is greater than 100,000 people.

2.2. Estimating the Water Distribution Network Flexibility Potential in the U.S.

We then extrapolate this data to the United States, where there are around 51,000 year-round water utilities [88]. We do not consider the 18,390 non-transient non-community water systems (e.g., schools and hospitals) and 83,470 transient non-community water systems (e.g., campgrounds or gas stations) because they are not open year-round. We calculate the average power capacities and energy capacities for each utility size classification in Wisconsin. Given the data on the number of utilities in the U.S. and their size, we extrapolate the Wisconsin averages to get the total estimated energy and power capacities by utility size in the United States. Cases 1 and 2 are shown in Tables 2.3 and 2.4, respectively. While these numbers are approximate, they do indicate that drinking water network pumping is a sizable flexibility resource. For comparison, California's energy storage mandate aims for 1.325 GW [91].

Table 2.3: Estimated Energy and Power Capacities for Water Utilities in the U.S. (Case 1 - Distribution)

	Very Small	Small	Medium	Large	Very Large	Total
Number of Utilities	28,462	13,737	4,936	3,802	419	51,346
Power Capacity (GW)	1.2	1.6	1.8	4.6	5.1	14.3
Energy Capacity (GWh)	100.7	88.6	76.2	127.1	90.3	482.9

Table 2.4: Estimated Energy and Power Capacities for Water Utilities in the U.S. (Case 2 - Treatment and Distribution)

	Very Small	Small	Medium	Large	Very Large	Total
Number of Utilities	28,462	13,737	4,936	3,802	419	51,346
Power Capacity (GW)	1.3	1.6	2.1	5.4	8.7	19.1
Energy Capacity (GWh)	106.0	92.4	85.0	143.6	140.7	567.7

However, there are five significant limitations to the accuracy of this estimate. First, the energy intensity and storage capacity of water networks vary significantly by region. For example, while the waste water and drinking water networks nationally consume around 4% of the electricity in the U.S., 19% of the electricity consumption in California goes to water related uses [28, 54]. Second, the actual energy capacity is highly variable upon current water demand. During peak water demands, the energy capacity would be smaller because the tanks would be able to supply the network for a shorter amount of time before being depleted

and vice versa for low demand times. For example, if we consider the average hourly water demand taken from the reported minimum daily demand (i.e., the reported minimum water pumped for any one day in 2019 for each utility), the energy capacity for water distribution network supply pumps in Wisconsin and the United States is 31.5 GWh and 2,733.6 GWh, respectively. Third, while we calculated the flexibility potential for all WDNs, prioritizing the use of larger utilities (e.g., large to very large) to provide power system services may make more sense economically. This is because larger utilities generally have more pumps and tanks and are therefore able to provide more demand response services. Fourth, this estimate only captures the temporal flexibility (i.e., the WDN shifting power consumption in time by storing water in elevated storage tanks) and not the spatial flexibility (i.e., shifting pumping load between different pumps) in the WDN. And fifth, the volume of a tank that can be used for operational storage is less than the physical storage capacity of the tank. This is because tanks are also needed to maintain system pressure as well as provide sufficient amounts of water for contingency firefighting. The specific volume that can be used can vary based on state-wide regulatory constraints and utility-specific requirements. For instance, there may be a required amount of ‘dead storage’ needed to meet minimum pressure requirements for all consumers [2]. It can be unclear in utility reports whether the tank capacity includes the volume of stored water designated as dead storage.

2.3. Chapter Conclusion

In this chapter, we estimated the flexibility potential of WDNs in Wisconsin and extrapolated the data to get a rough estimate of the flexibility potential of WDNs in the United States. We found that WDNs appear to be a sizable flexibility resource. By considering additional data—such as the seasonal and daily variation of water demand [20, 64], and the regional variation in water network energy intensities [117], and regulatory constraints on operation—we can further improve the reliability of the national water network potential estimate.

Chapter 3.

Incorporating Water Demand Uncertainty Sources in a Chance-Constrained Water Distribution Network Voltage Support Problem

This chapter presents a chance-constrained optimization problem to schedule water distribution network (WDN) pumping subject to water and power distribution network constraints while managing water demand uncertainty. We utilize a heuristic scenario-based approach to solve for this preliminary problem. We evaluate the impact of the power distribution network (PDN) parameters and voltage limits on the solution. This chapter is based on [112].

3.1. Notation

Sets

\mathcal{E}	Set of pipes in the WDN (indexed by e)
\mathcal{I}_k	Set of buses directly downstream of bus k in PDN (indexed by k)
\mathcal{J}	Set of junctions within the set of nodes in the WDN (indexed by j)
\mathcal{K}	Set of buses in the PDN (indexed by k)
\mathcal{N}	Set of nodes in the WDN (indexed by j)
\mathcal{P}	Set of pumps within the set of pipes in the WDN (indexed by e)

\mathcal{R}	Set of reservoir nodes within the set of nodes in the WDN (indexed by j)
\mathcal{V}	Set of valves within the set of pipes in the WDN (indexed by e)

Variables

c_e	Control policy parameter for pump e (-)
H_j	Hydraulic head at node j (m)
L_e	Head loss in pressure reducing valve e (m)
p_e	Real power demand of pump e (kW)
P_k	Real power flow downstream of bus k (kW)
$P_{L,k}$	Real power consumed at bus k (kW)
q_e	Reactive power demand of pump e (kVAr)
Q_k	Reactive power flow downstream of bus k (kVAr)
$Q_{L,k}$	Reactive power consumed at bus k (kVAr)
V_k	Voltage magnitude at bus k (V^2)
x_e	Volumetric water flow rate in pipe e (CMH)

Random Variables

\tilde{d}_j	Deviation in water demand of consumer j (CMH)
\tilde{H}_j	Deviation in hydraulic head at node j (m)
\tilde{x}_e	Deviation in water flow rate in pipe e (CMH)

Parameters

a_{je}	Element in incidence matrix A of nodes \times pipes (-)
d_j	Forecasted water demand of consumer j (CMH)
\bar{h}_j	Elevation head of node j (m)
h_j^{\max}	Maximum pressure head for node j (m)
h_j^{\min}	Minimum pressure head for node j (m)
\hat{H}_e	Pump e 's shut-off head (m)
k_e	Resistance coefficient for pipe e ($h^{1.852} \cdot m^{-3(1.852)-1}$)
m_e	Pump coefficient for pump e ($h^2 \cdot m^{-5}$)
N	Number of scenarios (-)
r_k	Resistance of the line downstream of bus k (Ω)
V_k^{\min}	Minimum voltage limit at bus k (kV)
V_k^{\max}	Maximum voltage limit at bus k (kV)
V_{set}	Voltage at feeder head (kV)
x_k	Reactance of the line downstream of bus k (Ω)

x_e^{\min}	Minimum water flow rate of pump e (CMH)
x_e^{\max}	Maximum water flow rate of pump e (CMH)
β	Constant in pump power consumption equation (kW/CMH · m)
ΔT	Length of time period (h)
δ	Number of optimization variables (-)
ϵ	User-selected violation level (%)
π_e	Forecasted energy price for pump e (\$/kWh)
ψ	User-selected confidence level (%)
μ_e	Ratio between real and reactive power of pump e (-)
ρ_k	Forecasted real power demand of consumers connected to bus k (kW)
ζ_k	Forecasted reactive power demand of consumers connected to bus k (kVAr)

Functions

$f(\mathbf{x}, \tilde{d})$ Constraints in chance-constraint with decision variables \mathbf{x} and uncertainty \tilde{d}

3.2. Chapter Introduction

The objective of this chapter is to develop an approach to schedule water pumping subject to the constraints of the water and power distribution networks. In contrast to past work that coordinates optimal WDN operation and PDN operation [32, 62, 74, 82, 130], we consider network uncertainty. Both networks are subject to uncertainty, for example, from stochastic water demand, power demand, and equipment outages. Here, we consider only uncertain water demand and we assume a control policy that allows the pumps to adjust in response to forecast error by modifying pumping operations. Our approach determines the nominal schedule of the pumps and the optimal control policy parameters.

The contributions of this chapter are 1) formulation of the optimization problem to operate the WDN subject to the WDN and PDN constraints, 2) reformulation of the problem as a chance-constrained optimization problem considering water demand forecast error, 3) application of a heuristic scenario-based approach to solve the chance-constrained problem, 4) assessment of the impact of PDN constraints on optimal pumping, and 5) investigation of the approach's performance.

The remainder of the chapter is organized as follows. Section 3.3 gives the problem description and assumptions. Section 3.4 formulates the deterministic and chance-constrained problems and describes the solution approach. Section 3.5 describes our case study and its results. Finally, Section 3.6 discusses the limitations of our approach and how these

limitations set the direction for the following chapters.

3.3. Problem Description and Assumptions

In this chapter, we develop an approach to schedule the pumps in a WDN to minimize pumping costs while ensuring WDN and PDN constraints are satisfied. Fig. 3.1 shows the topology of a coupled WDN and PDN. The pumps draw power from specific buses in the PDN. We first develop the deterministic optimization problem in which pumping costs are minimized subject to the water and power flow equations and inequality constraints limiting the hydraulic heads, pipe flows, voltages, and apparent power flows. We then reformulate the problem into a chance-constrained problem assuming uncertain water demand. We assume that the inequality constraints must hold probabilistically at a specified violation level, which is a design variable. In order to ensure that water demand is satisfied despite forecast error, we assume the pumps use an affine control policy to change their operation as a function of the total water demand forecast error. We optimize the control policy parameters together with the pump schedule. In this chapter, we do not consider water storage tanks; however, they could be added to the formulation, increasing the number of constraints and decision variables since storage tank inflow/outflow can be scheduled and controlled in real time like pumping.

The problem is solved over a single time period of length ΔT . The WDN is depicted as a directed graph $(\mathcal{N}, \mathcal{E})$ composed of sets of nodes \mathcal{N} and edges \mathcal{E} . The nodes consist of a disjoint set of junctions \mathcal{J} and reservoirs \mathcal{R} , i.e., $\mathcal{N} = \{\mathcal{J} \cup \mathcal{R}\}$. The edges that connect the nodes are pipes that may have pumps ($\mathcal{P} \subset \mathcal{E}$) or valves ($\mathcal{V} \subset \mathcal{E}$); there is at most one pump or valve on a pipe. We denote a pipe $e : g \rightarrow h$ where the water flowing in pipe e goes from sending node g to receiving node h . We assume that the water flow in the pipes does not change direction within the time period and the flow is indicated by the directed graph. We also assume that the on/off states of pumps are determined in advance of the scheduling period, i.e., we do not consider the possibility of turning off the pumps.

We assume the PDN is radial and includes a set of buses \mathcal{K} to which consumers and water pumps are connected. We also assume that the power distribution network is balanced and pumping actions have no impact on electricity prices, i.e., the WDN is a price taker. Finally, we assume we have full knowledge of the WDN and the PDN, while in practice they are usually operated by different entities.

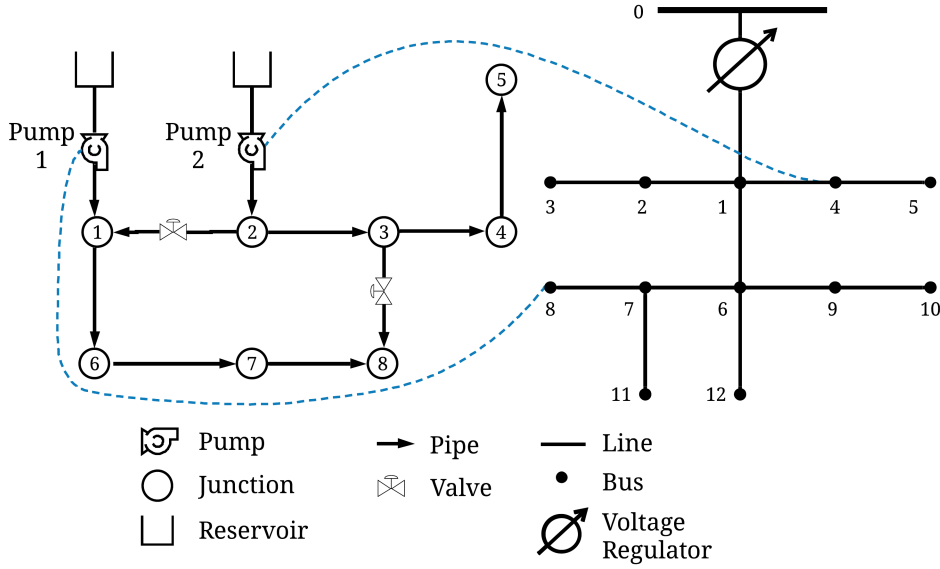


Figure 3.1: Water (left) and power (right) distribution networks. Dashed lines show where water pumps are connected in the power distribution network.

3.4. Problem Formulation

In this section, we develop the problem formulation. We first formulate the deterministic problem. Then, we introduce uncertain water demand and formulate the chance constraints. Finally, we describe our solution approach using a scenario-based method.

3.4.1. Water Constraints

We use the hydraulic constraints from [10]. We modify the formulation to include pressure reducing valves and reservoirs as defined in [32].

Nodes, \mathcal{N}

The total hydraulic head at node j , denoted H_j , is comprised of the elevation head \bar{h}_j and the pressure head. It is constrained to ensure sufficient water pressure

$$h_j^{\min} + \bar{h}_j \leq H_j \leq h_j^{\max} + \bar{h}_j \quad \forall j \in \mathcal{N}. \quad (3.1)$$

Reservoirs are treated as an infinite source of water and, therefore, have a fixed pressure head. We set the reservoirs' hydraulic head equal to the elevation head

$$H_j = \bar{h}_j \quad \forall j \in \mathcal{R}. \quad (3.2)$$

For junctions, we denote the forecasted water consumption at junction j as d_j . We assume the water consumption within the time step is constant, non-negative, and there is no storage at the junction. The flow continuity constraint is

$$\sum_{e \in \mathcal{E}} a_{je} x_e = d_j \quad \forall j \in \mathcal{J}, \quad (3.3)$$

which ensures that the water consumed at junction j must equal the sum of the volumetric flow rate x_e in the pipes entering and exiting that junction. The parameter a_{je} is an element in the node-edge incidence matrix A which describes the connections in $(\mathcal{N}, \mathcal{E})$. Row j corresponds to node $j \in \mathcal{N}$ and column e corresponds to pipe $e \in \mathcal{E}$. Within this matrix, 1 or -1 at (j, e) designates that node j is the receiving or sending end of pipe e , respectively. The remaining entries are 0.

Edges, \mathcal{E}

The head loss along a pipe is equal to the head difference between the sending and receiving node

$$\sum_{j \in \mathcal{N}} a_{je} H_j = \begin{cases} \hat{H}_e - m_e (x_e)^2 & \forall e \in \mathcal{P}, \\ -L_e & \forall e \in \mathcal{V}, \\ -k_e (x_e)^{1.852} & \forall e \in \mathcal{E} \setminus (\mathcal{P} \cup \mathcal{V}), \end{cases} \quad (3.4)$$

where \hat{H}_e and m_e are pump curve coefficients, and k_e is a resistance coefficient. The first case corresponds to pipes with pumps, the second to pipes with valves, and the third to the remaining pipes. For pipes with pressure reducing valves, the head loss $L_e \geq 0$ is a decision variable. The pipe flow is nonnegative and the pump flow is bounded

$$x_e^{\min} \leq x_e \leq x_e^{\max} \quad \forall e \in \mathcal{P}. \quad (3.5)$$

3.4.2. Power Constraints

The real and reactive power consumed at each bus are

$$P_{L,k} = \begin{cases} \rho_k + p_e, & \text{pump } e \text{ connected to bus } k \\ \rho_k, & \text{otherwise} \end{cases}, \quad (3.6)$$

$$Q_{L,k} = \begin{cases} \zeta_k + q_e, & \text{pump } e \text{ connected to bus } k \\ \zeta_k, & \text{otherwise} \end{cases}, \quad (3.7)$$

$\forall k \in \mathcal{K}$, where ρ_k and ζ_k are the real and reactive power demand of consumers connected to bus k , and p_e and q_e are the real and reactive power demand of pump e . While pumps are best modeled as motor loads, for simplicity, we assume that the pumps are constant power loads with a constant ratio of real to reactive power μ_e . To model the power flows, we use the branch flow model [7]

$$\sum_{n \in \mathcal{I}_{k+1}} P_n = P_k - r_k \frac{P_k^2 + Q_k^2}{V_k^2} - P_{L,k+1}, \quad (3.8)$$

$$\sum_{n \in \mathcal{I}_{k+1}} Q_n = Q_k - x_k \frac{P_k^2 + Q_k^2}{V_k^2} - Q_{L,k+1}, \quad (3.9)$$

$$V_{k+1}^2 = V_k^2 - 2(r_k P_k + x_k Q_k) + (r_k^2 + x_k^2) \frac{P_k^2 + Q_k^2}{V_k^2}, \quad (3.10)$$

$\forall k \in \mathcal{K}$, where P_k and Q_k are the real and reactive power flow downstream of bus k , r_k and x_k are the resistance and reactance of the line downstream of bus k , and V_k is the voltage at bus k . The set \mathcal{I}_{k+1} consists of all lines downstream of and directly connected to bus $k+1$. The voltage at the feeder head is regulated to V_{set} and the remaining voltages are constrained

$$V_k^{\min} \leq V_k \leq V_k^{\max} \quad \forall k \in \mathcal{K}. \quad (3.11)$$

We could also bound the apparent power flows but in practice PDNs usually hit their voltage limits first.

3.4.3. Objective

Our objective is to minimize the scheduled energy costs of pumping water over all pumps in the WDN, i.e.,

$$\min_{\mathbf{x}} \sum_{e \in \mathcal{P}} \pi_e p_e \Delta T, \quad (3.12)$$

where π_e is the price of energy for pump e . The decision variable \mathbf{x} includes x_e , H_j , L_e , P_k , Q_k , and V_k . The scheduled power consumption is a function of the flow rate x_e and head gain in the pump, which can be approximated by a quadratic function of x_e . For a fixed speed pump

$$p_e = \beta \left(\hat{H}_e - m_e (x_e)^2 \right) x_e \quad \forall e \in \mathcal{P}, \quad (3.13)$$

where β is a constant. This equation is modified from the pump power consumption equation in [130], which uses variable speed pumps. The objective function is a cubic function of the flow.

3.4.4. Chance Constraints

We next consider uncertainty in water demand. We define \tilde{d}_j as the water demand forecast error at junction j . We minimize the expected energy cost of pumping and since we assume the forecasts are unbiased, the objective function is equivalent to that in the deterministic case. The decision variable is expanded to $\mathbf{x} = \{c_e, x_e, H_j, L_e, P_k, Q_k, V_k\}$, where c_e is the control policy parameter of pump e . We assume an affine control policy that compensates for water demand forecast error by varying the output of supply pumps (i.e., pumps drawing from reservoirs not in-line booster pumps that increase pressure head)

$$\tilde{x}_e = c_e \sum_{j \in \mathcal{J}} \tilde{d}_j \quad \forall e \in \mathcal{P}, \quad (3.14)$$

$$\sum_{e \in \mathcal{P}} c_e = 1, \quad (3.15)$$

where \tilde{x}_e is the real-time deviation of water flows in pipes with pumps from the scheduled flow. In (3.14), the total water demand deviation is multiplied by the control policy parameters to determine how the pumps should adjust in order to compensate the forecast error. In (3.15), the control policy parameters sum to one so that the changes in pumping operation fully compensate the water demand forecast error.

Using tilde ($\tilde{\cdot}$) to refer to deviations in variables resulting from the real-time control of pumps compensating water demand forecast error, we can write the stochastic counterparts of the deterministic constraints. For example, (3.1) becomes

$$h_j^{\min} + \bar{h}_j \leq H_j + \tilde{H}_j \leq h_j^{\max} + \bar{h}_j \quad \forall j \in \mathcal{N}.$$

The stochastic inequality constraints can be written as $f(\mathbf{x}, \tilde{d}) \leq 0$ and transformed into a chance constraint

$$\mathbb{P}(f(\mathbf{x}, \tilde{d}) \leq 0) \geq 1 - \epsilon \quad (3.16)$$

where the constraints must hold jointly with a probability of $1 - \epsilon$, where ϵ is the user-selected violation level. The resulting problem cannot be directly solved. Possible solution approaches include i) assuming specific uncertainty distributions, allowing the chance constraints to hold individually rather than jointly, and reformulating into an equivalent deterministic problem; ii) distributionally robust optimization; and iii) scenario-based approaches. However, since our problem includes nonlinear and nonconvex constraints, existing methods for i) and ii) do not work. Therefore, we resort to iii).

3.4.5. Scenario Approach

We use the scenario approach [17] to solve our chance-constrained optimization problem. For convex problems, [17] gives a requirement for the number of randomly-selected scenarios N for which the stochastic constraints must hold to ensure feasibility at the chosen violation level [17]

$$N \geq \frac{2}{\epsilon} \left(\ln \frac{1}{\psi} + \delta \right), \quad (3.17)$$

where δ is the number of optimization variables and ψ is a user-selected confidence level. For example, for the case study presented in Section 3.5, a violation level of $\epsilon = 0.05$ and a confidence level of $\psi = 10^{-5}$ requires $N = 4,621$ scenarios. If the violation level is reduced to $\epsilon = 0.02$, the number of instances needed is $N = 11,552$. Since our problem is nonconvex, we apply the scenario approach heuristically; the guarantees derived in [17] no longer apply. Moreover, we test the approach with a varying number of scenarios with the goal of gaining insight into the performance and drawbacks of the method. In following chapters, we convexify the integrated power-water problem in order to apply the scenario approach with performance guarantees (Chapters 5 and 6) and plan to explore applying scenario-based approaches tailored to nonconvex problems, e.g., [41] (Chapter 7).

Table 3.1: Pump Parameters

Pump	\hat{H}_e (m)	m_e (h^2m^{-5})	x_e^{\min} (CMH)	x_e^{\max} (CMH)
1	100.5	0.0004	25	325
2	100.0	0.0001	50	700

3.5. Case Study

3.5.1. Set Up

We use a modified version of the WDN presented in [21]; the topology is shown in Fig. 3.1. Ref. [130] also uses this network but makes different modifications than we do. Specifically, we model the pumps in the pumping station as a single pump with equivalent head and flow, we do not model the booster pump, and we model pressure reducing valves (using the model from [130]) instead of control valves. The WDN consists of 2 reservoirs, 8 junctions, and 11 pipes with 2 fixed speed pumps and 2 pressure reducing valves. The consumer water demand and $k_e \forall e \in \mathcal{E} \setminus (\mathcal{P} \cup \mathcal{V})$ are from [21]. The nodal elevation, minimum pressure head, and pressure reducing valve placements are from [130]. Since we do not model the booster pump nor add a surface tank, we changed the elevations at junctions 4, 5, and 6 (to 0, 20, and 40 m, respectively) and the minimum pressure head at junction 6 (to 10 m). Pump parameters are shown in Table 3.1. We set $\beta = 6.97 \times 10^{-6}$ kg/CMH · m. The forecasted total water demand is 420 cubic meters per hour (CMH).

For the PDN, we use the topology of the IEEE 13-node feeder, shown in Fig. 3.1 [52]. Pumps 1 and 2 are connected to buses 8 and 4, respectively. The load at each bus is set to the average over the 3 phases. The distributed load along the line from bus 1 to 6 is placed at bus 1. The line impedance is calculated from the line lengths and the impedance of the first phase listed in the feeder specification sheet. The switch and transformer are each replaced with a line that has the same impedance as the other segment on the same lateral. The shunt admittance and shunt capacitors are neglected. We explore three consumer power demand levels: 105%, 108%, and 110% of the nominal load at all buses. We set the price of electricity to $\pi_e = \$100/\text{MWh} \forall e \in \mathcal{P}$, and the line to neutral voltage at the feeder head to $V_{\text{set}} = 4.16$ kV. The voltage limits are $V_k^{\min} = 0.95$ pu and $V_k^{\max} = 1.05$ pu $\forall k \in \mathcal{K}$. The ratio of real to reactive power consumed by the pumps is $\mu_e = 3 \forall e \in \mathcal{P}$.

We use a Gaussian probability density function to randomly generate water demand forecast error with mean 0 and standard deviation $0.10d_j \forall j \in \mathcal{J}$. The distribution is truncated

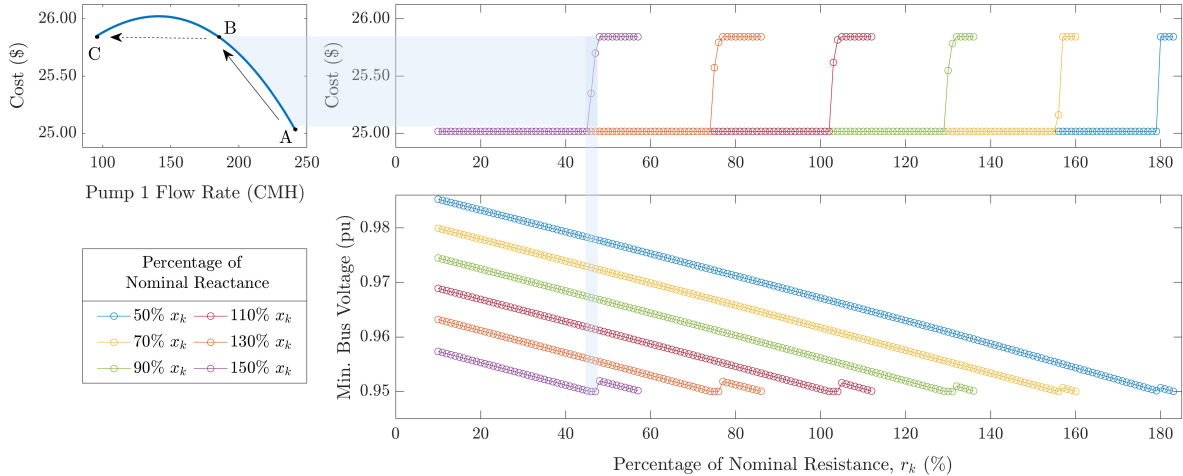


Figure 3.2: Impact of distribution line parameters on pumping costs. (Top left) Pumping cost as a function of pump 1’s flow rate and (Top right) as a percentage of the nominal line resistance and reactance. (Bottom right) Minimum bus voltage as a function of the percentage of the nominal line resistance and reactance.

and scaled using an acceptance/rejection approach [14] such that only points within three standard deviations of the mean are included. We assume the errors at each junction are independent. We explore cases with $N = 10, 50, 100$, and 1000 scenarios. For cases $N = 10$ and 50 we solved each case 100 times and for cases $N = 100$ and 1000 we solved each case 10 times, and report the average results. Cases with fewer scenarios exhibit higher variability in results, requiring a larger number of solution instances to obtain reliable averages. The solver was unable to find a feasible solution in one instance for the 110% consumer power demand level and $N = 1000$ case. We generated another instance so that we could compute the average across 10 instances, but recognize that, if this occurred in a real system with real uncertainty scenarios, this could be problematic.

We solve the problem using the optimization package JuMP in Julia with Ipopt [127]. Since the problem is nonconvex and the solver can only guarantee a local minimum, we solve each problem 40 times using different initial guesses for the decision variables and chose the solution with the lowest cost.

3.5.2. Impact of Power Network Parameters On Pumping

We first analyzed the impact of PDN line parameters on the deterministic solution. The objective function is a concave function of the pumps’ flow rates. The top left plot of Fig. 3.2

shows total pumping costs as a function of pump 1's flow rate. When the voltage constraints are not active, pump 1's optimal flow rate is at point A. As the line impedances increase, the voltages drop, approaching their lower limits. In the right two plots, we vary the line resistances r_k and reactances x_k as a percentage of their nominal values. The total pumping costs are shown in the top plot and the minimum bus voltages are shown in the bottom plot. Bus 8 always has the lowest voltage in the network. As the line resistance increases, the voltage at bus 8 gets closer to its lower limit of 0.95 pu. Once the voltage constraint becomes active, pump 1 must decrease its power consumption/flow rate to maintain the minimum bus voltage at 0.95 pu (i.e., move from point A toward point B), which increases pumping costs. This transition is shown by the light blue shaded area connecting the three plots. When pump 1 reaches point B, there is a second flow rate, i.e., point C, that yields the same total pumping cost. The minimum bus voltage increases when pump 1 switches to point C. The optimal flow rate for pump 1 remains at point C as the impedance continues to increase until the problem becomes infeasible. Note that when the PDN constraints become active and pumping is shifted from point A to point C, there is a 60% decrease in pump 1's flow rate. Pump 1 reduces its power consumption by 67.44 kW (51.23% power reduction).

All of the reactance curves in Fig. 3.2 exhibit the same behavior. Pump 1 moves from point A to point B when voltage constraints are active and resistances are increased, and then to point C when there is an equivalent cost. For higher reactance values, the solution will switch to point C for smaller resistance values (effectively shifting the curve left).

The effect of the consumer power demand level on the pump flow rates is shown in Fig. 3.3. The curves show pump 1's maximum flow rate as a function of pump 2's flow rate for different consumer power demand levels. Pump 1's maximum flow rate is constrained by PDN voltage constraints. The gray line shows all possible combinations of flow rates that meet the total forecasted water demand. The line is darkened for flow rates that satisfy the pump flow rate bounds (3.5). For the deterministic problem, the scheduled flow rates must fall on this darkened line. When pump 1's maximum flow rate is above this line there are feasible solutions; however, they become more limited as consumer power demand increases. For example, when the consumer power demand level is 115%, pump 1's maximum flow rate (red) is below the gray line for all pump 2 flow rates and so there is no feasible solution.

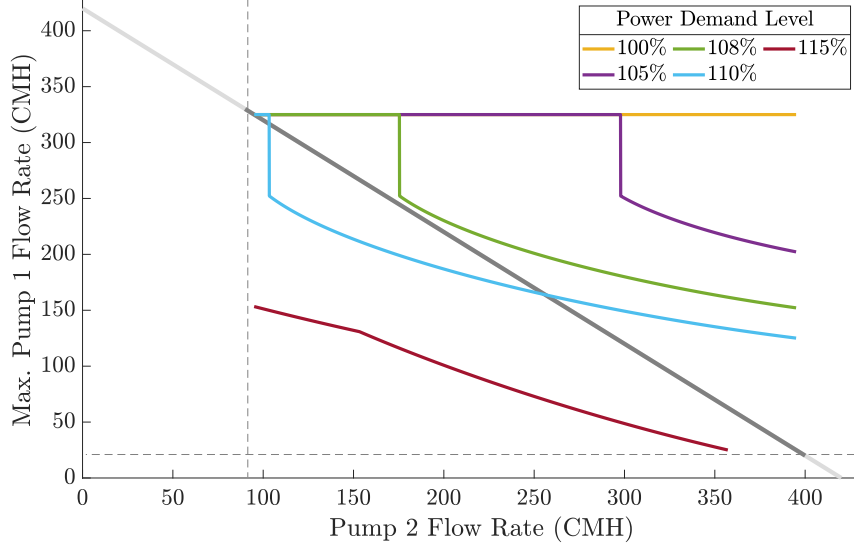


Figure 3.3: Pump 1’s maximum flow rate as a function of pump 2’s flow rate for different consumer power demand levels.

3.5.3. Control Policy Parameters

We next solved the chance-constrained optimization problem for each case and consumer power demand level. The time to solve the problem ranged from less than a second when $N = 10$ to around a minute when $N = 1000$. We report average control policy parameters for pump 1 in Table 3.2. In this formulation, a pump’s control policy parameter is equivalent to the percentage of the total real-time water demand deviation that the pump is responsible for offsetting. As the consumer power demand increases the set of feasible operating points reduces (as seen in Fig. 3.3), forcing pump 1 to point C. However, at point C pump 1 has more flexibility to respond to water demand forecast error than when it is at point A. Therefore, its control policy parameter increases to 46%. For $N = 1000$ we find that, usually, at least one scenario requires pump 1 to operate at point C and so pump 1’s control policy parameter is approximately 46%. We see more variation across solution instances as N and consumer power demand decreases. For $N < 1000$, pump 1’s average control policy parameter increases with increasing power demand. We do not observe a clear upwards or downwards trend in pump 1’s average control policy parameter as N increases.

Table 3.2: Pump 1's Average Control Policy Parameter (%)

Power Demand (%)	$N = 10$	$N = 50$	$N = 100$	$N = 1000$
105	28.9	27.7	25.3	46.2
108	44.9	31.9	37.0	46.2
110	46.2	46.2	46.2	46.1

Table 3.3: Violation Probability (%), Mean μ and Standard Deviation σ

Power Demand (%)	$N = 10$		$N = 50$		$N = 100$		$N = 1000$	
	μ	σ	μ	σ	μ	σ	μ	σ
105	8.40	9.83	3.85	3.81	1.86	1.06	1.32	0.13
108	2.27	6.49	1.47	1.19	1.19	0.36	1.11	0.07
110	1.52	3.55	1.17	0.11	1.20	0.12	1.14	0.13

3.5.4. Feasibility Range

In order to evaluate the solutions obtained for each case and consumer power demand level, we tested the solutions using 10,000 new sets of randomly generated water demands for all junctions. Specifically, for each solution instance and set of randomly generated water demands, we determined if the pumping schedule and real-time pump adjustments computed from the control policy parameters would lead to water and power flows that satisfy the WDN and PDN constraints. Table 3.3 shows the average and the sample standard deviation of the violation probabilities. As expected, the empirical violation probability generally decreases as N increases. We observe a slight increase in violation probability despite an increase in scenarios from $N = 50$ to 100 for the 110% consumer power demand level; however, this is due the specific scenarios drawn in those cases. Averaging more solution instances would likely eliminate this issue.

We observe that the heuristically-applied scenario approach is effective solving our problem and finding schedules and control policy parameters that lead to feasible solutions despite water demand forecast error. Empirically, we find that only $N = 100$ scenarios are needed to consistently achieve violation probabilities less than 5% for all consumer power demand levels. This is significantly less than the $N = 4,621$ scenarios computed with (3.17). Similarly, only $N = 1000$ scenarios are needed to consistently achieve violation probabilities less than 2%, as compared to $N = 11,552$ scenarios computed with (3.17). We also find that the violation probability varies with the consumer power demand level, where solutions com-

puted for higher power demands generally have lower violation probabilities. We note that our results are not generalizable to other coupled power and water distribution networks; however, this preliminary investigation shows that our approach is worth testing on realistic networks. We discuss the scalability of the scenario approach to larger networks and time horizons in Chapter 6.

3.6. Chapter Conclusion

We explored the performance of a heuristic scenario-based approach on a nonconvex chance-constrained optimal water pumping problem including water and power network constraints and water demand forecast error. By including power distribution network constraints in the problem, we can ensure that water pumping does not exacerbate voltage issues in power distribution networks. We computed both the optimal pumping schedule and the parameters of an affine control policy that would be used to modify pumping to respond to water demand forecast errors in real time. We found that the approach can achieve low chance constraint violation probabilities with a relatively small number of scenarios. However, we noted several challenges, namely that finding a solution requires reinitializing the nonlinear solver multiple times and no guarantee that the solution is the global minimum. Moreover, the approach confers no probabilistic guarantees when applied to a nonconvex problem. To address this, the subsequent chapters examine relaxation/approximation techniques when modeling the water and power networks to make the problem more computationally tractable. We also use solution approaches that guarantee a user-specified performance.

Chapter 4.

Incorporating Power Demand Uncertainty Sources in a Chance-Constrained Water Distribution Network Voltage Support Problem

In this chapter, we take into consideration power demand uncertainty. We improve the water distribution network (WDN) and power distribution network (PDN) model used and solve for the chance-constrained voltage support problem. The solution approach uses a scenario-based approach that provides performance guarantees for convex programs. Approximation and relaxation techniques are used to convexify the WDN and PDN constraints. This chapter is based on [114].

4.1. Notation

Sets

\mathcal{E}	Set of pipes in the WDN (indexed by e)
\mathcal{I}_k	Set of buses directly downstream of bus k in PDN (indexed by k)
\mathcal{J}	Set of junctions within the set of nodes in the WDN (indexed by j)
\mathcal{K}	Set of buses in the PDN (indexed by k)
\mathcal{N}	Set of nodes in the WDN (indexed by j)

\mathcal{P}	Set of pumps within the set of pipes in the WDN (indexed by e)
\mathcal{R}	Set of reservoir nodes within the set of nodes in the WDN (indexed by j)
\mathcal{S}	Set of storage tanks within the set of nodes in the WDN (indexed by j)
\mathcal{T}	Set of time steps in the scheduling problem (indexed by t)
\mathcal{V}	Set of valves within the set of pipes in the WDN (indexed by e)
Φ	Set of phases in the PDN (indexed by ϕ)

Decision Variables

C_e^t	Power control policy row vector for pump e at time t (-)
H_j^t	Hydraulic head at node j at time t (m)
$H_{j,\text{out}}^t$	Tank outlet hydraulic head for tank j at time t (m)
\hat{H}_e^t	Head loss of pipe e at time t (m)
L_e^t	Head loss in pressure reducing valve e at time t (m)
$p_{e,\phi}^t$	Real power demand of pump e at phase ϕ and time t (kW)
\mathbf{P}_k^t	Real power flow vector (all phases) entering bus k at time t (kW)
$P_{L,k,\phi}^t$	Real power consumed at bus k , phase ϕ at time t (kW)
$q_{e,\phi}^t$	Reactive power demand of pump e at phase ϕ and time t (kVAr)
\mathbf{Q}_k^t	Reactive power flow vector (all phases) entering bus k at time t (kVAr)
$Q_{L,k,\phi}^t$	Reactive power consumed at bus k , phase ϕ at time t (kVAr)
x_e^t	Volumetric flow rate in pipe $e : g \rightarrow h$ (from node g to h) at time t (CMH)
\mathbf{Y}_k^t	Voltage magnitude squared vector for all phases at bus k at time t (kV 2)

Functions

$f(\mathbf{x}, \tilde{\rho})$	Constraints in chance-constraint with decision variables \mathbf{x} and uncertainty $\tilde{\rho}$
$F^t(\cdot)$	Scheduled WDN operation cost at time t given decision variables
$\hat{Y}_{k,\phi}^t(\cdot)$	Voltage magnitude squared at bus k , phase ϕ , and time t given power demand

Random Variables

\tilde{s}^t	Binary variable indicating voltage limit violation occurrence (-)
$\tilde{\rho}_{k,\phi}^t$	Deviation in real power demand at bus k , phase ϕ , and time t (kW)

Parameters

a_{je}	Element in incidence matrix of nodes \times pipes (-)
b_e^1, b_e^0	Coefficients in upper bound for pipe headloss convex hull for pipe e (h/m 2 , m)
d_j^t	Forecasted water demand of consumer j at time t (CMH)
f_e^1, f_e^0	Convex hull upper bound coefficients for pump e 's power (m, h/m 4)
g	Power control policy weighting coefficient

\bar{h}_j	Elevation head of node j (m)
h_j^{\min}	Minimum pressure head for node j (m)
h_j^{\max}	Maximum pressure head for node j (m)
k_e	Resistance coefficient of pipe e (h^2/m^5)
\mathbf{M}_{kn}	Parameter matrix formed from impedances for line kn (Ohms)
M	Big-M coefficient (-)
m_e^1, m_e^0	Pump hydraulic function parameters for pump e ($\text{h}/\text{m}^2, \text{m}$)
N	Number of scenarios required (-)
\mathbf{N}_{kn}	Parameter matrix formed from impedances for line kn (Ohms)
V_k^{\min}	Minimum voltage limit at bus k (kV)
V_k^{\max}	Maximum voltage limit at bus k (kV)
V_{set}	Voltage at feeder head (kV)
x_e^{\max}	Maximum flow rate of pump e (CMH)
x_e^{\min}	Minimum flow rate of pump e (CMH)
β	Constant in pump power consumption equation ($\text{kW}/\text{CMH} \cdot \text{m}$)
ΔT	Length of time period (h)
δ	Number of decision variables in the optimization problem (-)
γ_j	Cross-sectional area of tank j (m^2)
ϵ	User-selected violation level (%)
μ_e	Ratio between real and reactive power of pump e (-)
π_e^t	Forecasted energy price at time t for pump e (\$/kWh)
ψ	User-selected confidence level (%)
$\rho_{k,\phi}^t$	Forecasted real power demand at bus k , phase ϕ at time t (kW)
$\zeta_{k,\phi}^t$	Forecasted reactive power demand at bus k , phase ϕ at time t (kVAr)

4.2. Chapter Introduction

The goal of this chapter is to develop an approach to schedule WDN operation given WDN and PDN constraints subject to power demand uncertainty at buses with loads. To ensure that PDN voltage constraints are satisfied in the presence of uncertainty, we formulate the problem as a chance-constrained optimization problem and develop a real-time control policy that adjusts the water supply pumps' flow rates (and consequently power consumption) from the scheduled operation as a function of forecast error when voltage violations happen. The optimization problem determines both the WDN schedule and the control policy parameters.

In chapter 3, we formulated a chance-constrained water pumping problem considering water demand uncertainty. In contrast, here, we consider power demand uncertainty, leading to a substantially different formulation. Moreover, we improve the formulation to include storage tanks, PDN unbalance, and multiple time periods. Importantly, the control policy in Chapter 3 and related work [95, 124] ensures supply and demand are balanced, whereas here the control policy determines corrective control actions that prevent constraint violations.

The contributions of this chapter are the 1) design of a corrective control policy that responds to voltage constraint violations in real time, 2) formulation of a chance-constrained optimization problem to choose a pumping schedule and control policy parameters considering power demand uncertainty, 3) reformulation of the problem into a chance-constrained convex quadratically constrained program using relaxations and approximations, 4) application of the scenario approach to solve the problem, and 5) assessment of the approach's performance through case studies.

4.3. Problem Description

We consider a coupled WDN and PDN where the water pumps are loads on the PDN. See Fig. 4.1 for an example, which will be used in our case studies. In this section, we first describe how the pumps are scheduled and controlled to satisfy network constraints. Then, we detail the WDN and PDN models and apply relaxations to make the problem convex. We introduce uncertainty and develop the control policy used to modify pump operation in real time. Last, we formulate the chance-constrained optimization problem.

4.3.1. Schedule and Real-time Control of WDN Pumps

We solve for the WDN operational schedule (i.e., pump flow rates and tank levels) over a scheduling horizon subject to WDN and PDN constraints. We ensure that the network constraints are satisfied for the WDN's scheduled operation given forecasted water and power demands. The scheduling horizon is a set of discrete periods $t \in \mathcal{T}$ of duration ΔT .

Since the consumer power demand is uncertain, some forecast errors may cause PDN constraint violations when the WDN is operated as scheduled. To address this, we develop a control policy that adjusts the water supply pumps given power demand forecast errors. Not all power demand forecast errors require corrective action by the water pumps. In those cases, the pumps maintain their schedule. We assume that the WDN operator has

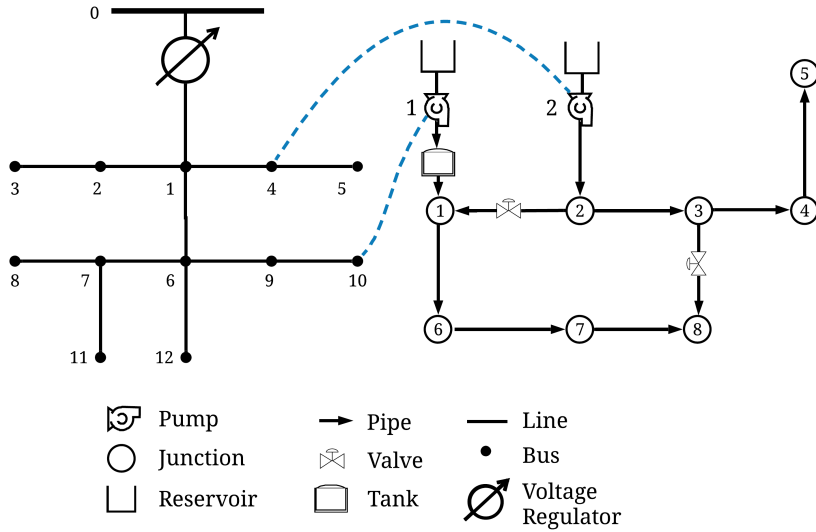


Figure 4.1: Power (left) and water (right) distribution networks. The dashed lines show where the supply pumps are connected in the PDN.

full knowledge of the PDN and the WDN operator determines when to use the control policy based on the realized power demand forecast error at each bus and phase. Although this assumption may be impractical due to the present lack of communication systems and information sharing between WDNs and PDNs, this work provides us insights into the best possible solution without considering these challenges. Section 4.3.6 develops the control policy and Section 4.4 describes how we jointly optimize the schedule and control policy parameters.

4.3.2. Power Distribution Network Model

We consider an unbalanced, radial PDN that includes a set of buses \mathcal{K} to which consumers and water pumps are connected. We use the 3-phase, linearized, unbalanced model presented in [3]; however, other convex formulations could be used, such as [34]. In [3], the authors neglect the loss terms and assume that the voltage unbalance at each bus is small. Let $\Phi = \{a, b, c\}$ denote the three phases of the network. The linearized power flow model is [3]

$$\mathbf{Y}_k^t = \mathbf{Y}_n^t - \mathbf{M}_{kn} \mathbf{P}_n^t - \mathbf{N}_{kn} \mathbf{Q}_n^t \quad \forall k \in \mathcal{K}, t \in \mathcal{T}, \quad (4.1)$$

$$\mathbf{P}_k^t = \mathbf{P}_{L,k}^t + \sum_{n \in \mathcal{I}_k} \mathbf{P}_n^t \quad \forall k \in \mathcal{K}, t \in \mathcal{T}, \quad (4.2)$$

$$\mathbf{Q}_k^t = \mathbf{Q}_{L,k}^t + \sum_{n \in \mathcal{I}_k} \mathbf{Q}_n^t \quad \forall k \in \mathcal{K}, t \in \mathcal{T}, \quad (4.3)$$

where $\mathbf{Y}_k^t := [Y_{k,\phi}^t]_{\phi \in \Phi}$ is a 3×1 vector of squared voltage magnitudes at bus k . Similarly, \mathbf{P}_k^t and \mathbf{Q}_k^t are 3×1 vectors of the real and reactive power flow entering bus k . The matrices \mathbf{M}_{kn} and \mathbf{N}_{kn} are formed from the line impedance matrices. The set \mathcal{I}_k contains all buses that are directly downstream of bus k . The variables $\mathbf{P}_{L,k}^t := [P_{L,k,\phi}^t]_{\phi \in \Phi}$ and $\mathbf{Q}_{L,k}^t := [Q_{L,k,\phi}^t]_{\phi \in \Phi}$ are 3×1 vectors of the power demand at bus k , where the real and reactive power consumed at each phase is

$$P_{L,k,\phi}^t = \begin{cases} \rho_{k,\phi}^t + p_{e,\phi}^t, & \text{if pump } e \text{ connected to bus } k \\ \rho_{k,\phi}^t, & \text{otherwise} \end{cases}, \quad (4.4)$$

$$Q_{L,k,\phi}^t = \begin{cases} \zeta_{k,\phi}^t + q_{e,\phi}^t, & \text{if pump } e \text{ connected to bus } k \\ \zeta_{k,\phi}^t, & \text{otherwise} \end{cases}, \quad (4.5)$$

$\forall k \in \mathcal{K}, \phi \in \Phi, t \in \mathcal{T}$, where $\rho_{k,\phi}^t$ and $\zeta_{k,\phi}^t$ are the forecasted real and reactive net load, i.e., actual load minus distributed generation (which we assume is uncontrollable), at bus k and phase ϕ . The variables $p_{e,\phi}^t$ and $q_{e,\phi}^t$ are the real and reactive power demands of pump e on phase ϕ . We model the pumps as balanced three-phase constant power loads with real-to-reactive power ratios of μ_e .

The bus voltages are constrained

$$(V_k^{\min})^2 \leq Y_{k,\phi}^t \leq (V_k^{\max})^2 \quad \forall k \in \mathcal{K}, \phi \in \Phi, t \in \mathcal{T}, \quad (4.6)$$

where V_k^{\min} and V_k^{\max} are the lower and upper voltage limits at bus k . The voltage at the feeder head is regulated to V_{set} . We could also include apparent power flow constraints on the lines; however, since a voltage limit violation is more likely to occur first, we neglect them.

4.3.3. Water Distribution Network Model

We consider an urban water distribution network. We assume the pipes' water flow does not change direction over the scheduling horizon. This assumption eliminates the need for binary variables when modeling pipes without pumps or valves. It is frequently used in the literature, e.g, in [31, 32, 130]. Note that pumps and valves only allow unidirectional water

flow. As a result, we can represent the WDN as a directed graph $(\mathcal{N}, \mathcal{E})$ composed of a set of nodes \mathcal{N} and a set of edges \mathcal{E} . Each node can be described as a junction $j \in \mathcal{J}$, reservoir $j \in \mathcal{R}$, or elevated storage tank $j \in \mathcal{S}$, i.e., $\mathcal{N} = \mathcal{J} \cup \mathcal{R} \cup \mathcal{S}$. The edges are pipes that connect nodes. A pipe may include a pump or a valve, $(\mathcal{P} \cup \mathcal{V}) \subseteq \mathcal{E}$. We assume a pump's on/off status is determined in advance of the scheduling problem. The WDN is described by the hydraulic head H_j^t at node j and the volumetric flow rate x_e^t through pipe e . Most urban WDNs are capable of operational control through their SCADA system [28]. We use the same hydraulic constraints as we did in Chapter 3 with several modifications: we include water storage tanks, we add time indexing so we can formulate a multiperiod problem, we approximate the pump characteristic curve with a linear function, and we use the Darcy-Weisbach method instead of the Hazen-Williams method to model the pipe head loss. The last two modifications allow us transform the optimization problem into a convex program.

Nodes, \mathcal{N}

The hydraulic head H_j^t is composed of the pressure head and the elevation \bar{h}_j . The node constraints are

$$h_j^{\min} + \bar{h}_j \leq H_j^t \leq h_j^{\max} + \bar{h}_j \quad \forall j \in \mathcal{N}, t \in \mathcal{T}, \quad (4.7)$$

$$H_j^t = \bar{h}_j \quad \forall j \in \mathcal{R}, t \in \mathcal{T}, \quad (4.8)$$

$$\sum_{e \in \mathcal{E}} a_{je} x_e^t = d_j^t \quad \forall j \in \mathcal{J}, t \in \mathcal{T}, \quad (4.9)$$

$$H_{j,\text{out}}^t = H_{j,\text{out}}^{t-1} + \frac{\Delta T}{\gamma_j} \sum_{e \in \mathcal{E}} -a_{je} x_e^t \quad \forall j \in \mathcal{S}, t \in \mathcal{T}, \quad (4.10)$$

where h_j^{\min} and h_j^{\max} are the minimum and maximum pressure heads at node j , d_j^t is the water consumption at junction j , a_{je} is an element in the node-edge incidence matrix describing the connection of nodes and pipes in the network, and γ_j is the cross-sectional area of tank j . In (4.7), the hydraulic head at each node is bounded.

Reservoirs \mathcal{R} are treated as an infinite source of water with a fixed pressure head. Therefore in (4.8), without loss of generality, the hydraulic head is set equal to the elevation head.

For junctions \mathcal{J} , (4.9) enforces that the sum of water flow rates entering and exiting a junction must equal the water consumption d_j^t at that junction.

For tanks \mathcal{S} , we use the same formulation as [31]. We model the hydraulic head going into and out of the tank, H_j^t and $H_{j,\text{out}}^t$, respectively, and assume the inlet of the water tank is

located at the top of the tank. In (4.10), the hydraulic head at the tank outlet is calculated from the hydraulic head at the previous time period and the net inflow of the tank. To ensure that the tanks are not simply depleted at the end of the scheduling horizon, we constrain the final tank outlet head to be greater than or equal to the initial tank outlet head (i.e., $H_{j,\text{out}}^{t=|\mathcal{T}|} \geq H_{j,\text{out}}^{t=0}$). Similar to (4.7), the tank outlet head is physically bounded by the height and elevation of the tank.

Pipes, \mathcal{E}

The difference in head between the sending and receiving node, $\hat{H}_e^t = -\sum_{j \in \mathcal{N}} a_{je} H_j^t$, is equal to the pipe's head loss

$$\hat{H}_e^t = \begin{cases} - (m_e^0 + m_e^1 x_e^t) & \forall e \in \mathcal{P}, \\ L_e^t & \forall e \in \mathcal{V}, \end{cases} \quad (4.11a)$$

$$\hat{H}_e^t = \begin{cases} k_e (x_e^t)^2 & \forall e \in \mathcal{E} \setminus (\mathcal{P} \cup \mathcal{V}), \end{cases} \quad (4.11b)$$

$$\forall t \in \mathcal{T}, \text{ where } m_e^0 \text{ and } m_e^1 \text{ are pump curve coefficients, and } k_e \text{ is the resistance coefficient.}$$

The first case corresponds to pipes containing a fixed speed pump, the second to pipes containing a pressure reducing valve, and the third case to pipes without a pump or valve. For pipes with pressure reducing valves, the head loss $L_e^t \geq 0$ is a decision variable. While pumps are traditionally modeled with a quadratic pump characteristic curve, we neglect the quadratic term since its contribution is usually very small compared to the linear term [61]. The power consumption of a pump is a function of the head gain and flow rate. The pumps' flow rates are bounded and nonnegative

$$p_{e,\phi}^t = -\beta \hat{H}_e^t x_e^t \quad \forall e \in \mathcal{P}, \phi \in \Phi, t \in \mathcal{T}, \quad (4.12)$$

$$x_e^{\min} \leq x_e^t \leq x_e^{\max} \quad \forall e \in \mathcal{P}, t \in \mathcal{T}, \quad (4.13)$$

where x_e^{\min} and x_e^{\max} are pump e 's flow rate limits, and β is a constant. Note that $p_{e,\phi}^t$ is a quadratic function of the pump's flow rate. The control policy described in Section 4.3.6 adjusts supply pumps drawing from reservoirs not in-line booster pumps that increase pressure head. To ensure that water supply meets water demand, our control policy formulation only applies to pumps bringing water into the network.

4.3.4. Deterministic Problem

The deterministic problem minimizes the pumps' electricity cost given the forecasted power demand subject to WDN and PDN constraints

$$\begin{aligned} \min_{\mathbf{x}} \quad & \sum_{t \in \mathcal{T}} F^t(\mathbf{x}) \\ \text{s.t.} \quad & (4.1) - (4.13), \end{aligned} \tag{D}$$

where the decision variables are $\mathbf{x} = \{x_e^t, H_j^t, H_{j,\text{out}}^t, L_e^t, \mathbf{Y}_k^t, \mathbf{P}_k^t, \mathbf{Q}_k^t, p_{e,\phi}^t\}$. The electricity consumption cost associated with the pump schedule at time t is

$$F^t(\mathbf{x}) := \sum_{e \in \mathcal{P}} \left(\pi_e^t \Delta T \sum_{\phi \in \Phi} p_{e,\phi}^t \right)$$

where π_e^t is the price of electricity at pump e and time t . We assume that the WDN is a price taker, i.e., the WDN's power consumption has no impact on electricity prices.

4.3.5. Convex Relaxations

The WDN constraints are nonconvex due to the pipe head loss (4.11c) and the pump power consumption (4.12). Nonconvex problems are difficult to solve and so we use a convex relaxation, specifically, we take the convex hull of both quadratic constraints [61]. Equations (4.11c) and (4.12) become

$$\hat{H}_e^t \geq k_e (x_e^t)^2 \quad \forall e \in \mathcal{E} \setminus (\mathcal{P} \cup \mathcal{V}), t \in \mathcal{T}, \tag{4.14a}$$

$$\hat{H}_e^t \leq b_e^0 + b_e^1 x_e^t \quad \forall e \in \mathcal{E} \setminus (\mathcal{P} \cup \mathcal{V}), t \in \mathcal{T}, \tag{4.14b}$$

$$p_{e,\phi}^t \geq -\beta \hat{H}_e^t x_e^t \quad \forall e \in \mathcal{P}, \phi \in \Phi, t \in \mathcal{T}, \tag{4.14c}$$

$$p_{e,\phi}^t \leq -\beta (f_e^0 + f_e^1 x_e^t) \quad \forall e \in \mathcal{P}, \phi \in \Phi, t \in \mathcal{T}, \tag{4.14d}$$

where coefficients b_e^0 and b_e^1 provide an upper limit on head loss, and coefficients f_e^0 and f_e^1 provide an upper limit on pump power consumption. By replacing (4.11c) and (4.12) with (4.14a)-(4.14d), (D) becomes a convex quadratically constrained program. An advantage of implementing a convex hull relaxation is that extreme points of the convex hull are often in the original nonconvex set [61]. Since the cost of pumping is minimized in (D), the convex hull relaxation of (4.12) will be tight at the optimum whenever we want to reduce the pump

power consumption, e.g., when there would be minimum voltage limit violations. In [61], the authors used a quasi-convex hull relaxation for (4.11c) (they did not assume flow direction) and found the relaxation was tight at the optimum in their case study.

4.3.6. Compensating Power Demand Uncertainty

Next, we consider uncertainty in consumer power demand; we denote $\tilde{\rho}_{k,\phi}^t$ as the change in power demand from the forecast at bus k and phase ϕ . We formulate a control policy to adjust the pumps' flow rates from the scheduled operation as a function of the demand forecast errors. Since we do not want to use the control policy for uncertainty realizations that do not lead to constraint violations, we introduce an auxiliary binary variable $\tilde{s}^t \in \{0, 1\}$ that equals 1 when a minimum or maximum voltage limit violation would occur given the scheduled pump power consumption and the power demand uncertainty realization at time t

$$\tilde{s}^t = \begin{cases} 0 & \text{if } (V_k^{\min})^2 \leq \hat{Y}_{k,\phi}^t(\tilde{\rho}^t, \mathbf{p}^t) \leq (V_k^{\max})^2 \quad \forall k \in \mathcal{K}, \phi \in \Phi \\ 1 & \text{otherwise} \end{cases} \quad (4.15)$$

where $\hat{Y}_{k,\phi}^t(\tilde{\rho}^t, \mathbf{p}^t)$ is the voltage magnitude squared at bus k and phase ϕ given the power demand forecast errors $\tilde{\rho}^t := [\tilde{\rho}_{k,\phi}^t]_{k \in \mathcal{K}, \phi \in \Phi}$ and the scheduled pump power consumption $\mathbf{p}^t := [p_{e,\phi}^t]_{e \in \mathcal{P}, \phi \in \Phi}$. Eqn. (4.15) can be reformulated

$$\hat{Y}_{k,\phi}^t(\tilde{\rho}^t, \mathbf{p}^t) - (V_k^{\min})^2 \geq -M\tilde{s}^t \quad \forall k \in \mathcal{K}, \phi \in \Phi, \quad (4.16)$$

$$(V_k^{\max})^2 - \hat{Y}_{k,\phi}^t(\tilde{\rho}^t, \mathbf{p}^t) \geq -M\tilde{s}^t \quad \forall k \in \mathcal{K}, \phi \in \Phi, \quad (4.17)$$

$\forall t \in \mathcal{T}$, where coefficient $M > 0$ is sufficiently large to ensure that when the left side of (4.16) or (4.17) is negative (i.e., a voltage violation occurs), the inequality is satisfied only when \tilde{s}^t equals 1.

The control policy changes the pumps' flow rates from the schedule by

$$\tilde{x}_e^t = \tilde{s}^t \mathbf{C}_e^t \tilde{\rho}^t \quad \forall e \in \mathcal{P}, t \in \mathcal{T}, \quad (4.18)$$

where \tilde{x}_e^t is a random variable and \mathbf{C}_e^t is a decision variable, specifically, a control policy parameter row vector that relates the power demand forecast error at bus k and phase ϕ to a change in pump e 's flow rate. Despite the pump flow rate adjustments, the pumps and tanks must provide the same amount of water to the network. In our formulation, the tanks are

not explicitly controlled, but compensate for the deviation between the supply and demand of water.

4.3.7. Chance-Constrained Optimization Problem

We can write the stochastic counterparts of the deterministic equality constraints (4.1)-(4.5), (4.8)-(4.11b) and inequality constraints (4.6)-(4.7), (4.13)-(4.14d) using $(\tilde{\cdot})$ to denote deviations in variables due to power demand uncertainty. The complete set of stochastic constraints also includes the control policy constraints (4.16)-(4.18). The decision variables in the chance-constrained optimization problem are

$$\mathbf{x}_1 = \{x_e^t, H_j^t, H_{j,\text{out}}^t, L_e^t, \mathbf{Y}_k^t, \mathbf{P}_k^t, \mathbf{Q}_k^t, p_{e,\phi}^t, \mathbf{C}_e^t\}.$$

Then the stochastic inequality constraints can be written compactly as $f(\mathbf{x}_1, \tilde{\boldsymbol{\rho}}) \leq 0$ and transformed into a chance-constraint

$$P(f(\mathbf{x}_1, \tilde{\boldsymbol{\rho}}) \leq 0) \geq 1 - \epsilon, \quad (4.19)$$

where the constraints must jointly hold for a probability of at least $1 - \epsilon$, where ϵ is a user-selected violation level. Then, the chance-constrained problem to choose the scheduled WDN operation and control policy parameters over a planning horizon is

$$\begin{aligned} & \min_{\mathbf{x}_1, J^t} \quad \sum_{t \in \mathcal{T}} F^t(\mathbf{x}_1) + gJ^t \\ & \text{s.t.} \quad (4.1) - (4.11b), (4.13) - (4.14d), (4.19), \\ & \quad \|\mathbf{C}^t\|_F^2 \leq J^t \quad \forall t \in \mathcal{T}, \end{aligned} \quad (\text{MICP})$$

where gJ^t is the flexibility cost at time t and g is a weighting coefficient. The flexibility cost models the cost associated with adjusting pumps from their schedule in real time (e.g., wear and tear on WDN components). To prevent control actions that are unnecessarily large, we minimize the magnitude of all parameters in the control policy. This is achieved by setting the variable J^t equal to the Frobenius norm squared of the control policy parameter matrix at time t . The resulting problem is a mixed-integer random convex program.

4.4. Solution Approach

To solve the chance-constrained problem, we use the convex scenario approach [17], which solves the problem robustly for a set of scenarios. The number of scenarios required for probabilistic guarantees is a function of the user-selected maximum violation level ϵ and confidence level ψ . While there exist scenario approaches tailored to mixed integer random convex programs, e.g., [16, 41], these methods require significantly more scenarios than the convex scenario approach in addition to requiring a more computationally intensive mixed-integer solver. To simplify the formulation, we remove the binary variable \tilde{s}^t and apply the control policy to all scenarios, i.e., (4.16)-(4.18) in the chance constraint (4.19) is replaced with

$$\tilde{x}_e^t = \mathbf{C}_e^t \tilde{\rho}^t \quad \forall e \in \mathcal{P}, t \in \mathcal{T}.$$

The simplified formulation, referred to as (CP), is a chance-constrained convex quadratically constrained program and so the convex scenario approach can be applied. The required number of scenarios N for user-selected ϵ and ψ is [17]

$$N \geq \frac{2}{\epsilon} \left(\ln \frac{1}{\psi} + \delta \right), \quad (4.20)$$

where δ is the number of decision variables. In Section 4.5.2, we verify the performance of (CP) against (MICP).

4.5. Case Study

4.5.1. Set Up

The WDN has 2 fixed speed pumps, 2 reservoirs, 2 pressure reducing valves, 8 junctions, and 11 pipes. We use the same WDN as Chapter 3 with some modifications. Specifically, we add a cylindrical storage tank upstream of junction 1, with a diameter of 25 m and a height of 30 m. The elevations at junction 6 and the reservoir upstream of pump 1 are 10 m, and the minimum pressure heads at junctions 7 and 8 are 20 m. The pump curve coefficients are $m_{e=1}^0 = 75$ m and $m_{e=1}^1 = 0.005 \frac{h}{m^2}$ for pump 1, and $m_{e=2}^0 = 90$ m and $m_{e=2}^1 = 0.001 \frac{h}{m^2}$ for pump 2. The pipe parameters from [21] are used to calculate the Darcy-Weisbach resistance coefficients k_e , see [10] for details. We set β equal to 2.322×10^{-3} kW/CMH · m.

Table 4.1: Case Studies

Case	# of Periods	Add Capacitive Load?	Demand Multipliers	
			Water	Power
A	1	No	1.00	1.50
B	1	Yes	1.00	1.50
C	3	No	[1.00,1.00,1.00]	[1.50,1.50,1.50]
D	3	No	[1.00,0.85,0.65]	[1.50,1.45,1.35]

For the PDN, the IEEE 13-bus feeder topology is used. Pumps 1 and 2 are connected to buses 10 and 4, respectively. The load and line parameters are from [52]. The distributed load along the line from bus 1 to 6 is placed at bus 1. The minimum and maximum voltage limits are 0.95 pu and 1.05 pu, respectively. We set the real-to-reactive pump power ratio to $\mu_e = 3$, i.e., a 0.949 lagging power factor. For each pump, there are 17 control policy parameters that correspond to each bus and phase where a load is present. We assume that all loads are wye-connected and constant power with a 0.9 lagging power factor. We ignore the voltage regulator and shunt admittance. We assume that the switch is closed and we do not model the transformer between buses 4 and 5. Also, we set the voltage at the feeder head equal to 4.16 kV line-to-neutral. The price of electricity is fixed for all periods at \$100/MWh. The weighting coefficient g is set to 1 $\$ \cdot \text{kW}^2/\text{CMH}^2$, and we explore how changing g effects the solution.

We explore four cases, see Table 4.1. The cases vary in number of periods and demand multipliers, which are used to modify the nominal water and/or power demand uniformly across all junctions and/or buses. The entries of the demand multiplier vectors corresponds to different periods. In Cases A, C, and D the PDN operates close to the minimum voltage limit. In Case B we add capacitive load, specifically, 500 kVAr at $k = 3$, $\phi = b$ and at $k = 6$, $\phi = \{a, b, c\}$ and 600 kVAr at $k = 10$, $\phi = b$, which increases the voltage and makes the system operate close to the maximum voltage limits.

Table 4.2 lists the number of scenarios needed for the case studies. We use a Gaussian probability distribution that is truncated 3 standard deviations from the mean to randomly generate independent power demand forecast error realizations for all buses and phases that have loads. The forecast error $\tilde{\rho}_{k,\phi}^t$ for bus k , phase ϕ , and time t has a mean of 0 and standard deviation of $\sigma \times \rho_{k,\phi}^t$ where σ is a percentage.

We solve the (MICP) and (CP) problems using the JuMP package in Julia with the GUROBI solver [42]. The optimization problems are solved on a 64-bit Intel i7 dual core

Table 4.2: Number of Scenarios Needed for Scenario Approach

User-selected Parameters		Number of Periods $ \mathcal{T} $	
ϵ (%)	ψ (%)	1	3
10	10^{-3}	2145	6065
5	10^{-3}	4289	12128
3	10^{-3}	7148	20214

Table 4.3: Comparison of MICP and CP solver solutions

Problem	Time (s)	Total Cost	Electricity Cost (\$)	Flexibility Cost
(MICP)	74488.43	25.805	25.071	0.734
(CP)	0.27	25.805	25.069	0.736

CPU at 3.40 GHz and 16 GB of RAM.

4.5.2. Results

MICP versus CP

First, we explore the effect of removing the binary variables \tilde{s}^t from our formulation. In the (CP) formulation, we apply the control policy to every scenario. Table 4.3 shows the results from (MICP) and (CP) for Case A with $N = 100$ randomly generated scenarios and $\sigma = 4\%$. Since g is 1, the flexibility cost is defined as $\sum_t \|\mathbf{C}^t\|_F^2$. The solutions are essentially identical but (CP) takes significantly less time. However, there are cases in which we would expect the formulations to produce different solutions, for example, those in which use of the control policy when the system does not need it would cause constraint violations. Further, different ways of representing the cost of flexibility could lead to different solutions from (CP) and (MICP).

Convex Scenario Approach

Next, we apply the convex scenario approach to (CP) for each of the cases in Table 4.1. The results are shown in Table 4.4 for each case, σ , and ϵ . We list the electricity and flexibility costs separately. As expected, when ϵ is reduced, the total cost increases. Additionally, there is less chance of constraint violations when σ is small resulting in smaller control policy parameters. For example, in Case D with $\sigma = 3\%$ and $\epsilon = 10\%$, it is cheaper to schedule the

Table 4.4: Scenario Approach Results

Case	σ (%)	ϵ (%)	Electricity	Flexibility	Comp.	Empirical	Violation
			Cost (\$)	Cost	Time (s)	Probability <i>General</i> (%)	Selected
A	3	10	24.03	0.288	18.39	0.035	0.035
		5	24.04	0.287	40.46	0.035	0.035
		3	24.23	0.802	54.64	0.015	0.015
	4	10	25.67	1.146	15.15	0.119	0.101
		5	25.67	1.146	30.04	0.119	0.101
		3	25.04	3.000	46.23	0.019	0.019
	B	3	23.73	0.023	22.94	0.484	0.000
		5	23.75	0.058	32.83	0.111	0.000
		3	23.75	0.058	68.43	0.091	0.000
		4	23.95	0.402	16.69	0.290	0.039
		5	23.97	0.569	38.28	0.209	0.044
		3	24.00	0.935	72.81	0.186	0.030
C	3	10	24.07	1.257	19.53	0.512	0.321
		5	24.32	2.051	36.20	0.340	0.242
		3	25.01	4.271	59.70	0.196	0.127
	4	10	71.75	1.162	654.82	0.123	0.123
		5	72.18	1.520	1717.05	0.082	0.082
		3	73.04	2.337	3200.44	0.029	0.029
	5	10	76.73	3.234	667.88	0.246	0.229
		5	76.06	5.301	1525.91	0.139	0.137
		3	75.00	9.356	2299.50	0.055	0.055
D	3	10	59.18	0.000	581.89	0.069	0.025
		5	59.19	0.000	1820.04	0.004	0.004
		3	59.19	0.000	2641.91	0.004	0.004
	4	10	59.24	0.002	749.27	0.055	0.047
		5	59.33	0.007	1330.84	0.034	0.029
		3	59.46	0.321	3021.37	0.010	0.009

WDN operation to satisfy the PDN constraints for all scenarios than to schedule the WDN at a cheaper operation point and use the control policy to shift pumping in real time. In Case D with $\sigma = 3\%$ and $\epsilon = 5\%$ or 3% , the flexibility costs round to zero but are non-zero because a small amount of flexibility is needed to manage the additional scenarios.

The solver computation times are reported in Table 4.4. As the number of periods increases, there is a significant increase in time and memory. We attempted a scheduling problem with 6 periods; however, for violation levels smaller than $\epsilon = 10\%$, we had memory storage errors. This problem could partially be addressed with more efficient coding and/or using methods to speed up the solver.

Table 4.4 also includes the empirical violation probabilities. For each case, σ , and ϵ , we test the optimal schedule and control policy parameters on 100,000 independent randomly generated scenarios and report the percent of scenarios for which there is at least one constraint violation. We compute the empirical violation probabilities two ways: *general* refers to the violation probability computed for the case in which the control policy is applied to all scenarios and *selected* refers to the violation probability computed for the case in which the control policy is applied only when needed (i.e., there is a voltage constraint violation). Therefore, the *general* violation probabilities correspond to the problem actually solved with the convex scenario approach, whereas the *selected* violation probabilities correspond to the more realistic case. Note that the *general* violation probability is always greater than or equal to its corresponding *selected* violation probability since applying the control policy when it is not needed can result in a constraint violation. Also note that all empirical violation probabilities are significantly less than the user-selected violation level, which is typical for problems solved with the scenario approach [125]. If we had chosen a more atypical probability distribution from which to draw scenarios, we would have achieved less conservative results.

Next, we investigate how the location of the forecast error impacts the control policy parameters. Fig. 4.2 shows the relative magnitude of the negative and positive control policy parameters associated with each bus and phase in Case A. We show the positive and negative control policy parameters separately since they serve different purposes. A negative control policy parameter reduces a pump's flow rate and power consumption given an increase in load. Therefore, the negative control policy parameters serve to correct voltage limit violations and the positive control policy parameters serve to balance water supply and demand. The magnitudes of the negative control policy parameters show which buses/phases are most likely to cause voltage limit violations, and the magnitudes of the positive control

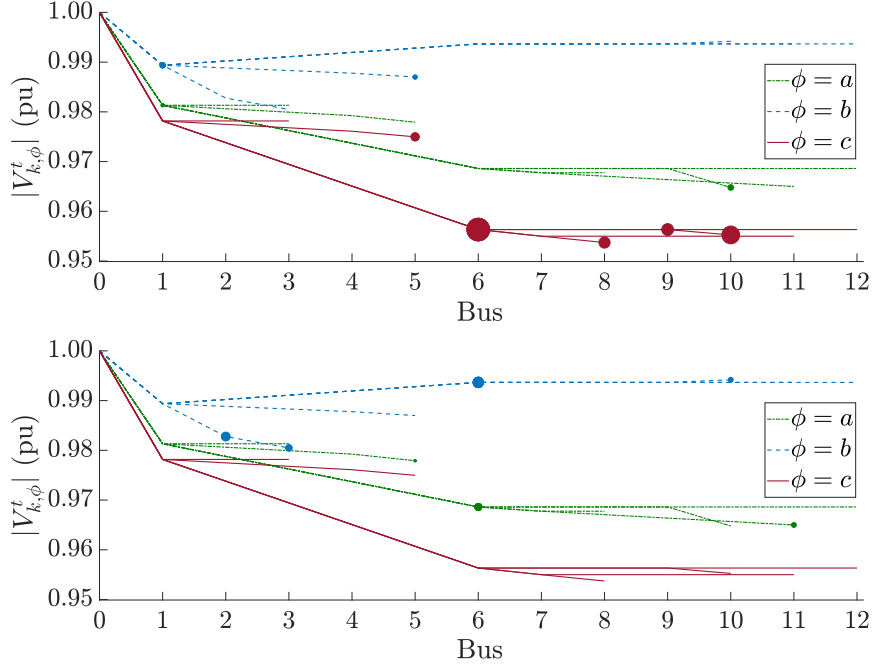


Figure 4.2: 3-phase PDN voltage profile for the optimal scheduled WDN operation in Case A ($\sigma = 4\%$, $\epsilon = 3\%$). The marker size at each bus and phase is scaled according to the magnitude of the pump's control policy parameters, where the top plot shows the magnitude of the negative control policy parameters and the bottom plot shows the magnitude of the positive control policy parameters. The magnitudes of the negative/positive control policy parameters show which buses and phases are most/least likely to cause voltage limit violations.

policy parameters show which buses/phases are least likely to cause voltage limit violations. The PDN is close to the minimum voltage limit on phase c and we observe that the negative control policy parameters are largest on phase c . In Case B (not shown), phase b is close to the maximum voltage limit and phase a is close to the minimum voltage limit. The negative control policy parameters are largest on phase b , followed by those on phase a .

Fig. 4.3 shows how considering uncertainty affects the optimal pump and tank schedule, specifically, it shows the optimal decisions from the scenario approach versus the deterministic approach for Cases C and D. The scenario approach decisions vary more over the scheduling horizon since they are co-optimized with the control policy parameters. The edges of the light and dark blue bands show the largest and average pump and tank adjustments from the scenario approach's schedule made by the control policy in the presence of a voltage violation (in computing the largest/average we exclude adjustments that violate constraints).

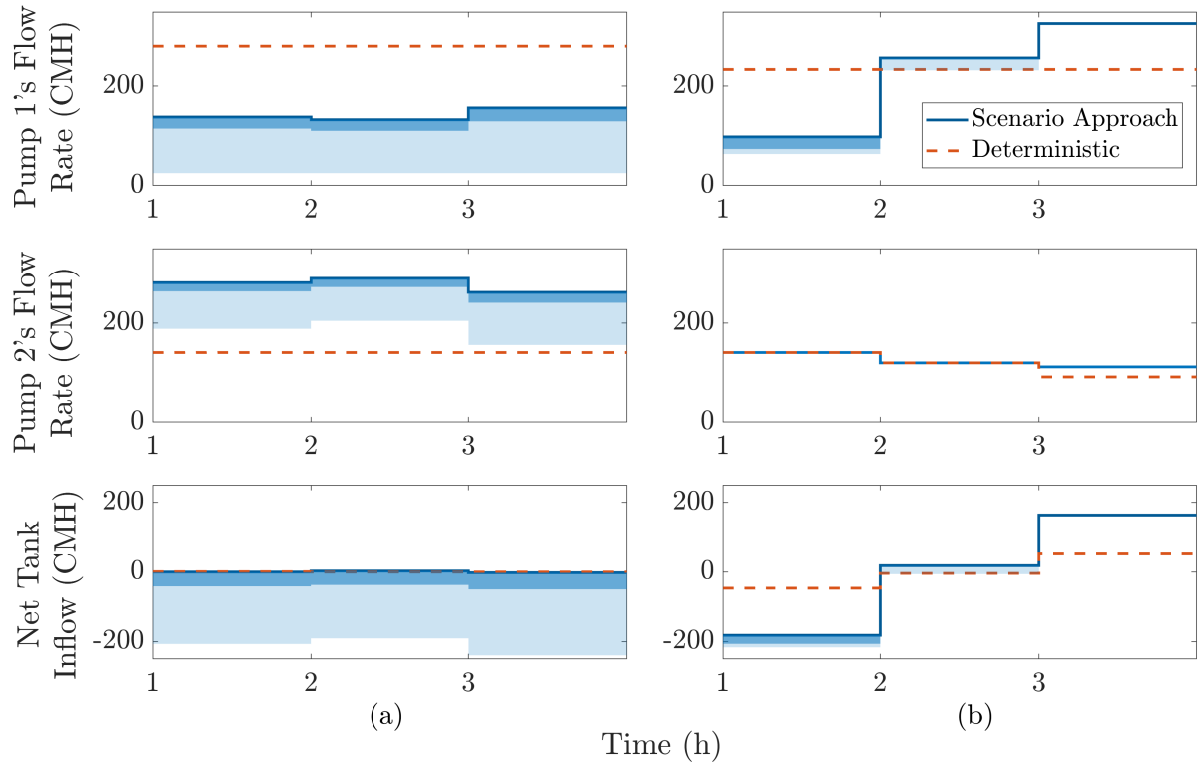


Figure 4.3: Pump and tank schedules for the scenario approach versus the deterministic approach for (a) Case C, $\sigma = 4\%$, $\epsilon = 3\%$, and (b) Case D, $\sigma = 4\%$, $\epsilon = 3\%$. The edges of light/dark blue bands show the largest/average pump and tank adjustments from the scenario approach's schedule made by the control policy.

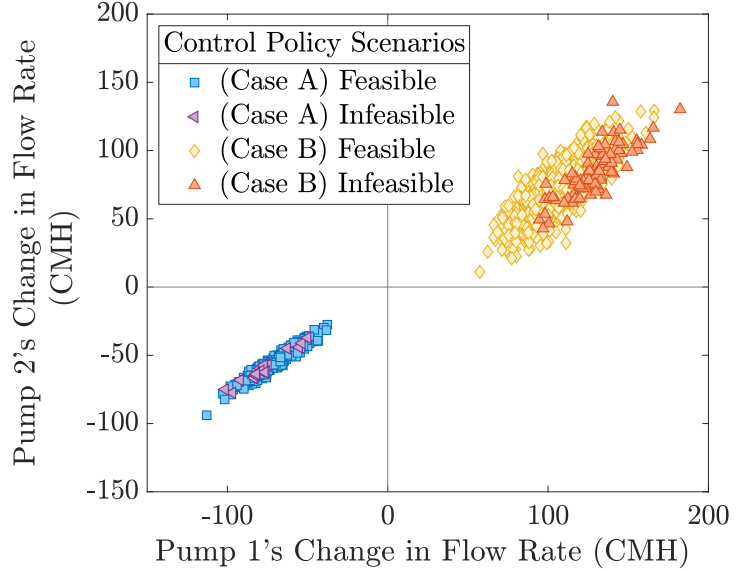


Figure 4.4: Change in pump flow rates for Case A ($\sigma = 4\%$, $\epsilon = 3\%$) and Case B ($\sigma = 5\%$, $\epsilon = 3\%$) for scenarios in the test set requiring the control policy.

In this case, the bands extend downward from the scheduled operation since the bus voltages are near the minimum voltage limit and the control policy is working to raise the voltage levels by decreasing pumping. For Case D, the bands are smaller since the pump and tank schedule is more conservative and less real-time control is required. Specifically, pumping is shifted to periods 2 and 3 when there is less power demand.

Fig. 4.4 shows the pump adjustments made by the control policy in the presence of a voltage violation for Cases A and B. For each scenario, we indicate whether the network constraints were satisfied after implementing the pump adjustment. The scenarios for Case A are in the lower right quadrant because the network experiences minimum voltage limit violations. Consequently, the pump power consumption is reduced in order to raise the voltage levels. The scenarios for Case B are in the upper right quadrant because the network experiences maximum voltage limit violations and pump power consumption needs to increase.

Fig. 4.5 shows how the control policy corrects voltage deviations. For Cases A and B, we compare the voltage profile associated with a power demand scenario before and after the control policy adjusts the pump operation. The voltage profile associated with the schedule is outside of the voltage limits. Once the pumps are adjusted, the voltage profile is within the voltage limits. The insets zoom in on the critical voltages.

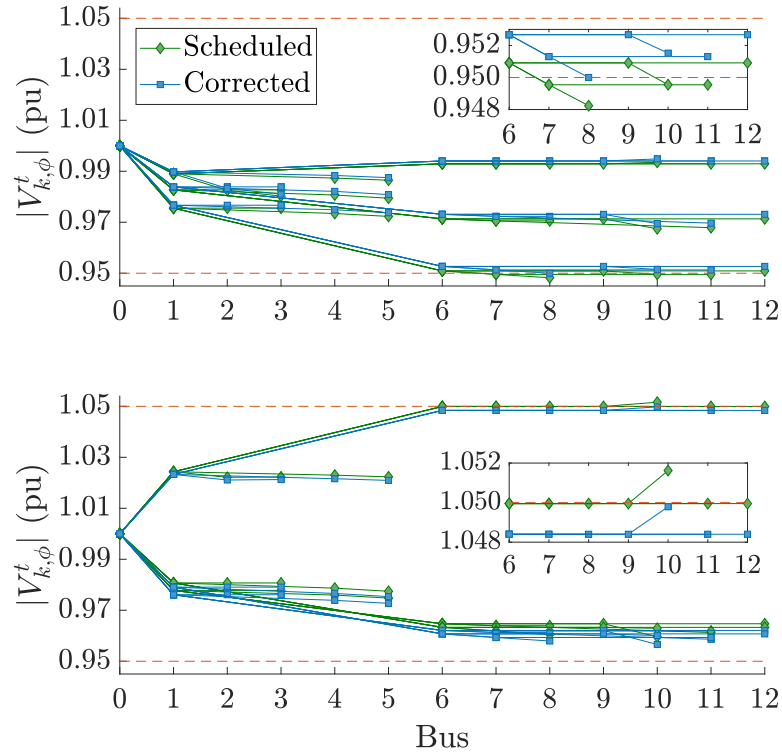


Figure 4.5: PDN voltage profile for a power demand scenario before (Scheduled) and after (Corrected) use of the control policy. Top: Case A ($\sigma = 4\%$, $\epsilon = 3\%$). Bottom: Case B ($\sigma = 5\%$, $\epsilon = 3\%$).

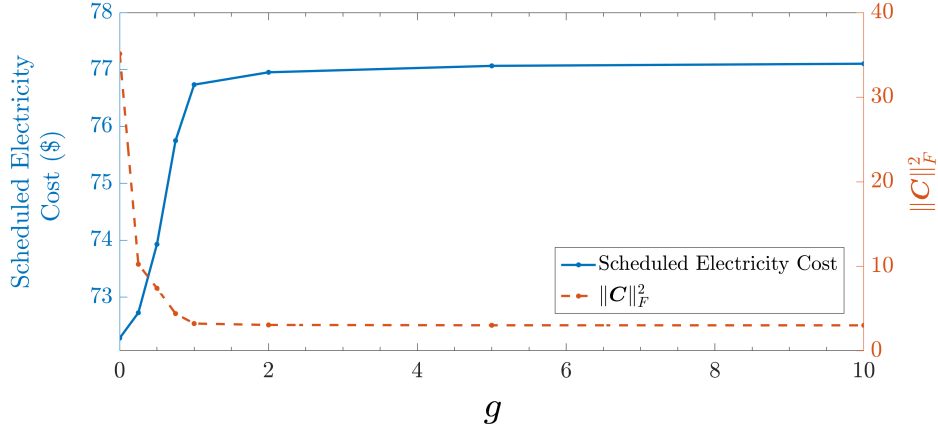


Figure 4.6: Comparison of scheduled electricity cost and flexibility as the weighting coefficient g varies, for Case C, $\sigma = 4\%$, $\epsilon = 10\%$.

The coefficient g determines the relative cost of the schedule versus the cost of the real-time control actions. Fig. 4.6 shows how the scheduled electricity cost and flexibility change as we vary g . The best choice of g would be a function of the real cost to WDN operators of changing pump schedules, and is a topic discussed further in Chapter 5.

Finally, we evaluate our WDN relaxations and PDN approximations. We find that, in our case study, the pump power consumption relaxation is tight for cases close to the minimum voltage limit, i.e., Cases A, C, and D. In Case B, the pump power consumption is increased above the convex hull's lower bound in order to fix the over-voltages. Additionally, the pipe head loss relaxation is not tight; however, we are able to recover the actual heads from the pump flow rates. In [107], the authors prove uniqueness of the water flow equations for several network configurations. Given the pump flow rates, the authors recover the head values by solving a convex energy minimization problem. While their proof does not extend to meshed networks that contain valves, our case study solutions appear unique and optimal when we test many solver initialization points. Additionally, the heads found in the relaxed problem are always less than or equal to the recovered heads. Since we are primarily concerned with head lower limits, we can be certain that the recovered heads are feasible. Lastly, we find that the voltage difference between the linearized unbalanced power flow and the ac power flow is minimal, e.g., for Case B, $\sigma = 5\%$, $\epsilon = 3\%$, the largest difference is 0.34%.

4.6. Chapter Conclusion

In this chapter, we formulated a chance-constrained water pumping problem subject to WDN and PDN constraints, and including power demand uncertainty. We utilized corrective control to adjust the pumps' flow rates to respond to PDN demand uncertainty in real time. We applied the convex scenario approach and found that we were able to successfully schedule and control the pumps to respond to voltage violations in the PDN. A drawback to this approach is the time needed to solve this problem when scaling to larger networks and longer optimization horizons. Improving the scalability of this approach is discussed further in Chapter 7. In Chapter 5, we will consider multiple sources of uncertainty.

Chapter 5.

Incorporating Multiple Uncertainty Sources in a Chance-Constrained Water Distribution Network Voltage Support Problem

In the chapter, we take into consideration both the water demand uncertainty and power demand uncertainty in the chance-constrained voltage support problem. We evaluate implementing balancing water and corrective power control policies and their relative importance on the optimal solution. Additionally, we explore the impact of the flexibility cost definitions and approximations on the water distribution network (WDN) and power distribution network (PDN) constraints as well as the trade-offs in conservativeness, computational tractability, and measurement requirements given the formulation and solution approach. This chapter is based on [111].

5.1. Notation

Sets

\mathcal{E}	Set of pipes in the WDN (indexed by e)
\mathcal{I}_k	Set of buses directly downstream of bus k in PDN (indexed by k)
\mathcal{J}	Set of junctions within the set of nodes in the WDN (indexed by j)
\mathcal{K}	Set of buses in the PDN (indexed by k)
\mathcal{L}	Set of lines in the PDN (indexed by l)

\mathcal{N}	Set of nodes in the WDN (indexed by j)
\mathcal{P}	Set of pumps within the set of pipes in the WDN (indexed by e)
\mathcal{R}	Set of reservoir nodes within the set of nodes in the WDN (indexed by j)
\mathcal{S}	Set of storage tanks within the set of nodes in the WDN (indexed by j)
\mathcal{T}	Set of time steps in the scheduling problem (indexed by t)
\mathcal{V}	Set of valves within the set of pipes in the WDN (indexed by e)
Φ	Set of phases in the PDN (indexed by ϕ)

Decision Variables

$c_{w,e}^t$	Water control policy parameter for pump/tank e at time t (-)
$C_{p,e}^t$	Power control policy parameter row vector for pump e at time t (-)
G_w^t	Component in water flexibility cost function
G_p^t	Component in power flexibility cost function
H_j^t	Hydraulic head at node j at time t (m)
$H_{j,out}^t$	Tank outlet hydraulic head for tank j at time t (m)
\hat{H}_e^t	Head loss of pipe e at time t (m)
L_e^t	Head loss in pressure reducing valve e at time t (m)
$p_{e,\phi}^t$	Real power demand of pump e at phase ϕ and time t (kW)
P_k^t	Real power flow vector (all phases) entering bus k at time t (kW)
$P_{L,k,\phi}^t$	Real power consumed at bus k , phase ϕ at time t (kW)
$q_{e,\phi}^t$	Reactive power demand of pump e at phase ϕ and time t (kVAr)
Q_k^t	Reactive power flow vector (all phases) entering bus k at time t (kVAr)
$Q_{L,k,\phi}^t$	Reactive power consumed at bus k , phase ϕ at time t (kVAr)
$R_{dn,w}^t$	Max. water control action decrease from scheduled pump power (kW)
$R_{up,w}^t$	Max. water control action increase from scheduled pump power (kW)
$R_{dn,p}^t$	Max. power control action decrease from scheduled pump power (kW)
$R_{up,p}^t$	Max. power control action increase from scheduled pump power (kW)
$V_{k,\phi}^t$	Voltage magnitude at bus k , phase ϕ at time t (kV)
$W_{dn,w}^t$	Max. water control action decrease from scheduled flow rate (CMH)
$W_{up,w}^t$	Max. water control action increase from scheduled flow rate (CMH)
$W_{dn,p}^t$	Max. power control action decrease from scheduled flow rate at time t (CMH)
$W_{up,p}^t$	Max. power control action increase from scheduled flow rate at time t (CMH)
x_e^t	Volumetric flow rate in pipe $e : g \rightarrow h$ (from node g to h) at time t (CMH)
\mathbf{Y}_k^t	Voltage magnitude squared vector for all phases at bus k at time t (kV ²)

$$\theta_{k,\phi}^t \quad \text{Voltage angle at bus } k, \text{ phase } \phi \text{ at time } t \text{ (rad)}$$

Functions and Constraint Sets

$\hat{p}_e(x_e^t)$	Pump power consumption of pump e given flow rate x_e^t
$F^t(\cdot)$	Cost of the scheduled WDN operation at time t given decision variables
$\nu_1(\cdot)$	PDN inequality constraints
$\nu_2(\cdot)$	WDN inequality constraints
$u_e(x_e^t)$	Pump e 's hydraulic function
$z_1(\cdot)$	PDN equality constraints
$z_2(\cdot)$	WDN equality constraints

Random Variables

\tilde{d}_j^t	Deviation in water demand at junction j and time t (CMH)
$\tilde{\rho}_{k,\phi}^t$	Deviation in real power demand at bus k and phase ϕ , at time t (kW)

Parameters

a_{je}	Element in incidence matrix of nodes \times pipes (-)
b_e^1, b_e^0	Coefficients in upper bound for pipe headloss convex hull for pipe e (h/m ² , m)
d_j^t	Forecasted water demand of consumer j at time t (CMH)
f_e^1, f_e^0	Convex hull upper bound coefficients for pump e 's power (m, h/m ⁴)
g_w^t	Water control policy weighting coefficient
g_p^t	Power control policy weighting coefficient
\bar{h}_j	Elevation head of node j (m)
h_j^{\min}	Minimum pressure head for node j (m)
h_j^{\max}	Maximum pressure head for node j (m)
k_e	Resistance coefficient of pipe e (h ² /m ⁵)
\mathbf{M}_{kn}	Parameter matrix formed from impedances of line kn (Ohms)
m_e^1, m_e^0	Pump hydraulic function parameters for pump e (h/m ² , m)
n	Pipe head loss function exponent (-)
N	Number of scenarios required (-)
\mathbf{N}_{kn}	Parameter matrix formed from impedances of line kn (Ohms)
$S_{l,\phi}^{\max}$	Maximum apparent power flow for line l and phase ϕ (MVA)
V_k^{\min}	Minimum voltage limit at bus k (kV)
V_k^{\max}	Maximum voltage limit at bus k (kV)
x_e^{\max}	Maximum flow rate of pump e (CMH)
x_e^{\min}	Minimum flow rate of pump e (CMH)

β_ϕ	Constant in pump power consumption equation for phase ϕ (kW/CMH · m)
ΔT	Length of time period (h)
δ	Number of decision variables in the optimization problem (-)
γ_j	Cross-sectional area of tank j (m^2)
ϵ	User-selected violation level (%)
π_e^t	Forecasted energy price at time t for pump e (\$/kWh)
ψ	User-selected confidence level (%)
$\rho_{k,\phi}^t$	Forecasted real power demand at bus k , phase ϕ , and time t (kW)
$\zeta_{k,\phi}^t$	Forecasted reactive power demand at bus k , phase ϕ , and time t (kVAr)

5.2. Chapter Introduction

We formulate an optimization problem to schedule pumping and tank levels subject to both WDN and PDN constraints and considering uncertainty in both nodal net power demands and the water demands. There are two challenges to solving this problem. First, the networks include nonlinear and nonconvex constraints. The second challenge is how to handle the uncertainty. We address the former by using convex approximations and relaxations, and provide a discussion on how they impact the solution. We address the latter by developing affine real-time control policies to respond to water and power demand forecast errors and formulating the problem as a chance-constrained optimization problem that jointly solves for the WDN schedule and control policies' parameters. Since these are critical infrastructure networks, we care more about feasibility than minimizing costs, and chance constraints allow us to achieve constraint satisfaction at high probability levels. However, we also acknowledge that a chance-constrained programming formulation has certain limitations, and highlight these within the chapter.

In Chapter 3, we only considered water demand uncertainty while, in Chapter 4, we only considered power demand uncertainty. In this chapter, we consider both, allowing us to formulate the complete problem and gain substantive additional insights into the solutions of real-world problems. Chapter 3 developed a first version of a *balancing* control policy that adjusts pump flow rates in real time to compensate water demand forecast error; in this chapter, we extend the balancing control policy to include actions from tanks. Also, in Chapter 3, we formulated the problem as a nonconvex program and applied a heuristic scenario-based approach to solve it, whereas in this chapter we use convex approximations and relaxations so that we can obtain probabilistic guarantees on the solution generated by

the scenario approach [17], though the guarantees apply to the approximate/relaxed problem. Chapter 4 developed a first version of a *corrective* control policy that adjusts pump flow rates in real time to respond to voltage violations; in this chapter, we extend it to improve the computational tractability of our solution approach.

The contributions of this chapter are 1) the formulation of an optimal multi-period WDN operation and control problem subject to WDN and PDN constraints and considering uncertainty in both water and power demand; 2) the development of real-time control policies that adjust pump flow rates in response to water and power demand forecast error; 3) the reformulation of the problem into a convex deterministic problem via convex approximations, convex relaxations, and application of the scenario approach; and 4) case studies on a coupled WDN-PDN with pumps, tanks, PDN unbalance, and significant water and power demand uncertainty. Within the case studies, we explore the impact of the approximations and relaxations, an approach to improve computational tractability, and trade-offs in the way we define the cost of real-time control actions. By including both the balancing and corrective control policies, we are able to analyze their relative importance and impact on the optimal solution.

5.3. Problem Description

Our goal is to minimize WDN electricity costs over a scheduling horizon by choosing supply pump flow rates and tank net outflows together with the parameters of real-time control policies enabling response to water and power demand forecast errors. First, ignoring uncertainty, we can formulate the deterministic optimization problem as

$$\begin{aligned} \min_{\mathbf{x}} \quad & \sum_{t \in \mathcal{T}} F^t(\mathbf{x}) \\ \text{s.t.} \quad & z_1(\mathbf{x}, \boldsymbol{\xi}) = 0, \quad v_1(\mathbf{x}, \boldsymbol{\xi}) \leq 0, \\ & z_2(\mathbf{x}, \boldsymbol{\xi}) = 0, \quad v_2(\mathbf{x}, \boldsymbol{\xi}) \leq 0, \end{aligned} \tag{D1}$$

where \mathbf{x} are the decision variables including supply pump flow rates and tank net outflows (defined later), and $\boldsymbol{\xi}$ are the network parameters including the forecasted water and power

demands (also defined later). The cost in discrete time period $t \in \mathcal{T}$ of duration ΔT is

$$F^t(\mathbf{x}) := \sum_{e \in \mathcal{P}} \left(\pi_e^t \Delta T \sum_{\phi \in \Phi} (p_{e,\phi}^t) \right) \quad \forall t \in \mathcal{T}, \quad (5.1)$$

where π_e^t is the actual or forecasted price of electricity for pump $e \in \mathcal{P}$ and $p_{e,\phi}^t$ is the power consumption of pump e on PDN phase $\phi \in \Phi = \{a, b, c\}$. Functions $z_1(\mathbf{x}, \boldsymbol{\xi})$ and $v_1(\mathbf{x}, \boldsymbol{\xi})$ are the PDN's equality and inequality constraints, and $z_2(\mathbf{x}, \boldsymbol{\xi})$ and $v_2(\mathbf{x}, \boldsymbol{\xi})$ are the WDN's equality and inequality constraints. In general, the problem is nonconvex due to nonlinear and nonconvex WDN and PDN constraints. The formulation assumes the WDN has full knowledge of the PDN. While this may be unrealistic, it is still valuable to solve this problem as it gives us insight into the optimal solution achievable without considering limitations on measurements, communication systems, and information sharing by the PDN.

In this section, we first explain the PDN model that defines $z_1(\mathbf{x}, \boldsymbol{\xi})$ and $v_1(\mathbf{x}, \boldsymbol{\xi})$ and then the WDN model that defines $z_2(\mathbf{x}, \boldsymbol{\xi})$ and $v_2(\mathbf{x}, \boldsymbol{\xi})$. Then, we describe a number of convex approximations and relaxations we use, resulting in a convex deterministic problem. Finally, we describe how we incorporate uncertainty, define the cost of flexibility, and formulate our chance-constrained optimization problem.

5.3.1. Power Distribution Network Model

The consumers and pumps are connected to a PDN through a set of buses $k \in \mathcal{K}$. The PDN equality constraints $z_1(\mathbf{x}, \boldsymbol{\xi})$ include the three-phase unbalanced AC power flow equations

$$f^t (\mathbf{P}_L^t(\mathbf{p}^t), \mathbf{Q}_L^t(\mathbf{q}^t), \mathbf{V}^t, \boldsymbol{\theta}^t, \boldsymbol{\xi}^t) = 0 \quad \forall t \in \mathcal{T}, \quad (5.2)$$

where $\mathbf{P}_L^t := [P_{L,k,\phi}^t]_{k \in \mathcal{K}, \phi \in \Phi}$ and $\mathbf{Q}_L^t := [Q_{L,k,\phi}^t]_{k \in \mathcal{K}, \phi \in \Phi}$ are vectors of the real and reactive power loads at each bus and phase; $\mathbf{V}^t := [V_{k,\phi}^t]_{k \in \mathcal{K}, \phi \in \Phi}$ and $\boldsymbol{\theta}^t := [\theta_{k,\phi}^t]_{k \in \mathcal{K}, \phi \in \Phi}$ are vectors of the voltage magnitudes and angles at each bus and phase; and $\mathbf{p}^t := [p_{e,\phi}^t]_{e \in \mathcal{P}, \phi \in \Phi}$ and $\mathbf{q}^t := [q_{e,\phi}^t]_{e \in \mathcal{P}, \phi \in \Phi}$ are vectors of the real and reactive pump power consumption for each pump and phase. The load at each bus and phase is

$$P_{L,k,\phi}^t = \begin{cases} \rho_{k,\phi}^t + p_{e,\phi}^t, & \text{if pump } e \text{ connected to bus } k \\ \rho_{k,\phi}^t, & \text{otherwise} \end{cases}, \quad (5.3)$$

$$Q_{\text{L},k,\phi}^t = \begin{cases} \zeta_{k,\phi}^t + q_{e,\phi}^t, & \text{if pump } e \text{ connected to bus } k \\ \zeta_{k,\phi}^t, & \text{otherwise} \end{cases}, \quad (5.4)$$

$\forall k \in \mathcal{K}, \phi \in \Phi, t \in \mathcal{T}$, where $\rho_{k,\phi}^t$ and $\zeta_{k,\phi}^t$ are network parameters, specifically, the forecasted real and reactive net load, i.e., actual load minus distributed generation, e.g., from solar photovoltaics, at each bus, phase, and time period. The PDN equality constraints also include

$$\theta_{0,a}^t = 0^\circ, \quad \theta_{0,b}^t = -120^\circ, \quad \theta_{0,c}^t = 120^\circ \quad \forall t \in \mathcal{T}, \quad (5.5)$$

$$V_{0,a}^t = V_{0,b}^t = V_{0,c}^t = 1 \text{ pu} \quad \forall t \in \mathcal{T}, \quad (5.6)$$

which specify that the substation (i.e., bus 0, without loss of generality) has a fixed and balanced voltage.

The PDN inequality constraints $v_1(\mathbf{x}, \boldsymbol{\xi}) \leq 0$ include limits on the bus voltages' magnitudes

$$V_k^{\min} \leq V_{k,\phi}^t \leq V_k^{\max} \quad \forall k \in \mathcal{K}, \phi \in \Phi, t \in \mathcal{T}, \quad (5.7)$$

where V_k^{\min} and V_k^{\max} are the lower and upper voltage magnitude limits at bus k . They can also include limits on the apparent power flows along lines $l \in \mathcal{L}$

$$(P_{l,\phi}^t)^2 + (Q_{l,\phi}^t)^2 \leq (S_{l,\phi}^{\max})^2 \quad \forall l \in \mathcal{L}, \phi \in \Phi, t \in \mathcal{T}, \quad (5.8)$$

where $S_{l,\phi}^{\max}$ is the apparent power flow limit for line l and phase ϕ .

We do not model existing voltage regulating equipment (i.e., tap changing transformers, switched capacitors, etc.) as it would introduce binary variables, making the problem much harder to solve. Moreover, this allows us to explore the impact of WDN actions alone on PDN voltage levels. Future work will explore how best to model this equipment in our formulation and how this equipment and WDNs can work together to regulate voltages in the most cost-effective manner.

5.3.2. Water Distribution Network Model

We assume supply pump on/off statuses are determined in advance of the scheduling horizon. We also assume pipe water flows do not change direction during the scheduling horizon. These assumptions are commonly used in the literature, e.g., by [31, 32, 81, 130], to eliminate

the need for binary variables. Consequently, we can formulate the WDN as a directed graph $(\mathcal{N}, \mathcal{E})$ composed of a set of nodes \mathcal{N} and a set of edges \mathcal{E} . Nodes can be categorized as junctions $j \in \mathcal{J}$, reservoirs $j \in \mathcal{R}$, or elevated storage tanks $j \in \mathcal{S}$, i.e., $\mathcal{N} = \mathcal{J} \cup \mathcal{R} \cup \mathcal{S}$. The main distinction between tanks and reservoirs is that tanks allow bidirectional flow whereas reservoirs model the water supply source (i.e., treatment plant clearwells). Water is pumped into elevated storage tanks (e.g., during periods of low demand) so that the tanks can release pressurized water using gravity at a later time period (e.g., during periods of high demand). Edges are pipes connecting the nodes; they can contain a supply pump $e \in \mathcal{P}$ or a pressure reducing valve $e \in \mathcal{V}$, i.e., $(\mathcal{P} \cup \mathcal{V}) \subseteq \mathcal{N}$. The WDN can be described by its hydraulic head H_j^t at node j and the volumetric flow rate x_e^t through pipe e . Fig. 5.1 shows the relationships between elevation, hydraulic head, flow rate, demand, and head loss along two pipe segments.

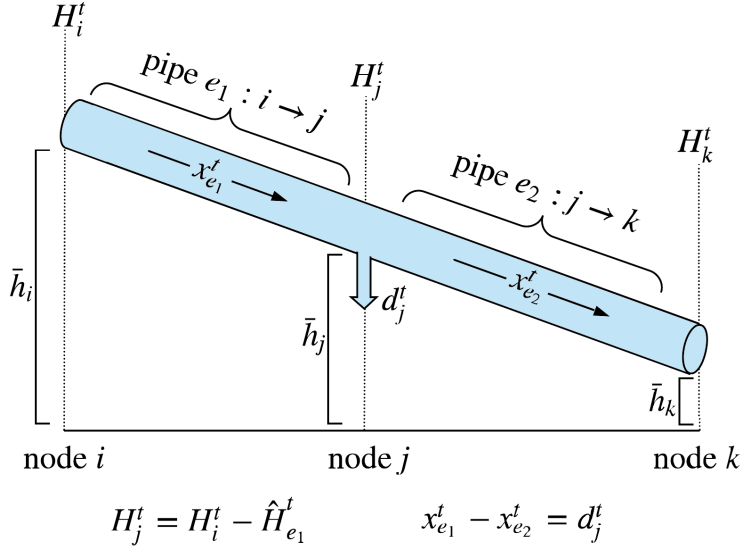


Figure 5.1: WDN visualization including elevation and hydraulic head with respect to an elevation reference, flow rate, and head loss. Example equations of conservation of hydraulic head (5.15) and conservation of water (5.11) are included.

Nodes, \mathcal{N}

The hydraulic head H_j^t at node j is composed of the elevation \bar{h}_j and the pressure head. The WDN nodal constraints are

$$h_j^{\min} + \bar{h}_j \leq H_j^t \leq h_j^{\max} + \bar{h}_j \quad \forall j \in \mathcal{N}, t \in \mathcal{T}, \quad (5.9)$$

$$H_j^t = \bar{h}_j \quad \forall j \in \mathcal{R}, t \in \mathcal{T}, \quad (5.10)$$

$$\sum_{e \in \mathcal{E}} a_{je} x_e^t = d_j^t \quad \forall j \in \mathcal{J}, t \in \mathcal{T}, \quad (5.11)$$

$$H_{j,\text{out}}^t = H_{j,\text{out}}^{t-1} + \frac{\Delta T}{\gamma_j} \sum_{e \in \mathcal{E}} a_{je} x_e^t \quad \forall j \in \mathcal{S}, t \in \mathcal{T}, \quad (5.12)$$

$$h_j^{\min} + \bar{h}_j \leq H_{j,\text{out}}^t \leq h_j^{\max} + \bar{h}_j \quad \forall j \in \mathcal{S}, t \in \mathcal{T}, \quad (5.13)$$

where h_j^{\min} and h_j^{\max} are the lower and upper pressure head limits at node j . For tanks, these are set to the minimum and maximum tank levels. Parameter d_j^t is the forecasted water demand at junction j , γ_j is the cross-sectional area of tank j , and $a_{je} \in \{0, 1, -1\}$ is an element in the node-edge incidence matrix which describes the connection of edges and nodes in the network. In (5.9), the hydraulic head at each node is limited. We treat reservoirs \mathcal{R} as infinite sources with fixed pressure heads. Consequently in (5.10), we set the hydraulic head equal to elevation without loss of generality. For junctions \mathcal{J} , we ensure that the conservation of water is satisfied. Therefore, in (5.11), the sum of water entering and exiting a junction must equal the consumer water demand d_j^t . We model tanks \mathcal{S} with separate inflow and outflow pipes, where the inlet is at the top of the tank and the outlet is at the bottom [122]. The inlet is treated as a junction, where its head H_j^t is computed the same way as any junction (i.e., the upstream hydraulic head minus the head loss through the connecting pipe, described below). The outlet tank hydraulic head $H_{j,\text{out}}^t$ is a function of the previous period's outlet tank hydraulic head and the tank net inflow, as shown in (5.12). Equation (5.13) limits the outlet head by the physical volume of the tank. Since we do not want to simply deplete the tank over the scheduling horizon, we constrain the final outlet tank hydraulic head to be greater than or equal to the initial outlet tank hydraulic head

$$H_{j,\text{out}}^{t=|\mathcal{T}|} \geq H_{j,\text{out}}^{t=0}. \quad (5.14)$$

Edges, \mathcal{E}

We denote the frictional head loss along pipe e as $\hat{H}_e^t = -\sum_{j \in \mathcal{N}} a_{je} H_j^t$. The head loss equation for each pipe is dependent on whether it contains a pump or valve

$$\hat{H}_e^t = \begin{cases} u_e(x_e^t) & \forall e \in \mathcal{P}, \\ L_e^t & \forall e \in \mathcal{V}, \end{cases} \quad (5.15a)$$

$$\hat{H}_e^t = \begin{cases} k_e \cdot (x_e^t)^n & \forall e \in \mathcal{E} \setminus (\mathcal{P} \cup \mathcal{V}), \end{cases} \quad (5.15c)$$

$\forall t \in \mathcal{T}$. The first case corresponds to pipes containing fixed speed pumps, where pump e 's hydraulic function u_e is dependent on its flow rate x_e^t . It is usually approximated with a quadratic function. The second case corresponds to pumps containing pressure reducing valves, where the valve head loss $L_e^t \geq 0$ is a decision variable. The third case corresponds to pipes without a pump or valve, where k_e is the resistance coefficient for pipe e and n is the exponent.

Additionally, the pump flow rates are limited

$$x_e^{\min} \leq x_e^t \leq x_e^{\max} \quad \forall e \in \mathcal{P}, t \in \mathcal{T}, \quad (5.16)$$

where $x_e^{\min} > 0$ and x_e^{\max} are the lower and upper flow rate limits for pump e . The power consumption of pump e is a function of its head gain $-\hat{H}_e^t$ and flow rate

$$p_{e,\phi}^t = -\beta_\phi \hat{H}_e^t x_e^t \quad \forall e \in \mathcal{P}, \phi \in \Phi, t \in \mathcal{T}, \quad (5.17)$$

where β_ϕ is a constant with units of kW/CMH · m that both converts $\hat{H}_e^t x_e^t$ to units of power and assigns a portion of the pump power consumption to each phase ϕ , e.g., one third to each phase if the load is balanced.

The WDN equality constraints are collected to form $z_2(\mathbf{x}, \boldsymbol{\xi}) = 0$ and the inequality constraints are collected to form $v_2(\mathbf{x}, \boldsymbol{\xi}) \leq 0$. The water decision variables are $\mathbf{x} := [x_e^t]_{e \in \mathcal{E}, t \in \mathcal{T}}$, $\mathbf{H} := [H_j^t]_{j \in \mathcal{N}, t \in \mathcal{T}}$, $\mathbf{H}_{\text{out}} := [H_{j,\text{out}}^t]_{j \in \mathcal{S}, t \in \mathcal{T}}$, and $\mathbf{L} := [L_e^t]_{e \in \mathcal{V}, t \in \mathcal{T}}$.

5.3.3. Deterministic Problem: Nonconvex Formulation

Using the constraints defined in the previous subsections, the full deterministic problem is

$$\min_{\mathbf{x}_1} \quad \sum_{t \in \mathcal{T}} F^t(\mathbf{x}_1) \quad (\mathbf{D2})$$

$$\begin{aligned} \text{s.t. } & (5.2) - (5.8), \\ & (5.9) - (5.17), \end{aligned}$$

where the decision variables are $\mathbf{x}_1 = \{\mathbf{x}, \mathbf{H}, \mathbf{H}_{\text{out}}, \mathbf{L}, \mathbf{P}_L, \mathbf{Q}_L, \mathbf{V}, \boldsymbol{\theta}, \mathbf{p}, \mathbf{q}\}$. The problem is nonconvex.

5.3.4. Approximations and Relaxations

Since nonconvex problems can be difficult to solve, we use convex approximations and relaxations to convexify our formulation. For the PDN, we use a linearized 3-phase unbalanced power flow model for radial networks; however, our approach can easily be extended to other convex PDN formulations, such as [34, 100], where [100] approximates system losses. The formulation we use neglects the losses and assumes that the voltage unbalance at each bus is small [3]

$$\mathbf{Y}_k^t = \mathbf{Y}_n^t - \mathbf{M}_{kn} \mathbf{P}_n^t - \mathbf{N}_{kn} \mathbf{Q}_n^t \quad \forall k \in \mathcal{K}, t \in \mathcal{T}, \quad (5.18)$$

$$\mathbf{P}_k^t = \mathbf{P}_{L,k}^t + \sum_{n \in \mathcal{I}_k} \mathbf{P}_n^t \quad \forall k \in \mathcal{K}, t \in \mathcal{T}, \quad (5.19)$$

$$\mathbf{Q}_k^t = \mathbf{Q}_{L,k}^t + \sum_{n \in \mathcal{I}_k} \mathbf{Q}_n^t \quad \forall k \in \mathcal{K}, t \in \mathcal{T}, \quad (5.20)$$

where $\mathbf{Y}_k^t \in \mathbb{R}^{3 \times 1}$ contains the three-phase voltage magnitudes squared at bus k and time t , i.e., $Y_{k,\phi}^t = (V_{k,\phi}^t)^2$; $\mathbf{P}_k^t \in \mathbb{R}^{3 \times 1}$ and $\mathbf{Q}_k^t \in \mathbb{R}^{3 \times 1}$ contain the three-phase real and reactive power flows entering bus k at time t ; and parameter matrices \mathbf{M}_{kn} and \mathbf{N}_{kn} are formed from the line impedances. The set \mathcal{I}_k contains all buses that are connected directly downstream of bus k .

For the WDN, the head loss in pipes without pumps or valves (5.15c), the pump hydraulic function (5.15a), and the pump power consumption (5.17) are nonconvex. Head loss is usually modeled with the Darcy-Weisbach or Hazen-Williams formulas; see [10] for details. Both are nonconvex. Using the approach from [61], we relax the Darcy-Weisbach formula, in which $n = 2$, by replacing (5.15c) with its convex hull

$$\hat{H}_e^t \geq k_e \cdot (x_e^t)^2 \quad \forall e \in \mathcal{E} \setminus (\mathcal{P} \cup \mathcal{V}), t \in \mathcal{T}, \quad (5.21a)$$

$$\hat{H}_e^t \leq b_e^0 + b_e^1 x_e^t \quad \forall e \in \mathcal{E} \setminus (\mathcal{P} \cup \mathcal{V}), t \in \mathcal{T}, \quad (5.21b)$$

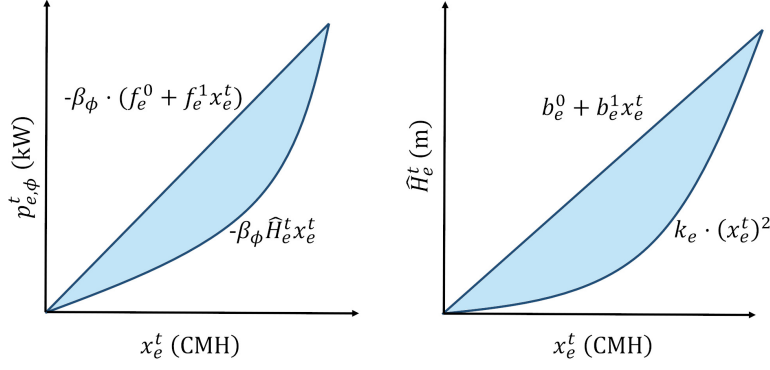


Figure 5.2: Convex hull for the pump power consumption (left) and pipe head loss (right).

where b_e^0 and b_e^1 are parameters that provide the upper bound for the convex hull. In Fig. 5.2 (right), we illustrate the convex hull of the pipe head loss.

As mentioned, the pump hydraulic function (5.15a) is usually approximated with a quadratic function; however, the coefficient in front of the quadratic term is usually small and negative [10]. Therefore, like [61], we neglect the quadratic term since its contribution is small compared to the linear term and approximate the pump hydraulic function as

$$\hat{H}_e^t = - (m_e^0 + m_e^1 x_e^t) \quad \forall e \in \mathcal{P}, t \in \mathcal{T}. \quad (5.22)$$

where m_e^0 and m_e^1 are parameters.

The pump power consumption is a quadratic function of the flow rate x_e^t . Since it is included in the linearized power flow equations, it makes them nonconvex. Again, using the approach from [61], we replace (5.17) with its convex hull

$$p_{e,\phi}^t \geq -\beta_\phi \hat{H}_e^t x_e^t \quad \forall e \in \mathcal{P}, \phi \in \Phi, t \in \mathcal{T}, \quad (5.23a)$$

$$p_{e,\phi}^t \leq -\beta_\phi \cdot (f_e^0 + f_e^1 x_e^t) \quad \forall e \in \mathcal{P}, \phi \in \Phi, t \in \mathcal{T}, \quad (5.23b)$$

where f_e^0 and f_e^1 are parameters that provide the upper bound for the convex hull. In Fig. 5.2 (left), we illustrate the convex hull for the pump power consumption. When pumping costs are minimized subject to the pump power consumption convex hull, the solution will lie on the lower edge of the hull, i.e., the original constraint.

5.3.5. Deterministic Problem: Convex Formulation

Assuming the PDN experiences voltage problems before apparent power flows violate line limits, which is often the case in radial distribution networks, we neglect the line flow limits (5.8). Then, using the relaxations and approximations from Section 5.3.4, we can formulate the deterministic problem as a convex program

$$\begin{aligned} \min_{\mathbf{x}_2} \quad & \sum_{t \in \mathcal{T}} F^t(\mathbf{x}_2) \\ \text{s.t.} \quad & (5.3) - (5.4), (5.7), (5.9) - (5.14), \\ & (5.15b), (5.16), (5.18) - (5.23b) \end{aligned} \tag{D3}$$

where the decision variables are $\mathbf{x}_2 = \{\mathbf{x}, \mathbf{H}, \mathbf{H}_{\text{out}}, \mathbf{L}, \mathbf{P}, \mathbf{Q}, \mathbf{Y}, \mathbf{p}, \mathbf{q}\}$.

5.3.6. Incorporating Uncertainty

Next, we consider water and power demand uncertainty. We denote the water demand forecast error at junction j as \tilde{d}_j^t and the power demand forecast error at bus k , phase ϕ as $\tilde{\rho}_{k,\phi}^t$. We develop control policies to adjust the supply pump flow rates and the tank net outflows from their scheduled operation in real time to *balance* the mismatch in water supply and demand resulting from water demand forecast error and to *correct* voltage constraint deviations resulting from power demand forecast error. Note that we do not apply control policies to booster pumps that increase pressure head.

The *balancing* control policy adjusts pumping and tank levels to compensate for water demand forecast error. We also refer to it as the water control policy. We assume the pumps receive a measurement of the *total* water demand forecast error and change their flow rates from their schedule by $\tilde{x}_{w,e}^t$ as a function of the total error $\sum_{j \in \mathcal{J}} \tilde{d}_j^t$

$$\tilde{x}_{w,e}^t = c_{w,e}^t \sum_{j \in \mathcal{J}} \tilde{d}_j^t \quad \forall e \in \mathcal{P}, t \in \mathcal{T}, \tag{5.24}$$

where $\tilde{x}_{w,e}^t$ is a random variable and $c_{w,e}^t$ is a scalar water control policy parameter associated with pump e and a decision variable in our optimization problem. The tanks are passive and adjust their net outflow by

$$\sum_{e \in \mathcal{E}} -a_{je} \tilde{x}_{w,e}^t = c_{w,j}^t \sum_{i \in \mathcal{J}} \tilde{d}_i^t \quad \forall j \in \mathcal{S}, t \in \mathcal{T} \tag{5.25}$$

to compensate any water demand and supply mismatch, where $c_{w,j}^t$ is a scalar water control policy parameter associated with tank j and a decision variable in our optimization problem. Note that on the right side of the equation we use subscript i rather than j to sum over the water demand forecast errors at all junctions since subscript j is used elsewhere in the equation. To ensure the water supply equals the water demand we set

$$\sum_{e \in \mathcal{P}} c_{w,e}^t + \sum_{j \in \mathcal{S}} c_{w,j}^t = 1 \quad \forall t \in \mathcal{T}. \quad (5.26)$$

Our preliminary work in Chapter 3 introduced a first version of this control policy, but it did not consider storage tanks or multiple time periods.

The *corrective* control policy adjusts pumping and tank levels to compensate power demand forecast error when there is a voltage constraint violation. We also refer to it as the power control policy. We assume that pumps receive notice of voltage constraint violations along with measurements of the power demand forecast error for each bus and phase of the PDN. When violations occur, they change their flow rates from their schedule by $\tilde{x}_{p,e}^t$ as a function of the error vector $\tilde{\rho}^t := [\tilde{\rho}_{k,\phi}^t]_{k \in \mathcal{K}, \phi \in \Phi}$

$$\tilde{x}_{p,e}^t = \mathbf{C}_{p,e}^t \tilde{\rho}^t \quad \forall e \in \mathcal{P}, t \in \mathcal{T}, \quad (5.27)$$

where $\tilde{x}_{p,e}^t$ is a random variable and $\mathbf{C}_{p,e}^t$ is a power control policy parameter row vector that relates the power demand deviations at load bus k and phase ϕ to a change in pump e 's flow rate. The latter is a decision variable in our optimization problem. Note that (5.27) does not explicitly control tank levels (recall that tanks do not consume power so they have no direct impact on voltages); however, tanks still compensate for deviations between water supply and demand.

Our preliminary work in Chapter 4 introduced (5.27) and found that solving for power control policy parameters corresponding to every load bus and phase was computationally cumbersome. Therefore, in Section 5.4.4, we explore the impact of aggregating forecast errors over phases/buses, which reduces the number of decision variables and therefore the size of the optimization problem. Chapter 4 also explored use of the power control policy for all power demand forecast errors versus only when needed to correct a voltage constraint violation. While always applying the power control policy would result in unnecessary control actions, it would also eliminate the need for real-time notice of voltage constraint violations. Moreover, modeling the usage/non-usage of the power control policy in the optimization for-

mulation requires introduction of binary variables, which significantly increases computation time. It is also possible to formulate the optimization problem assuming the power control policy is used for all power demand forecast errors, but only apply it when needed. However, this may result in a sub-optimal policy. In this chapter, we formulate the optimization problem assuming the power control policy is used for all power demand forecast errors and also apply it in this way.

For notational simplicity, we define the water control policy parameter column vector, which includes all pump and tank control policy parameters, as $\mathbf{c}_w^t := \langle [c_{w,e}^t]_{e \in \mathcal{P}}, [c_{w,j}^t]_{j \in \mathcal{S}} \rangle$, where we use angle brackets to vertically stack column vectors. We also define the power control policy matrix $\mathbf{C}_p^t = [\mathbf{C}_{p,e}^t]_{e \in \mathcal{P}}$, which includes all pumps. Note that the control policy parameters may vary over the scheduling horizon. Both control policies contribute to the total change in pump flow rate

$$\tilde{x}_e^t = \tilde{x}_{w,e}^t + \tilde{x}_{p,e}^t \quad \forall e \in \mathcal{P}, t \in \mathcal{T}. \quad (5.28)$$

5.3.7. Flexibility Costs

Using pumps to respond to forecast errors in real time would incur some cost, i.e., more frequent changes in output, larger changes in output, and/or faster changes in output would lead to more wear and tear on WDN components, such as pumps and valves. We refer to this cost as a *flexibility cost*. However, it is not clear how best to formulate that cost and so we explore several options. We define the objective function of the chance-constrained optimization problem as $\sum_{t \in \mathcal{T}} (F^t(\mathbf{x}_2) + g_w^t G_w^t + g_p^t G_p^t)$, where $g_w^t G_w^t$ and $g_p^t G_p^t$ are flexibility cost functions associated with the water and power control policies, respectively, and g_w^t and g_p^t are weighting coefficients. The dimensions of g_w^t and g_p^t are chosen such that the terms $g_w^t G_w^t$ and $g_p^t G_p^t$ are scalars. Three options for defining the flexibility cost follow.

Option 1

The flexibility costs are a function of the squared norms of the water and power control policy parameters:

$$G_{w,1}^t := \|\mathbf{c}_w^t\|_2^2, \quad (5.29)$$

$$G_{p,1}^t := \|\mathbf{C}_p^t\|_F^2. \quad (5.30)$$

Specifically, we use the squared Euclidean norm of the water control policy parameter vector and the squared Frobenius norm of the power control policy parameter matrix. Therefore, $G_{w,1}^t$ and $G_{p,1}^t$ are scalars. Option 1 penalizes all parameters within the control policy to prevent excessive control actions. For the water control policy, this formulation spreads the control actions amongst the pumps/tanks rather than using only a small subset of pumps/tanks to compensate water demand deviations. For the power control policy, the system is underdetermined, i.e., different choices of power control parameters can achieve the same control action given the same power demand forecast error. This formulation chooses the set of parameters that minimizes their squared norm.

Option 2

The flexibility costs are a function of the range of pump *flow rate* adjustments

$$G_{w,2}^t := \langle \mathbf{W}_{up,w}^t, \mathbf{W}_{dn,w}^t \rangle, \quad (5.31)$$

$$G_{p,2}^t := \langle \mathbf{W}_{up,p}^t, \mathbf{W}_{dn,p}^t \rangle, \quad (5.32)$$

where column vectors $\mathbf{W}_{up,w}^t, \mathbf{W}_{dn,w}^t \in \mathbb{R}_+^{|\mathcal{P} \cup \mathcal{S}| \times 1}$ define the flexibility band around the scheduled flow rate for water control policy actions and $\mathbf{W}_{up,p}^t, \mathbf{W}_{dn,p}^t \in \mathbb{R}_+^{|\mathcal{P}| \times 1}$ define the flexibility band for power control policy actions. Specifically, $\mathbf{W}_{up,w}^t, \mathbf{W}_{dn,w}^t, \mathbf{W}_{up,p}^t$, and $\mathbf{W}_{dn,p}^t$ are decision variables related to the control policies through the following element-wise inequalities

$$-\mathbf{W}_{dn,w}^t \leq \mathbf{c}_w^t \sum_{j \in \mathcal{J}} \tilde{d}_j^t \leq \mathbf{W}_{up,w}^t \quad \forall t \in \mathcal{T}, \quad (5.33)$$

$$-\mathbf{W}_{dn,p}^t \leq \mathbf{C}_p^t \tilde{\rho}^t \leq \mathbf{W}_{up,p}^t \quad \forall t \in \mathcal{T}. \quad (5.34)$$

In contrast to Option 1, Option 2 considers the largest flow rate changes over all of the scenarios instead of penalizing the control policy parameters, which may be more reasonable if pump wear-and-tear is related to the magnitude of fast changes in flow rate.

Option 3

The flexibility costs are a function of the range of pump *power* deviations, which is similar to specifying reserve capacities in electric power systems,

$$G_{w,3}^t := \langle \mathbf{R}_{up,w}^t, \mathbf{R}_{dn,w}^t \rangle, \quad (5.35)$$

$$G_{p,3}^t := \langle \mathbf{R}_{\text{up,p}}^t, \mathbf{R}_{\text{dn,p}}^t \rangle, \quad (5.36)$$

where column vectors $\mathbf{R}_{\text{up,w}}^t, \mathbf{R}_{\text{dn,w}}^t \in \mathbb{R}_+^{|\mathcal{P}| \times 1}$ define the flexibility band around the scheduled pump power consumption due to water control policy actions and $\mathbf{R}_{\text{up,p}}^t, \mathbf{R}_{\text{dn,p}}^t \in \mathbb{R}_+^{|\mathcal{P}| \times 1}$ define the flexibility band for power control policy actions. While we could specify these values per phase, we make the realistic assumption that pumps are balanced three-phase motors and power deviations are identical in each phase. Therefore, $\mathbf{R}_{\text{up,w}}^t, \mathbf{R}_{\text{dn,w}}^t, \mathbf{R}_{\text{up,p}}^t$, and $\mathbf{R}_{\text{dn,p}}^t$ are identical for each phase, and so we do not specify the phase. Since the pump power consumption curve (5.17) is monotonically increasing, the largest pump power deviations occur with the largest flow rate adjustments. Therefore, decision variables $\mathbf{R}_{\text{up,w}}^t, \mathbf{R}_{\text{dn,w}}^t, \mathbf{R}_{\text{up,p}}^t$, and $\mathbf{R}_{\text{dn,p}}^t$ are directly related to $\mathbf{W}_{\text{up,w}}^t, \mathbf{W}_{\text{dn,w}}^t, \mathbf{W}_{\text{up,p}}^t$, and $\mathbf{W}_{\text{dn,p}}^t$, i.e.,

$$R_{\text{dn,w},e}^t = p_e^t - \hat{p}_e(x_e^t - W_{\text{dn,w},e}^t) \quad \forall e \in \mathcal{P}, t \in \mathcal{T}, \quad (5.37)$$

$$R_{\text{dn,p},e}^t = p_e^t - \hat{p}_e^t(x_e^t - W_{\text{dn,p},e}^t) \quad \forall e \in \mathcal{P}, t \in \mathcal{T}, \quad (5.38)$$

$$R_{\text{up,w},e}^t = \hat{p}_e^t(x_e^t + W_{\text{up,w},e}^t) - p_e^t \quad \forall e \in \mathcal{P}, t \in \mathcal{T}, \quad (5.39)$$

$$R_{\text{up,p},e}^t = \hat{p}_e^t(x_e^t + W_{\text{up,p},e}^t) - p_e^t \quad \forall e \in \mathcal{P}, t \in \mathcal{T}, \quad (5.40)$$

where the function $\hat{p}_e(x_e^t)$ returns the power consumption of pump e for the flow rate x_e^t . Again, since p_e^t and power deviations are identical in each phase, we do not specify the phase. In contrast to Option 2, there is a nonlinear mapping between the pump adjustments and the flexibility cost, and so using this cost option makes the problem more difficult to solve. Specifically, Option 3 requires (5.33)-(5.34) and (5.37)-(5.40); however, the latter are nonconvex. We replace them with their convex hulls as in Section 5.3.2; however, $\mathbf{R}_{\text{dn,p}}^t$ and $\mathbf{R}_{\text{dn,w}}^t$ will be inexact, leading to a reduced downwards flexibility band.

We discuss the trade-offs associated with these options in Section 5.4.5.

5.3.8. Chance-constrained Optimization

To formulate the full chance-constrained optimization problem, we first write the stochastic counterparts of the deterministic equality constraints (5.3)-(5.4), (5.10)-(5.12), (5.15b), (5.18)-(5.20), (5.22) and inequality constraints (5.7), (5.9), (5.13)-(5.14), (5.16), (5.21a)-(5.21b), (5.23a)-(5.23b) replacing $\rho_{k,\phi}^t$ with $\rho_{k,\phi}^t + \tilde{\rho}_{k,\phi}^t$ and d_j^t with $d_j^t + \tilde{d}_j^t$. For flexibility cost Option 1, the full set of stochastic constraints comprise these constraints along with (5.24), (5.25), (5.27), and (5.28). Options 2 and 3 require additional constraints defined in the

previous subsection. Eliminating the stochastic equality constraints through substitutions into the stochastic inequality constraints, the stochastic inequality constraints can be put into the form $f(\mathbf{x}_2, \mathbf{c}_w, \mathbf{C}_p, \tilde{\mathbf{d}}, \tilde{\boldsymbol{\rho}}) \leq 0$ and then transformed into a chance constraint

$$\mathbb{P} \left(f(\mathbf{x}_2, \mathbf{c}_w, \mathbf{C}_p, \tilde{\mathbf{d}}, \tilde{\boldsymbol{\rho}}) \leq 0 \right) \geq 1 - \epsilon, \quad (5.41)$$

where the constraints should be satisfied jointly for a probability level of at least $1 - \epsilon$, where ϵ is the violation level. WDN constraints within the chance constraint are the hydraulic head limits and pump flow rate limits. Because tanks are passive, tanks act to maintain water balance when pump flow rate limits are encountered. PDN constraints within the chance constraint correspond to the voltage limits. Therefore, the chance constraint limits the probability of a hydraulic head, pump flow rate, or voltage violation. Finally, we can write the chance-constrained optimization problem. For example, for flexibility cost Option 1, the problem is

$$\begin{aligned} \min_{\mathbf{x}_2, \mathbf{c}_w, \mathbf{C}_p} \quad & \sum_{t \in \mathcal{T}} (F^t(\mathbf{x}_2) + g_w^t J_w^t + g_p^t J_p^t) \\ \text{s.t.} \quad & (5.3) - (5.4), (5.7), (5.9) - (5.14), \\ & (5.15b), (5.16), (5.18) - (5.23b), \\ & (5.26), (5.41), \\ & G_{w,1}^t \leq J_w^t \quad \forall t \in \mathcal{T}, \\ & G_{p,1}^t \leq J_p^t \quad \forall t \in \mathcal{T}, \end{aligned} \quad (\text{CCO})$$

where slack variables J_w^t and J_p^t are upper bounds on the flexibility costs. Since these variables are minimized, the optimal solution will be to set them equal to G_w^t and G_p^t .

We solve this problem using the scenario approach for convex problems [17] for a number of reasons. First, the uncertainty impacts the constraints in complex ways and it is not clear how to analytically reformulate the constraints using known uncertainty distributions. Second, we are unlikely to know the uncertainty distributions in practice and the scenario approach does not require this information. Third, the scenario approach gives us a way to enforce the constraints jointly, rather than individually as is typical with approaches that rely on analytical formulation. A drawback of the scenario approach is that it requires a significant amount of data. Additionally, it is often very conservative in practice [125], leading to empirical violation probabilities much lower than the user-selected violation level ϵ and,

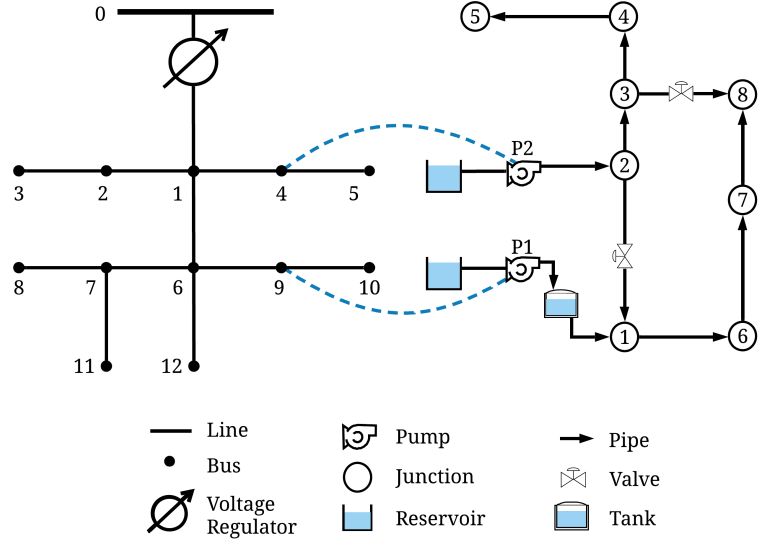


Figure 5.3: Coupled power (left) and water (right) distribution network. The dashed lines show where the water supply pumps are connected to the PDN. The water tank is passive. We show the single-phase equivalent PDN but we used a three-phase unbalanced network model. The pumps are modeled as balanced three-phase loads.

subsequently, higher costs. Specifically, in the approach, the constraints are enforced for a large set of uncertainty realizations resulting in a large convex deterministic optimization problem. The number N of scenarios required for probabilistic reliability guarantees is determined based on a user-selected violation level ϵ and confidence level ψ [17]

$$N \geq \frac{2}{\epsilon} \left(\ln \frac{1}{\psi} + \delta \right), \quad (5.42)$$

where δ is the number of decision variables in the optimization problem. In our case, the probabilistic guarantees apply to the convex (approximate and relaxed) problem, not the nonconvex problem. While there are some related approaches and results for nonconvex problems, they do not appear to apply directly to the form of our nonconvex problem.

5.4. Case Studies

In our case studies, we use the coupled WDN and PDN shown in Fig. 5.3, which we also used in Chapter 4. We first describe the set up and then present and interpret the results. Additionally, we explore the impact of the convex relaxations on the WDN constraints, an

approach to reduce the dimension of our power control policy parameters, and the choice of the flexibility cost formulation.

5.4.1. Set Up

The WDN was originally presented in [21]; it is based on an actual WDN. We have modified it to include a cylindrical storage tank (25 – m diameter, 30 – m height, 30 – m elevation), removed the booster pump, and converted the resistance coefficients from Hazen-Williams coefficients to Darcy-Weisbach coefficients. We changed the elevations at junction 6 and the reservoir upstream of pump 1 to 10 m and the minimum pressure heads at junctions 7 and 8 to 20 m. The pump hydraulic function coefficients are $m_{e=1}^0 = 75$ m and $m_{e=1}^1 = 0.005 \frac{\text{h}}{\text{m}^2}$ for pump 1 and $m_{e=2}^0 = 90$ m and $m_{e=2}^1 = 0.001 \frac{\text{h}}{\text{m}^2}$ for pump 2. We set $\beta_\phi = 2.322 \times 10^{-3} \text{ kW/CMH} \cdot \text{m } \forall \phi \in \Phi$.

The unbalanced three-phase PDN uses the IEEE 13-bus feeder topology, where the real power load and line parameters are from [52]. We assume that all loads are wye-connected and constant power. Consumer loads have a 0.9 lagging power factor and pumps have a real-to-reactive power ratio of 3 (i.e., a 0.949 lagging power factor). The distributed load between buses 1 and 6 is placed at bus 1. The minimum and maximum voltage limits are 0.95 pu and 1.05 pu. We set the voltage at the feeder head equal to 4.16 kV line-to-neutral. We assume the switch is closed and ignore the voltage regulator, shunt admittances, and the transformer between buses 4 and 5. Since we have no voltage regulator, we add capacitive loads (i.e., reactive power injections) to increase the system voltages: 100 kVAr at bus 8, phase c and 200 kVAr at bus 10, all phases. For the base case power control policy, each pump has 17 control policy parameters corresponding to the number of buses and phases that have a load present.

We set the price of electricity to \$100/MWh for all pumps and time periods in the scheduling horizon. We set the flexibility cost weighting coefficients g_w^t and g_p^t to 1 or **1**, where the latter is a row vector of ones and the units are selected to ensure that the flexibility costs are in \$ (specifically, the units of g_w^t , g_p^t are [\$], $[\$ \cdot \text{kW}^2/\text{CMH}^2]$ for Option 1; $[\$/\text{CMH}]$ for Option 2; and $[\$/\text{kW}]$ for Option 3). We conduct a sensitivity analysis to study the impact of varying g_w^t and g_p^t in Section 5.4.5. Unless otherwise stated, we use flexibility cost Option 1 to generate our results; however, Section 5.4.5 compares all options. We set the chance constraint confidence level $\psi = 10^{-4}$ and vary ϵ .

To generate water and power demand forecast error scenarios, we draw samples from

Table 5.1: Case Studies

Case	Number of Periods	Demand Multipliers		Required Scenarios
		Water	Power	
A	1	1.00	1.50	4,369
B	3	[1.00,1.00,1.00]	[1.50,1.50,1.50]	13,107
C	3	[1.00,0.85,0.65]	[1.50,1.45,1.35]	13,107

Gaussian probability distributions that are truncated at three standard deviations from the mean. For water demand forecast errors \tilde{d}_j^t , we use a mean of 0 and a standard deviation of $0.10\tilde{d}_j^t$. For power demand forecast errors, we use a mean of 0 and a standard deviation of $0.04\rho_{k,\phi}^t$. We do not model correlations in water and power demand forecast error, correlations across time, or correlations across space. While we would not expect actual forecast errors to be Gaussian and uncorrelated, these simplistic assumptions allow us to demonstrate how the approach works. Importantly, the approach works for forecast errors following any distribution and with any correlations; if sufficient amounts of real data were available, we could use it directly within our formulation.

We solve the problem with the JuMP package in Julia using the Gurobi solver [42]. We use a 64-bit Intel i7 dual core CPU at 3.40 GHz and 16 GB RAM.

To evaluate the reliability of our solutions, we use the Monte Carlo method to test whether all WDN and PDN constraints are satisfied for each of the 100,000 randomly-generated uncertainty realizations. We draw these realizations from the same water and power demand forecast error probability distributions as we used to generate the scenarios needed to reformulate the chance-constrained optimization problem. We use the realizations to compute the real-time control actions. The empirical violation probability is defined as the percentage of realizations for which at least one constraint is not satisfied.

5.4.2. Illustrative Results

We conduct three case studies described in Table 5.1. The water and power demand multipliers are used to modify the nominal water and power demands uniformly across all junctions in the WDN and all buses in the PDN. When expressed as a vector, each entry corresponds to one time period. We also report the number of forecast error scenarios required by the scenario approach when $\epsilon = 5\%$.

Fig. 5.4 shows the pump/tank scheduled flow rates corresponding to the chance-constrained problem (CCO) presented in Section 5.3.8 versus the convex deterministic problem (D3) pre-

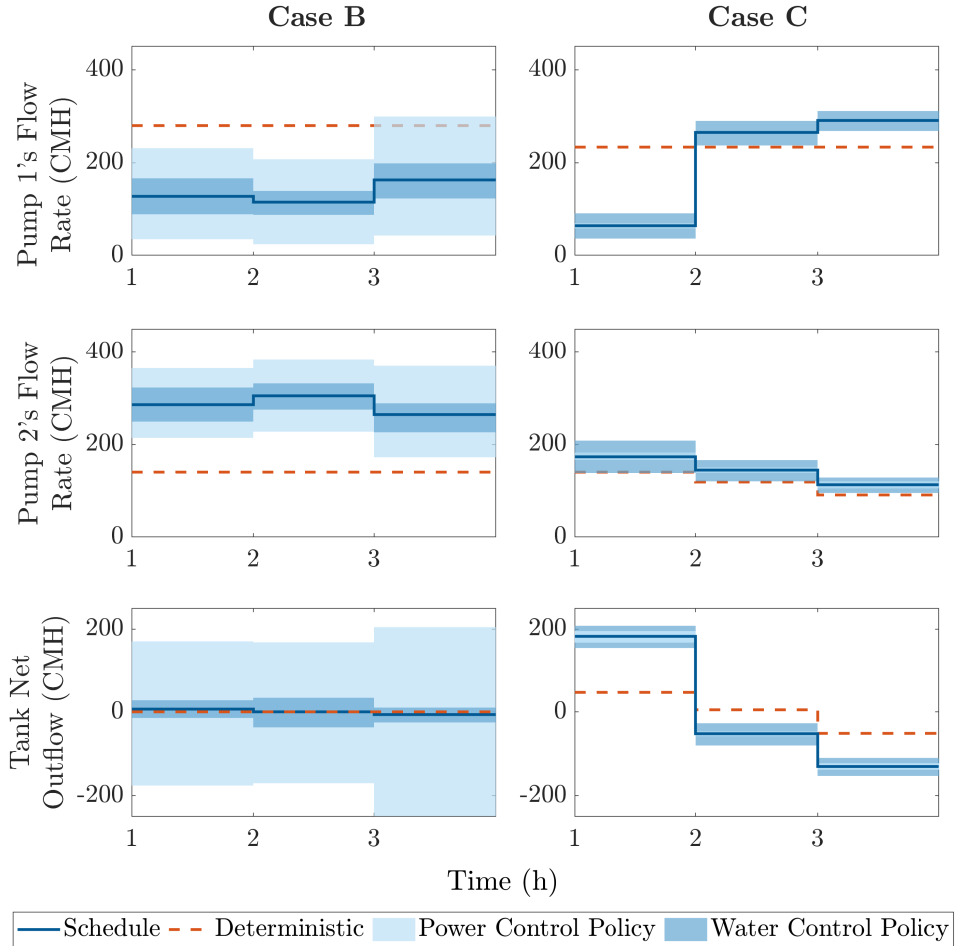


Figure 5.4: Pump and tank schedules for Case B, $\epsilon = 5\%$ (left) and Case C, $\epsilon = 5\%$ (right). Dark and light blue shading show the flexibility bands around the scheduled flow rate associated with the water and power control policy, respectively. The schedule obtained from solving the deterministic problem is also shown.

sented in Section 5.3.5 for Case B, $\epsilon = 5\%$ (left) and Case C, $\epsilon = 5\%$ (right). Case B has constant high water and power demand whereas Case C has decreasing water and power demand. The figure also shows the flow rate flexibility bands associated with the water and power control policies, which can be calculated using (5.33) and (5.34), respectively. The flexibility bands are set to the largest pump flow adjustments and tank net outflow deviations obtained by applying the control policies to the forecast error scenarios used to solve (CCO). The empirical violation probabilities are 0.13% for Case B and 0.16% for Case C, both much smaller than ϵ .

We observe that the pump and tank schedules obtained from (CCO) vary more from period to period than those obtained from (D3). This is necessary to ensure that the forecast error scenarios do not lead to violations of the PDN constraints. Pump 1 is more efficient (and thus less expensive) than pump 2. However, pump 1 is located at bus 9, which is closer to its minimum voltage limit than bus 4 (where pump 2 is located). In order to satisfy the voltage constraints corresponding to the scenarios in Case B, pump 1's scheduled flow rate is lower than that obtained from solving the deterministic problem while pump 2's scheduled flow rate is higher than that obtained from solving the deterministic problem. This results in a more expensive operating point.

In Case C, pump 1's and the tank's schedules vary more from period to period than in Case B. Specifically, in Case C, when the power demand is highest (period 1), pumping is reduced and the tank is used to meet a significant portion of the water demand in order to satisfy the voltage constraints corresponding to the scenarios. Later, when demands are lower, extra pumping is used to refill the tank. In each period the system is operating far from the PDN constraints; in the first period, this is because of the reduction in pumping, and in subsequent periods, this is because of the reduction in water and power demand. Therefore, the power control policy parameters and associated flexibility bands are extremely small. In contrast, in Case B, there is less opportunity for pump load shifting and tank usage due to the high constant demands. Further, the optimal schedule results in an operating point much closer to the PDN constraints, requiring much larger power control policy parameters and resulting in much larger flexibility bands. In both cases, we find that the flexibility bands associated with the water control policy remain approximately constant. This is expected since the water control policy is balancing water supply and demand.

Fig. 5.5 displays the pump flow rate adjustments from the schedule for Case A, $\epsilon = 3\%$. They are obtained by applying the water control policy, power control policy, and both control policies to the 100,000 water and power demand forecast error realizations used to

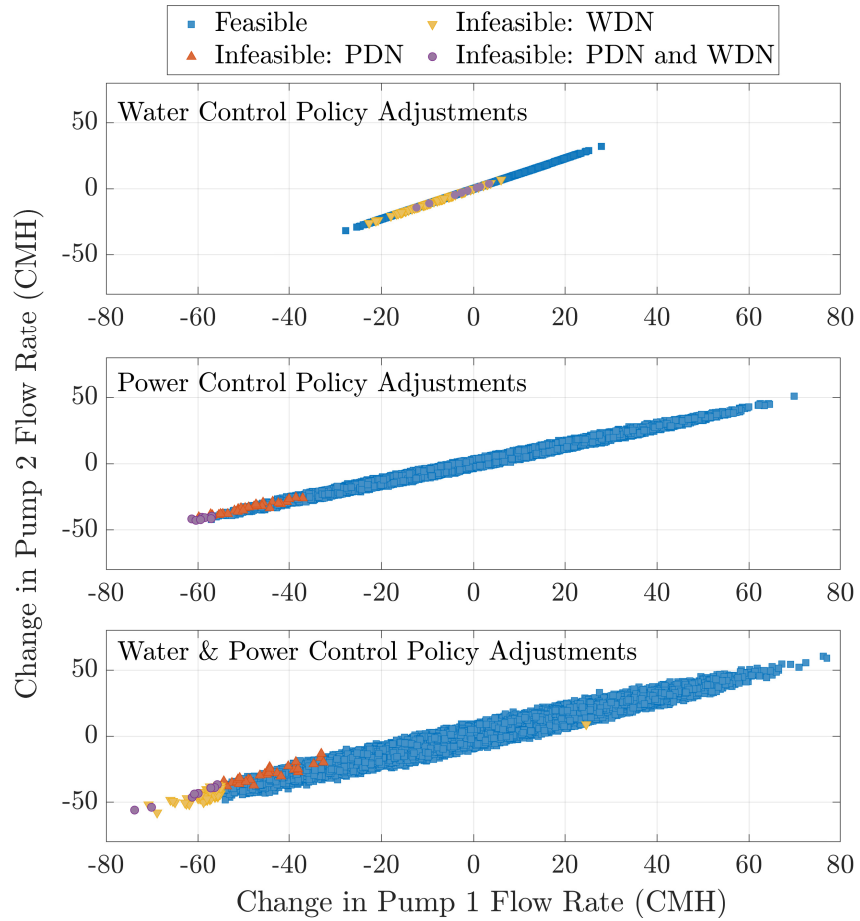


Figure 5.5: Feasible and infeasible pump flow rate adjustments given water and power demand uncertainty for Case A, $\epsilon = 3\%$.

calculate the empirical violation probabilities. We differentiate between actions that i) satisfy WDN and PDN constraints, ii) satisfy WDN constraints but violate PDN constraints, iii) satisfy PDN constraints but violate WDN constraints, and iv) violate both WDN and PDN constraints. The overall empirical violation probability is 0.11%, which is much smaller than the ϵ we have selected. Of the set of realizations that violate any constraints, only 7.27% violate both WDN and PDN constraints. From the figure, we can also see that pump 1's adjustments are usually larger than pump 2's. This is because its power control policy parameters are larger (also visible in Fig. 5.4). Pump 1 has a more direct impact on PDN constraint satisfaction since it is located at bus 9, which is closer to its minimum voltage limit than bus 4 (where pump 2 is located). To visualize this, in Fig. 5.6 we plot the relative magnitude of each pump's negative power control policy parameters per bus and per phase on the PDN's three-phase voltage profile. The significant voltage unbalance is due to uneven, heavy loading. The power control policy generally contains both negative and positive parameters. Given an increase in power demand, a negative parameter reduces the pump's flow rate and power consumption to respond to a minimum voltage limit violation, while a positive parameter increases the pump's flow rate to maintain the water supply. Therefore, by only showing the magnitude of the negative parameters, we can see the buses and phases where an increase in load is most likely to cause voltage limit violations, and which pump needs to reduce its power consumption more. We observe that pump 1's negative parameters always have a larger magnitude (and therefore a larger pump flow rate adjustment) than pump 2's negative parameters. Additionally, the control policy parameters associated with phase c are the largest since the voltages are close to the minimum voltage limit on phase c .

Next, we investigate how the water control policy parameters differ when we include only water demand uncertainty versus both water and power demand uncertainty. Fig. 5.7 shows the water control policy parameters for Case A, $\epsilon = 3\%$. With only water demand uncertainty, pump 1's scheduled flow rate is higher than that of pump 2 and pump 1 contributes more to balancing water demand forecast error. However, with both water and power demand uncertainty, the solution becomes more conservative, i.e., pump 1 reduces its flow rate and its contribution to water balancing. In our case studies, we find that power demand forecast error has a larger impact on the optimal schedules; however, it may have a larger or smaller impact than water demand forecast error on real-time pump adjustments, as shown in Fig. 5.4.

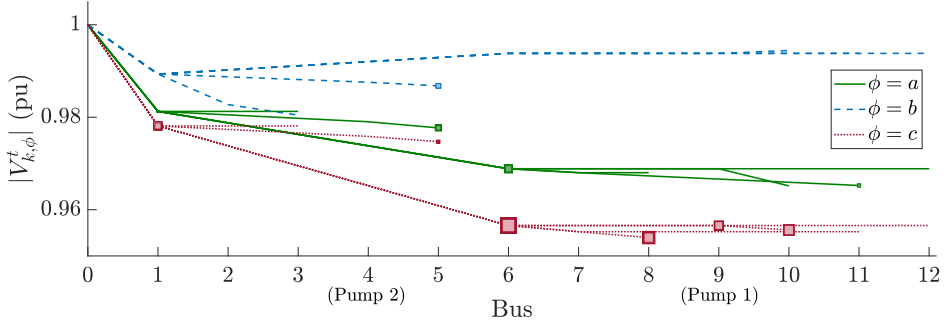


Figure 5.6: Three-phase PDN voltage profile for the schedule in Case A, $\epsilon = 3\%$. The square markers at each bus and phase are scaled according to the magnitude of the power control policy parameters. The dark squares represent pump 1's control policy parameters. The overlaying light squares correspond to pump 2's control policy parameters.

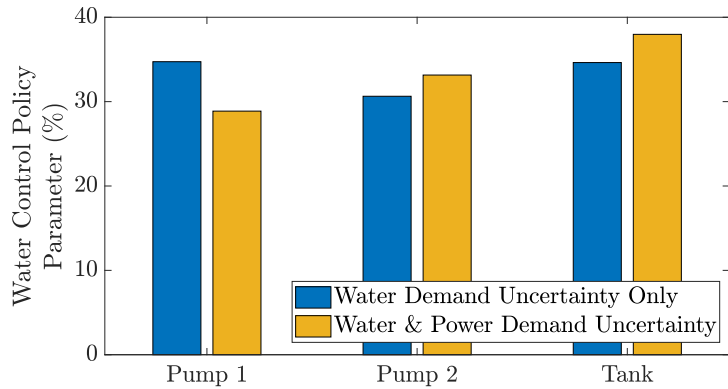


Figure 5.7: Water control policy pump and tank contribution given (i) only water demand uncertainty and (ii) water and power demand uncertainty for Case A, $\epsilon = 3\%$.

5.4.3. Impact of Convex Approximations and Relaxations

In this section, we first analyze the impact of i) the convex hull relaxation of the pipe head loss equation, ii) the approximate (linearized) pump hydraulic function, and iii) the convex hull relaxation of the pump power consumption curve. Considering only water demand uncertainty, we solve two variants of (CCO). The first replaces the pipe head loss convex hull (5.21a)-(5.21b) with the original nonconvex head loss constraint (5.15c) where $n = 2$. The second replaces the linearized pump hydraulic function (5.22) with a quadratic one, where the quadratic coefficients for pump 1 and 2 are $-1.0941 \times 10^{-4} \frac{\text{h}}{\text{m}^2}$ and $-1 \times 10^{-5} \frac{\text{h}}{\text{m}^2}$, respectively. We solve both variants with the scenario approach using the same number of scenarios as needed for the convex formulation. However, since neither variant is convex, the scenario approach solution no longer comes with probabilistic guarantees.

Table 5.2 shows the scheduled pump flow rates and the hydraulic heads for Case A, $\epsilon = 5\%$ for (CCO) and both variants. (CCO) finds the same scheduled pump flow rates as the variant using the quadratic pipe head loss equation. However, the hydraulic heads obtained using the quadratic pipe head loss equation are all greater than or equal to the heads found in (CCO) since the actual head loss is the lower bound of the convex hull's feasible region, shown in Fig. 5.2. Since we are primarily concerned with minimum hydraulic head limits, use of the convex hull ensures that the solution does not violate those limits. While the hydraulic heads found using the convex hull of the pipe head loss are not exact, in our case studies we found that we can recover the exact hydraulic heads; however, this may not always be possible. In [107], the authors prove uniqueness of the water flow equations for radial networks and certain meshed networks, e.g., WDNs that have meshed network sections that do not contain pumps or valves, and meshed network sections with pumps that are not in cycles. They recovered the hydraulic heads by solving a convex energy minimization problem given the pump flow rates. While their proof does not extend to meshed networks containing pressure reducing valves, like ours, the solutions to our case studies appear unique and we are able to recover the heads corresponding to the quadratic pipe head loss equation in Table 5.2.

Table 5.2: Relaxation and Approximation Comparison

Formulation (CCO)	Scheduled Flow		Head (m)						Tank Head (m)			
	Pump 1	Pump 2	1	2	3	4	5	6	7	8	Inlet	Outlet
Quadratic pipe head loss equation	248.80	171.20	44.43	95.17	94.57	91.71	89.93	29.96	31.86	41.38	86.24	45.00
Quadratic pump hydraulic function	248.88	171.12	44.43	94.88	94.09	91.34	89.65	30.51	32.65	41.55	79.47	45.00

The linear pump hydraulic function overestimates the head gain and power consumption of the pumps. As a result, (CCO) overestimates hydraulic heads at junctions downstream of pumps. Components such as storage tanks and pressure reducing valves act as buffers, helping to correct the downstream hydraulic heads. For example, the outlet tank head is dependent on the tank water level; even if there is a difference in the inlet hydraulic head between (CCO) and the variant with the quadratic pump hydraulic function, the outlet head is identical for both formulations. We find that the formulations produce similar scheduled pump flow rates and slightly different hydraulic heads (see Table 5.2). As expected, the inlet tank head obtained using the quadratic pump hydraulic function is lower than that obtained from (CCO). The outlet tank heads are identical. Additionally, the hydraulic heads for junctions 2-5 are smaller when we use the quadratic pump hydraulic function since (CCO) overestimates pump 2's head gain.

The convex hull relaxation of the pump power consumption curve (5.23a)-(5.23b) does not impact the solution. This is because, when minimizing the WDN's electricity cost, the solution will lie on the lower bound of the convex hull, i.e., the original constraint (5.17).

Lastly, we used the Monte Carlo method to evaluate the performance of the solutions of (CCO) within both the convexified network constraints and the original, nonconvex network constraints. Table 5.3 shows the empirical violation probabilities for each case and violation level. The nonconvex constraints are violated much more frequently than the convex constraints. All scenarios that violate the convex constraints also violate the nonconvex constraints. The additional violations of the nonconvex constraints are all voltage limit violations, indicating that the WDN approximations and relaxations are reasonable for this test system. We summarize the statistics of the additional voltage violations in the last two columns of the table, which show the minimum and average of the set of voltages below the minimum voltage limit corresponding to scenarios that violate the nonconvex constraints, but not the convex constraints. The minimum is just below the 0.95 pu minimum voltage limit indicating that the convex PDN model slightly overestimates the minimum voltages, as also shown in Fig. 5.8. We find that the difference between the actual voltage and the voltage calculated using the convex model (again, considering only the voltages that violate the nonconvex constraints, but not the convex constraints) is always less than or equal to 0.33%. Therefore, a simple way to cope with this issue would be to heuristically adjust the minimum voltage limit in the convex formulation to 0.955 pu. Alternatively, one could use a more accurate convex PDN power flow model, e.g., one that includes loss approximations. For example, using the linearized, unbalanced three-phase power flow formulation

Table 5.3: Empirical Violation Probabilities for Convex and Nonconvex Constraints

Case	ϵ (%)	Probability (%)		Voltage Violations (pu)	
		Convex	Nonconvex	Minimum	Average
A	5	0.11	10.98	0.94717	0.94937
	3	0.11	10.98	0.94717	0.94940
B	5	0.12	35.16	0.94693	0.94935
	3	0.10	34.29	0.94697	0.94937
C	5	0.13	5.41	0.94732	0.94943
	3	0.05	4.23	0.94724	0.94944

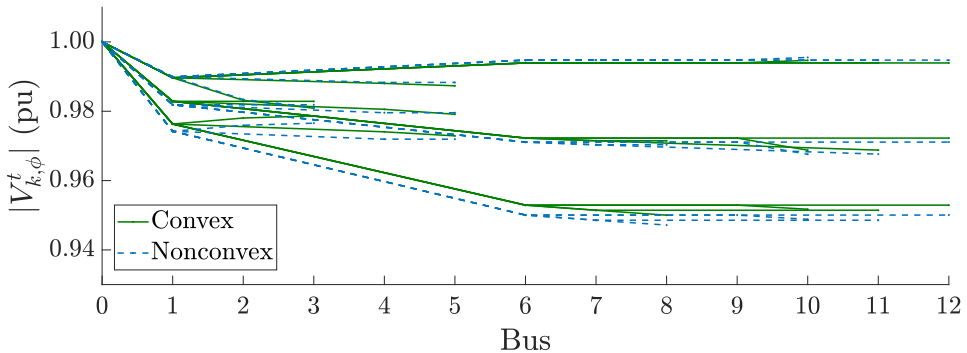


Figure 5.8: Comparison of the three-phase PDN voltage profile corresponding to the approximate, convex power flow model and the original, nonconvex power flow model for a scenario in Case A, $\epsilon = 5\%$.

with approximated losses from [100] instead of the lossless formulation from [3] on Case A, $\epsilon = 5\%$, and with the power demand multiplier reduced from 1.500 to 1.465, we find that the empirical nonconvex violation probability decreases from 5.354% to 0.210%. Note that we reduced the multiplier because Case A was tuned to represent extreme conditions and so the problem was infeasible with the power flow formulation with approximated losses.

These observations call attention to the fact that our approach gives us no insight into or way to manage the magnitude or duration of constraint violations. This is a drawback of the type of chance constraint we are using. In future work, we plan to explore alternative formulations that allow us to model and control constraint violations in a way that better matches the application-specific needs of the system, e.g., allowing deviations but assigning a cost related to the magnitude of the deviation, or allowing deviations for a limited time duration.

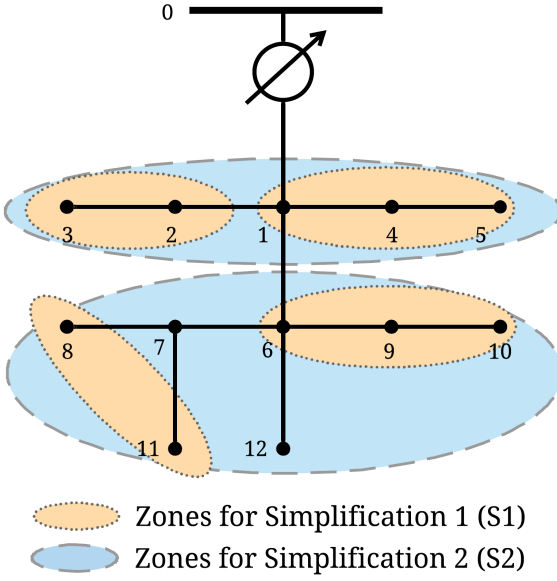


Figure 5.9: Grouping of buses associated with power control policy parameters for simplification 1 (S1) and simplification 2 (S2).

5.4.4. Simplifying the Power Control Policy

In this section, we investigate the impact of reducing the number of power control policy parameters to improve the computational tractability of our approach. The power control policy (5.27) uses a separate control policy parameter for each bus and phase with a load present, resulting in up to $3|\mathcal{K}|$ power control policy parameters. We refer to this as the *base case*. Here, we explore associating control policy parameters with groups of buses e.g., all buses on a lateral. To compute the control action, the control policy parameter is multiplied by the sum of power demand forecast errors in that group. With fewer control policy parameters, we need fewer scenarios since the number of scenarios is a function of the number of decision variables; this improves the computational tractability of the approach. Further, this approach requires fewer measurements and simpler communication systems, which would reduce the implementation costs. We consider two *simplifications*, referred to as simplification 1 (S1) and simplification 2 (S2). Fig. 5.9 shows the groups of buses, referred to as zones, used for S1 and S2. We do not group phases. For example, in S2 there are two zones but six control policy parameters, one for each phase in each zone. We solve the base case and cases corresponding to both simplifications for Case A using flexibility cost Option 2

Table 5.4: Power Control Policy Simplification Results

	Zones	Parameters per Pump	ϵ (%)	Scenarios	Solver Time (s)	Energy Cost (\$)	Flexibility Cost	Violation Probability (%)
Base Case	9	17	10	2,145	18.48	25.304	142.211	0.131
			5	4,289	29.95	25.304	145.581	0.116
			3	7,148	68.89	25.304	154.412	0.080
S1	4	9	10	1,825	7.49	25.304	155.925	0.135
			5	3,649	16.50	25.304	156.346	0.098
			3	6,081	29.83	25.304	158.751	0.056
S2	2	6	10	1,705	4.32	25.304	160.558	0.081
			5	3,409	14.47	25.304	162.684	0.066
			3	5,681	20.71	25.304	163.400	0.064

and considering only power demand uncertainty. We choose flexibility cost Option 2 instead of Option 1 so that the flexibility costs are comparable across the cases. Flexibility cost Option 1 uses the Frobenius norm of the power control policy parameter matrix, which is a different size in each case, meaning the costs are not comparable across cases.

Table 5.4 shows the results including the number of power control policy parameters per pump and the number of scenarios for different values of ϵ . The table also reports the solver time, the energy cost associated with the schedule, the flexibility cost associated with the power demand control policy, and the empirical violation probability. As expected, the solver time generally decreases with fewer zones, meaning fewer decision variables and fewer scenarios. We expect the reduction in solver time would be more important in larger networks and/or for problems with longer scheduling horizons. Investigating other methods to improve the computational tractability of our approach is discussed in Chapters 6 and 7.

In this case study, we find that S1 and S2 generally have lower empirical violation probabilities and higher objective costs than the base case. The base case has more degrees of freedom than S1 or S2 and so it is less conservative and lower cost. The control policy parameters associated with the simplifications cause coarser, larger, and more costly adjustments, which are more likely to be feasible against unseen scenarios. All cases have empirical violation probabilities much lower than ϵ , demonstrating that the scenario approach is conservative, which is typical [125]. Further, all approaches produce the same schedule and energy costs. The base case has the lowest flexibility cost (i.e., it makes the smallest pump/tank adjustments to respond to power demand forecast errors) while satisfying the desired violation level ϵ , and therefore it exhibits the best cost/performance trade-off.

Table 5.5: Flexibility Cost Comparison

Option	Simplification	Solver	Energy	Scheduled Flow Rate (CMH)		Flexibility Cost		Violation Probability (%)
		Time (s)	Cost (\$)	Pump 1	Pump 2	Water	Power	
1	Base Case	38.04	25.64	77.55	342.34	0.34	1.19	0.109
	S1	17.95	24.82	160.01	259.99	0.33	1.24	0.044
2	Base Case	52.52	25.28	113.62	306.38	130.20	177.00	0.216
	S1	32.75	25.26	115.64	304.36	143.35	177.00	0.175
3	Base Case	252.28	25.31	110.95	309.06	0	76.54	0.117
	S1	73.29	25.31	110.95	309.06	0	82.32	0.096

5.4.5. Comparison of Flexibility Cost Formulations

In this section, we explore the advantages and disadvantages of the three flexibility cost formulations presented in Section 5.3.7. We evaluate each flexibility cost formulation using Case A, $\epsilon = 5\%$ and present the results in Table 5.5 for both the base case and simplification S1. We report the solver time, energy costs associated with the schedule, the scheduled flow rates, the flexibility costs associated with the water control policy and the power control policy, and the empirical violation probabilities, which are all much lower than ϵ .

Option 1 has the smallest solver time, but it is difficult to interpret the flexibility costs and determine the weighting coefficients g_w^t and g_p^t such that the flexibility costs can be fairly compared against the energy costs. Further, as mentioned above, the flexibility costs are not comparable across simplifications. In Table 5.5, we observe that the water flexibility cost is approximately 1/3, which implies that the three pumps/tanks were used approximately equally to compensate water demand forecast error, which is a direct result of the flexibility cost formulation.

In Fig. 5.10, we show how the choice of water and power flexibility cost weighting coefficients impact the scheduled energy cost, $G_{w,1}^t$, and $G_{p,1}^t$ for Case A, $\epsilon = 5\%$. Comparing the left and right plots, we see that as g_p^t increases, the scheduled energy cost increases and $G_{p,1}^t$ decreases. This trade-off is intuitive: as power flexibility becomes more expensive relative to the scheduled energy cost, $G_{p,1}^t$ is reduced but the schedule becomes more expensive. The water flexibility cost weighting coefficient g_w^t has a negligible impact on the scheduled energy cost and $G_{p,1}^t$, and a small impact on $G_{w,1}^t$ in Option 1. There are several reasons for this. The first is that the magnitude of $G_{w,1}^t$ is small relative to the other costs in the objective function. The second is that the water flexibility cost has a limited range given the nature of the water control policy and Option 1. Since the water control policy splits the response

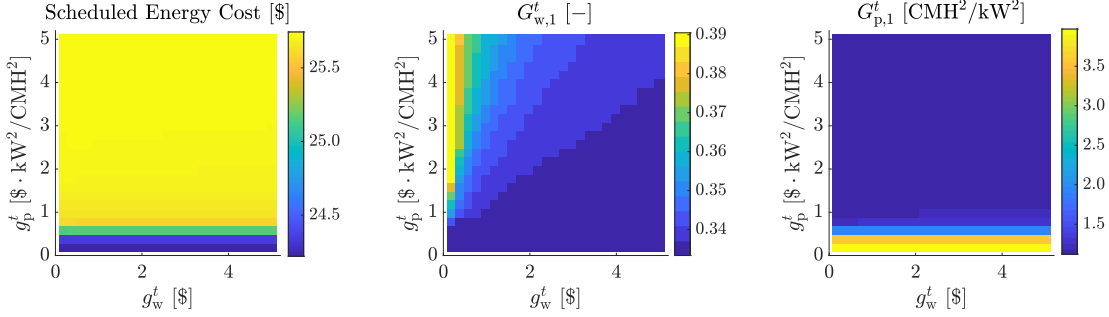


Figure 5.10: Sensitivity analysis showing how the scheduled energy cost, $G_{w,1}^t$, and $G_{p,1}^t$ change when varying the weighting coefficients g_w^t [\\$] and g_p^t [\\$·kW²/CMH²] for Case A, $\epsilon = 5\%$, and flexibility cost Option 1.

between 2 pumps and 1 tank, the feasible range of $G_{w,1}^t$ is $[\frac{1}{3}, 1]$, where $G_{w,1}^t = \frac{1}{3}$ when the split is equal. Changes in $G_{w,1}^t$ depend upon the magnitude of g_w^t relative to g_p^t , e.g., $G_{w,1}^t$ is large when g_p^t is large relative to g_w^t . This sensitivity analysis highlights that the weighting coefficients would need to be tuned for the system of interest.

Option 2 provides more intuition on the flexibility costs, which are based on the largest pump flow rate adjustment required to address the scenarios needed for the scenario approach. For example, in Table 5.5, we can see that the power control policy produces larger maximum flow rate deviations than the water control policy, for both the base case and S1. Similar to Option 1, it is difficult to determine weighting coefficients that allows us to fairly compare flexibility costs to energy costs.

Option 3 uses the largest increase and decrease in pump power consumption from the scheduled consumption to define the flexibility costs. An advantage of this approach is that the flexibility cost and the energy cost are both a function of pump power consumption. However, there are two disadvantages to this approach. First, Option 3 has the largest solver time. Second, $\mathbf{R}_{dn,p}^t$ and $\mathbf{R}_{dn,w}^t$ will be inexact when using convex hulls, leading to a reduced downwards flexibility band. Unlike the other flexibility cost options, Option 3 does not include tank flexibility costs since only pumps consume power. Therefore, the water control policy relies solely on the tank to balance water demand, and the water flexibility cost is 0, as shown in Table 5.5. By not including tank flexibility costs, there is no way to specify additional opportunity costs. However, tanks may be best equipped to respond to water demand forecast error since their purpose is to hedge against water demand variability [122].

Based on these results, it is not clear which flexibility cost option is best; however, Option 2 seems to exhibit good trade-offs between tractability and interpretability. Also, in contrast

to Option 3, it gives us a way to include the flexibility cost of the tanks.

5.5. Chapter Conclusion

In this chapter, we formulated a chance-constrained water pumping problem subject to water and power distribution network constraints given water and power demand uncertainty. We developed power and water control policies that can be used in real time to respond to forecast errors. Control policy parameters are included as decision variables in the chance-constrained optimization problem. We reformulated the problem using convex approximations and relaxations and solved it with the scenario approach. Case studies explored solution patterns, which were found to be conservative (i.e., highly reliable at a high cost), in addition to the impact of the approximations and relaxations, an approach to simplify the power control policy, and the impact of different flexibility cost formulations.

We found that temporal and spatial shifting of WDN pumping load can be used support the PDN. We also found that convex approximations and relaxations used for the WDN were reasonable in that scenarios that violated the nonconvex constraints also violated the convexified constraints. However, the convex PDN model overestimated the smallest voltages leading to a large difference in the empirical violation probabilities corresponding to the convex constraints and the nonconvex constraints. Fortunately, this is easy to fix (heuristically) by slightly increasing the minimum voltage limit. Further, we found that the approach is computationally heavy and does not currently scale to large networks or problems with long planning horizons. We proposed one way to simplify the power control policy, which reduces required measurements and also improves computational tractability, but results in more conservative solutions.

Chapter 6.

Tractable Uncertainty-Aware Methods for Leveraging Water Pumping Flexibility for Power Networks

In this chapter, we explore solution approaches and formulations to control the pump power consumption in water distribution networks (WDNs) in a computationally tractable way that can be scaled to large networks and problems with long time horizons. To do so, we leverage monotonicity properties to reformulate the problem as a computationally tractable affinely adjustable robust counterpart. Building upon robust and chance-constrained reformulation approaches, we develop an analytically reformulated probabilistic problem that manages uncertainty differently in the water and power network. We find that our proposed probabilistic approach is computationally tractable and is less conservative than the robust approach, indicating that our formulation would be scalable to larger networks. This chapter is based on [115] and [110].

6.1. Notation

Sets

\mathcal{E}	Set of pipes in the WDN (indexed by ij)
\mathcal{I}_k	Set of buses directly downstream of bus k in PDN (indexed by k)
\mathcal{J}	Set of junctions within the set of nodes in the WDN (indexed by j)

\mathcal{K}	Set of buses in the PDN (indexed by k)
\mathcal{N}	Set of nodes in the WDN (indexed by j)
\mathcal{P}	Set of pumps within the set of pipes in the WDN (indexed by ij)
\mathcal{P}_k	Set of pumps connected to bus k (indexed by ij)
\mathcal{R}	Set of reservoir nodes within the set of nodes in the WDN (indexed by j)
\mathcal{S}	Set of storage tanks within the set of nodes in the WDN (indexed by j)
\mathcal{T}	Set of time steps in the scheduling problem (indexed by t)
\mathcal{U}	Uncertainty set (indexed by ρ)
Φ	Set of phases in the PDN (indexed by ϕ)

Decision Variables

C_e^t	Control policy parameter row vector for pump e at time t (-)
H_j^t	Hydraulic head at node j and time t (m)
\tilde{H}_j^t	Auxiliary head variable for tank j at time t (m)
ℓ_j^t	Water level of tank j at time t (m)
p_e^t	Real-time single-phase real power demand of pump e at time t (kW)
$p_{\text{nom},e}^t$	Scheduled single-phase real power demand of pump e at time t (kW)
\mathbf{P}_k^t	Real power flow vector (all phases) entering bus k at time t (kW)
\mathbf{Q}_k^t	Reactive power flow vector (all phases) entering bus k at time t (kVAr)
$R_{\text{dn},e}^t$	Max. three-phase pump power decrease from the scheduled pump power consumption due to voltage support services for pump e and time t (kW)
$R_{\text{up},e}^t$	Max. three-phase pump power increase from the scheduled pump power consumption due to voltage support services for pump e and time t (kW)
x_{ij}^t	Volumetric flow rate of water through pipe ij at time t (CMH)
\mathbf{x}	Operational variables
\mathbf{y}	Adjustable variables
\mathbf{Y}_k^t	Three-phase voltage magnitude squared at bus k and time t (kV)
α_j^t	Connection status binary of tank j at time t (0,1)
β_j^t	Filling binary of tank j at time t (0,1)

Functions

$b_e(\cdot)$	Pump power consumption function
$F(\cdot)$	Cost function
$f_{ij}(\cdot)$	Head loss function for edge ij
$f^{-1}(\cdot)$	Inverse cumulative distribution function

$g_j(\cdot)$	Tank head function of tank j
$Y_{k,\phi}^t(\cdot)$	Voltage magnitude squared function at bus k , phase ϕ , and time t

Constraint Sets

$\mathcal{W}_1(\cdot)$	Power flow constraint set
$\mathcal{W}_2(\cdot)$	Voltage support constraint set
$\mathcal{W}_3(\cdot)$	Water flow constraint set
$\widehat{\mathcal{W}}_1(\cdot)$	Robust reformulation of power flow constraint set
$\widehat{\mathcal{W}}_2(\cdot)$	Robust reformulation of voltage support constraint set
$\widehat{\mathcal{W}}_3(\cdot)$	Robust reformulation of water flow constraint set
$\mathcal{W}_p(\cdot)$	Power flow and voltage support constraint set
$\mathcal{W}_w(\cdot)$	Water flow constraint set
$\Gamma_{\text{scheduled}}(\cdot)$	Deterministic WDN constraints given the scheduled pump power
$\Gamma_{\text{extreme}}(\cdot)$	Deterministic WDN constraints given the max. or min. pump power

Random Variables, ω

$\Delta\rho_{k,\phi}^t \in \Delta\rho^t$	Deviation in real power demand at bus k , phase ϕ , and time t (kW)
ρ_k^t	Real-time three-phase real power demand at bus k and time t (kW)
ζ_k^t	Real-time three-phase reactive power demand at bus k and time t (kVAr)

Parameters

d_j^t	Forecasted water demand of consumer j at time t (CMH)
\hat{h}_j	Elevation head of node j (m)
$H_{\min,j}$	Minimum pressure head for node j (m)
$H_{\max,j}$	Maximum pressure head for node j (m)
h_{ij}^1, h_{ij}^0	Pump power parameters for pump ij (h/m, kW)
k_{ij}	Resistance coefficient of pipe ij (h^2/m^5)
$\ell_{\min,j}$	Minimum water level in tank j (m)
$\ell_{\max,j}$	Maximum water level in tank j (m)
M	Large number in big-M method
\mathbf{M}_{kn}	Line parameter matrix formed from impedances for line kn (Ohms)
m_{ij}^1, m_{ij}^0	Quadratic pump hydraulic function parameters for pump ij
m_{ij}^3, m_{ij}^2	Linear pump hydraulic function parameters for pump ij
\mathbf{N}_{kn}	Line parameter matrices formed from impedances for line kn (Ohms)
V_{\min}	Minimum bus voltage magnitude limit (kV)
V_{\max}	Maximum bus voltage magnitude limit (kV)

$x_{\min,ij}$	Minimum flow rate of pump ij (CMH)
$x_{\max,ij}$	Maximum flow rate of pump ij (CMH)
ΔT	Duration of time period (h)
γ_j	Cross-sectional area of tank j (m^2)
ϵ_p	User-selected violation level in power flow component (%)
ϵ_w	User-selected violation level in water flow component (%)
η_e	Ratio between real and reactive power of pump e (-)
π_e^t	Forecasted energy price at time t for pump e at time t (\$/kWh)
$\pi_{vs,e}^t$	Voltage support capacity cost for pump e at time t (\$/kWh)
μ	Mean of power demand forecast error (kW)
Σ	Covariance of power demand forecast error (kW^2)
$\hat{\rho}_k^t$	Forecasted three-phase real power demand at bus k and time t (kW)
σ	Parameter to scale power demand forecast error (-)

6.2. Chapter Introduction

In this chapter, we consider optimizing water pumping to provide voltage support under power demand uncertainty. Specifically, we schedule and control supply pump power to ensure that bus voltages in the power distribution network (PDN) remain within their safe operating limits. In Chapter 5, we formulated a chance-constrained power-water optimization problem considering water and power demand uncertainty and solved it using the scenario approach [17]. One drawback of the scenario approach is that it requires a large amount of data and does not scale well to larger problems. In this chapter, we formulate the problem as an Adjustable Robust Optimization (ARO) problem and develop a solution approach to make the problem tractable by leveraging the monotonicity properties.

Monotonicity properties allow us to replace the semi-infinite water network constraints with two sets of deterministic network constraints representing the extreme operating scenarios. By doing so, we provide feasibility guarantees for the entire range of operating scenarios between the two extreme cases. To do this, we leverage the monotonicity properties of dissipative flow networks developed in [126]. This work was extended in [76] for transient gas network modeling and applied in an uncertainty management framework for an integrated gas-power problem in [98]. These papers focus on applying monotonicity properties to gas networks specifically. In this chapter, we show how the monotonicity properties of dissipative flow networks apply to WDNs and identify the water tank formulation assump-

tions required for monotonicity and the impact these assumptions have on the solution space. Using these properties, along with affine control policies and constraint approximations, we reformulated the problem as an Affinely Adjustable Robust Counterpart (AARC) that is much more scalable than our chance-constrained approach solved via the scenario approach. However, a drawback is that the robust problem tends to be excessively conservative.

To address this, we also propose a computationally tractable and less conservative probabilistic approach. Our approach combines a chance-constrained formulation to manage the uncertainty in the power distribution network and a probabilistically robust formulation to manage the impact of the PDN's uncertainty on the WDN. The formulation ensures that the real-time control actions satisfy the network constraints at a user-specified probability level. To achieve computational tractability, we assume uncertainty distributions are known and build upon the robust approach to analytically reformulate the probabilistic power and water constraints, resulting in a fast-to-solve deterministic problem. This enables application to large networks. The approach is much less conservative than robust approaches, but may perform poorly if assumed uncertainty distributions are inaccurate. We compare the performance (e.g., the computational time, cost, and empirical violation probabilities) of our approach with the robust approach and evaluate how practical these approaches would be when scaling the integrated PDN-WDN formulation to larger networks.

The contributions of this chapter are 1) formulating an ARO problem to schedule and control water pumping subject to PDN and WDN constraints and power demand uncertainty; 2) deriving water tank operation assumptions to ensure monotonicity properties hold for the WDN; 3) tractably reformulating the AARC using monotonicity properties, convex approximations, and affine control policies; 4) development of a tractable probabilistic formulation of the voltage support problem under power demand uncertainty subject to probabilistically robust WDN constraints and chance-constrained PDN constraints; and 5) exploration of the performance and computational trade-offs between the robust and probabilistic optimization methods in case studies.

The remainder of the chapter is organized as follows. Section 6.3 provides an overview of the robust optimization framework and network modeling. Sections 6.4 and 6.5 present the monotonicity properties and water flow approximations to get a tractable robust problem. The deterministic problem is presented in Section 6.6 as a point of comparison and we examine at the robust performance in a case study in Section 6.7. In Section 6.8, we propose a new probabilistic approach. We solve the robust and probabilistic approaches for a case study in Section 6.9 and compare their performances. Lastly, we provide concluding remarks

in Section 6.10.

6.3. Adjustable Robust Voltage Support Problem

We first present a robust formulation of the water pumping problem to provide voltage support. Our goal is to robustly optimize the water pump power consumption subject to the PDN and WDN constraints and power demand uncertainty. Specifically, we seek to determine the scheduled pump power consumption and the parameters of a control policy that determines the real-time pump power consumption adjustments so that the PDN voltage limit constraints are never violated over the scheduling horizon. This formulation can also be interpreted as an optimal power flow problem with water pumps acting as distributed energy resources where the WDN constraints further limit the feasible operation of the water pumps.

In this chapter, we do not consider water demand uncertainty. In Chapter 5, we simultaneously solved for two separate control policies to adjust pumping as a function of both water and power demand uncertainty. However, the tanks are already designed to hedge against water demand uncertainty [122] and we found that the range of tank flow rate adjustments remains approximately constant over time. Therefore, it is reasonable to assume that a portion of the tank is reserved for responding to water demand uncertainty considered in close-to-real-time operational planning problems (similar to how portions of tanks are reserved for emergency fire flow scenarios).

We first formulate the ARO problem as

$$\begin{aligned} \min_{\mathbf{x}} \quad & F(\mathbf{x}, \mathbf{y}(\boldsymbol{\rho}, \mathbf{x})) \\ \text{s.t.} \quad & \forall \boldsymbol{\rho} \in \mathcal{U}, \exists \mathbf{y}, \\ & \mathcal{W}_1(\mathbf{x}, \mathbf{y}(\boldsymbol{\rho}, \mathbf{x}), \boldsymbol{\rho}), \\ & \mathcal{W}_2(\mathbf{x}, \mathbf{y}(\boldsymbol{\rho}, \mathbf{x}), \boldsymbol{\rho}), \\ & \mathcal{W}_3(\mathbf{x}, \mathbf{y}(\boldsymbol{\rho}, \mathbf{x}), \boldsymbol{\rho}). \end{aligned} \tag{ARO}$$

The ARO is a multi-stage robust optimization problem containing random variable $\boldsymbol{\rho}$ in the uncertainty set \mathcal{U} , the operational ('here-and-now') variable \mathbf{x} which is feasible for all uncertainty realizations within the uncertainty set \mathcal{U} , and the adjustable ('wait-and-see') variable $\mathbf{y}(\boldsymbol{\rho}, \mathbf{x})$ which can be decided given a specific uncertainty realization [8]. In our

problem, the uncertainty $\boldsymbol{\rho}$ is the power demand at every bus and phase, the operational variable \mathbf{x} includes the scheduled pump power consumption, and the adjustable variable $\mathbf{y}(\boldsymbol{\rho}, \mathbf{x})$ includes the pump power consumption adjustment which is a function of the power demand forecast error. The constraint sets $\mathcal{W}_1(\cdot)$ and $\mathcal{W}_3(\cdot)$ contain the quasi-steady state PDN and WDN constraints (i.e., steady state operation for every time step of duration ΔT within the scheduling horizon \mathcal{T}). Function $\mathcal{W}_2(\cdot)$ links the WDN and PDN; specifically, it contains the real-time pump adjustments which impact both the power flow and water flow. The cost function $F(\cdot)$ includes the cost of the pump schedule and real-time adjustments.

ARO is less conservative than classic robust optimization problems because decisions can be updated in real-time [8]. Unlike a chance-constrained optimization problem in which the constraints must be satisfied at a specified probability, ARO constraints must be satisfied for all uncertainty realizations within the uncertainty set.

We next model the PDN $\mathcal{W}_1(\cdot)$ and the pump adjustments $\mathcal{W}_2(\cdot)$ which ensure that the minimum and maximum voltage limits are satisfied. Then, we present the basic form of the AARC. In the next section, we derive the WDN constraints $\mathcal{W}_3(\cdot)$ that limit the pump power consumption and present the full AARC.

6.3.1. Power Distribution Network Modeling

We first define $\mathcal{W}_1(\cdot)$. We consider an unbalanced, radial PDN that includes a set of buses \mathcal{K} and phases Φ to which the uncontrollable net loads (i.e., actual load minus distributed generation) and the controllable pumps are connected. To facilitate the derivation of the robust counterpart, we use a linearized power flow model, specifically, the three-phase unbalanced power flow model from [3, 34] also referred to as Lin3DistFlow. It should be noted that other linear three-phase unbalanced power flow models could be used, e.g., [9, 100]. Empirically, Lin3DistFlow and its variants perform very well. For example, [121] found that the voltage magnitude accuracy of Lin3DistFlow consistently outperformed a second order cone relaxation in a case study of 500 existing Belgium feeders. It is also possible that more accurate nonlinear three-phase unbalanced power flow models could be used; however, this would complicate our formulation and, since our focus is on the WDN, we leave this to future work. The power flow equations are [3]

$$\mathbf{P}_k^t = \boldsymbol{\rho}_k^t + \sum_{e \in \mathcal{P}_k} \mathbf{p}_e^t + \sum_{n \in \mathcal{I}_k} \mathbf{P}_n^t \quad \forall k \in \mathcal{K}, t \in \mathcal{T}, \quad (6.1)$$

$$\mathbf{Q}_k^t = \zeta_k^t + \sum_{e \in \mathcal{P}_k} \eta_e \mathbf{p}_e^t + \sum_{n \in \mathcal{I}_k} \mathbf{Q}_n^t \quad \forall k \in \mathcal{K}, t \in \mathcal{T}, \quad (6.2)$$

$$\mathbf{Y}_k^t = \mathbf{Y}_n^t - \mathbf{M}_{kn} \mathbf{P}_n^t - \mathbf{N}_{kn} \mathbf{Q}_n^t, \quad \forall k \in \mathcal{K}, t \in \mathcal{T}, \quad (6.3)$$

where (6.1) and (6.2) represent the active and reactive power balance at each node k and (6.3) represents the voltage drop across the line. The parameter \mathbf{Y}_k^t is the three-phase voltage magnitude squared at bus k and time t , \mathbf{P}_k^t and \mathbf{Q}_k^t are the three-phase real and reactive power flows entering bus k , \mathbf{M}_{kn} and \mathbf{N}_{kn} are the parameter matrices for line kn , ρ_k^t and ζ_k^t are the three-phase real and reactive uncontrollable power demand at bus k (load minus distributed generation), \mathbf{p}_e^t is the three-phase power consumption of pump e (where the pumps are modeled as balanced three-phase constant power loads with constant power factor), and \mathcal{I}_k is the set of buses directly downstream bus k . The set \mathcal{P}_k contains all pumps that are connected to bus k . The pump power consumption \mathbf{p}_e^t is zero if there are no pumps connected to bus k . The parameter η_e is the real-to-reactive power consumption ratio of pump e . Additionally, we want to ensure that the voltages at each bus k and phase ϕ are within their safe operating limits, i.e.,

$$(V_{\min})^2 \leq Y_{k,\phi}^t \leq (V_{\max})^2 \quad \forall k \in \mathcal{K}, \phi \in \Phi, t \in \mathcal{T}, \quad (6.4)$$

where parameters V_{\min} and V_{\max} are the lower and upper voltage magnitude limits.

6.3.2. Real-Time Pump Adjustments Responding to Uncertainty

We next define $\mathcal{W}_2(\cdot)$. The source of uncertainty is the real-time uncontrollable power demand vector $\rho^t := \hat{\rho}^t + \Delta\rho^t$, which is composed of the forecasted power demand $\bar{\rho}^t$ (a known parameter) and the uncertain but bounded forecast error $\Delta\rho^t := [\Delta\rho_{k,\phi}^t]_{k \in \mathcal{K}, \phi \in \Phi}$. We assume that water supply pumps in the WDN are adjusted according to a decision rule that is a function of $\Delta\rho^t$. Specifically, we define an affine pump power control policy and solve for the policy parameters as ‘here and now’ decisions. Using an affine policy allows us to represent the response of the system without needing to resolve the problem for each uncertainty realization. This makes it easier for water utilities to implement the control policy in real time. However, the use of an affine policy also restricts the feasible space, meaning that our solutions may be conservative. The control policy allows us to write the adjustable power variables (e.g., voltage magnitude squared) as affine functions of the

random variables. The real-time single-phase pump power consumption is

$$p_e^t = p_{\text{nom},e}^t + \mathbf{C}_e^t \Delta \boldsymbol{\rho}^t \quad \forall e \in \mathcal{P}, t \in \mathcal{T}, \quad (6.5)$$

where $p_{\text{nom},e}^t$ is the scheduled single-phase power consumption of pump e at time t , \mathbf{C}_e^t is a control policy parameter row vector that determines the single-phase adjustment of pump e at time t as a function of $\Delta \boldsymbol{\rho}^t$, and \mathcal{P} is the set of pumps. To implement this, the water system operator needs real-time data on the power demand forecast error at each bus and phase. While this may be unrealistic at the present time, this formulation and results point to the value of real-time pump adjustments; future work will explore whether this value outweighs the costs of the infrastructure needed to support it. Note that the pump power's phase is not specified since we assume the pumps are balanced loads and so p_e^t is the same in each phase.

We additionally assume that the cost of the real-time pump adjustments is a function of the adjustment range and define \mathbf{R}_{up} and \mathbf{R}_{dn} as the largest increase and decrease in pump power, i.e.,

$$-R_{\text{dn},e}^t \leq 3\mathbf{C}_e^t \Delta \boldsymbol{\rho}^t \leq R_{\text{up},e}^t \quad \forall e \in \mathcal{P}, t \in \mathcal{T}, \quad (6.6a)$$

$$R_{\text{up},e}^t, R_{\text{dn},e}^t \geq 0 \quad \forall e \in \mathcal{P}, t \in \mathcal{T}, \quad (6.6b)$$

where we multiply the single-phase pump power adjustment by three to get the total three-phase power demand.

6.3.3. Basic Form of the AARC

The objective function minimizes the cost of the scheduled pump power and the cost associated with adjusting the pump power in real time (e.g., the wear-and-tear on the pumps from more frequent and larger magnitude real-time pump adjustments). It is unclear how to best represent the real-time pump power cost; Chapter 5 explored several options. However, if pump wear-and-tear is affected by the magnitude of the pump adjustments, then it is reasonable to incorporate the real-time voltage support capacity into the cost function. The cost, which is now only a function of the operational variables, can be written as

$$F(\mathbf{x}) = \sum_{t \in \mathcal{T}} \sum_{e \in \mathcal{P}} 3\pi_e^t p_{\text{nom},e}^t + \pi_{\text{vs},e}^t (R_{\text{up},e}^t + R_{\text{dn},e}^t), \quad (6.7)$$

where π_e^t is the cost of electricity for the pump e at time t and $\pi_{\text{vs},e}^t$ is the cost associated with the voltage support capacity at time t . The operational decision variables in the PDN constraints include \mathbf{p}_{nom} , \mathbf{C} , \mathbf{R}_{dn} , and \mathbf{R}_{up} . The adjustable decision variables in the PDN constraints include the voltage magnitude squared \mathbf{Y} and are linear in the random variables $\Delta\rho$ and so we can tractably reformulate $\mathcal{W}_1(\cdot)$, i.e., the power flow equations and constraints (6.1)-(6.4), and $\mathcal{W}_2(\cdot)$, i.e., the affine control policy and associated constraints (6.5)-(6.6b), given the uncertainty set \mathcal{U} . We use explicit maximization [65] to derive the robust counterpart of $\mathcal{W}_1(\cdot)$ and $\mathcal{W}_2(\cdot)$. Assuming we can also obtain the robust counterpart of the WDN constraints $\mathcal{W}_3(\cdot)$, we can write the basic form of the AARC as

$$\begin{aligned} \min_{\mathbf{x}} \quad & (6.7) \\ \text{s.t.} \quad & \widehat{\mathcal{W}}_1(\mathbf{x}), \\ & \widehat{\mathcal{W}}_2(\mathbf{x}), \\ & \widehat{\mathcal{W}}_3(\mathbf{x}), \end{aligned} \tag{AARC}$$

where constraint sets $\widehat{\mathcal{W}}_1(\mathbf{x})$, $\widehat{\mathcal{W}}_2(\mathbf{x})$ represent the robust reformulation of (6.1)-(6.6b) and $\widehat{\mathcal{W}}_3(\mathbf{x})$ is the robust reformulation of the WDN constraints, which we derive in the next section.

6.4. Incorporating WDN Constraints

We need to ensure that the WDN constraints are satisfied for any real-time pump power consumption determined by the affine control policy (6.5). As a result, the flow rates, hydraulic heads, and tank levels are adjustable variables. In this section, we present the WDN constraints that are included in the ARO, show how the monotonicity properties in [126] apply to the WDN which allows us to tractably reformulate the WDN constraints, and describe the tank formulation assumptions required to ensure monotonicity.

6.4.1. Water Distribution Network Modeling

The WDN can be represented as a connected directed graph $(\mathcal{N}, \mathcal{E})$, where \mathcal{N} is the set of nodes and \mathcal{E} is the set of edges. Set \mathcal{N} is composed of disjoint subsets of junctions \mathcal{J} , reservoirs \mathcal{R} , and elevated storage tanks \mathcal{S} , i.e., $\mathcal{N} = \mathcal{J} \cup \mathcal{R} \cup \mathcal{S}$. The edges are bi-directional pipes that connect the nodes in the network, e.g., $ij \in \mathcal{E}$ is a pipe connecting node i to

node j . The water flow through a pipe may be positive or negative, where the sign indicates the direction that the water is moving. A pipe may contain at most one supply pump, i.e., $\mathcal{P} \subseteq \mathcal{E}$. A pump is restricted to a non-negative water flow rate since pumps can only pump in one direction. The WDN at time t can be characterized by the hydraulic heads $\mathbf{H}^t := [H_j^t]_{\forall j \in \mathcal{N}}$ at all nodes (which is equal to the sum of elevation and pressure head) and the volumetric flow rates $\mathbf{x}^t := [x_{ij}^t]_{\forall ij \in \mathcal{E}}$ through all pipes going from node i to node j .

WDNs are dissipative flow networks [126] and are governed by the following quasi-steady state equations

$$\sum_{i:ij \in \mathcal{E}} x_{ij}^t + d_j^t = 0 \quad \forall j \in \mathcal{N}, t \in \mathcal{T}, \quad (6.8)$$

$$x_{ij}^t = -x_{ji}^t \quad \forall ij \in \mathcal{E}, t \in \mathcal{T}, \quad (6.9)$$

$$H_i^t - H_j^t = f_{ij}(x_{ij}^t) \quad \forall ij \in \mathcal{E}, t \in \mathcal{T}, \quad (6.10)$$

where d_j^t is the injection of water at node j and time t , where positive values indicate an injection into the network and negative values indicate a withdrawal from the network. Customer water demands at junctions are assumed to be known and non-positive. In (6.8), the conservation of water at each node is enforced. Since the flow along pipes can be bi-directional, (6.9) enforces skew symmetry along pipe ij at time t . The head loss equation (6.10) describes the relationship between hydraulic head at nodes and flow rate over a pipe or pump connecting them. The head loss function $f_{ij}(\cdot)$ is continuous and increasing with respect to flow rate x_{ij}^t . The pipe head loss function is commonly modeled using the Darcy-Weisbach formulation [10]

$$f_{ij}(x_{ij}^t) = k_{ij}|x_{ij}^t|x_{ij}^t \quad \forall ij \in \mathcal{E} \setminus \mathcal{P}, t \in \mathcal{T},$$

where parameter k_{ij} is the resistance coefficient of pipe ij . The pump head is typically modeled as a quadratic function

$$f_{ij}(x_{ij}^t) = -(m_{ij}^0 - m_{ij}^1(x_{ij}^t)^2) \quad \forall ij \in \mathcal{P}, t \in \mathcal{T},$$

where m_{ij}^0 and m_{ij}^1 are the head loss parameters of pump ij . Additional constraints needed to model the WDN are given next by component type.

Junctions

The hydraulic head, which is composed of the elevation head and the pressure head, is bounded at all nodes

$$H_{\min,j} \leq H_j^t \leq H_{\max,j} \quad \forall j \in \mathcal{N}, t \in \mathcal{T}, \quad (6.11)$$

where $H_{\min,j}$ and $H_{\max,j}$ are the minimum and maximum heads.

Tanks

Tanks are connected to a single node in the WDN, where we separately model the tank's inflow and outflow from the node (see Fig. 6.1). The tank inlet is typically located at the top of the tank. The tank constraints are

$$\ell_j^{t=|\mathcal{T}|} \geq \ell_j^{t=0} \quad \forall j \in \mathcal{S}, \quad (6.12a)$$

$$\ell_j^t = \ell_j^{t-1} + \frac{\Delta T}{\gamma_j} \sum_{i:i \in \mathcal{E}} x_{ij}^t \quad \forall j \in \mathcal{S}, t \in \mathcal{T}, \quad (6.12b)$$

$$\ell_{\min,j} \leq \ell_j^t \leq \ell_{\max,j} \quad \forall j \in \mathcal{S}, t \in \mathcal{T}, \quad (6.12c)$$

$$g_j(\mathbf{x}^t, \ell_j^t) \leq 0 \quad \forall j \in \mathcal{S}, t \in \mathcal{T}, \quad (6.12d)$$

where ℓ_j^t is the water level (including elevation) at tank j and time t and γ_j is the cross-sectional area of tank j . In (6.12a), we ensure that the tanks are not depleted over the scheduling horizon by setting the final tank level to be greater than or equal to the initial tank level. The water level ℓ_j^t is defined in (6.12b) and bounded in (6.12c) to reflect the physical volume of the tank. Function $g_j(\cdot)$ in (6.12d) contains tank head constraints that depend upon our tank formulation which we will describe in more detail in Section 6.4.2. The tank head determines whether the tank is storing or supplying water to the network. When the tank in Fig. 6.1 has no valves or pumps, it stores water if the tank head is greater than the head associated with the maximum tank level and supplies water if the tank head is equal to the head associated with the tank level. In order for WDN monotonicity to hold, we need to make certain assumptions about tank equipment and operation, which will be discussed in Section 6.4.2.

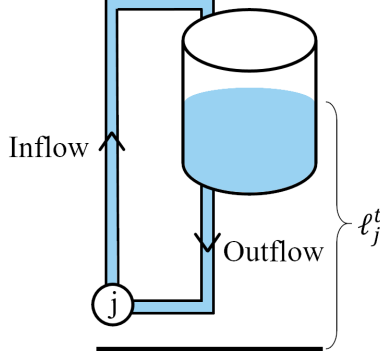


Figure 6.1: Water storage tank diagram.

Reservoirs

Reservoirs are modeled as infinite sources and the head is fixed

$$H_j^t = \hat{h}_j \quad \forall j \in \mathcal{R}, t \in \mathcal{T}, \quad (6.13)$$

where \hat{h}_j is the elevation at reservoir j .

Pipes and Pumps

Pipes without pumps can have positive or negative flows. Pumps have bounded unidirectional flows, i.e.,

$$0 \leq x_{\min,ij} \leq x_{ij}^t \leq x_{\max,ij} \quad \forall ij \in \mathcal{P}, t \in \mathcal{T}, \quad (6.14)$$

We consider fixed speed supply pumps whose on/off status is unchanged throughout the scheduling horizon. The single-phase pump power consumption is

$$p_e^t = b_e(x_{ij}^t) \quad \forall e = ij \in \mathcal{P}, t \in \mathcal{T}, \quad (6.15)$$

where function $b_e(\cdot)$ calculates the power consumed by pump e and assigns a third of the total pump power consumption to each phase. For fixed speed pumps, this function is traditionally modeled as a cubic [31, 81], quadratic [61], or linear function [13, 63, 108] of flow rate or head gain. Here, we assume a linear function of flow rate

$$p_e^t = h_{ij}^0 + h_{ij}^1 x_{ij}^t \quad \forall e = ij \in \mathcal{P}, t \in \mathcal{T},$$

where h_{ij}^0 and h_{ij}^1 are parameters.

Including these WDN constraints within the problem results in a semi-infinite program since (6.8)-(6.15) represent infinitely many constraints and adjustable variables x_{ij}^t , ℓ_j^t , and H_j^t associated with every possible realization of the power demand forecast error in the uncertainty set. However, we can leverage monotonicity properties to tractably reformulate the WDN constraints.

6.4.2. Monotonicity of WDNs

Next, we establish that the hydraulic heads \mathbf{H}^t and tank levels $\boldsymbol{\ell}^t$ are monotonic functions of the reservoir water injection and controllable pump power consumption. This allows us to replace the semi-infinite water flow equations with two sets of deterministic constraints that consider only the minimum and maximum water injections.

In order to formulate the equivalent deterministic water constraints, we must first prove the uniqueness of the water flow solution given the water injections. If there exists a unique solution, we can write the adjustable variables as functions of the injections and evaluate the relationship between the water injections and the adjustable variables. Next, we need to prove that the adjustable variables are monotonic functions of the water injections (which vary based on the uncertain power demand in the PDN). We build our analysis on the monotonicity proofs for dissipative flow networks in [76, 126]; however, there are several key differences. The WDN requires additional formulation assumptions to ensure monotonicity because of the additional adjustable variables in the WDN (i.e., the tank levels) and the external constraints on tank head. For example, we must ensure that the tank level is a monotonic function of the reservoir water injections since the tank level is a bounded adjustable variable.

Network Assumptions

We need to make the following three assumptions for the monotonicity properties to apply to the WDN.

- Assumption 1: The head loss function $f_{ij}(x_{ij}^t) \forall ij \in \mathcal{E}$ and pump power consumption are increasing in flow rate. This assumption is in [126]. In the WDN, this assumption holds for head loss in pipes and pumps whose on/off status (potentially time-varying) is determined before the scheduling horizon. The pipe head loss function is commonly modeled using the experimental Hazen-Williams equation or theoretical

Darcy-Weisbach equation, and in both equations, the head loss is increasing with flow rate. We assume the pump power consumption is increasing in flow rate, which follows general power characteristic curves [88].

- Assumption 2: If $d_j^{t,(1)} \leq d_j^{t,(2)} \forall j \in \mathcal{R}$ and $d_j^{t,(1)} = d_j^{t,(2)} \forall j \in \mathcal{J}$, then $d_j^{t,(1)} \geq d_j^{t,(2)} \forall j \in \mathcal{S}$. Given an increase in reservoir water injections, we need to assume all tank injections decrease. This assumption is always true for a single tank network since water injections must sum to zero. However, for this to be true in a multiple tank case, we need an additional constraint that limits tank injection adjustments to all be in the same direction. This limits the possible feasible WDN solutions.
- Assumption 3: The tank head is not strictly dependent on the tank level. If the tank head *is* strictly dependent on the tank level, an increase in reservoir water injection would cause an increase in tank level and, consequently, tank head. As a result, the junction heads surrounding the tank may not be monotonically decreasing. We next consider two tank formulations that satisfy this assumption and derive the associated head constraints (6.12d). In both formulations, the tank water injections become decision variables.

Tank Formulation 1. We assume that a valve is connected to the tank's outlet pipe so that we can control the outlet flow rate/head, similar to [108, 122]. In this set up, the tank heads must satisfy additional inequality constraints if the tank is storing or supplying water. The constraints included in (6.12d) in this formulation are

$$-M\alpha_j^t \leq d_j^t \leq M\alpha_j^t \quad \forall j \in \mathcal{S}, t \in \mathcal{T}, \quad (6.16a)$$

$$-M\beta_j^t \leq d_j^t \leq M(1 - \beta_j^t) \quad \forall j \in \mathcal{S}, t \in \mathcal{T}, \quad (6.16b)$$

$$-M(1 - \alpha_j^t) \leq \tilde{H}_j^t - H_j^t \leq M(1 - \alpha_j^t) \quad \forall j \in \mathcal{S}, t \in \mathcal{T}, \quad (6.16c)$$

$$\ell_{\max,j} - M(1 - \beta_j^t) \leq \tilde{H}_j^t \leq \ell_j^t + M\beta_j^t \quad \forall j \in \mathcal{S}, t \in \mathcal{T}, \quad (6.16d)$$

$$\alpha_j^t, \beta_j^t \in \{0, 1\} \quad \forall j \in \mathcal{S}, t \in \mathcal{T}, \quad (6.16e)$$

where $M > 0$ is a large number, α_j^t is a binary variable that determines whether tank j is connected, and β_j^t is a binary variable that determines whether tank j is filling. Constraint (6.16a) sets the tank water injection to zero if the tank is not connected. In (6.16b), the tank is filling or emptying given a positive or negative tank injection. In (6.16c), \tilde{H}_j^t is an auxiliary head variable. If the tank is connected, then the head

at the tank node is equal to \tilde{H}_j^t ; otherwise the constraint holds trivially. In (6.16d), if tank j is emptying, then $H_j^t \leq \ell_j^t$. If tank j is filling, then $H_j^t \geq \ell_{\max,j}$.

Tank Formulation 2. The tank level has no impact on the tank head, similar to [59, 61]. For this assumption to be feasible, the tank's inlet and outlet pipes need a booster pump and a valve, respectively. This formulation provides the most flexibility in the water flow solution. No additional head constraints are needed in (6.12d). A drawback to this formulation is that the tank is no longer passive and the booster pump consumes energy.

In Fig. 6.2, we demonstrate the feasible water flow solutions for tank formulations 1 and 2 using the coupled PDN-WDN presented in Section 6.7. For combinations of pump and tank injections, we check if there exists a water flow solution given the mixed-integer nonconvex water flow constraints. Tank formulation 1 is less flexible than tank formulation 2 because the head and water level of the tanks limit when the tank can store or supply water. Additionally, Fig. 6.2 also shows the feasible solutions that satisfy monotonicity (i.e., the addition of Assumption 2 since Assumptions 1 and 3 are already met). For this case study, we found that the feasible range of pump flow rates is the same regardless of the monotonicity constraint; however, the feasible combinations of tank injections are significantly limited. However, tank injection combinations that are not feasible under monotonicity are cases in which the tanks are counteracting each other, and so may correspond to more expensive (i.e., suboptimal) operating points. In our case study, we use tank formulation 2 since the WDN has more flexibility and can provide more voltage support. Our current formulation does not consider the power consumption of the tank's booster pump which we plan to model in future work.

Existence and Uniqueness

Existence and uniqueness of WDNs has been proven many times in the literature. Given the water injections at all nodes, if the water flow equations (6.8)-(6.10) are feasible and the head loss equation is monotonically increasing in flow, then there exists a unique solution to the water flow equations [107, 116].

Monotonicity of Head with Water Injections

We use the Aquarius Theorem from [126] to show monotonicity of the junction heads given reservoir water injections. The Aquarius Theorem is summarized for comprehensiveness:

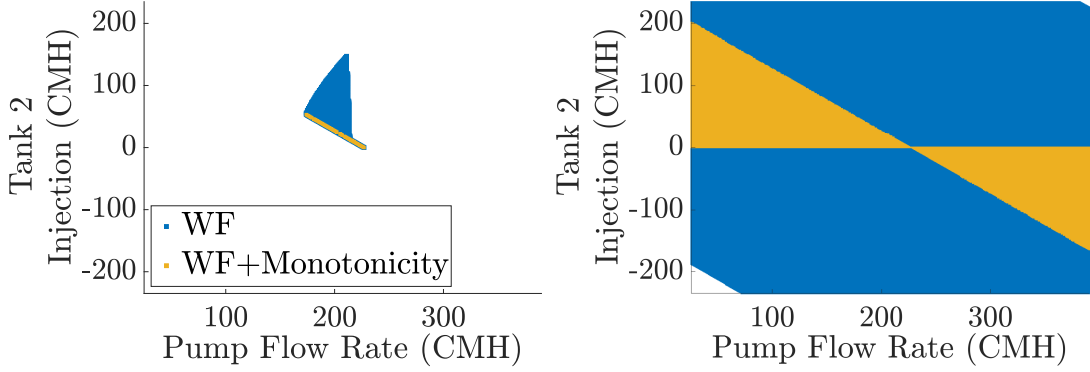


Figure 6.2: The feasible water flow solutions for tank formulation 1 (Left) and tank formulation 2 (Right) are shown in blue with an overlaid orange area indicating the feasible water flow solutions when enforcing monotonicity.

Aquarius Theorem [126]: Consider two sets of flow rates $\mathbf{x}^{(1)}$ and $\mathbf{x}^{(2)}$ that satisfy (6.8) for injection vectors $\mathbf{d}^{(1)}$ and $\mathbf{d}^{(2)}$. Let $\mathcal{B} \subset \mathcal{N}$. If $d_i^{(1)} \geq d_i^{(2)} \forall i \in \mathcal{B}$, then for every $i \in \mathcal{B}$, there exists a nonintersecting path i_1, \dots, i_K , where $i_1 \in \mathcal{N} \setminus \mathcal{B}$ and $i_K = i$ such that $x_{i_k i_{k+1}}^{(1)} \leq x_{i_k i_{k+1}}^{(2)} \forall k = 1, \dots, K - 1$.

The Aquarius Theorem states that given an ordered water injection, there is a path of ordered water flows. Therefore, we can make the following statement:

Proposition 1. Consider the solutions $(\mathbf{x}^{(1)}, \mathbf{H}^{(1)})$ and $(\mathbf{x}^{(2)}, \mathbf{H}^{(2)})$ satisfying the conservation of water equation (6.8) and the head loss equation (6.10) for water injection vectors $\mathbf{d}^{(1)}$ and $\mathbf{d}^{(2)}$. If $d_i^{(1)} \leq d_i^{(2)}$ for all $i \in \mathcal{R}$, then $H_j^{(1)} \geq H_j^{(2)}$ for every node $j \in \mathcal{N} \setminus \mathcal{R}$.

Proof. We define sets $\mathcal{B} = \{\mathcal{S} \cup \mathcal{J}\}$ and $\mathcal{N} \setminus \mathcal{B} = \mathcal{R}$. Given Assumption 2, we know that $d_j^{(1)} \geq d_j^{(2)} \forall j \in \mathcal{S}$ since $d_i^{(1)} \leq d_i^{(2)} \forall i \in \mathcal{R}$. Using the Aquarius Theorem, we know there is a nonintersecting path between every node in \mathcal{B} to a node in \mathcal{R} that has an ordered flow rate since $d_i^{(1)} \geq d_i^{(2)}$ for all $i \in \mathcal{B}$ (i.e., $d_i^{(1)} \geq d_i^{(2)}$ for all $i \in \mathcal{S}$ and $d_i^{(1)} = d_i^{(2)}$ for all $i \in \mathcal{J}$). We calculate the cumulative head loss along the nonintersecting path i_1, \dots, i_{K-1} defined in the Aquarius Theorem from $j \in \mathcal{R}$ to $i \in \mathcal{B}$, i.e.,

$$H_j - H_i = \sum_{k=1}^{K-1} f_{i_k i_{k+1}}(x_{i_k i_{k+1}}) \quad \forall i \in \mathcal{B}, \exists j \in \mathcal{R}.$$

We know that $H_j^{(1)} = H_j^{(2)}$ for all $j \in \mathcal{R}$ since reservoirs are treated as infinite sources with fixed pressure heads. Since $d_i^{(1)} \geq d_i^{(2)}$, through the Aquarius Theorem, we know that

$x_{i_k i_{k+1}}^{(1)} \leq x_{i_k i_{k+1}}^{(2)}$ $\forall k = 1,..,K-1$ along the path and

$$\begin{aligned} H_i^{(1)} &= H_j^{(1)} - \sum_{k=1}^{K-1} f_{i_k i_{k+1}}(x_{i_k i_{k+1}}^{(1)}) \geq \\ &H_j^{(2)} - \sum_{k=1}^{K-1} f_{i_k i_{k+1}}(x_{i_k i_{k+1}}^{(2)}) = H_i^{(2)}. \end{aligned}$$

Therefore, if $d_i^{(1)} \leq d_i^{(2)}$ for all $i \in \mathcal{R}$ then $H_j^{(1)} \geq H_j^{(2)}$ for every node $j \in \mathcal{N} \setminus \mathcal{R}$. Conversely, if $d_i^{(1)} \geq d_i^{(2)}$ for all $i \in \mathcal{R}$ then $H_j^{(1)} \leq H_j^{(2)}$ for every node $j \in \mathcal{N} \setminus \mathcal{R}$. \square

This implies that the maximum head occurs at the minimum reservoir water injection. Conversely, the minimum head occurs at the maximum reservoir water injection.

Monotonicity of Tank Level with Water Injections

Proposition 2. Consider the solutions $(\mathbf{x}^{(1)}, \mathbf{H}^{(1)})$ and $(\mathbf{x}^{(2)}, \mathbf{H}^{(2)})$ satisfying the conservation of water equation (6.8) and the head loss equation (6.10) for water injection vectors $\mathbf{d}^{(1)}$ and $\mathbf{d}^{(2)}$. If $d_i^{(1)} \geq d_i^{(2)}$ for all $i \in \mathcal{R}$, then $\ell_j^{(1)} \geq \ell_j^{(2)}$ for every tank $j \in \mathcal{S}$.

Proof. An increase in reservoir injection causes a decrease in tank injection (Assumption 2). Since the tank level increases given a decreasing tank injection (6.12b), we know that the tank level increases with increasing reservoir injection. \square

We are able to extend the monotonicity properties in Propositions 1 and 2 to the pump power consumption since we are considering supply pumps that are directly downstream of reservoirs. For these pumps, an increase in the reservoir water injection is directly related to an increase in water flow through the pump. Since the power consumption increases with flow (Assumption 1), we know that the power consumption increases with increasing reservoir injection.

Therefore $\mathcal{W}_3(\cdot)$ in the ARO can be replaced with the two extreme sets of pump power consumption and the scheduled pump power consumption

$$\Gamma_{\text{scheduled}}(\mathbf{p}_{\text{nom}}), \quad (6.17a)$$

$$\Gamma_{\text{extreme}}(\bar{\mathbf{p}}), \quad (6.17b)$$

$$\Gamma_{\text{extreme}}(\mathbf{p}), \quad (6.17c)$$

where $\Gamma_{\text{scheduled}}(\cdot)$ is the set of WDN equations (6.8)-(6.15) for the scheduled operation and $\Gamma_{\text{extreme}}(\cdot)$ is the set of WDN equations (6.8)-(6.11), (6.12b)-(6.15) for the extreme cases. We use an overbar and underbar to denote the sets of WDN variables for the maximum and minimum extreme cases, e.g., $\overline{\mathbf{H}}$ and $\underline{\mathbf{H}}$. The maximum and minimum pump power consumptions are defined by the scheduled pump power consumption, \mathbf{R}_{up} , and \mathbf{R}_{dn} ,

$$\bar{p}_e^t = p_{\text{nom},e}^t + (1/3)R_{\text{up},e}^t \quad \forall e \in \mathcal{P}, t \in \mathcal{T}, \quad (6.18a)$$

$$\underline{p}_e^t = p_{\text{nom},e}^t - (1/3)R_{\text{dn},e}^t \quad \forall e \in \mathcal{P}, t \in \mathcal{T}. \quad (6.18b)$$

Since the pumps are balanced three-phase loads, we divide the magnitude of the largest pump power adjustments by three to get the single-phase pump power consumption. Additionally, we enforce Assumption 2 in the extreme cases by including

$$\bar{d}_j^t \leq d_{\text{nom},j}^t \quad \forall j \in \mathcal{S}, t \in \mathcal{T}, \quad (6.19a)$$

$$\underline{d}_j^t \geq d_{\text{nom},j}^t \quad \forall j \in \mathcal{S}, t \in \mathcal{T}, \quad (6.19b)$$

in (6.17b) and (6.17c), respectively, where $d_{\text{nom},j}^t$ is the scheduled reservoir water injection and \bar{d}_j^t , \underline{d}_j^t corresponds to the water injections in the extreme scenarios.

6.4.3. Full AARC

Finally, we replace the general expression of the robust reformulation of the WDN constraints $\omega_3(\mathbf{x})$ with three sets of deterministic constraints to obtain the full AARC

$$\begin{aligned} & \min_{\mathbf{x}} && (6.7) \\ & \text{s.t.} && \widehat{\mathcal{W}}_1(\mathbf{x}), \\ & && \widehat{\mathcal{W}}_1(\mathbf{x}), \\ & && (6.17), (6.18), \end{aligned} \quad (\text{AARC})$$

where $\mathbf{x} = \{\mathbf{p}_{\text{nom}}, \mathbf{p}, \bar{\mathbf{p}}, \mathbf{R}_{\text{up}}, \mathbf{R}_{\text{dn}}, \mathbf{C}, \mathbf{H}, \ell, \mathbf{x}, \underline{\mathbf{H}}, \underline{\ell}, \underline{\mathbf{x}}, \overline{\mathbf{H}}, \bar{\ell}, \bar{\mathbf{x}}\}$.

6.5. WDN Approximations

Additionally, we approximate the pipe and pump head loss equations (6.10) to make the water constraints convex. Importantly, these approximations are not necessary to guarantee robustness; the monotonicity properties used in Section 6.4 guarantee robustness for the nonconvex WDN constraints. We replace the nonconvex head loss function $f_{ij}(x_{ij}^t)$ for pipes with a quasi-convex hull of the Darcy-Weisbach formulation⁴ so we can model pipes with bi-directional flow [61]

$$\begin{aligned} H_i^t - H_j^t &\leq (2\sqrt{2} - 2)k_{ij}x_{\max,ij}x_{ij}^t + (3 - 2\sqrt{2})k_{ij}x_{\max,ij}^2, \\ H_i^t - H_j^t &\geq (2\sqrt{2} - 2)k_{ij}|x_{\min,ij}|x_{ij}^t - (3 - 2\sqrt{2})k_{ij}x_{\min,ij}^2, \\ H_i^t - H_j^t &\geq 2k_{ij}x_{\max,ij}x_{ij}^t - k_{ij}x_{\max,ij}^2, \\ H_i^t - H_j^t &\leq 2k_{ij}|x_{\min,ij}|x_{ij}^t + k_{ij}x_{\min,ij}^2, \end{aligned} \quad (6.20)$$

$\forall ij \in \mathcal{E} \setminus \mathcal{P}, t \in \mathcal{T}$. Parameters $x_{\min,ij}$ and $x_{\max,ij}$ are the lower and upper limits on pipe ij 's flow rate. We under-approximate the pump head gain as a linear function

$$H_i^t - H_j^t = m_{ij}^3 x_{ij}^t + m_{ij}^2 \quad \forall ij \in \mathcal{P}, t \in \mathcal{T}, \quad (6.21)$$

where m_{ij}^3 and m_{ij}^2 are parameters. Therefore, the convexified (AARC) replaces (6.10) in (6.17) with (6.20)-(6.21). While the robust approach in Section 6.4.3 and the proposed probabilistic approach in Section 6.8 do not require convex WDN constraints, we utilize the approximations to improve computation time. Additionally, the scenario-based probabilistic approach developed in Chapter 5 requires convex constraints in order for the scenario approach to be applicable. Chapter 5 and [61] investigated the impact of the WDN approximations used and found that they were reasonable. For example, Chapter 5 empirically observed that the solutions of an approximated formulation using the linearized pump head-flow function (6.21) satisfied the original, nonconvex water constraints.

⁴The formulation in [61] is formulated specifically for the Darcy-Weisbach headloss formula. This can be generalized to also apply to the Hazen-Williams headloss formula. In Appendix A, we generalized the relaxation to work for all commonly used head loss formulas.

6.6. Deterministic Problem

To provide a point of comparison for the uncertainty-aware methods, this section describes the decoupled, convex, deterministic problem. We present the formulation in which the WDN solves for the pump schedule with no knowledge of the PDN and the power demand uncertainty. We use the deterministic problem – a formulation in which the PDN is not explicitly considered – as a way to evaluate and compare the solutions and performance of the uncertainty-aware approaches presented in Sections 6.3 and 6.8. Specifically, we evaluate the reduction in violation probabilities and the impact of the PDN on the water pumping. The deterministic, decoupled water pumping formulation is

$$\begin{aligned} \text{minimize}_{\mathbf{x}} \quad & \sum_{t \in \mathcal{T}} \sum_{e \in \mathcal{P}} 3\pi_e^t p_e^t \\ \text{subject to} \quad & (6.8) - (6.9), (6.11) - (6.15), (6.20) - (6.21), \end{aligned} \tag{D}$$

where $\mathbf{x} := \{p_e^t \in \mathbf{p}, H_j^t \in \mathbf{H}, \ell_j^t \in \boldsymbol{\ell}, x_{ij}^t \in \mathbf{x}\}$. The pump power decision variable p_e^t is equivalent to the scheduled pump power $p_{\text{nom},e}^t$ since there are no real-time pump adjustments.

6.7. Robust Case Study

In our case study, we use a coupled PDN and WDN shown in Fig. 6.3. We first describe the case study set up and then present our case study results for the robust problem.

6.7.1. Set Up

The WDN is a test network (NET1) included with EPANET, a free WDN modeling and simulation software program developed by the U.S. Environmental Protection Agency [87]. We pull the network data from the EPANET input file and make the following modifications. We added an additional tank (tank 2) in order to evaluate a case study that requires the tank injection monotonicity constraints (6.19). We reduced the volume of the first tank so that the total water storage capacity remains the same. The updated tank data is $\gamma_j = 94.53 \text{ m}^2$, $\ell_j^0 = 327.06 \text{ m}$, $\ell_{\min,j} = 319.56 \text{ m}$, and $\ell_{\max,j} = 334.56 \text{ m}$ for tank 1 and $\gamma_j = 94.54 \text{ m}^2$, $\ell_j^0 = 339.02 \text{ m}$, $\ell_{\min,j} = 331.52 \text{ m}$, and $\ell_{\max,j} = 346.52 \text{ m}$ for tank 2. The minimum head limit at each junction is equal to the elevation plus a minimum pressure head of 20 m. The pump performance coefficients are $h_{ij}^1 = 1.09 \text{ kW/CMH}$, $h_{ij}^0 = -22.88 \text{ kW}$, $m_{ij}^1 = -9.08 \times$

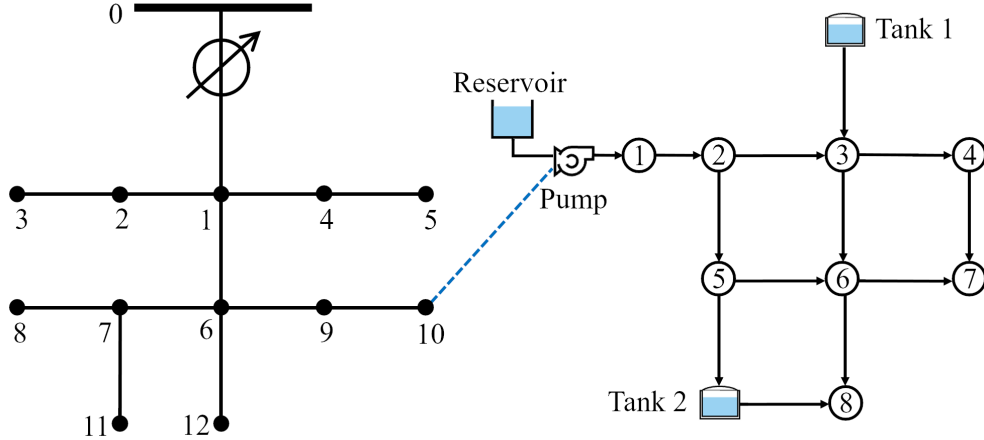


Figure 6.3: Coupled PDN (left) and WDN (right). The blue dashed line indicates where the water supply pump is connected to the PDN.

10^{-2} m/CMH, and $m_{ij}^0 = 103.73$ m with a minimum and maximum flow rate of $x_{\min,ij} = 25$ CMH and $x_{\max,ij} = 390$ CMH, respectively.

For the three-phase unbalanced PDN, we use the IEEE 13-bus feeder topology [52] with the same modifications and assumptions as Chapter 5. The pump is connected to bus 10. We set η_e to 3. The minimum and maximum voltage limits are 0.95 pu and 1.05 pu, respectively. The nominal power demands at each bus and phase are multiplied by 1.5 so that the PDN is heavily loaded and the voltages are close to their minimum voltage limit. The power demand forecast error is uncertain but bounded between $[-\sigma \bar{\rho}_{k,\phi}^t, \sigma \bar{\rho}_{k,\phi}^t]$ at each bus and phase with a load present, where σ indicates a percentage of the forecasted load. We set $\pi_e^t = \$100/\text{MWh}$ and $\pi_{\text{vs},e}^t = \$10/\text{MWh}$. We solve the problem with the JuMP package in Julia using the SCIP [33] and Gurobi [42] solvers.

6.7.2. Results

We first evaluate the robust solutions for a single time period while varying the size of the uncertainty set (i.e., by varying σ). In Table 6.1, we present the objective cost, the scheduled pump power consumption, and the full range of real-time pump power adjustments $R^t = R_{\text{up}}^t + R_{\text{dn}}^t$ for the robust voltage support problem with convex WDN constraints. For all cases in Table 6.1, the scheduled pump power consumption is constant because the tank injections must be non-positive (6.12a) and the scheduled pump power consumption is minimized (i.e., the scheduled tank injection is zero). When $\sigma = 2\%$, the PDN does not

Table 6.1: Single-Period Results

σ (%)	Objective Cost (\$)	Sched. Pump Power (kW)	R^t (kW)
2	67.16	671.61	0
3	68.79	671.61	162.90
4	71.87	671.61	470.58
5	74.94	671.61	778.20

experience voltage limit violations for any realization of uncertain power demand. Therefore, the control policy is zero and the water pumps do not adjust their operation in real time. As the power demand uncertainty increases, a non-zero control policy is needed to handle some of the uncertainty realizations. Consequently, the objective cost and R^t increase.

We check the robustness of the solutions in Table 6.1 with the original, nonconvex WDN constraints and the linearized PDN constraints. We randomly generated 1,000 uniformly distributed power demand forecast error scenarios within the uncertainty set. Given the scheduled pump power consumption and the parameters of the pump power control policy, we calculated the real-time pump power adjustments and verified that the power flow equations and the nonconvex water flow equations are satisfied. We found that the solutions are feasible in the robust nonconvex problem for all uncertainty scenarios tested.

Next, we solve the robust voltage support problem for a 24-hour period. In Fig. 6.4, we compare the solution of the robust problem to that of a deterministic problem that uses only the forecasted demands. We observe that the robust schedule (6.17a) varies less than the deterministic schedule. This is because the robust solution needs to be feasible for the entire range of pump power adjustments around the schedule, i.e., $-R_{dn,e}^t$ and $+R_{up,e}^t$. The range of pump power adjustments results in robust bounds around the WDN's adjustable variables (e.g., the pump flow rates and the tank levels). We illustrate the range of bounds for the extreme cases (6.17b)-(6.17c) in Fig. 6.4 with a blue shaded area.

The robust bounds of the tanks in Fig. 6.4 demonstrate the propagation of uncertainty over multiple time periods. In our formulation, the water level in the tank is a function of the tank level in the previous time period. As a result, the tank's robust bounds are dependent on the uncertainty from previous time periods. As expected, the tank bounds increase over time due to propagation of uncertainty across time periods. We were unable to robustly solve the 24-hour problem for larger uncertainty levels (e.g. $\sigma = 5\%$), indicating that the solution becomes increasingly conservative as the uncertainty accumulates over the scheduling horizon until the robust problem becomes infeasible. There are methods to deal

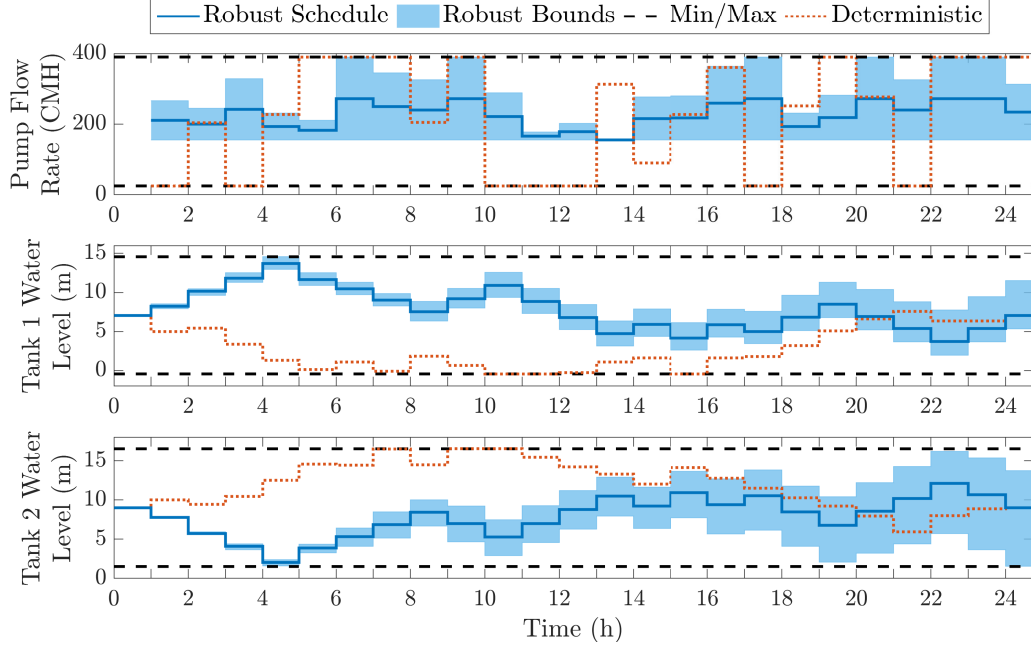


Figure 6.4: Pump flow rates and tank levels in the multi-period convex robust problem ($\sigma = 4\%$) for the robust schedule (solid blue lines) and the deterministic schedule based on forecasted demands (red dotted lines). The bounds on the robust pump flow rate and tank levels are shown with blue shading around the schedule. The black dashed lines are the minimum and maximum pump flow rates and tank levels.

with uncertainty propagation, such as compensating for recently observed forecast error [45], but we leave this to future work.

Next, we verify the computational tractability of the robust voltage support problem by comparing the solver time of the robust problem with that of the chance-constrained voltage support formulation solved via the scenario approach in Chapter 4. The results in Chapter 4 are generated using a comparably sized WDN. When solving the voltage support problem for three time periods, the robust problem's solver time was less than a second whereas the chance-constrained problem's solver time was 10-50 minutes. For a scheduling horizon of 24 hours, we were unable to solve the chance-constrained problem due to memory issues whereas solving the robust problem takes less than 2 seconds. This comparison demonstrates the computational tractability of our proposed formulation.

6.8. Probabilistic Problem Formulation

To reduce the conservativeness of the solution while maintaining computational tractability, we propose an uncertainty-aware optimization framework that contains chance-constrained power constraints and probabilistically robust water constraints. Specifically, the chance-constrained power constraints guarantee feasibility of the PDN operation under power demand uncertainty with a high probability. The probabilistically robust water constraints guarantee feasibility of the real-time voltage support control policy on WDN operation with a high probability. Using probabilistic constraints is a reasonable approach since there are other components in the PDN that can provide voltage support. Additionally, small deviations outside of system limits for short periods of time may be acceptable.

We derive an analytical reformulation of the integrated PDN-WDN problem utilizing the monotonicity properties discussed in Section 6.4.2 and assuming knowledge of the uncertainty distribution. We rewrite the joint chance constraints as individual chance constraints. Unlike joint chance constraints, individual chance constraints do not significantly increase the computational complexity. Additionally, individual chance constraints are effective at reducing the joint violation probability and are less conservative than explicitly formulated joint chance constraints [43]. Furthermore, there is added flexibility in identifying active constraints and tuning constraint violation levels individually. We evaluate the empirical joint and individual reliability in the case study in Section 6.9.

Our new probabilistic approach builds on the robust reformulation (AARC) and existing approaches for chance-constraints. The benefits and disadvantages of these methods are explored in the case study in Section 6.9. The proposed probabilistic optimization problem is of the form

$$\underset{\mathbf{x}}{\text{minimize}} \quad (6.7) \quad (6.22a)$$

$$\text{subject to} \quad \mathcal{W}_p(\mathbf{x}, \Delta\rho), \quad (6.22b)$$

$$\mathcal{W}_w(\mathbf{x}, \Delta\rho), \quad (6.22c)$$

where the constraint sets $\mathcal{W}_p(\mathbf{x}, \Delta\rho)$ and $\mathcal{W}_w(\mathbf{x}, \Delta\rho)$ contain the quasi-steady state power flow (including the voltage support constraints) and water flow constraints, respectively. These sets of constraints are functions of the decision variables $\mathbf{x} \in \mathbb{R}^d$ and the random variables $\Delta\rho \in \mathbb{R}^n$ (which in this case is the power demand forecast error).

6.8.1. Power Distribution Network Constraints, $\mathcal{W}_p(\mathbf{x}, \Delta\rho)$

With the use of the affine control policy and Lin3DistFlow, the power constraints are linear. To analytically reformulate the power constraints, the voltage limit constraints are separated to form $2 \times |\mathcal{K}| \times |\Phi| \times |\mathcal{T}|$ individual chance constraints

$$\mathbb{P}\left[Y_{k,\phi}^t(\mathbf{x}, \Delta\rho) \leq V_{\max}^2\right] \geq 1 - \epsilon_p \quad \forall k \in \mathcal{K}, \phi \in \Phi, t \in \mathcal{T}, \quad (6.23)$$

$$\mathbb{P}\left[V_{\min}^2 \leq Y_{k,\phi}^t(\mathbf{x}, \Delta\rho)\right] \geq 1 - \epsilon_p \quad \forall k \in \mathcal{K}, \phi \in \Phi, t \in \mathcal{T}. \quad (6.24)$$

The function $Y_{k,\phi}^t(\mathbf{x}, \Delta\rho)$ returns the voltage magnitude squared at bus k , phase ϕ , and time t which is an affine function of the power demand forecast errors $\Delta\rho$, the scheduled pump power \mathbf{p}_{nom} , and the control policy parameters $\mathbf{C}_e^t \in \mathbf{C}$ at time t . The chance constraints ensure that each voltage limit is satisfied for a user-specified probability level $1 - \epsilon_p$, where ϵ_p is the individual violation level. It should be noted that the individual violation level can be different for each individual chance constraint. We analytically reformulate the power chance-constraints assuming that the power demand forecast error follows a normal distribution with a known mean $\mu \in \mathbb{R}^n$ and covariance $\Sigma \in \mathbb{R}^{n \times n}$. Ref. [99] found that a reformulation based on a normal distribution is reasonable (i.e., provides good trade-offs between cost and security) in systems with a large number of uncertain variables, e.g., uncertain power demands. The individual chance constraints can be equivalently written in the following deterministic form [12, 99]

$$\begin{aligned} \mathbb{P}[a(\mathbf{x}) + b(\mathbf{x})\Delta\rho \leq c] &\geq 1 - \epsilon \\ \Leftrightarrow a(\mathbf{x}) &\leq c - b(\mathbf{x})\mu - f^{-1}(1 - \epsilon)\|b(\mathbf{x})\Sigma^{1/2}\|_2, \end{aligned} \quad (6.25)$$

where $a(\mathbf{x}) \in \mathbb{R}$ and $b(\mathbf{x}) \in \mathbb{R}^{1 \times n}$ are affine functions of the decision variables, $c \in \mathbb{R}$ is a constant, and $f^{-1}(\cdot)$ is either the inverse cumulative distribution function or a probability inequality [99]. Since we assume a normal distribution, $f^{-1}(\cdot)$ is the inverse cumulative distribution function of the standard normal distribution.

6.8.2. Water Distribution Network Constraints, $\mathcal{W}_w(\mathbf{x}, \Delta\rho)$

For the water constraints (6.22c), we build on a probabilistically robust method presented in [72] to make the probabilistically robust method applicable and tractable for our formulation. In [72], the authors determine an uncertainty set and solve for the probabilistically

robust constraints in two sequential steps. Our formulation concurrently solves these two steps, which allows us to incorporate the probabilistically robust water constraints into an optimization framework that manages power constraints in a different way. In [72], the uncertainty set is determined via a scenario-based approach, where the number of samples generated depends on the number of uncertainty sources and a user-specified violation level. Since our problem considers many sources of uncertainty (i.e., every bus and phase over the entire scheduling horizon), this approach would be very conservative for our formulation. It should also be noted that scenario-based approaches are generally conservative in practice [125]. However, our approach may have more requirements on our formulation (for example, distribution assumptions) than the method in [72].

To tractably reformulate the water constraints, we analytically solve for a bounded set \mathcal{D} given the uncertainty $\Delta\rho$. We ensure that \mathcal{D} encloses a user-specified probability density. The water constraints are then solved robustly, i.e., (6.17), given set \mathcal{D} . Since the robust reformulation of the water constraints relies on the extreme pump powers, we solve for a range of extreme pump powers, i.e., $p_{\text{nom},e}^t - \underline{R}_e^t$ and $p_{\text{nom},e}^t + \overline{R}_e^t$ that need to be feasible in (6.17b) and (6.17c). In other words, we ensure that the probability density of the real-time pump adjustments within $[\underline{\mathbf{R}}, \overline{\mathbf{R}}]$ is at least $1 - \epsilon_w$, i.e.,

$$\mathbb{P} \left[\mathbf{C}_e^t \Delta \rho^t \leq \overline{R}_e^t \right] \geq 1 - \epsilon_w \quad \forall e \in \mathcal{P}, t \in \mathcal{T}, \quad (6.26)$$

$$\mathbb{P} \left[-\underline{R}_e^t \leq \mathbf{C}_e^t \Delta \rho^t \right] \geq 1 - \epsilon_w \quad \forall e \in \mathcal{P}, t \in \mathcal{T}, \quad (6.27)$$

where ϵ_w is the individual violation level. Therefore, the uncertainty set \mathcal{D} is the hyper-rectangle of the voltage support capacities, i.e., $\mathcal{D} := \times_{e=1}^{|\mathcal{P}|} \times_{t=1}^{|\mathcal{T}|} [\underline{R}_e^t, \overline{R}_e^t]$ where \times is the Cartesian product. Given the robust water constraints (6.17) are satisfied, the water flow constraints are feasible for pump power set points inside $[\mathbf{p}_{\text{nom}} - \underline{\mathbf{R}}, \mathbf{p}_{\text{nom}} + \overline{\mathbf{R}}]$. Equations (6.26) and (6.27) can be reformulated as deterministic constraints using the format presented in (6.25).

6.8.3. Full Probabilistic Problem

The deterministic reformulation of the probabilistically robust water distribution network constraints and the analytical reformulation of the voltage limit chance constraints are com-

bined into a single optimization formulation

$$\begin{aligned} & \underset{\mathbf{x}}{\text{minimize}} && (6.7) \\ & \text{subject to} && \mathcal{W}_p(\mathbf{x}) \leq 0, \\ & && \mathcal{W}_w(\mathbf{x}) \leq 0, \\ & && (6.17), \end{aligned} \tag{P}$$

where $\mathcal{W}_p(\mathbf{x}) \leq 0$ represents the analytical reformulation (6.25) of the probabilistic voltage limit constraints (6.23)-(6.24) and $\mathcal{W}_w(\mathbf{x}) \leq 0$ represents the analytical reformulation of the probabilistically robust voltage support capacity constraints (6.26)-(6.27). The decision variable \mathbf{x} contains \mathbf{p}_{nom} , \mathbf{R} , $\bar{\mathbf{R}}$, \mathbf{C} , \mathbf{H} , $\underline{\mathbf{H}}$, $\bar{\mathbf{H}}$, ℓ , $\underline{\ell}$, $\bar{\ell}$, \mathbf{x} , $\underline{\mathbf{x}}$, and $\bar{\mathbf{x}}$.

The benefits and trade-offs of the probabilistic and robust approach are then explored for a case study in Section 6.9.

6.9. Probabilistic Case Study

In our case study, we consider the coupled PDN and WDN depicted in Fig. 6.5. We first describe the case study and then present the results.

6.9.1. Set Up

We use the coupled PDN and WDN from [115]. The WDN is based on an example network provided in EPANET, an open-source hydraulic modeling and simulation software program [87]. For the PDN, we use the IEEE 13-bus topology [52]. All modifications and parameter values are provided in [115] except the following change to the water and power demands. In order to make the case study more realistic, the nominal water demand at each junction is multiplied by a time-varying constant. Similarly, the nominal power demand at each bus and phase is multiplied by a time-varying constant. The dashed blue curve and the solid red curve in the top plot of Fig. 6.6 depict the water and power demand multipliers over a twelve-hour scheduling horizon where each time period has a duration ΔT of one hour. Additionally, we pulled electricity prices π^t for the Midcontinent Independent System Operator (MISO) for July 21st, 2021, 7:00-18:00 from [75]. These electricity prices are shown in the bottom plot of Fig. 6.6. We set $\pi_{\text{vs}} = 5 \$/\text{MWh}$. The minimum and maximum voltage limits are 0.95 pu and 1.05 pu, respectively.

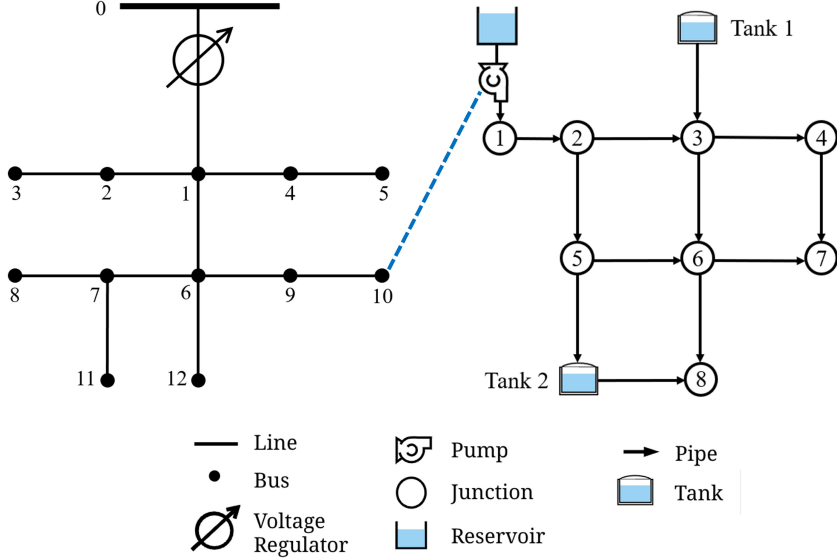


Figure 6.5: Topology of the case study’s coupled three-phase unbalanced PDN (left) and WDN (right). The blue dashed line indicates where the three-phase balanced water supply pump is located in the PDN.

We consider two different types of uncertainty distributions – a normal distribution and a student t-distribution. In the probabilistic approach (P) presented in Section 6.8, we assume that the distribution of the power demand forecast error is normal, which may not be realistic. To observe how this approach performs when the actual distribution is not well known, we fit a multivariate normal distribution to 500 randomly drawn samples from the actual distribution, which is either a multivariate normal distribution or multivariate t-distribution. Student t-distributions have heavier tails than a normal distribution, leading to more extreme power demand forecast errors. It should be noted that we can also reformulate the chance-constraints assuming that the distribution is a t-distribution [99]. However, a focus of this case study is evaluating the performance when the underlying uncertainty is different than what we assume.

For the multivariate t-distribution, we set the degrees of freedom equal to 3, the correlation coefficients to 0.2, and scale the distribution such that the standard deviation is equal to $\alpha \hat{\rho}_{k,\phi}^t$ where α is a percentage and $\hat{\rho}_{k,\phi}^t$ is the forecasted power demand. Additionally, we truncate the t-distribution at ten times the standard deviation. For the multivariate normal distribution, we generate samples from a load forecast error model that consists of a zero-mean normally distributed global error (with standard deviation $\sigma_0 \hat{\rho}_{k,\phi}^t$) and a zero-mean normally distributed nodal error (with standard deviation $\sigma_{\text{node}} \hat{\rho}_{k,\phi}^t$), similar to [51]. The

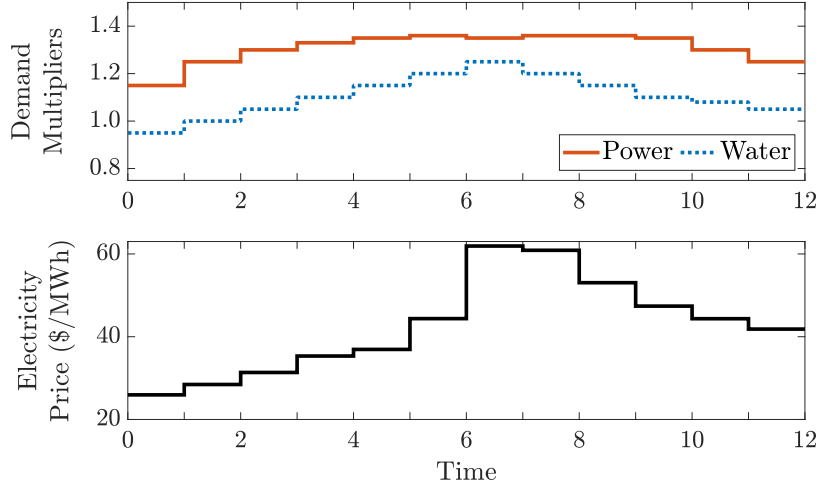


Figure 6.6: Time-varying water and power demand multipliers (top) and electricity price (bottom) over the scheduling horizon.

Table 6.2: Case Studies

Case	Actual Distribution	Parameters
A	t-distribution	$\alpha = 8\%$
B	t-distribution	$\alpha = 1.5\%$
C	normal distribution	$\sigma_0 = 1.01\%$, $\sigma_{\text{node}} = 3.98\%$

normal distribution is truncated at three standard deviations from the mean. We consider three cases, which are described in Table 6.2.

The estimated multivariate normal distribution used in the probabilistic approach (P) is fitted using maximum likelihood estimation from 500 randomly generated samples drawn from the actual distribution. We compare our solution to the adjustable robust approach (R), where the power demand is uncertain but bounded. The bounds are set to the maximum values of 2,000 samples randomly generated from the actual distribution, i.e., $\Delta\rho_{k,\phi}^t \in [-\Delta\rho_{\max,k,\phi}^t, \Delta\rho_{\max,k,\phi}^t]$ for all $k \in \mathcal{K}$, $\phi \in \Phi$, and $t \in \mathcal{T}$ where $\Delta\rho_{\max,k,\phi}^t = \max_{i \in \mathcal{U}_{2000}} |\Delta\rho_{k,\phi,i}^t|$ and \mathcal{U}_{2000} is the set of 2,000 randomly drawn samples.

To evaluate the solution performance of each approach, we use the Monte Carlo method to determine the empirical violation probabilities given the actual distribution and the fitted normal distribution. We calculate the empirical violation probability under both distributions so that we can evaluate the performance given the actual and expected distribution.

We generate 50,000 power demand forecast error scenarios for the twelve-hour scheduling horizon and determine the corresponding real-time pump power adjustments from the pump schedule. We determine the joint empirical violation probability by determining whether there exists a water and/or power network violation for any scenario in the scenario set.

For simplicity, we set all individual violation levels for the voltage limits constraints ϵ_p to be the same and all individual violation levels for the voltage support capacity constraints ϵ_w to be the same. The problems are solved with the Gurobi solver [42] using the JuMP package in Julia on a computer with a 64-bit Intel i7 dual core CPU at 3.40 GHz and 16 GB RAM.

6.9.2. Results

We solve the robust (R), probabilistic (P), and deterministic (D) formulations from Sections 6.4.3, 6.8.3, and 6.6, respectively. Table 6.3 displays the solver time, the total cost (6.7) and the cost of the pump schedule (i.e., the first term in (6.7)) as percent increases from the deterministic cost (which has the same total and pump schedule cost), and the average three-phase up and down voltage support capacity over the twelve-hour scheduling horizon for the probabilistic and robust approaches as we vary the user-selected individual violation levels and the uncertainty distribution. As the individual violation levels decrease and the uncertainty distribution's standard deviation increases, the pump operation shifts to a more expensive operating point and larger real-time control actions are needed to respond to the uncertainty realizations. As a result, the costs and the voltage support capacity increase. In Table 6.3, Case A has the largest forecast error standard deviation and costs while Case B has the smallest forecast error standard deviation and costs. It should be noted that the real-time up and down voltage support capacities for the probabilistic approach are not equal because the fitted normal distribution is not necessarily zero mean.

Table 6.3: Probabilistic and Robust Results

Case	Problem Type	ϵ_p (%)	ϵ_w (%)	Solver Time (s)	Total Cost (% Increase)	Scheduled Cost (% Increase)	Average \bar{R} (kW)	Average \underline{R} (kW)
A	(P)	1 × 10 ⁻²	1 × 10 ⁻²	1.36	11.53	4.90	184.90	183.37
	(P)	5 × 10 ⁻³	1 × 10 ⁻³	1.46	15.40	7.63	216.77	215.13
	(P)	3 × 10 ⁻³	1 × 10 ⁻⁴	1.44	18.88	8.78	281.59	279.60
	(R)	—	—	—	—	Infeasible	—	—
B	(P)	1 × 10 ⁻⁵	1 × 10 ⁻⁵	0.49	0	0	0	0
	(R)	—	—	0.40	2.86	1.54	36.80	36.80
C	(P)	1 × 10 ⁰	1 × 10 ⁰	0.48	0	0	0	0
	(P)	1 × 10 ⁻³	1 × 10 ⁻³	0.94	0.49	0.49	0	0
	(P)	1 × 10 ⁻⁹	1 × 10 ⁻⁹	1.21	6.30	3.78	69.98	69.69
	(R)	—	—	0.49	26.86	12.21	407.31	407.31

(P): Probabilistic approach

(R): Robust approach

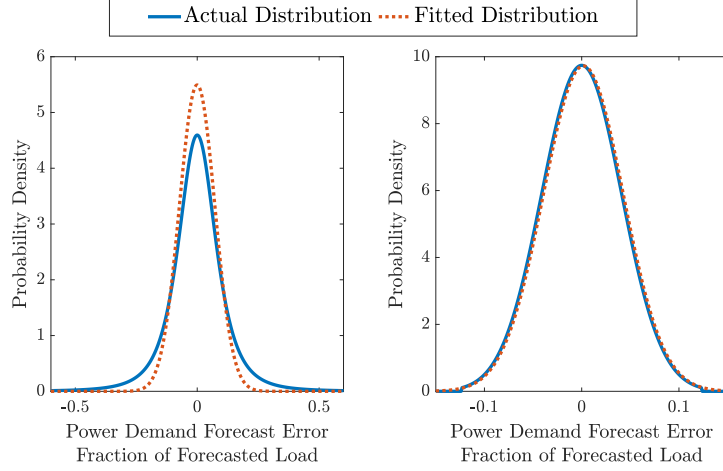


Figure 6.7: Example probability density functions of the actual distributions (solid lines) for bus 8, phase c , and $t = 1$ compared with the estimated normal distribution (dashed lines) fitted using maximum likelihood estimation with 500 samples. The actual distributions are Case A (left) and Case C (right).

The robust solution requires a more expensive pump schedule and larger real-time voltage support capacity than the probabilistic solution. This is because the robust solution has to be feasible for all uncertainty realizations whereas the probabilistic solution needs to be feasible for a certain probability density of the uncertainty realizations. For example, in Case C, the total robust cost is a 26.86% increase from the deterministic cost whereas the probabilistic case ($\epsilon_p, \epsilon_w = 1 \times 10^{-9}\%$) is a 6.30% increase from the deterministic cost. In many cases, the probabilistic formulation provides a solution whereas the robust formulation is infeasible. This illustrates the additional flexibility of a probabilistic solution versus a robust solution. However, the difference between the probabilistic and robust approaches intensifies when the fitted distribution is not representative of the actual distribution. This is illustrated in Fig. 6.7, which shows an example of the probability density functions for the actual distribution and its corresponding fitted normal distribution for Cases A and C. In Cases A and B, the actual distributions have heavier tails than the fitted distributions. In these cases, the probability of drawing a value from the fitted distribution that is near the robust bounds (which are formed from the actual distribution) is negligible. This indicates that the probabilistic approach using the fitted normal distribution may perform poorly if the assumed uncertainty distribution is inaccurate.

The solver times for the probabilistic and robust solutions are shown in Table 6.3. The probabilistic and robust solver times are comparable. We find that the probabilistic approach

would reasonably scale to larger networks since the probabilistic approach in the case studies solve in less than two seconds. For comparison, the scenario-based chance constrained formulation was unable to solve for a comparable PDN-WDN system due to memory issues.

Fig. 6.8 illustrates how the uncertainty impacts the pump schedule for Case A ($\epsilon_p = 3 \times 10^{-3}\%$ and $\epsilon_w = 1 \times 10^{-4}\%$) and Case C ($\epsilon_p, \epsilon_w = 1 \times 10^{-9}\%$). We compare the probabilistic schedule (solid blue line), the deterministic schedule (dotted red line), and the robust schedule (dashed green line). The probabilistic and robust schedules vary less between time periods compared to the deterministic schedule and are more centered within the pump power limits. This is because the uncertainty-aware approaches need to respond to the uncertain power demand forecast error to ensure that the voltages remain within their limits. The range of real-time voltage support adjustments around the schedule are depicted with the blue and green bands for the probabilistic and robust solutions, respectively. In Case A, the robust problem is infeasible and the pump in the probabilistic solution almost uses its full pumping range to provide real-time voltage support. In Case C, the standard deviation of the forecast error is smaller so the probabilistic problem does not need as much voltage support capacity. Here, the robust solution is also feasible. As expected, the robust solution's real-time voltage support capacity is much larger than the probabilistic solution's voltage support capacity.

Next, we verify that the empirical violation probabilities of the individual chance constraints are below the user-selected violation levels, ϵ_p and ϵ_w when the samples are generated from the fitted, multivariate normal distribution. In general, we found that many empirical violation probabilities are well below the user-specified violation level. To demonstrate this, let's consider the voltage constraints in Case A ($\epsilon_p = 5 \times 10^{-3}\%$ and $\epsilon_w = 1 \times 10^{-3}\%$). The empirical voltage violation probabilities range from 0% to $4 \times 10^{-3}\%$, with a mean of $8.8 \times 10^{-5}\%$ and standard deviation of $4.9 \times 10^{-4}\%$. This indicates that many individual chance constraints are never active. We found that the violations only occurred on phase c at the end of the network (buses 6-12), where a majority of all violations (around 47%) occurred at bus 8.

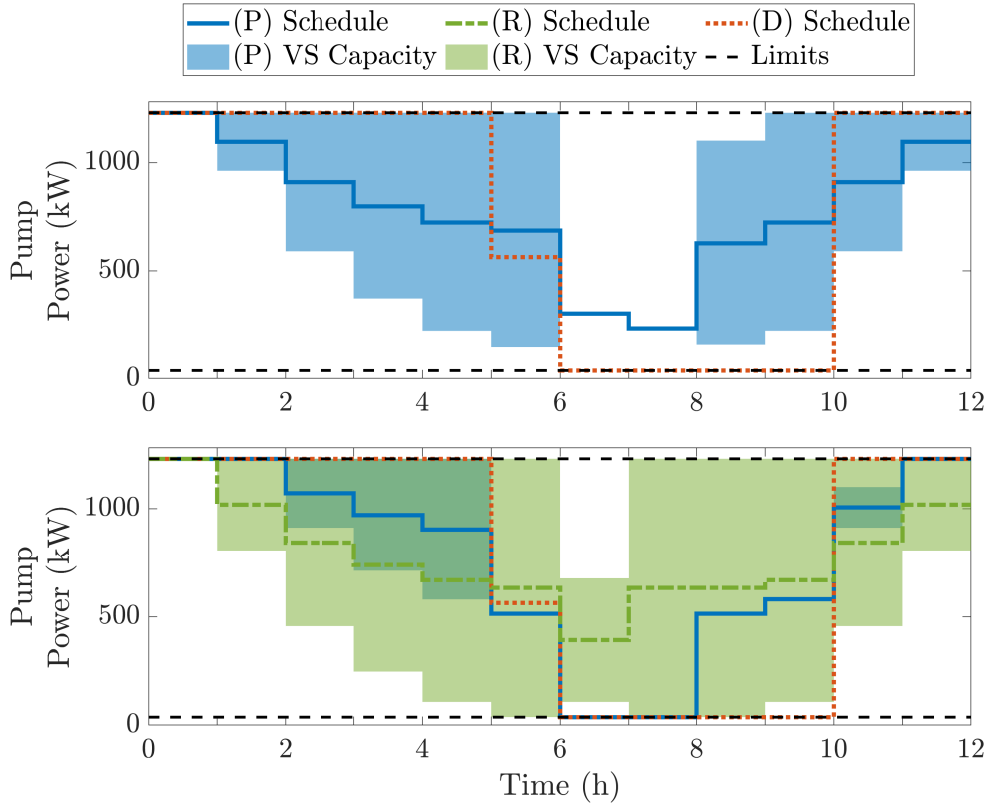


Figure 6.8: Comparison of pump power schedules for the probabilistic (solid blue line), deterministic (dotted red lines), and robust (dashed green lines) solutions for (top) Case A ($\epsilon_p = 3 \times 10^{-3}\%$ and $\epsilon_w = 1 \times 10^{-4}\%$) and (bottom) Case C ($\epsilon_p = 1 \times 10^{-9}\%$ and $\epsilon_w = 1 \times 10^{-9}\%$). The blue and green bands indicate the range of real-time voltage support adjustments of the pump around the probabilistic and robust schedule, respectively. The black dashed lines indicate the pump power limits.

Table 6.4: Empirical Joint Violation Probabilities (%)

Case	Problem Type	ϵ_p (%)	ϵ_w (%)	Fitted Distribution				Actual Distribution		
				Joint Power	Joint Water	Total	Joint Power	Joint Water	Total	
A										
(P)	(D)	—	—	5.37	0	5.37	11.11	0	11.11	
	(P)	1×10^{-2}	1×10^{-2}	0.04	0.01	0.05	5.02	2.40	7.12	
	(P)	5×10^{-3}	1×10^{-3}	0.02	0	0.02	4.75	1.69	6.19	
	(P)	3×10^{-3}	1×10^{-4}	0.01	0	0.01	4.43	1.25	5.49	
	(R)	—	—	Infeasible						
B										
(P)	(D)	—	—	0	0	0	0	0	0	
	(P)	1×10^{-5}	1×10^{-5}	0	0	0	0	0	0	
	(R)	—	—	0	0	0	0	0	0	
C										
(P)	(D)	—	—	0	0	0	0.01	0	0.01	
	(P)	1×10^0	1×10^0	0	0	0	0.01	0	0.01	
	(P)	1×10^{-3}	1×10^{-3}	0	0	0	0	0	0	
	(P)	1×10^{-9}	1×10^{-9}	0	0	0	0	0	0	
	(R)	—	—	0	0	0	0	0	0	

(P): Probabilistic approach

(R): Robust approach

(D): Deterministic approach

Table 6.4 evaluates the joint empirical violation probabilities. The joint water, joint power, and overall joint empirical violation probabilities are displayed for both the fitted and actual distributions. We observe that Cases B and C both have probabilistic solutions that have the same empirical violation probabilities as the robust solution, despite having lower costs. As expected, the empirical violation probability decreases as the violation level decreases. Additionally, the actual distribution generally had worse empirical violation probabilities than the fitted distribution when the fitted distribution was not representative of the actual distribution's probability distribution (e.g., Case A). However, we observe that by decreasing the individual violation levels ϵ_w and ϵ_p , we are able to improve the joint empirical violation probability of the actual distribution, despite the distribution being different than we expect. We also compare the empirical violation probabilities of the probabilistic approach with the deterministic approach. The joint power and overall joint empirical violations are generally much higher in the deterministic approach since the WDN and PDN operation is completely decoupled. This illustrates the benefits of coupled operation to the power network and the coupled power-water system as a whole. As expected, the WDN does not experience any constraint violations in the deterministic case. In the probabilistic case, water constraint violations can occur since WDN operation is impacted by the uncertainty in the PDN. This can be seen in the joint water violation probabilities for Case A in Table 6.4. However, the empirical violation probabilities can be tuned by the individual constraint violation levels to provide a certain amount of reliability to each network. A benefit of individual chance constraints over joint chance constraints is that there is more flexibility in identifying and tuning important individual constraints for system security [43].

6.10. Chapter Conclusion

In this chapter, we formulated an ARO problem that controls water pumping in the WDN to provide voltage support to the PDN given power demand uncertainty. We apply the monotonicity properties from [126] to the WDN and identify the tank operation assumptions needed to ensure monotonicity. We found that the assumptions needed to enforce monotonicity may significantly restrict the feasible water flow solutions. Using these properties, along with affine control policies and constraint approximations, we reformulated the problem as a tractable AARC. In our case study, we demonstrated the robustness and computational tractability of our approach. As an alternative formulation, we proposed a computationally tractable analytical reformulation of a probabilistic water pumping problem

to provide voltage support to the PDN. The problem is subject to the probabilistically robust WDN constraints and chance-constrained PDN constraints and manages power demand uncertainty. We compared this approach with the ARO method to evaluate the computational and solution performance. We found that the probabilistic approach is significantly less conservative than the robust approach and that it is able to find solutions when the robust approach is infeasible. By adjusting individual violation levels, we can target network constraints that are important for system reliability. A drawback to the probabilistic approach is that we assume the uncertainty distribution is known, and so the probabilistic approach may perform poorly if the distribution is inaccurate. The probabilistic approach has a comparable computational performance to the robust approach. Therefore, this approach can be applied to large networks.

Chapter 7.

Coordination of Multiple Services

This chapter presents a robust water pumping optimization problem to provide multiple grid services concurrently. We reformulate the problem into a deterministic, convex, and sequential optimization problem that employs analytical robust reformulations. We evaluate the benefits and challenges of providing multiple services together. This chapter is based on [113].

7.1. Notation

Sets

\mathcal{E}	Set of pipes in the WDN (indexed by ij)
\mathcal{I}_k	Set of buses directly downstream of bus k in PDN (indexed by k)
\mathcal{J}	Set of junctions within the set of nodes in the WDN (indexed by j)
\mathcal{K}	Set of buses in the PDN (indexed by k)
\mathcal{N}	Set of nodes in the WDN (indexed by j)
\mathcal{P}	Set of pumps within the set of pipes in the WDN (indexed by ij)
\mathcal{R}	Set of reservoir nodes within the set of nodes in the WDN (indexed by j)
\mathcal{S}	Set of storage tanks within the set of nodes in the WDN (indexed by j)
\mathcal{T}	Set of time steps in the scheduling problem (indexed by t)
\mathcal{U}	Uncertainty set (indexed by ω)
Φ	Set of phases in the PDN (indexed by ϕ)

Decision Variables

$C_{\text{vs},e}^t$	VS control policy parameter row vector for pump e at time t (-)
$C_{\text{fr,up},e}^t$	Up FR control policy parameter for pump e at time t (-)

$C_{\text{fr,dn},e}^t$	Down FR control policy parameter for pump e at time t (-)
$F_{\text{dn},e}^t$	Auxiliary decision variable to replace $C_{\text{fr,dn},e}^t R_{\text{fr,dn}}^t$ (kW)
$F_{\text{up},e}^t$	Auxiliary decision variable to replace $C_{\text{fr,up},e}^t R_{\text{fr,up}}^t$ (kW)
H_j^t	Hydraulic head at node j and time t (m)
ℓ_j^t	Water level of tank j at time t (m)
p_e^t	Real-time single-phase real power demand of pump e at time t (kW)
$p_{\text{nom},e}^t$	Scheduled single-phase real power demand of pump e at time t (kW)
\mathbf{P}_k^t	Real power flow vector (all phases) entering bus k at time t (kW)
\underline{p}_e^t	Minimum single-phase power consumption at pump e and time t (kW)
\bar{p}_e^t	Maximum single-phase power consumption at pump e and time t (kW)
\mathbf{Q}_k^t	Reactive power flow vector (all phases) entering bus k at time t (kVAr)
$\mathbf{R}_{\text{fr,dn}}^t$	Single-phase down frequency regulation capacity at time t (kW)
$\mathbf{R}_{\text{fr,up}}^t$	Single-phase up frequency regulation capacity at time t (kW)
$\mathbf{R}_{\text{vs,dn},e}^t$	Max. single-phase pump power decrease from the schedule due to voltage support services for pump e and time t (kW)
$\mathbf{R}_{\text{vs,up},e}^t$	Max. single-phase pump power increase from the schedule due to voltage support services for pump e and time t (kW)
x_{ij}^t	Volumetric flow rate of water through pipe ij at time t (CMH)
\mathbf{x}	Operational variables
\mathbf{Y}_k^t	Three-phase voltage magnitude squared at bus k and time t (kV)
Y_{\min}^t	Min. \mathbf{Y}_k^t across all buses and phases at time t (kV^2)
\mathbf{y}	Adjustable variables

Functions

$F(\cdot)$	Cost function
$\Delta p_{\text{vs},e}^t(\cdot)$	Real time voltage support adjustment function at pump e and time t
$\Delta p_{\text{fr},e}^t(\cdot)$	Real time frequency regulation adjustment function at pump e and time t
$\mathbb{Y}_{k,\phi}^t$	Voltage magnitude squared at bus k , phase ϕ , and time t

Constraint Sets

$\Psi_1(\cdot)$	Voltage support constraint set
$\Psi_2(\cdot)$	Frequency regulation constraint set
$\Psi_3(\cdot)$	Power flow constraint set
$\Psi_4(\cdot)$	Water flow constraint set
$\hat{\Psi}_{\text{vs}}(\cdot)$	Robust reformulation of power flow constraints in VS problem

$\hat{\Psi}_{\text{fr}}(\cdot)$	Robust reformulation of power flow constraints in FR problem
$\Gamma_{\text{scheduled}}(\cdot)$	Deterministic WDN constraints given the scheduled pump power
$\Gamma_{\text{extreme}}(\cdot)$	Deterministic WDN constraints given the max. or min. pump power

Random Variables, ω

$\tilde{s}_{\text{dn}}^t \in [0, 1]$	Down frequency regulation signal at time t (-)
$\tilde{s}_{\text{up}}^t \in [-1, 0]$	Up frequency regulation signal at time t (-)
$\Delta\rho_{k,\phi}^t \in \Delta\rho^t$	Deviation in real power demand at bus k and phase ϕ , at time t (kW)
ρ_k^t	Real-time three-phase real power demand at bus k and time t (kW)
ζ_k^t	Real-time three-phase reactive power demand at bus k and time t (kVAr)

Parameters

d_j^t	Forecasted water demand of consumer j at time t (CMH)
\bar{h}_j	Elevation head of node j (m)
\underline{H}_j^{\min}	Minimum pressure head for node j (m)
\overline{H}_j^{\min}	Maximum pressure head for node j (m)
h_{ij}^1, h_{ij}^0	Pump power parameters for pump ij (kW/CMH, kW)
k_{ij}	Resistance coefficient of pipe ij (h^2/m^5)
$\underline{\ell}_j$	Minimum water level in tank j (m)
$\overline{\ell}_j$	Maximum water level in tank j (m)
M_{kn}	Line parameter matrix formed from impedances for line kn (Ohms)
m_{ij}^1, m_{ij}^0	Pump hydraulic function parameters for pump ij (m/CMH, m)
N_{kn}	Line parameter matrix formed from impedances for line kn (Ohms)
\underline{V}_k	Minimum 3-phase voltage magnitude limit at bus k (kV)
\overline{V}_k	Maximum 3-phase voltage magnitude limit at bus k (kV)
\underline{x}_{ij}	Minimum flow rate of pump ij (CMH)
\overline{x}_{ij}	Maximum flow rate of pump ij (CMH)
ΔT	Duration of time period (h)
γ_j	Cross-sectional area of tank j (m^2)
ν_j	Recovered water deficit in tank j from previous scheduling horizon (m^3)
η_e	Ratio between real and reactive power of pump e (-)
π_e^t	Forecasted energy price at for pump e at time t (\$/kWh)
$\pi_{\text{vs},e}^t$	Voltage support capacity cost for pump e at time t (\$/kWh)
$\pi_{\text{vs,up},e}^t$	Up frequency regulation prices for pump e at time t (\$/kWh)
$\pi_{\text{vs,dn},e}^t$	Down frequency regulation prices for pump e at time t (\$/kWh)

$\pi_{vs,up,e}^t$	Up frequency regulation prices for pump e at time t (\$/kWh)
\bar{p}_k^t	Forecasted three-phase real power demand at bus k and time t (kW)
σ	Parameter to scale power demand forecast error (-)

7.2. Chapter Introduction

The WDN can provide several local and grid level services to the power grid. However, for any one service, the flexibility in the WDN may be underutilized. To improve utilization, the WDN can be operated to simultaneously provide local and grid-level services, which provides more overall benefit to the power system and also can increase the value proposition to the WDN operator. The goal of this chapter is to use WDNs to provide multiple simultaneous grid services. In particular, we focus on providing voltage support to the power distribution network and frequency regulation to the bulk transmission system. In order to provide robust guarantees on the safe operation of the PDN and WDN, we need to account for network demand uncertainty.

To do this, we formulate a robust water pumping problem to simultaneously provide voltage support and frequency regulation subject to power and water distribution network constraints in the presence of power demand uncertainty. We first develop the full optimization problem where the scheduled WDN operation, voltage support, and frequency regulation are co-optimized. The formulation is nonconvex and mixed-integer, and so we reformulate the problem into multiple sub-problems and solve the problems sequentially. We then evaluate the performance trade-offs of the co-optimized and sequential problems.

The contributions of this chapter are the 1) formulation of a robust optimization problem to simultaneously solve for the pump schedule, voltage support control actions, and frequency regulation capacity subject to WDN and PDN constraints while managing uncertainty in power demand and the frequency regulation signal, 2) tractable reformulation of the problem into a robust, mixed-integer convex sequential problem, 3) evaluation of the challenges associated with providing voltage support and frequency regulation together, and 4) demonstration of the performance of the proposed solution approach through a case study.

7.3. Problem Description

Our goal is to optimize the WDN's operation and capacity allocated to grid services subject to PDN and WDN constraints while managing power demand uncertainty over the schedul-

ing horizon \mathcal{T} . Specifically, the operation of the supply pumps in the WDN should not violate WDN or PDN constraints. We co-optimize the WDN’s scheduled operation and the capacities reserved for voltage support and asymmetric up and down frequency regulation.

There are several sources of uncertainty in this problem. The power demand at each bus, phase, and time period $t \in \mathcal{T}$ is uncertain but bounded. We define the power demand at time t as the sum of the known, forecasted demand and the uncertain power demand forecast error vector $\Delta\rho^t$, which includes the error at all buses and phases. Additionally, in order to provide frequency regulation, the WDN pumps need to adjust their power consumption based on uncertain up and down frequency regulation signals $\tilde{s}_{\text{up}}^t \in [-1, 0]$ and $\tilde{s}_{\text{dn}}^t \in [0, 1]$, respectively. The frequency regulation signals are scaled by the up and down frequency regulation capacities, which are decision variables, to obtain the required change in power. We define the uncertainty as ω , i.e., $\omega = [\Delta\rho^t, \tilde{s}_{\text{up}}^t, \tilde{s}_{\text{dn}}^t]_{t \in \mathcal{T}} \in \mathcal{U}$ where \mathcal{U} is the uncertainty set.

We formulate the problem as an adjustable robust optimization problem [8] where \mathbf{x} contains the operational variables and \mathbf{y} contains the adjustable variables that are dependent on the uncertainty ω , specifically,

$$\begin{aligned} \min_{\mathbf{x}} \quad & F(\mathbf{x}, \mathbf{y}(\omega, \mathbf{x})) && \text{(Co-optimized)} \\ \text{s.t.} \quad & \forall \omega \in \mathcal{U}, \exists \mathbf{y}, \\ & \Psi_1(\mathbf{x}, \mathbf{y}(\omega, \mathbf{x}), \omega), \\ & \Psi_2(\mathbf{x}, \mathbf{y}(\omega, \mathbf{x}), \omega), \\ & \Psi_3(\mathbf{x}, \mathbf{y}(\omega, \mathbf{x}), \omega), \\ & \Psi_4(\mathbf{x}, \mathbf{y}(\omega, \mathbf{x}), \omega). \end{aligned}$$

The cost function $F(\cdot)$ includes the costs of scheduled pump operation and real-time adjustments to provide voltage support and frequency regulation. The constraint sets $\Psi_1(\cdot)$ and $\Psi_2(\cdot)$ include the voltage support and frequency regulation capacities and control actions, respectively. The constraint sets $\Psi_3(\cdot)$ and $\Psi_4(\cdot)$ are the quasi-steady state PDN and WDN constraints for every time step $t \in \mathcal{T}$ of duration ΔT .

In our problem, the operational variable \mathbf{x} includes the WDN schedule (in particular, the scheduled pump power consumption), the pump power capacity needed to provide voltage support, and the up and down frequency regulation capacity. Additionally, we solve for the affine control policy parameters used for voltage support and frequency regulation real-

time adjustments. While an affine control policy restricts the feasible space of $\mathbf{y}(\boldsymbol{\omega}, \mathbf{x})$, a computationally tractable problem can be formulated and the real-time implementation of the control policy is simple for water utilities. The adjustable variables \mathbf{y} are dependent on the control policy adjustments, e.g., the real-time pump power consumption and the bus voltages. We can define the real-time single-phase pump power consumption in terms of its schedule and real-time voltage support and frequency regulation adjustments

$$p_e^t = p_{\text{nom},e}^t + \Delta p_{\text{vs},e}^t(\boldsymbol{\omega}^t) + \Delta p_{\text{fr},e}^t(\boldsymbol{\omega}^t), \quad (7.1)$$

$\forall \boldsymbol{\omega} \in \mathcal{U}, e \in \mathcal{P}, t \in \mathcal{T}$, where \mathcal{P} is the set of pumps in the WDN, $\Delta p_{\text{vs},e}^t$ is the real-time voltage support adjustment based on the power demand forecast error, and $\Delta p_{\text{fr},e}^t$ is the real-time frequency regulation adjustments based on the up and down frequency regulation signals from the bulk transmission system. We assume that the pumps are balanced three-phase loads and therefore we do not specify the phase of the pump power consumption; the power consumed in each phase is equal. These real-time voltage support and frequency regulation control policies are described in Sections 7.3.1 and 7.3.2. We next model the voltage support $\Psi_1(\cdot)$, frequency regulation $\Psi_2(\cdot)$, PDN $\Psi_3(\cdot)$, and WDN $\Psi_4(\cdot)$ constraints. The constraints are semi-infinite, since they must hold true for all uncertainty realizations. However, we discuss how to tractably reformulate the constraints in Sections 7.3.4 and 7.4.

7.3.1. Voltage Support, $\Psi_1(\cdot)$

We first consider the set of constraints that make up $\Psi_1(\cdot)$. In order to ensure that voltages in the PDN are within safe operating conditions for all power demand uncertainty, we formulate a control policy to adjust the pump power setpoints in response to the real-time power demand forecast error realizations, leveraging the approach in Chapter 5. The voltage support pump power adjustment in (7.1) can then be written as

$$\Delta p_{\text{vs},e}^t = \mathbf{C}_{\text{vs},e}^t \boldsymbol{\Delta \rho}^t \quad \forall e \in \mathcal{P}, t \in \mathcal{T}, \quad (7.2)$$

where decision variable $\mathbf{C}_{\text{vs},e}^t$ is the voltage support control policy parameter row vector for pump e . The control policy relates the power demand forecast error at each bus and phase to a change in pump e 's power consumption. We can define the range of up and down pump

power adjustments needed for voltage support by bounding the control policy

$$-R_{\text{vs,dn},e}^t \leq C_{\text{vs},e}^t \Delta \rho^t \leq R_{\text{vs,up},e}^t \quad \forall e \in \mathcal{P}, t \in \mathcal{T}, \quad (7.3a)$$

$$R_{\text{vs,up},e}^t, R_{\text{vs,dn},e}^t \geq 0 \quad \forall e \in \mathcal{P}, t \in \mathcal{T}, \quad (7.3b)$$

where $R_{\text{vs,dn},e}^t$ and $R_{\text{vs,up},e}^t$ are the largest decrease and increase in single-phase pump power consumption due to voltage support services.

7.3.2. Frequency Regulation, $\Psi_2(\cdot)$

We next define the set of frequency regulation constraints that make up $\Psi_2(\cdot)$. We consider both up and down frequency regulation services. Using generator sign convention, up frequency regulation corresponds to a decrease in pump power consumption and down frequency regulation corresponds to an increase in pump power consumption. We solve for the amount of capacity that the WDN can provide at each time period as well as the participation of each pump in response to the up and down frequency regulation signals. The frequency regulation pump power adjustment in (7.1) can be written as

$$\Delta p_{\text{fr},e}^t = C_{\text{fr,up},e}^t R_{\text{fr,up}}^t \tilde{s}_{\text{up}}^t + C_{\text{fr,dn},e}^t R_{\text{fr,dn}}^t \tilde{s}_{\text{dn}}^t \quad \forall e \in \mathcal{P}, t \in \mathcal{T}, \quad (7.4)$$

where decision variables $R_{\text{fr,up}}^t$ and $R_{\text{fr,dn}}^t$ are the up and down single-phase frequency regulation capacities at time t . Decision variables $C_{\text{fr,up},e}^t$ and $C_{\text{fr,dn},e}^t$ are the up and down control policy parameters of pump e at time t . The frequency regulation capacities are non-negative and the frequency regulation control policy parameters must sum to one to ensure that the requested power adjustment is being fully met by the pumps, i.e.,

$$R_{\text{fr,up}}^t, R_{\text{fr,dn}}^t \geq 0 \quad \forall t \in \mathcal{T}, \quad (7.5)$$

$$\sum_{e \in \mathcal{P}} C_{\text{fr,up},e}^t = 1 \quad \forall t \in \mathcal{T}, \quad (7.6)$$

$$\sum_{e \in \mathcal{P}} C_{\text{fr,dn},e}^t = 1 \quad \forall t \in \mathcal{T}. \quad (7.7)$$

To remove the bilinear terms in the control policy, we can replace the frequency regulation control policy parameters and capacity terms in (7.4)-(7.7) with

$$F_{\text{up},e}^t := C_{\text{fr,up},e}^t R_{\text{fr,up}}^t \quad \forall e \in \mathcal{P}, t \in \mathcal{T}, \quad (7.8)$$

$$F_{\text{dn},e}^t := C_{\text{fr,dn},e}^t R_{\text{fr,dn}}^t \quad \forall e \in \mathcal{P}, t \in \mathcal{T}, \quad (7.9)$$

$$F_{\text{up},e}^t, F_{\text{dn},e}^t \geq 0 \quad \forall e \in \mathcal{P}, t \in \mathcal{T}, \quad (7.10)$$

where $F_{\text{up},e}^t$ and $F_{\text{dn},e}^t$ are decision variables in $\Psi_2(\cdot)$. Then we can recover the up and down frequency regulation capacities and control policy parameters *a posteriori*, e.g., the recovered down frequency regulation variables are

$$R_{\text{fr,dn}}^t := \sum_{e \in \mathcal{P}} F_{\text{dn},e}^t \quad \forall t \in \mathcal{T}, \quad (7.11)$$

$$C_{\text{fr,dn},e}^t := \frac{F_{\text{dn},e}^t}{\sum_{e \in \mathcal{P}} F_{\text{dn},e}^t} \quad \forall e \in \mathcal{P}, t \in \mathcal{T}. \quad (7.12)$$

7.3.3. Power Distribution Network Modeling, $\Psi_3(\cdot)$

Next, we define $\Psi_3(\cdot)$, the power distribution network model. We consider a radial power distribution network that contains uncontrollable net loads (i.e., actual loads minus distributed generation) and controllable pumping loads that are connected to a set of buses \mathcal{K} and phases $\Phi = \{a, b, c\}$. We must ensure a feasible power flow where the minimum and maximum voltage limit constraints are satisfied, i.e.,

$$\underline{\mathbf{V}}_k^2 \leq \mathbf{Y}_k^t \leq \overline{\mathbf{V}}_k^2 \quad \forall k \in \mathcal{K}, t \in \mathcal{T}, \quad (7.13)$$

where \mathbf{Y}_k^t is the three-phase voltage magnitude squared at bus k and time t . The voltage magnitude squared is calculated from the linearized, three-phase unbalanced power flow equations, which are commonly referred to as Lin3DistFlow [3]

$$\mathbf{Y}_k^t = \mathbf{Y}_n^t - \mathbf{M}_{kn}\mathbf{P}_n^t - \mathbf{N}_{kn}\mathbf{Q}_n^t \quad \forall k \in \mathcal{K}, t \in \mathcal{T}, \quad (7.14)$$

$$\mathbf{P}_k^t = \boldsymbol{\rho}_k^t + \mathbf{p}_e^t + \sum_{n \in \mathcal{I}_k} \mathbf{P}_n^t \quad \forall k \in \mathcal{K}, t \in \mathcal{T}, \quad (7.15)$$

$$\mathbf{Q}_k^t = \boldsymbol{\zeta}_k^t + \eta_e \mathbf{p}_e^t + \sum_{n \in \mathcal{I}_k} \mathbf{Q}_n^t \quad \forall k \in \mathcal{K}, t \in \mathcal{T}, \quad (7.16)$$

where \mathbf{P}_k^t and \mathbf{Q}_k^t are the real and reactive three-phase power flows entering bus k at time t , \mathbf{M}_{kn} and \mathbf{N}_{kn} are 3×3 parameter matrices formed from the line impedance matrices, and \mathcal{I}_k is the set of buses directly downstream of bus k . The three-phase real and reactive uncontrollable power demand at bus k and time t is denoted $\boldsymbol{\rho}_k^t$ and $\boldsymbol{\zeta}_k^t$, respectively. The

variable \mathbf{p}_e^t is the three-phase pump power consumption vector of pump e at time t . In (7.15) and (7.16), the pump power consumption is zero if there are no pumps present at bus k . We model the pumps as three-phase balanced loads, with a constant power factor (i.e., η_e is the real-to-reactive power ratio of pump e). We note that other three-phase unbalanced linearized power flow formulations could be used, e.g., [9].

7.3.4. Water Distribution Network Modeling, $\Psi_4(\cdot)$

Last, we define $\Psi_4(\cdot)$, the water distribution network model. The WDN can be represented as a directed graph composed of a set of nodes \mathcal{N} and a set of edges \mathcal{E} . The nodes are made up of disjoint sets of junctions \mathcal{J} , elevated storage tanks \mathcal{S} , and reservoirs \mathcal{R} . The edges, or pipes, are bidirectional and connect nodes in the network, e.g., $ij \in \mathcal{E}$ is a pipe going from node i to node j . A pipe may contain a supply pump, i.e., $\mathcal{P} \subseteq \mathcal{E}$. A WDN's water flow can be described by the hydraulic head H_j^t for each node $j \in \mathcal{N}$ and the volumetric flow rate x_{ij}^t of water through each pipe $ij \in \mathcal{E}$. We do not explicitly consider water demand uncertainty. In Chapter 5, we found it reasonable to assume that a portion of the tank volume is reserved to hedge against water demand uncertainty. To ensure safe operation, the hydraulic heads (which are composed of the elevation and pressure head) must be between the minimum and maximum head limits, i.e.,

$$\underline{H}_j \leq H_j^t \leq \bar{H}_j \quad \forall j \in \mathcal{N}, t \in \mathcal{T}. \quad (7.17)$$

Additionally, the tank water levels ℓ_j^t and supply pump flow rates are bounded

$$\underline{\ell}_j \leq \ell_j^t \leq \bar{\ell}_j \quad \forall j \in \mathcal{S}, t \in \mathcal{T}, \quad (7.18)$$

$$0 \leq \underline{x}_{ij} \leq x_{ij}^t \leq \bar{x}_{ij} \quad \forall ij \in \mathcal{P}, t \in \mathcal{T}, \quad (7.19)$$

where $\underline{\ell}_j$ and $\bar{\ell}_j$ are the minimum and maximum tank levels of tank j , and \underline{x}_{ij} and \bar{x}_{ij} are the minimum and maximum flow rates of pump $ij \in \mathcal{P}$. The hydraulic heads and flow rates are governed by the water flow equations

$$\sum_{i:ij \in \mathcal{E}} x_{ij}^t = -d_j^t \quad \forall j \in \mathcal{N}, t \in \mathcal{T}, \quad (7.20)$$

$$x_{ij}^t = -x_{ji}^t \quad \forall ij \in \mathcal{E}, t \in \mathcal{T}, \quad (7.21)$$

$$H_j^t - H_i^t = k_{ij} x_{ij}^t |x_{ij}^t| \quad \forall ij \in \mathcal{E} \setminus \mathcal{P}, t \in \mathcal{T}, \quad (7.22)$$

$$H_i^t - H_j^t = m_{ij}^1 x_{ij}^t + m_{ij}^0 \quad \forall ij \in \mathcal{P}, t \in \mathcal{T}, \quad (7.23)$$

$$H_j^t = \bar{h}_j \quad \forall j \in \mathcal{R}, t \in \mathcal{T}, \quad (7.24)$$

$$\ell_j^t = \ell_j^{t-1} + \frac{\Delta T}{\gamma_j} \sum_{i:ij \in \mathcal{E}} x_{ij}^t \quad \forall j \in \mathcal{S}, t \in \mathcal{T}, \quad (7.25)$$

where d_j^t is the water injection at node j and time t , k_{ij} is the resistance coefficient of pipe ij , m_{ij}^1 and m_{ij}^0 are head loss parameters of pump ij , γ_j is the cross-sectional area of tank j , and \bar{h}_j is the elevation of node j . Conservation of water is ensured by (7.20) and (7.21) specifies skew symmetry of water flow through the pipes. In (7.22)-(7.23), the head loss and head gain as a function of flow rate is defined for pipes and pumps that are operating, respectively. The pipe head loss function is modeled using the Darcy-Weisbach formulation [10]. When a pump is on, the pump head gain of a fixed speed pump is generally modeled in the literature with either a linear or quadratic function of the flow rate through the pump. Here, we use a linear form. When the pump is off, the pump behaves like a closed valve and the pump head gain is arbitrary. To formulate this, we can introduce a binary pump status variable and use the big-M method to formulate this equation. Reservoirs are modeled as infinite sources of water with a fixed head, which is specified in (7.24). In (7.25), the water level of tank j is calculated based on the tank level in the previous time period and the net flow of water into and out of the tank.

The single-phase pump power consumption is generally modeled as a linear, quadratic, or cubic function of the flow rate through the pump. Here, we model it with a linear function

$$p_e^t = h_{ij}^1 x_{ij}^t + h_{ij}^0 \quad \forall e = ij \in \mathcal{P}, t \in \mathcal{T}, \quad (7.26)$$

where h_{ij}^1 and h_{ij}^0 are parameters. The water distribution network constraints are semi-infinite since the constraints must hold for all realizations of uncertainty (which enters the WDN constraints in the real-time pump power consumption equation (7.26)).

We tractably reformulate the semi-infinite WDN constraints into three sets of deterministic constraints using the monotonicity properties of dissipative flow networks [76]. In order to apply the monotonicity properties to the WDN, several assumptions must be made (see Chapter 6). We assume that the tank head is not strictly dependent on the tank level (i.e., there is either a booster pump and/or valve connected to the tank inlet and outlet pipe), the head loss functions are increasing in flow rate, and that an increase in reservoir water injections cause the deviation in tank water injections to be non-positive for all tanks

(i.e., the tanks do not also increase their water injection). We also assume that the pump statuses do not change in real-time (i.e., the real-time on/off pump statuses are the same as the schedule) to minimize pump wear-and-tear and ensure monotonicity. The robustness proof and implications of these assumptions are further discussed in Chapter 6. With these assumptions, we can prove that the hydraulic heads at all nodes, the tank levels, and pump flows are monotonic functions of the reservoir water injections (which vary based on the voltage support and frequency regulation control actions). The WDN constraints can then be reformulated as the scheduled and extreme cases of the pump power consumption

$$\Gamma_{\text{scheduled}}(\mathbf{p}_{\text{nom}}) \leq 0, \quad (7.27a)$$

$$\Gamma_{\text{extreme}}(\bar{\mathbf{p}}) \leq 0, \quad (7.27b)$$

$$\Gamma_{\text{extreme}}(\mathbf{p}) \leq 0, \quad (7.27c)$$

where $\Gamma_{\text{scheduled}}(\mathbf{p}_{\text{nom}})$, $\Gamma_{\text{extreme}}(\bar{\mathbf{p}})$, and $\Gamma_{\text{extreme}}(\mathbf{p})$ are the sets of deterministic WDN constraints (7.17)-(7.26) given the scheduled, minimum, and maximum power consumption

$$\bar{p}_e^t = p_{\text{nom},e}^t + R_{\text{vs,up},e}^t + R_{\text{fr,dn},e}^t \quad \forall e \in \mathcal{P}, t \in \mathcal{T}, \quad (7.28)$$

$$\underline{p}_e^t = p_{\text{nom},e}^t - R_{\text{vs,dn},e}^t - R_{\text{fr,up},e}^t \quad \forall e \in \mathcal{P}, t \in \mathcal{T}, \quad (7.29)$$

where the pumps are balanced three-phase loads.

7.3.5. Providing Both Voltage Support and Frequency Regulation

When treating the WDN as a flexible load, we must ensure that the tanks are not simply depleted over the scheduling horizon. This issue is magnified when we include asymmetric frequency regulation services. We address this by specifying a total volume of water that must be in the storage tanks at the end of the scheduling horizon

$$\sum_{j \in \mathcal{S}} \gamma_j \ell_j^{t=|\mathcal{T}|} = \hat{v} + \sum_{j \in \mathcal{S}} \gamma_j \ell_j^{t=0}, \quad (7.30)$$

where \hat{v} is the water deficit from the previous scheduling horizon that must be recovered. We include (7.30) in (7.27a). Alternatively, if we wished to correct the tank levels in each time period, we could incorporate a random variable that compensates for the previous time period's water deviation from the scheduled operation, but we leave this to future work.

A challenge with providing both voltage support and frequency regulation simultaneously

is to ensure that the frequency regulation services are not creating voltage issues within the PDN. The goal of voltage support is to provide the smallest pump power adjustments to ensure that the bus voltages are within their limits. Therefore, any additional pump adjustment in the opposite direction of the voltage support adjustments will counteract the voltage support control action and either require more voltage support capacity or cause voltage limit violations. To address this, we consider asymmetric frequency regulation services and require indicator functions to ensure up or down frequency regulation are only provided if it does not cancel out the voltage support control action. This can be done by checking whether there are maximum or minimum voltage limit violations given the scheduled pump operation and power demand uncertainty. For example, if a PDN is experiencing voltages that violate the minimum voltage limit, the voltage support control policy would reduce the pump power consumption which would then increase the voltages. In this case, no down frequency regulation services (increase pump power consumption) can be provided without requiring a larger voltage support capacity to counteract it. However, up frequency regulation (decrease pump power consumption) can still be provided. If there are no voltage limit violations given the scheduled pump operation and power demand uncertainty, both up and down frequency regulation can be provided. In Section 7.4, we tractably reformulate the problem as a robust, mixed-integer convex sequential problem.

7.4. Sequential Reformulation

The formulation presented in Section 7.3 is a mixed-integer adjustable robust optimization problem due to the presence of the indicator functions and binary pump status variables. While there are some related approaches and results to tractably reformulate mixed-integer robust problems, they do not appear to directly apply to our problem. Instead, we solve this problem sequentially as three sub-problems. We first solve the robust voltage support and pump scheduling problem. Next, we identify whether the WDN is capable of providing up and/or down frequency regulation at each time period by solving for the worst-case voltages (i.e., minimum and maximum voltages) given the pump schedule and power demand forecast error. Last, we solve the appropriate robust frequency regulation problem.

By separating **(Co-optimized)** into three sub-problems, we are able to eliminate the indicator functions needed to identify the direction(s) of frequency regulation that the WDN can provide and allows us to solve computationally tractable robust reformulations. Each sub-problem is described in the subsections below. It should be noted that the solution of the

sequential problem will be a feasible solution of the **(Co-optimized)** problem; however, it may not be the optimal solution. The separate optimization problems no longer experience a trade-off between the cost of the WDN schedule and the profit of providing frequency regulation. In Section 7.5.2, we explore this trade-off by comparing the solutions of the sequential problem with special cases of **(Co-optimized)** problem, specifically, those in which we know in advance the type of frequency regulation that can be provided. This allows us to neglect the indicator functions so we can tractably reformulate **(Co-optimized)**. Further investigation of how to tractably reformulate the adjustable robust optimization problem while ensuring that the voltage support and frequency regulation do not cancel each other out is a subject for future research.

7.4.1. Step 1: Voltage Support Problem

In the first sub-problem, we solve the scheduled pump power consumption and voltage support control policy parameters while satisfying WDN and PDN constraints and managing power demand uncertainty. The decision variables are the scheduled pump power consumption $p_{\text{nom},e}^t$, the voltage support control policy parameters $\mathbf{C}_{\text{vs},e}^t$, and the voltage support capacities $R_{\text{vs,up},e}^t$ and $R_{\text{vs,dn},e}^t$ for all pumps $e \in \mathcal{P}$ and all time periods $t \in \mathcal{T}$. The optimization problem can be written as

$$\begin{aligned} \min_{\mathbf{x}} \quad & \sum_{t \in \mathcal{T}} \sum_{e \in \mathcal{P}} 3\pi_e^t p_{\text{nom},e}^t + 3\pi_{\text{vs},e}^t (R_{\text{vs,up},e}^t + R_{\text{vs,dn},e}^t) \\ \text{s.t.} \quad & (7.27), \quad \hat{\Psi}_{\text{vs}}(\mathbf{x}) \leq 0, \quad (\text{Seq-VS}) \\ & \bar{p}_e^t = p_{\text{nom},e}^t + R_{\text{vs,up},e}^t \quad \forall e \in \mathcal{P}, t \in \mathcal{T}, \\ & \underline{p}_e^t = p_{\text{nom},e}^t - R_{\text{vs,dn},e}^t \quad \forall e \in \mathcal{P}, t \in \mathcal{T}, \end{aligned}$$

where π_e^t and $\pi_{\text{vs},e}^t$ are the costs of electricity and voltage support capacity. We can substitute the power flow constraints (7.14)-(7.16), the voltage support control policy constraints (7.2)-(7.3b), and the coupling constraint between the pump load and power demand forecast error (i.e., $p_e^t = p_{\text{nom},e}^t + \Delta p_{\text{vs},e}^t(\Delta \boldsymbol{\rho}^t)$) into (7.13). Since the resulting inequalities are linear in the decision variables and uncertainty, we can use explicit maximization [65] to robustly reformulate the problem. We denote the robust reformulation of the power constraints as $\hat{\Psi}_{\text{vs}}(\mathbf{x})$.

In (7.27), we approximate the pipe head loss constraints using a quasi-convex hull proposed in [61]. While this approximation is not necessary to reformulate the semi-infinite water

constraints as deterministic sets of constraints, it does make the formulation mixed-integer convex.

7.4.2. Step 2: Frequency Regulation Preprocessing

Before solving the frequency regulation problem, we need to identify the direction(s) of frequency regulation the WDN can provide. We robustly solve for the worst-case minimum and maximum voltages within the PDN at each time period given the pump schedule and all power demand forecast error uncertainty realizations. For example, to solve for the minimum voltage over all buses and phases at time t , the robust problem is

$$\begin{aligned} & \max_{Y_{\min}^t} Y_{\min}^t && (\text{Seq-Vmin}) \\ & \text{s.t. } Y_{\min}^t \leq \mathbb{Y}_{k,\phi}^t(\mathbf{p}_{\text{nom}}^t, \Delta\rho^t) \quad \forall \Delta\rho \in \mathcal{U}. \end{aligned}$$

where $\mathbb{Y}_{k,\phi}^t(\mathbf{p}_{\text{nom}}^t, \Delta\rho^t)$ is the voltage magnitude squared at bus k and phase ϕ which is an affine function of the power demand forecast errors $\Delta\rho^t$ and the scheduled three-phase pump power consumption vector $\mathbf{p}_{\text{nom}}^t$. The robust problem can be reformulated as the deterministic robust counterpart and solved for the worst-case minimum and maximum voltage magnitudes. At each time period, there are four possible cases: i) if the voltage limits are satisfied, then the WDN can provide both up and down frequency regulation; ii) if the minimum and maximum voltage limits are violated, then the WDN cannot provide frequency regulation; iii) if only the maximum voltage limits are violated, then the WDN can only provide down frequency regulation; and iv) if only the minimum voltage limits are violated, then the WDN can only provide up frequency regulation.

7.4.3. Step 3: Frequency Regulation

In the third and final sub-problem, we solve for the up and down frequency regulation capacities subject to the WDN and PDN constraints while managing power demand forecast error and frequency regulation signals. If the WDN cannot provide either up or down frequency regulation, we force the respective up or down frequency regulation capacity to zero. We solve for $F_{\text{fr,up},e}^t$ and $F_{\text{fr,dn},e}^t$ and recover the frequency regulation capacity and control policy

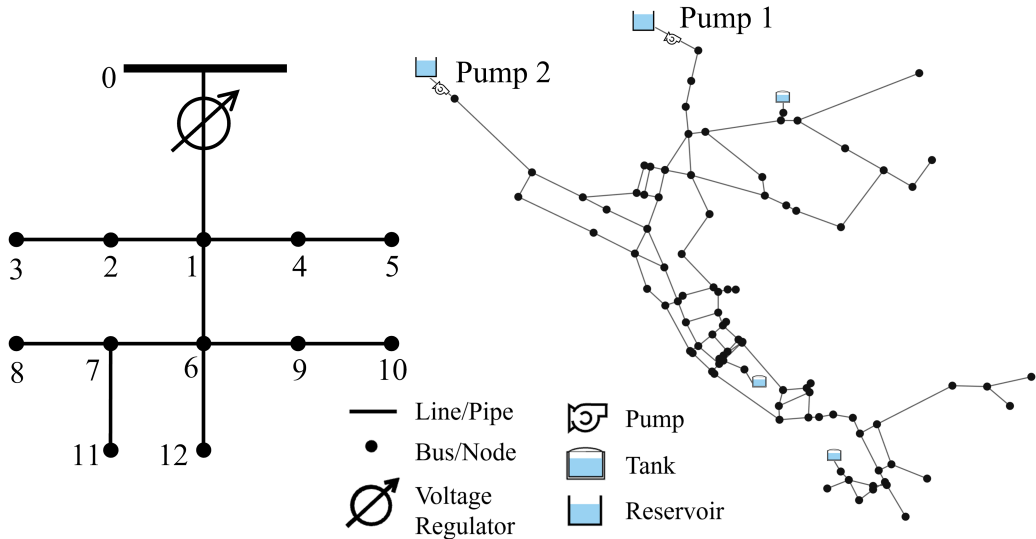


Figure 7.1: Coupled power (left) and water (right) distribution networks. Pumps 1 and 2 are connected to buses 10 and 5, respectively.

parameters *a posteriori*. The robust frequency regulation optimization problem is then

$$\begin{aligned} \max_{\mathbf{x}} \quad & \sum_{t \in \mathcal{T}} \sum_{e \in \mathcal{P}} \pi_{\text{fr},\text{up},e}^t F_{\text{fr},\text{up},e}^t + \pi_{\text{fr},\text{dn},e}^t F_{\text{fr},\text{dn},e}^t && (\text{Seq-FR}) \\ \text{s.t.} \quad & (7.27b) - (7.29), \\ & \hat{\Psi}_{\text{fr}}(\mathbf{x}) \leq 0 \end{aligned}$$

where $\pi_{\text{fr},\text{up},e}^t$ and $\pi_{\text{fr},\text{dn},e}^t$ are the prices associated with providing up and down frequency regulation, $\hat{\Psi}_{\text{fr}}(\mathbf{x})$ is the robust reformulation of the power flow constraints (7.13)-(7.16), the frequency regulation control policy constraints (7.4), (7.8)-(7.10), and the coupling constraint between the pump load and real-time uncertainty (7.1).

7.5. Case Study

In our case study, we consider a coupled PDN-WDN system, shown in Fig. 7.1. We first describe the set up of the case study and then present the results of the sequential problem. Additionally, we explore the value of co-optimizing the WDN schedule and the frequency regulation capacity.

7.5.1. Set Up

The WDN is an example network (NET3) included in the EPANET software, a WDN simulator [87]. The network parameters are from the EPANET input file with several modifications. The pump parameters are $h_{ij}^1 = [0.12, 0.08]$ kW/CMH, $h_{ij}^0 = [53.22, 8.42]$ kW, $m_{ij}^1 = [-1.09 \times 10^{-2}, -1.35 \times 10^{-2}]$ m/CMH, and $m_{ij}^0 = [60.96, 31.70]$ m with a minimum and maximum flow rate of $\underline{x}_{ij} = [0, 0]$ CMH and $\bar{x}_{ij} = [2700, 905]$ CMH for pumps 1 and 2, respectively. The minimum head at each node is the sum of the elevation and a minimum pressure head of 15 m.

For the PDN, we use the IEEE-13 bus topology [52] with the same modifications and assumptions as Chapter 5. Pumps 1 and 2 are connected to buses 10 and 5, respectively. The voltage is constrained to 0.95–1.05 pu. We multiply the power demand loads by 1.4 in order to have a heavily loaded network that is close to the minimum voltage limit. The power demand forecast error at each bus, phase, and time period is unknown but bounded by a percentage of the forecasted load $\bar{\rho}_{k,\phi}^t$, i.e., $[-\sigma \bar{\rho}_{k,\phi}^t, \sigma \bar{\rho}_{k,\phi}^t]$ where σ is a user-specified percentage. We select different σ values to change the size of the uncertainty set.

We consider a 12-hour scheduling horizon. We set $\hat{v} = 10$ m³, $\pi_{vs,e}^t = 0.025$ \$/kWh, and $\pi_{fr,e}^t = 0.025$ \$/kWh. The electricity prices are from the Midcontinent Independent System Operator (MISO) on July 21st, 2021 [75]. We solve the mixed-integer convex sequential problem using the Gurobi solver [42] and the JuMP package in Julia.

7.5.2. Results

We first solve the sequential problem where $\sigma = 7.5\%$. In Fig. 7.2, the scheduled pump power consumption, the range of voltage support capacity and frequency regulation capacity around the schedule are depicted for each pump. In this case, we see that the voltage support capacity is nonzero. This indicates that, given the pump schedule and the power demand uncertainty set, voltage limit violations would occur without real-time voltage support control actions. In this case, the preprocessing sub-problem found that the PDN would violate the minimum voltage limit without the voltage support control actions. The voltage support control policy is responsible for taking the smallest pump power control action to reduce pumping so that the voltages are within the safe operating range. Any increase in pump power consumption would counteract the voltage support control policy. As a result, the WDN can only provide up frequency regulation capacity.

Table 7.1 evaluates the robust sequential solutions as we vary the size of the uncertainty

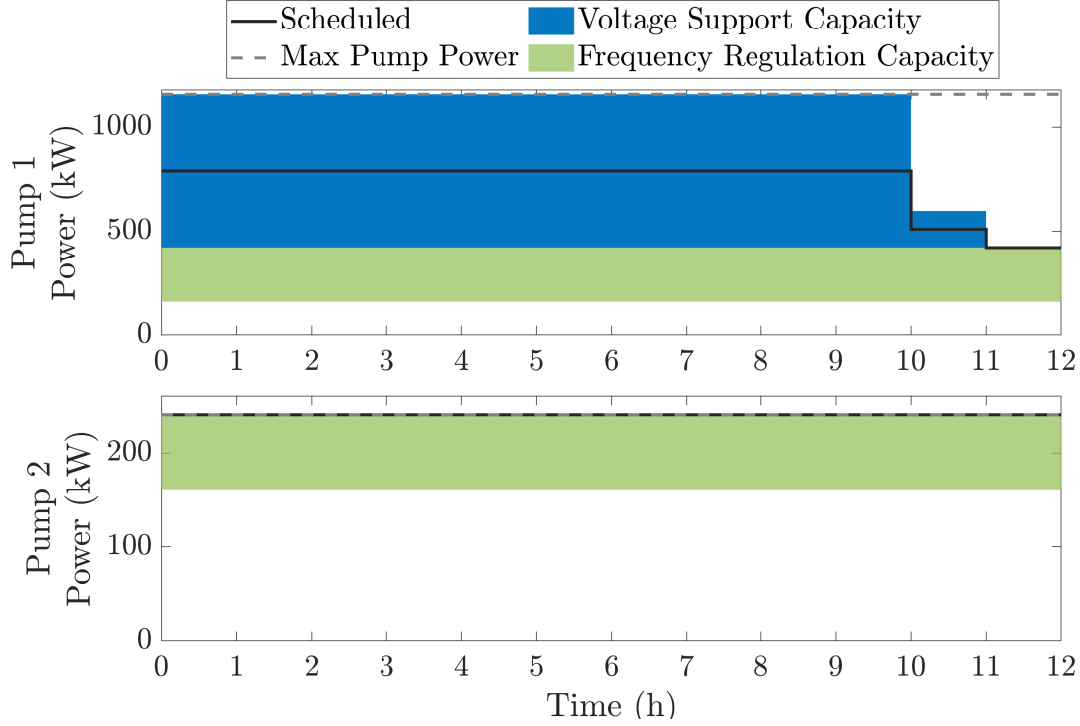


Figure 7.2: Three-phase pump power consumption in the sequential problem ($\sigma = 7.5\%$). The solid black lines indicates the schedule, blue and green bands indicate the range of pump power adjustments allocated for voltage support and frequency regulation.

set (i.e., by varying σ). We present the average range of three-phase voltage support pump power adjustments (i.e., $R_{vs}^t = \sum_{e \in \mathcal{P}} 3 \cdot (R_{vs,up,e}^t + R_{vs,dn,e}^t)$) and the average three-phase up and down frequency regulation capacity over the scheduling horizon. For $\sigma = 3.5\text{--}4.5\%$, there are no power demand uncertainty realizations that cause voltage limit violations (i.e., the voltage support control policy parameters and R_{vs} are zero). As a result, the WDN can provide both up and down frequency regulation capacity. We observe that the WDN is generally able to provide more up capacity (consume less power) than down capacity (consume more power) since the network is closer to the minimum voltage limit. As σ increases, the worst-case voltages given the scheduled pump power consumption and power demand uncertainty set are closer to or at the minimum voltage limit, reducing the amount of down frequency regulation that the WDN can provide. For $\sigma = 5.5\text{--}8.0\%$, there are now minimum voltage limit violations and the voltage support control policy has non-zero parameters. Because of this, the WDN can only provide up frequency regulation. As σ increases, the frequency regulation capacity decreases since an increased amount of capacity

Table 7.1: Average Three-Phase Results over 12-hour Scheduling Horizon

σ (%)	R_{vs} (kW)	$R_{fr,up}$ (kW)	$R_{fr,dn}$ (kW)
3.5	0	355.4	128.5
4.5	0	401.5	65.7
5.5	53.4	465.8	0
6.5	340.6	465.8	0
7.5	627.7	341.7	0
8.0	771.3	269.9	0

is needed for voltage support and larger power demand uncertainty realizations cause the PDN to be closer to voltage limit violations. For σ values larger than 8.0%, the WDN is unable to provide voltage support fully and so the problem is infeasible.

One drawback with the sequential problem formulation is that the optimization problem no longer considers the trade-off between the pump scheduling cost and frequency regulation profit since they are now two separate optimization problems. In Fig. 7.2, the WDN operates pump 2 at its maximum setpoint. Pump 1 is used to provide the remaining water demand since it is more expensive than pump 2. In a sequential problem, the WDN cannot evaluate the cost/profit trade-offs of operating at a slightly more expensive schedule and providing more frequency regulation.

We next investigate the affect that the WDN schedule has on the frequency regulation capacity. We do this by comparing the solutions of the sequential problem with a special case of the co-optimized problem where the type of frequency regulation that the WDN can provide is known. Under this assumption, the sequential problem can be tractably reformulated into a deterministic, mixed-integer convex program. We focus on the specific case where the power demand uncertainty does not cause voltage violations in the PDN. In this case, the WDN does not provide voltage support (i.e., zero voltage support control policy parameters). We compare the solutions of the sequential problem and three co-optimized problems with differing up and down frequency regulation prices.

Table 7.2 reports the average three-phase up and down frequency regulation capacity over the scheduling horizon. Since the WDN can provide both up and down frequency regulation when $\sigma = 4.5\%$, we can observe the trade-off between minimizing the cost of the pumping schedule and the profit from allocating frequency regulation capacity. In the first co-optimized case, the WDN provides more frequency regulation capacity than in the sequential case. As we decrease the frequency regulation prices $\pi_{fr,up}$ and $\pi_{fr,dn}$, the co-optimized problem prioritizes minimizing the scheduled pumping operation cost over the

Table 7.2: Comparison of Sequential and Co-optimized Solutions ($\sigma = 4.5\%$)

Case	$\pi_{fr,up}$ (\$/kWh)	$\pi_{fr,dn}$ (\$/kWh)	$R_{fr,up}$ (kW)	$R_{fr,dn}$ (kW)
Sequential	0.025	0.025	401.5	65.7
Co-optimized-1	0.025	0.025	465.8	116.9
Co-optimized-2	0.005	0.005	452.6	116.9
Co-optimized-3	0.001	0.001	401.5	65.7

profit from frequency regulation. In the third co-optimized case, the schedule and frequency regulation capacity are the same as in the sequential case. While not illustrated in this example, we have also found that if the profit from up and down frequency regulation are different, the co-optimized problem may shift the scheduled pumping operation to a more expensive operating point to provide larger levels of the more profitable type of frequency regulation. When the WDN can only provide up or down frequency regulation, we can expect to see the co-optimized problem shifting the pump operation away from the least expensive operating point to realize higher profits from frequency regulation services. Last, we discuss the impact of the WDN approximations on our solution. While it is not required in the analytical reformulation of the semi-infinite robust water flow constraints, we employ approximations (i.e., quasi-convex hull relaxation of the pipe head loss equation (7.22) and an affine approximation of the pump performance curves (7.26)) to make the WDN mixed-integer convex. Ref. [61] empirically observed that the quasi-convex hull relaxation was exact when minimizing the pump power consumption. However, our formulation also maximizes a feasible range of pump power consumption and may cause the hydraulic heads to be inexact. We compared the scheduled pump power consumption of our solution using the approximated model with the original nonlinear pump curves. We found that the maximum relative error for pumps 1 and 2 was 8% and 15%, respectively. This motivates future work to evaluate and improve the accuracy of the approximated model.

7.6. Chapter Conclusion

In this chapter, we formulated a robust water pumping problem subject to WDN and PDN constraints that provides voltage support and frequency regulation concurrently. We separate the problem into three sub-problems and solve for the solution to the robust reformulation sequentially. In a case study, we demonstrated the ability of the WDN to provide multiple

services at the same time. One drawback we found was that the sequential formulation no longer considers the trade-offs between the cost of the pump schedule and the profits from frequency regulation services. However, the sequential solution will always be feasible within the co-optimized formulation. Future research includes exploring approaches to solve the co-optimized robust optimization problem with mixed integer adjustable variables in order to incorporate a binary voltage support control policy that is only implemented when needed and indicator functions to determine the type of frequency regulation to apply.

Chapter 8.

Assessing the Resilience of an Optimal Water Pumping Control Strategy to Provide Frequency Regulation

In this chapter, we evaluate the performance of optimal water pumping strategies against traditional rule-based controls. We investigate the ability of the WDN to respond to a hazard event when the supply pumps are optimally scheduled and controlled to provide grid services. We consider optimal water pumping problems that minimize the electricity costs of water pumping and can also provide frequency regulation. We assess the water network's performance during a wind-based hazard under different control strategies with a hydraulic simulator, EPANET.

8.1. Notation

Sets

\mathcal{E}	Set of pipes in the WDN (indexed by ij)
\mathcal{J}	Set of junctions within the set of nodes in the WDN (indexed by j)
\mathcal{K}	Set of buses in the PDN (indexed by k)
\mathcal{L}	Set of lines in the PDN (indexed by ℓ)
\mathcal{N}	Set of nodes in the WDN (indexed by j)
\mathcal{P}	Set of pumps within the set of pipes in the WDN (indexed by ij)
\mathcal{R}	Set of reservoirs within the set of nodes in the WDN (indexed by j)
\mathcal{S}	Set of storage tanks within the set of nodes in the WDN (indexed by j)

\mathcal{T} Set of time steps in the scheduling problem (indexed by t)

Variables

F_{ij}^t	Frequency regulation capacity of pump ij at time t (kW)
H_j^t	Hydraulic head at node j at time t (m)
$H_{j,E}^t$	Hydraulic head at node j at time t under extreme operation (m)
$H_{j,N}^t$	Hydraulic head at node j at time t under normal operation (m)
p_{ij}^t	Single-phase real power demand of pump ij at time t (kW)
$p_{ij,\text{down}}^t$	Maximum single-phase real power demand of pump ij at time t (kW)
$p_{ij,\text{up}}^t$	Minimum single-phase real power demand of pump ij at time t (kW)
P_E^t	Network performance metric for extreme operating case
P_N^t	Network performance metric for normal operating case
R	Network resilience metric (-)
R_{tank}	Final tank water availability resilience metric (-)
R_{pressure}	Pressure met resilience metric (-)
R_{line}	Active lines resilience metric (-)
R_{load}	Connected loads resilience metric (-)
w_{ij}^t	Normalized speed of pump ij at time t (-)
x_{ij}^t	Volumetric flow rate of water through pipe ij at time t (CMH)
\mathbf{x}	Decision variables
z_{ij}^t	Binary on/off status of pump ij at time t (0,1)
$\alpha_{\ell,E}^t$	Active line status of line ℓ at time t in extreme operating scenario (0,1)
$\alpha_{\ell,N}^t$	Active line status of line ℓ at time t in normal operating scenario (0,1)
$\beta_{k,E}^t$	Connection status of bus k at time t in extreme operating scenario (0,1)
$\beta_{k,N}^t$	Connection status of bus k at time t in normal operating scenario (0,1)

Functions

$P_f(\cdot)$	Probability of failure
$\Phi(\cdot)$	Cumulative distribution function
$\mu(\cdot)$	Mean of lognormal distribution
$\sigma(\cdot)$	Standard deviation of lognormal distribution
$\eta(\cdot)$	Pump efficiency function
$\text{sgn}(\cdot)$	Sign function

Constraint Sets

$\mathcal{W}_{\text{scheduled}}(\cdot)$ WDN constraints given the scheduled pump power consumption

$\mathcal{W}_{\text{extreme}}(\cdot)$ WDN constraints given the max. or min. pump power consumption

Parameters

A_c	Conductor area (m^2)
b_{ij}^1, b_{ij}^0	Coefficients in head gain function for pump ij
c_{ij}	Exponent in head gain function of pump ij
$c_{ij,2}, c_{ij,1}, c_{ij,0}$	Parameters in power consumption approximation of pump ij
d_j^t	Forecasted water demand of consumer j at time t (CMH)
d_c	Conductor diameter (m)
$f_{ij,0}^t, f_{ij,1}^t$	Pipe ij 's head loss approximation parameters at time t
$f_{ij,2}^t, f_{ij,3}^t, f_{ij,4}^t$	Parameters in head gain approximation of pump ij
\hat{h}_j	Elevation head of node j (m)
h	Height of pole (m)
\underline{H}_j	Minimum pressure head for node j (m)
\bar{H}_j	Maximum pressure head for node j (m)
k_{ij}	Resistance coefficient of pipe ij
L_c	Span length between poles (m)
M	Large number (-)
N	Number of scenarios (-)
n	Pipe head loss exponent (-)
n_c	Number of conductors (-)
V_t	Three-second gust wind speed (m/s)
\underline{w}_{ij}	Minimum normalized speed of pump ij (-)
\bar{w}_{ij}	Maximum normalized speed of pump ij (-)
\underline{x}_{ij}	Minimum flow rate of pump ij (CMH)
\bar{x}_{ij}	Maximum flow rate of pump ij (CMH)
y	Modified age of the utility pole (years)
θ	Angle between wind direction and conductors (degrees)
ΔT	Duration of time period (h)
κ	Pump power consumption parameter
γ_j	Cross-sectional area of tank j (m^2)
π_{ij}^t	Energy price at time t for pump ij at time t (\$/kWh)
π_{fr}^t	Price of frequency regulation capacity at time t (\$/kWh)

8.2. Chapter Introduction

In the previous chapters, we proposed leveraging the drinking water distribution network (WDN) to provide services to the power grid. However, we need to ensure that new water pumping control strategies do not negatively impact network performance, reliability, or resiliency. In this chapter, we evaluate the operational resiliency of the WDN to hazard events when the WDN operation is optimized to minimize pump electricity costs and provide frequency regulation to the bulk transmission system. Specifically, metrics are used to quantify the resiliency of the distribution networks after a wind event that causes power outages. The optimal pump control strategies are compared with conventional rule-based water system operation. We explore ways to incorporate resilience metrics into the optimal water pumping and grid services provision problem to improve upon or maintain current levels of resilience. We also evaluate the feasibility and impact of water network approximation and relaxation techniques within a hydraulic simulation. The contributions of this chapter are 1) assessing three operational water pumping strategies within a hydraulic simulator, 2) simulating a wind-based hazard event and investigating the water network's operational resiliency in a case study, and 3) highlighting the importance of considering resilience metrics in optimal coupled power-water problems.

The rest of this chapter is organized as follows: Section 8.3 provides an overview of our approach and the considered pump control strategies. In Section 8.4, we present the hazard modeling and simulation methods as well as discuss how we quantify and compare the operational resilience of the power and water network under different control strategies and hazard intensities. The optimal pumping problems are fully described in Section 8.5. Last, we present the results of a case study in Section 8.6 and provide concluding remarks in Section 8.7.

8.3. Problem Description

We consider a coupled power and water distribution network that is experiencing a wind event that may damage the utility poles in the power distribution network (PDN). Power outages in the PDN cause water pumping stations to shut down which can lead to reduced water pressures and water shortages in the WDN. However, power outages do not typically cause long-term damage on the WDN [30]. We compare how the WDN's performance given a hazard event can be impacted by different supply pump operational strategies. We consider

three different strategies – a conventional rule-based operation, an optimal pump schedule that minimizes pump electricity costs, and an optimal pump schedule that minimizes pump electricity costs and maximizes the profit of providing frequency regulation. We consider the frequency regulation service because we are able to explore the trade-offs of the WDN operating costs and the amount of frequency regulation capacity provided while considering the network performance and wind hazard intensities. To evaluate the operational resilience of the WDN’s operation to a wind-based hazard, we simulate large wind events and evaluate the power network’s (and correspondingly the water network’s) vulnerability to the considered hazard under different operational schemes.

8.3.1. Problem Approach

Below is a general outline of our approach to evaluate the operational resiliency of the WDN under different optimal operational strategies and power outage cases.

1. Planned Day-Ahead Operation: We first solve for the planned pump operation given the forecasted power and water demands over the scheduling horizon. We consider three different operational strategies – a rule-based operation, an optimal pump schedule that minimizes pumping costs, and an optimal pump schedule that minimizes pumping costs and maximizes profit from providing frequency regulation. These control strategies are outlined in Section 8.3.2 and the optimal pumping formulations are presented in Section 8.5.
2. Wind Event Simulations: To consider the performance of the networks under a range of scenarios, we next generate N outage scenarios from the probabilistic utility pole fragility curves given the three-second gust wind speeds for each time period within the scheduling horizon. The steps to generate the N outage scenarios are described in Section 8.4.1. Given the utility pole outages, we determine the corresponding PDN line/bus outages and WDN pump outages (i.e., time of failure and duration of pump outage). For each scenario, we also consider the wind event start time and utility pole repair time to be uncertain.
3. Pump Outages and Restoration Operation: In this work, we are focused on how different control strategies set up a WDN to respond to extreme events. For all control strategies, we chose that the water network reverts to rule-based control when the WDN experiences an outage. Given this, the only aspect that changes between simulations is

what strategy is used before the outage occurs. While we could also update the optimal water pumping problem given a partial outage, we do not have information on how the water system operators would make changes to the rule-based operation during an outage event. Because of this, we use a rule-based control during the contingency and restoration phase to make the results between each control strategy comparable.

4. Evaluate Network Operation and Resilience: For each scenario, we run a hydraulic analysis given the pump outages and restorations with the EPANET hydraulic simulator [102] in the Python package WNTR [55]. We then compute the resilience metrics for each scenario as well as the average results over the set the scenarios. We discuss the hydraulic simulator in Section 8.4.2 and the resilience metrics in Section 8.4.3.

8.3.2. WDN Operational Control Strategies

In this work, we consider the performance of the WDN under different operational strategies. Below are the three strategies that we consider.

Rule-Based Control (Rule)

In this strategy, we consider the rule-based controls that are traditionally used by water system operators. In our case study, we use the control rules that are included in the EPANET input file (INP) of our test network. Control rules in EPANET can adjust the status and setting of pumps and valves based on simulation time triggers (e.g., turn pump 2 off at 5:00 am) or network conditions (e.g., turn on pump 1 if the tank pressure goes below five meters).

Optimal Water Flow Control (OWF)

We optimize the water pump operation subject to the water flow constraints while minimizing water pump electricity costs. We formulate this problem as an iterative mixed-integer linear program, which is described in Section 8.5.2.

Optimal Water Flow Control + Frequency Regulation (OWF+FR)

In this strategy, we optimize the water pump operation to provide frequency regulation subject to the water flow constraints. We minimize the operational costs, i.e., the electricity costs of pump power consumption minus the profit associated with providing frequency

regulation. We solve for the pump schedule and frequency regulation capacity over a 24-hour scheduling horizon. In real-time, we adjust the pump speed to respond to the frequency regulation signal using the affinity laws [102, 104]. The OWF+FR formulation and the frequency regulation signal adjustments are described in Section 8.5.3.

8.4. Hazard Event Modeling and Simulation

In this section, we first describe modeling wind hazard events and the subsequent damage states of the wooden utility poles in the PDN. We then describe the hydraulic simulator and the metrics used to evaluate the resiliency of the power network.

8.4.1. Hazard Simulation and Outage States

We consider a multi-time period wind event that can damage wooden utility poles in the PDN. The damage status of the wooden utility poles determines the outage status of the lines and buses within the power distribution network as well as the power outage status of pumps in the WDN. We consider N scenarios, or replications, of a wind hazard event in order to consider the performance of the networks under a range of damage state outcomes. Below are the steps used to generate the damage state of the PDN given a wind event.

1. *Simulate wind speeds, overlaid over the PDN feeder.* Similar to [48], we assume time-varying, deterministic wind speeds that are uniform over the entire PDN. It should be noted that we could also simulate the wind fields with spatial resolution; for instance, [46, 129] map a maximum wind speed value and wind decay model within a wind field model to calculate storm radius, wind distribution, maximum three-second gust wind speeds, and duration of wind speeds above 20 m/s. For each scenario, the start time of the event is randomly generated from a uniform distribution. We do this in order to consider the impact of the hazards occurring at different times during the simulation period.
2. *Generate fragility curves.* For each scenario, we determine the damage state of the wooden utility poles in the PDN using fragility curves. A fragility curve is a probabilistic analysis of a specific network component's reliability under extreme conditions. For example, a wooden utility pole in the PDN can have a probability of failure from zero (unaffected) to one (critical, 100% chance of failure) given the wind speed intensity. We use the fragility curves of wooden utility poles for strong wind events

developed in [27]. In [27], the probability of failure during wind events is estimated given information on the poles (class, age, and height), conductors (number, diameter, orientation, and span length), and wind (speed and direction). The fragility curve is modeled as a lognormal cumulative distribution function (CDF)

$$P_f(V_t, y, \theta, A_c, h) = \Phi\left(\frac{\ln(2.23694 \times V_t) - \mu(y, \theta, A_c, h)}{\sigma(y, \theta, A_c, h)}\right), \quad (8.1)$$

where P_f is the probability of failure, V_t is the three-second gust wind speed at time step t (m/s), y is the modified age of the pole (years), θ is the angle between wind direction and conductors (degrees), A_c is the conductor area (m^2), h is the height of pole (m), $\mu(\cdot)$ and $\sigma(\cdot)$ return the parameters of the lognormal distribution, and $\Phi(\cdot)$ is the cumulative distribution function of the standard normal distribution. The conductor area and modified pole age are expressed as

$$A_c = n_c \times d_c \times L_c, \quad (8.2)$$

$$y = \max(\text{age}, 25), \quad (8.3)$$

where n_c is the number of conductors, d_c is the conductor diameter (m), and L_c is the span length between poles (i.e., length of conductor) (m). Estimations of μ and σ are determined with second-degree multivariable polynomials which are functions of θ , A_c , y , and h . The fragility parameter values in the polynomials—which are fitted using a generalized linear model given 20,000 training points—are provided in lookup tables for μ and σ for different pole classes [27]. It should be noted that the fragility curve in [27] may not depict the full damage impact of wind events on the PDN, since it does not consider downed lines from vegetation. This can be accounted for by using a different shifted fragility curve model in this framework.

3. *Create N multi-time period scenarios given fragility curves, where each scenario includes the damage states for all utility poles over the scheduling horizon.* Given the span length L_c and the distance between buses in the PDN, we determine the number of wooden utility poles between connected buses. For each wooden utility pole, we determine if a utility pole is damaged during the wind hazard event for all scenarios N . Whether a pole fails within a scenario is determined by randomly generating a

uniformly distributed number $r_t \in (0, 1)$ for all time steps t during the hazard event. If $P_f(V_t, y, \theta, A_c, h) > r_t$, then the pole fails. We randomly generate a utility pole repair time from a Gaussian distribution to determine how long the utility pole remains damaged.

4. *Given the PDN damage states in the N scenarios, determine what distribution lines and WDN pumps are experiencing outages.* This can be determined by solving for which buses are experiencing outages due to damaged utility poles. The pump and line outage information is needed for running the hydraulic analysis (Section 8.4.2) and solving for the power and water network resiliency metrics (Section 8.4.3).

8.4.2. Hydraulic Simulation

We simulate the WDN operation using the WNTR (Water Network Tool for Resilience) package in Python [55]. WNTR includes EPANET’s hydraulic simulator [87] as well as the ability to include stochastic simulations of disruptive events, outages, and recovery/repair actions. Since we are considering cases where there may be low pressure levels and unmet water demands, we use pressure-driven demand water flow analysis (as opposed to demand-driven water flow analysis, which is only reasonable under normal operating conditions). Within WNTR, we run hydraulic simulations over all N scenarios, where we can include information on pump power outages and restorations as well as pump control strategies.

8.4.3. Evaluating Operational Resilience

Ensuring the resilience of the power and water distribution networks to disruptive events is critical. When discussing resiliency and reliability, we consider the network’s ability to anticipate, absorb, adapt to, and recover from disruptive events. Operational resiliency, in particular, is related to supply and demand availability, effectiveness of corrective actions, and the operational status and capability of assets [48]. While there are many existing metrics used to define resilience, we use the concept of resilience metrics to quantify the network performance over the response and recovery to a hazard event [86, 89]. Resilience metrics can examine different performance factors, such as loss of load and water pressure violations. The overall estimated network resilience R is defined as the ratio between the network performance surrounding a hazard event and the network performance under normal

operation over the scheduling horizon

$$R = \frac{\sum_{t \in \mathcal{T}} P_E^t}{\sum_{t \in \mathcal{T}} P_N^t}, \quad (8.4)$$

where P_E^t and P_N^t are the time-varying performance curves for the extreme and normal operating cases and \mathcal{T} is the operational horizon. Note that the value of R is between zero and one, where one indicates that the network performance is unaffected by the hazard event. Below, we describe the power and water network factors that we consider.

Power Distribution Network

Similar to [89], we consider the number of active lines and connected loads in the extreme operating scenarios compared to the normal operating case for the PDN performance curves, i.e.,

$$R_{\text{line}} = \frac{\sum_{t \in \mathcal{T}} \sum_{\ell \in \mathcal{L}} \alpha_{\ell,E}^t}{\sum_{t \in \mathcal{T}} \sum_{\ell \in \mathcal{L}} \alpha_{\ell,N}^t}, \quad (8.5)$$

$$R_{\text{load}} = \frac{\sum_{t \in \mathcal{T}} \sum_{k \in \mathcal{K}} \beta_{k,E}^t}{\sum_{t \in \mathcal{T}} \sum_{k \in \mathcal{K}} \beta_{k,N}^t}, \quad (8.6)$$

where $\alpha_{\ell,E}^t \in \{0, 1\}$ and $\alpha_{\ell,N}^t \in \{0, 1\}$ are the active line statuses of line ℓ at time t for the extreme and normal operating case and \mathcal{L} is the set of lines in the PDN. The variables $\beta_{k,E}^t \in \{0, 1\}$ and $\beta_{k,N}^t \in \{0, 1\}$ are the connected load statuses of bus k at time t for the extreme and normal operating case, where \mathcal{K} is the set of buses in the PDN. It should be noted that resilience metrics based on similar performance indicators could be used given the particular objectives of the resilience analysis. The PDN resilience metrics help quantify the intensity of the wind events. Given the wooden utility pole damage statuses, we calculate the PDN resilience metrics for each scenario.

Water Distribution Network

For the WDN, we quantify resilience in terms of the water service availability R_{wsa} (i.e., the ratio of delivered water to expected water demand), pressure met R_{pressure} (i.e., demand junctions where the hydraulic head is above the minimum head limit \underline{H}_j), and the available

capacity of the tank R_{tank} (i.e., cumulative tank levels at the end of the scheduling horizon)

$$R_{\text{pressure}} = \frac{\sum_{t \in \mathcal{T}} \sum_{j \in \mathcal{J}} \mathbb{I}(H_{j,E}^t \geq \underline{H}_j)}{\sum_{t \in \mathcal{T}} \sum_{j \in \mathcal{J}} \mathbb{I}(H_{j,N}^t \geq \underline{H}_j)}, \quad (8.7)$$

$$R_{\text{tank}} = \frac{\sum_{j \in \mathcal{S}} H_{j,E}^{t=|\mathcal{T}|}}{\sum_{j \in \mathcal{S}} H_{j,N}^{t=|\mathcal{T}|}}, \quad (8.8)$$

where $H_{j,E}^t$ and $H_{j,N}^t$ are the hydraulic heads at junction or tank j at time t for the extreme and normal operating case, \mathcal{J} is the set of junctions in the WDN, \mathcal{S} is the set of water storage tanks in the WDN, and \mathbb{I} is an indicator function (i.e., $\mathbb{I}(A)$ returns one if A is true otherwise it returns zero).

8.5. Optimal Coupled Power-Water Frameworks

In this section, we summarize the network constraints and the problem formulation for the optimal water pumping formulations. The problem is solved over a set of time periods \mathcal{T} of duration ΔT .

8.5.1. Modeling Water Flow Constraints

The WDN can be represented as a directed graph with a set of nodes \mathcal{N} and edges \mathcal{E} connecting the nodes. Each node can be classified as either a junction \mathcal{J} , reservoir \mathcal{R} , or storage tank \mathcal{S} . The edges are either pumps \mathcal{P} or pipes (i.e., $\mathcal{E} \setminus \mathcal{P}$). We can characterize the water flow at time t by the volumetric flow rate x_{ij}^t through pipe ij (i.e., from node i to node j) for all $ij \in \mathcal{E}$ and the hydraulic head H_j^t at node j for all $j \in \mathcal{N}$. We consider pumps with variable speed drives. Below, we outline the water flow constraints by component.

Nodes. The conservation of water throughout the WDN must be satisfied

$$\sum_{i:ij \in \mathcal{E}} x_{ij}^t + d_j^t = 0 \quad \forall j \in \mathcal{N}, t \in \mathcal{T}, \quad (8.9)$$

where d_j^t is the water injection at node j and time t . The consumer water demands at junctions are non-positive values and the reservoir water supplies are non-negative values. During low pressure situations, fully meeting the consumer demand may be infeasible. In the hydraulic analysis, we use a pressure dependent demand simulation, where the water demand provided may be reduced if a demand junction is below the required pressure levels.

Additionally, the hydraulic head (elevation plus pressure head) at junctions must be within safe operating limits

$$\underline{H}_j \leq H_j^t \leq \bar{H}_j \quad \forall j \in \mathcal{J}, t \in \mathcal{T}, \quad (8.10)$$

where \underline{H}_j and \bar{H}_j are the minimum and maximum head limits at junction j .

Pipes. The frictional head loss along a pipe is commonly modeled with the empirical Hazen-Williams or theoretical Darcy-Weisbach head loss formulas of the form

$$H_i^t - H_j^t = \text{sgn}(x_{ij}^t) \cdot k_{ij} \cdot |x_{ij}^t|^n \quad \forall ij \in \mathcal{E} \setminus \mathcal{P}, t \in \mathcal{T},$$

where k_{ij} is the pipe resistance coefficient of pipe ij , n is the pipe head loss exponent, and function $\text{sgn}(x)$ returns the sign of x . The Hazen-Williams and Darcy-Weisbach head loss formulas are both nonconvex. In this chapter, we use the Hazen-Williams formula in order to be consistent with the head loss formula used within the WNTR simulator [55].

To reformulate the problem as an iterative mixed-integer linear program, we use a first-order Taylor series approximation around a flow rate to model the head loss along a pipe $ij \in \mathcal{E}$ at time t

$$H_i^t - H_j^t = f_{ij,0}^t + f_{ij,1}^t \cdot x_{ij}^t \quad \forall ij \in \mathcal{E} \setminus \mathcal{P}, t \in \mathcal{T} \quad (8.11)$$

where $f_{ij,0}^t$ and $f_{ij,1}^t$ are parameters. During each iteration, $f_{ij,0}^t$ and $f_{ij,1}^t$ are updated given the flow rate from the previous iteration. This is described in Algorithm 1.

Pumps. We consider variable speed supply pumps. We denote w_{ij}^t as the normalized speed setting of pump $ij \in \mathcal{P}$ at time t and $z_{ij}^t \in \{0, 1\}$ indicates whether pump $ij \in \mathcal{P}$ is on at time t . The pump flow rate and pump speed are enforced to operate within a certain range when the pump is on

$$\underline{x}_{ij} \cdot z_{ij}^t \leq x_{ij}^t \leq \bar{x}_{ij} \cdot w_{ij}^t \quad \forall ij \in \mathcal{P}, t \in \mathcal{T}, \quad (8.12)$$

$$\underline{w}_{ij} \cdot z_{ij}^t \leq w_{ij}^t \leq \bar{w}_{ij} \cdot z_{ij}^t \quad \forall ij \in \mathcal{P}, t \in \mathcal{T}, \quad (8.13)$$

$$z_{ij}^t \in \{0, 1\} \quad \forall ij \in \mathcal{P}, t \in \mathcal{T}, \quad (8.14)$$

where \underline{w}_{ij} and \bar{w}_{ij} are the minimum and maximum normalized pump speeds. The parameters $\underline{x}_{ij} \geq 0$ and \bar{x}_{ij} are the minimum and maximum pump flow rates when the pump is on and operating at the normalized pump speed. The maximum pump flow rate in (8.12) scales with

the pump speed, following the affinity laws. The affinity laws approximate how changes in pump speeds (i.e. pump speed w_1 to pump speed w_2) impact the pump characteristics [71]

$$\frac{x_1}{x_2} = \frac{w_1}{w_2}, \quad \frac{\hat{H}_1}{\hat{H}_2} = \left(\frac{w_1}{w_2}\right)^2, \quad \frac{p_1}{p_2} = \left(\frac{w_1}{w_2}\right)^3, \quad (8.15)$$

where x , \hat{H} , and p represents the flow rate, head gain, and pump power, respectively. The subscripts ‘1’ and ‘2’ are used to denote two different operating points. The big-M method is used to formulate the on and off characteristics of the pump performance curve. When the pump is off, the flow rate and speed are zero; when the pump is on, the head gain across the pump can be modeled with the power law [24, 102].

$$g_{ij}^t + M \cdot (1 - z_{ij}^t) \leq H_j^t - H_i^t \leq g_{ij}^t + M \cdot (1 - z_{ij}^t), \quad (8.16)$$

$$g_{ij}^t = (w_{ij}^t)^2 (b_{ij}^0 + b_{ij}^1 \cdot (x_{ij}^t / w_{ij}^t)^{c_{ij}}), \quad (8.17)$$

$\forall ij \in \mathcal{P}, t \in \mathcal{T}$, where M is a large number, g_{ij}^t is the pump head gain when pump ij is on and b_{ij}^0 , b_{ij}^1 , and c_{ij} are the pump curve parameters of pump ij . When the pump is off, there is no flow through the pump and the head gain is arbitrary. We define the pump curve using the single-point curves in EPANET and WNTR. In this case, $c_{ij} = 2$ and the head gain simplifies to

$$g_{ij}^t = b_{ij}^0 \cdot (w_{ij}^t)^2 - b_{ij}^1 \cdot (x_{ij}^t)^2 \quad \forall ij \in \mathcal{P}, t \in \mathcal{T}. \quad (8.18)$$

To aid in our reformulation of an iterative mixed-integer linear problem (MILP), we use a first-order Taylor series approximation around an initial flow rate of the pump head gain (8.18), similar to (8.11). We replace (8.18) with

$$g_{ij}^t = f_{ij,2}^t + f_{ij,3}^t w_{ij}^t + f_{ij,4}^t x_{ij}^t \quad \forall ij \in \mathcal{P}, t \in \mathcal{T}, \quad (8.19)$$

where $f_{ij,2}^t$, $f_{ij,3}^t$ and $f_{ij,4}^t$ are parameters that are updated every iteration; this is further described in Section 8.5.2.

The single-phase pump power consumption is dependent on the head gain and the flow rate across the pump

$$p_{ij}^t = \kappa \cdot 1/\eta(x_{ij}^t) \cdot (H_j^t - H_i^t) \cdot x_{ij}^t \quad \forall ij \in \mathcal{P}, t \in \mathcal{T}, \quad (8.20)$$

where κ is a parameter and $\eta(x_{ij}^t)$ is the pump efficiency function. The pump efficiency – which is dependent on the pump flow rate and speed – can be modeled as a quadratic or cubic polynomial [119]. We assume that the pumps are balanced three-phase loads with constant power factors. We approximate the pump power consumption as a linear function around the optimal operating point (specified in the EPANET INP file) at the nominal speed,

$$p_{ij}^t = c_{ij,0} + c_{ij,1} \cdot w_{ij}^t + c_{ij,2} \cdot x_{ij}^t \quad \forall ij \in \mathcal{P}, t \in \mathcal{T}, \quad (8.21)$$

where parameters $c_{ij,0}$, $c_{ij,1}$ and $c_{ij,2}$ are determined from the first order Taylor series approximation around the normalized pump speed and the desired operating point (where the efficiency is at its peak).

Tanks. Tanks are modeled the same as the EPANET constraints

$$H_j^{t=|\mathcal{T}|} \geq H_j^{t=0}, \quad (8.22a)$$

$$H_j^t = H_j^{t-1} - \frac{\Delta T}{\gamma_j} d_j^t \quad \forall t \in \mathcal{T}, \quad (8.22b)$$

$$\underline{H}_j \leq H_j^t \leq \bar{H}_j \quad \forall t \in \mathcal{T}, \quad (8.22c)$$

$\forall j \in \mathcal{S}$, where H_j^t is equivalent to the elevation and water level of tank j at time t and γ_j is the cross-sectional area of tank j . In (8.22a), we ensure that the final tank levels are greater than or equal to the initial tank levels. Since the water demands follow a daily pattern, this constraint helps enforce that the tank is not depleted over the scheduling horizon. The tank heads are updated in (8.22b) given the previous time period's head and the tank water injection in the current period. The tank head (and level) are bounded in (8.22c).

Reservoirs. We model the reservoirs as infinite sources with a fixed hydraulic head \hat{h}_j , i.e.,

$$H_j^t = \hat{h}_j \quad \forall j \in \mathcal{R}, t \in \mathcal{T}. \quad (8.23)$$

8.5.2. Optimal Water Flow Pumping Control (OWF)

We first present the OWF control strategy, where the WDN system operator minimizes the electricity costs of pumping subject to the water flow constraints and the water demand forecasts. We formulate the problem as an iterative MILP. The description of the algorithm is presented in Algorithm 1, where the convex optimization problem solved during each

iteration is

$$\begin{aligned} \min_{\mathbf{x}} \quad & \sum_{t \in \mathcal{T}} \sum_{ij \in \mathcal{P}} 3\pi_{ij}^t p_{ij}^t \Delta T \\ \text{s.t.} \quad & (8.9) - (8.14), (8.16), (8.19), (8.21) - (8.23). \end{aligned} \quad (\text{OWF})$$

where the parameter π_{ij}^t is the cost of electricity at pump ij and time t . The decision variable \mathbf{x} includes the pump power consumptions $p_{ij}^t \forall ij \in \mathcal{P}$, pump statuses $z_{ij}^t \forall ij \in \mathcal{P}$, pump speeds $w_{ij}^t \forall ij \in \mathcal{P}$, flow rates $x_{ij}^t \forall ij \in \mathcal{E}$, and hydraulic heads $H_j^t \forall j \in \mathcal{N}$ for all time periods $t \in \mathcal{T}$. During each iteration k , we update $\langle \mathbf{f} \rangle_k := \langle [f_{ij,0}^t, f_{ij,1}^t, f_{ij,2}^t, f_{ij,3}^t, f_{ij,4}^t] \rangle_k$ given the flow rates and pump speed from the previous iteration. We define the error as the difference between the flow rates and pump speeds between each consecutive iteration. We stop iterating when the error is below a certain threshold or we reach a maximum number of iterations.

Algorithm 1 Iterative OWF MILP Algorithm

Input: WDN topology, initial tank conditions $H_j^{t=0} \forall j \in \mathcal{S}$, and forecasted electricity prices $\pi_{ij}^t \forall ij \in \mathcal{P}, t \in \mathcal{T}$ and water demands $d_j^t \forall j \in \mathcal{J}, t \in \mathcal{T}$

Output: Pump power consumption p_{ij}^t , status z_{ij}^t , and speed $w_{ij}^t \forall ij \in \mathcal{P}, t \in \mathcal{T}$

1: Set $k \leftarrow 0$, tolerance = 0.01, maxIter = 100, error = 100

2: Initialize $\langle \mathbf{f} \rangle_k$, and $\langle \mathbf{x}, \mathbf{w} \rangle_k$ in (8.11) and (8.19)

3: while error \geq tolerance OR $k \leq$ maxIter do

4: $k \leftarrow k + 1$

5: Solve (OWF) $_k$ using $\langle \mathbf{f} \rangle_{k-1}$ to obtain $\langle \mathbf{x} \rangle_k := \langle x_{ij}^t \forall ij \in \mathcal{E}, t \in \mathcal{T} \rangle_k$ and $\langle \mathbf{w} \rangle_k := \langle w_{ij}^t \forall ij \in \mathcal{P}, t \in \mathcal{T} \rangle_k$

6: Calculate $\langle \mathbf{f} \rangle_k$ given $\langle \mathbf{x}, \mathbf{w} \rangle_k$

7: Calculate error := $\|\langle \mathbf{x}, \mathbf{w} \rangle_k - \langle \mathbf{x}, \mathbf{w} \rangle_{k-1}\|_2$

8: end while

The WDN operator sets pump status $z_{ij}^t := \langle z_{ij}^t \rangle_k$ and speed $w_{ij}^t := \langle w_{ij}^t \rangle_k$.

8.5.3. Optimal Water Pumping Control + Frequency Regulation (OWF+FR)

We next present the (OWF+FR) control strategy, where the WDN system operator minimizes the costs associated with pump electricity consumption and with providing frequency regulation subject to the water flow constraints. To provide frequency regulation in real time, the pumps adjust their power consumption as a function of the frequency regulation

signal, i.e., $\tilde{s} \in [-1, 1]$, which is scaled by the frequency regulation capacity. We assume a generator sign convention where up frequency regulation (or a positive signal) corresponds to a decrease in pump power consumption and down frequency regulation corresponds to an increase in pump power consumption.

In our formulation, we solve for the scheduled pump operation as well as the available frequency regulation capacity to adjust the pump power consumption given a frequency regulation signal. We assume that the WDN needs to be capable of providing the offered frequency regulation capacity over the entire hour time step t which is consistent with CAISO day-ahead market requirements for energy storage. This also allows us to use the same timescale as the quasi-steady state water flow constraints in our optimization problem. Additionally, we assume that there is an offsetting mechanism so that the frequency regulation signal is ‘energy neutral’ over the contracted period. We consider the maximum pump power consumption $p_{ij,\text{down}}^t$ and minimum pump power consumption $p_{ij,\text{up}}^t$ if the full down and up frequency regulation were used

$$p_{ij,\text{down}}^t = p_{ij}^t + F_{ij}^t \quad \forall ij \in \mathcal{P}, t \in \mathcal{T}, \quad (8.24)$$

$$p_{ij,\text{up}}^t = p_{ij}^t - F_{ij}^t \quad \forall ij \in \mathcal{P}, t \in \mathcal{T}, \quad (8.25)$$

$$F_{ij}^t \geq 0 \quad \forall ij \in \mathcal{P}, t \in \mathcal{T}, \quad (8.26)$$

where F_{ij}^t is the maximum symmetric up and down frequency regulation capacity that pump ij can provide at time t . The total frequency regulation capacity at time t is the cumulative capacity for all pumps at time t , i.e., $F^t = \sum_{ij \in \mathcal{P}} F_{ij}^t$.

The OWF+FR problem is also solved in the same iterative method as (OWF), where the optimization problem solved is

$$\begin{aligned} \min_{\mathbf{x}} \quad & \sum_{t \in \mathcal{T}} \sum_{ij \in \mathcal{P}} 3\pi_{ij}^t p_{ij}^t \Delta T - \pi_{\text{fr}}^t F_{ij}^t \Delta T \\ \text{s.t.} \quad & \mathcal{W}_{\text{scheduled}}(\mathbf{p}), \\ & \mathcal{W}_{\text{FR}}(\mathbf{p}_{\text{down}}), \\ & \mathcal{W}_{\text{FR}}(\mathbf{p}_{\text{up}}), \\ & (8.24) - (8.26) \end{aligned} \quad (\text{OWF+FR})$$

where π_{fr}^t is the price associated with offering frequency regulation. The scheduled water flow constraint set $\mathcal{W}_{\text{scheduled}}(\cdot)$ contains (8.9)-(8.14), (8.16), (8.19), and (8.21)-(8.23). The

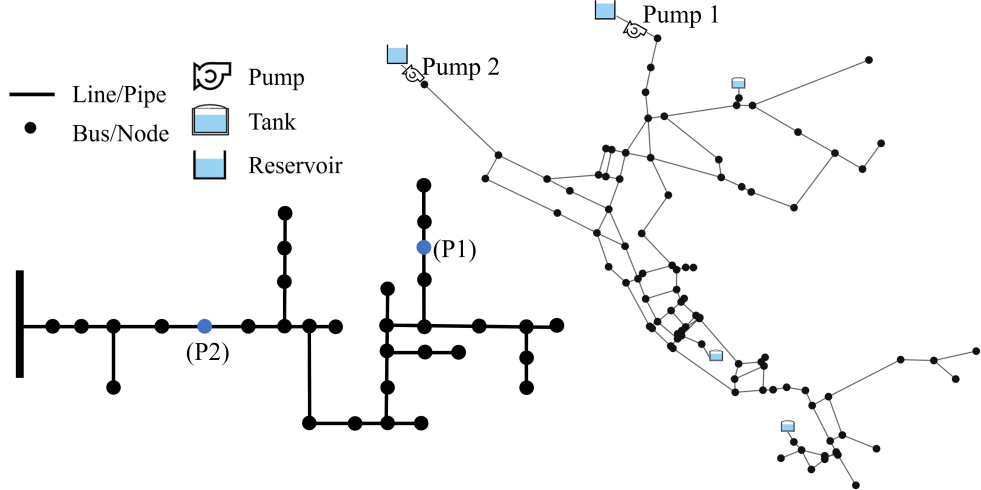


Figure 8.1: Topology of the coupled power distribution network (Left) and water distribution network (Right). Blue nodes in the power distribution network are used to indicate where the pumps are connected.

frequency regulation up and down water flow constraint sets $\mathcal{W}_{\text{FR}}(\cdot)$ contains (8.9)-(8.14), (8.16), (8.19),(8.21), and (8.22b)-(8.23). The decision variable \mathbf{x} includes the water flow variables associated with the schedule and frequency regulation capacity for all time periods.

Once we have determined the scheduled pump power consumption, scheduled pump speed, and frequency regulation capacities for each pump, the real-time frequency regulation pump power adjustment is determined by affinity laws (8.15) given the frequency regulation signal \tilde{s}

$$\hat{w}_{ij} = w_{ij,\text{nom}}^t \cdot \left(1 + \frac{F_{ij}^t \tilde{s}}{p_{ij,\text{nom}}^t}\right)^{1/3} \quad \forall ij \in \mathcal{P}, t \in \mathcal{T} \quad (8.27)$$

where \hat{w}_{ij} is the real-time pump speed. The scheduled pump speed $w_{ij,\text{nom}}^t$, scheduled pump power consumption $p_{ij,\text{nom}}^t$, and frequency regulation capacity F_{ij}^t are given for each time period of ΔT . The real-time pump speed is updated with changes in the frequency regulation signal on a faster time scale (i.e., every two seconds). This relationship applies for when the pump is on and providing frequency regulation.

8.6. Case Study

We consider a case study with a coupled PDN and WDN. The topology of the water and power networks are shown in Fig. 8.1. We consider a 24-hour scheduling horizon.

8.6.1. Set Up

In our case study, we consider a coupled PDN and WDN. The WDN is an example network (NET3) included in the EPANET software, which is also used in Chapter 7. NET3 has two reservoirs, three storage tanks, two supply pumps, and around 90 junctions. The minimum pressure head at junctions is set to 20 psi (approximately 14 m). The maximum pump flow (for pumps that are on) is $(b_{ij}^0/b_{ij}^1)^{1/c_{ij}}$ CMH (same as the definition in WNTR). The pump curves are determined using EPANET's single point curve definition given the desired flow rate and head at nominal speed provided in the EPANET INP file. The minimum and maximum normalized pump speeds are 0.7 and 1.3, respectively. We do not consider changes in efficiency curves given speed adjustments since the pump speed remains within $\pm 33\%$ of the normalized speed [71, 104]. The peak wire-to-water efficiency of both pumps is 75%.

We use the IEEE 34-node test feeder for the PDN. We assume that all of the utility poles are the same within the PDN, i.e., 50-year old class five poles. Class five poles were selected since distribution systems in the United States generally have class four and five poles [131]. We assume a span length of 46 meters (151 feet), $A_c = 2 \text{ m}^2$, and height of 12.2 meters. The pumps are connected to buses 844 and 814.

For the wind-based hazard, we assume the three-second gust wind speed is spatially uniform (yet with temporal variations) over the feeder. The wind event duration is five hours. The nominal gust wind speed during the hazard event is shown in Fig. 8.2. To consider different storm intensities, we use a multiplier to scale the three-second wind gust speed up, e.g., when we report results for a 175% wind speed intensity, the wind speeds in Fig. 8.2 are multiplied by 1.75. The wind direction is north-northeast (i.e., 30 degrees from due east). The fragility curves developed in [27] map a wooden utility pole's probability of failure to the three-second gust wind speed. In our case study, we assume that the poles and conductors are uniform throughout the PDN (e.g., all poles are 50 year old class 5 poles). As a result, the ‘steepness’ of the fragility curve is only dependent on θ , the angle between the conductors and the wind direction. In Fig. 8.3, we can observe that as θ increases to 90 degrees (i.e., wind is perpendicular to the conductors), the probability of failure is higher at smaller wind speeds.

There can be multiple pole outages that impact the outage of a line in the PDN. The time to repair for each pole is randomly generated from a Gaussian distribution with a mean of five hours and standard deviation of 2.5 hours [86]. It is assumed that no repairs are made during the storm for safety purposes. Therefore, the random time to repair starts at the end of the wind event. We do not consider queuing of repairs given the number of

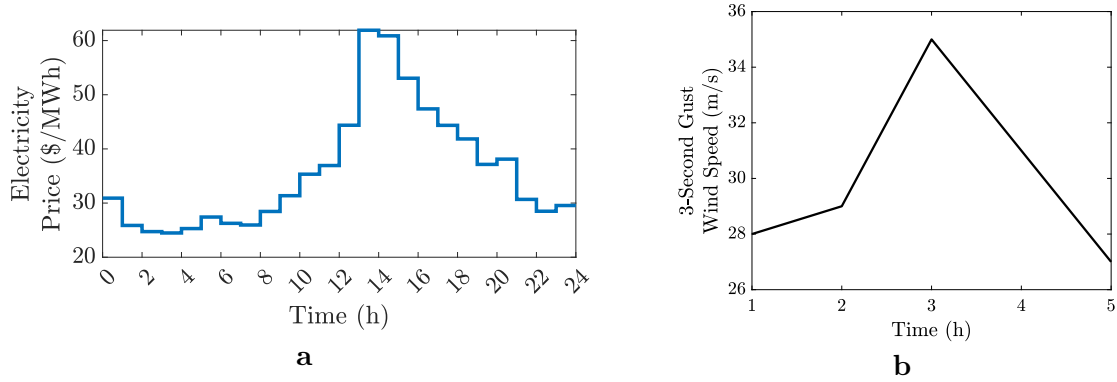


Figure 8.2: (a) Electricity prices over scheduling horizon and (b) Nominal three-second wind gust speed during the hazard event.

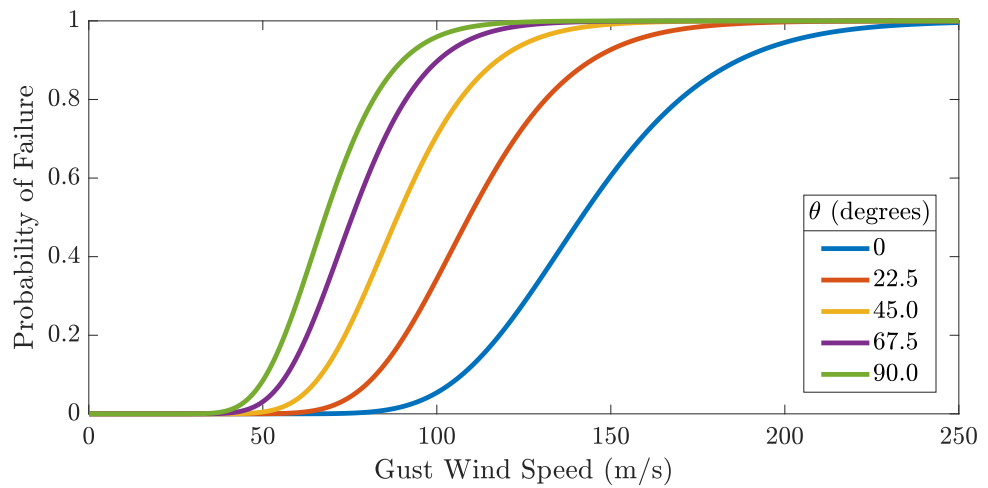


Figure 8.3: Probability of wooden utility pole failure as a function of the three-second gust wind speed. Fragility curves are depicted given the pole parameters used in the case study for varying θ values.

available repair crews since the focus of our work is comparing the performance of rule-based and optimal water network operation under the same set of scenarios. The wind event is randomly generated from a uniform distribution $U[t=10,t=15]$ since we want to consider the impact of when the event occurs and want to ensure that the full wind event concludes during the scheduling horizon. We consider 50 scenarios.

For the rule-based control strategy, we use the pre-existing controls in NET3's input file. For the optimal control strategies, we convert the controls to be rules and add a second condition so that the rules are not used under normal condition (i.e., before any pump outages occur). This is done by rewriting the controls as rules with an additional simulation time condition. We use a hydraulic time step and reporting time step of two seconds. With the optimal control strategies, we set the pump speed using a time series pattern and set the pump status using simulation time condition rules. We use the EPANET simulator within the WNTR package since the EPANET simulator can adjust the speed in variable speed pumps. For the frequency regulation signal within the real-time simulation, we use PJM's RegD signal from January 1, 2020 [92]. We set the frequency regulation price to \$0.20/kWh. The electricity price is shown in Fig. 8.2.

8.6.2. Results

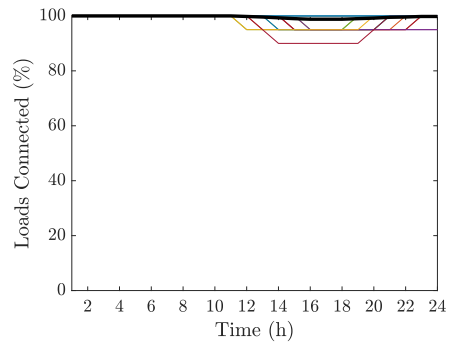
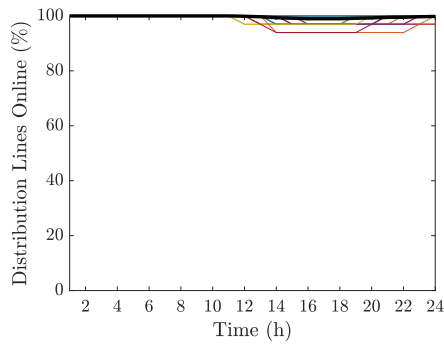
Power Distribution Network Resilience

We first consider the impact of the wind hazard on the PDN. In Fig. 8.4, we plot the active line and connected load performance curves of the PDN over each scenario while varying the three-second wind gust speed intensity. The average performances over all the scenarios is shown with bold black lines. The PDN performance curves can be used to better understand the implications of storm intensity. We calculate the resilience metrics of the active distribution lines R_{lines} and connected loads R_{load} —using the definitions in (8.5) and (8.6)—in Table 8.1. As expected, we can observe that the loss in loads and lines increases as the wind speed intensity increases.

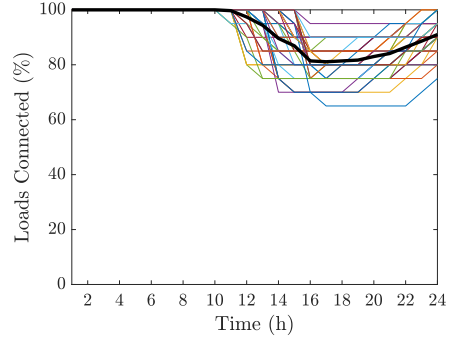
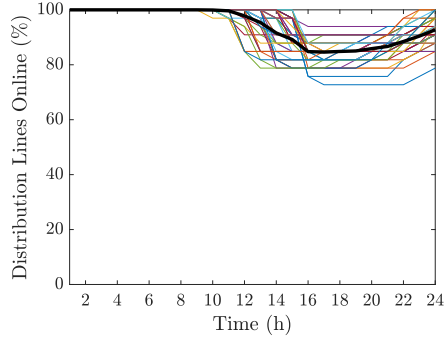
Comparison of Water Network Operation Strategies under Normal Operation

We next compared the operation of the control strategies under normal operation. Figure 8.5 depicts the tank levels and pump power consumption for each control strategy. For all control strategies, WNTR was able to find a feasible solution that met the required hydraulic head limits and did not deplete the final tank level. The pump power consumption between the

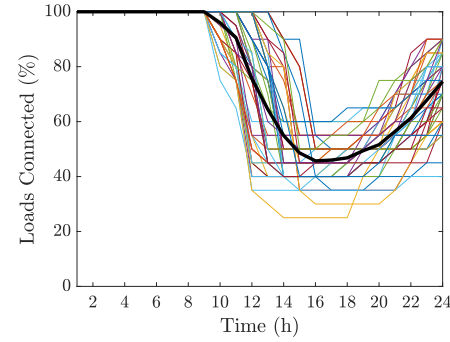
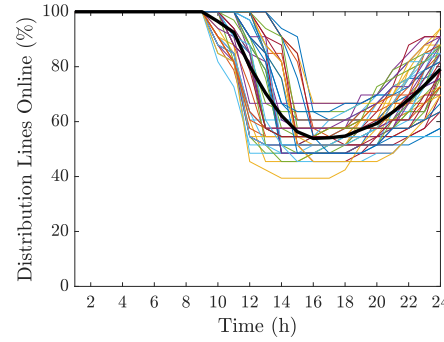
Wind speed, 100%



Wind speed, 125%



Wind speed, 150%



Wind speed, 175%

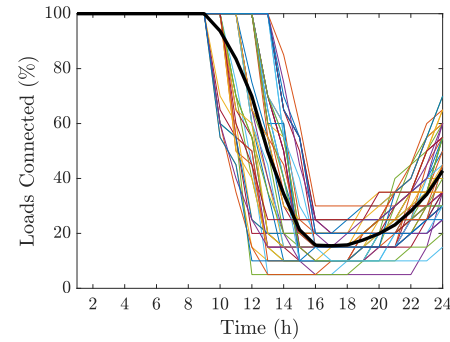
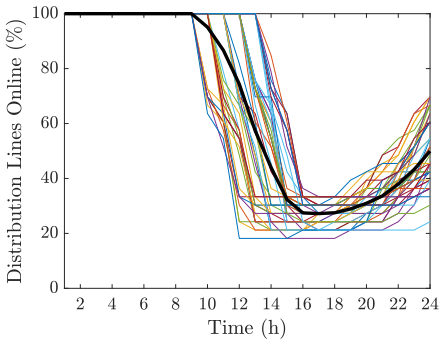


Figure 8.4: Power distribution network performance indicator functions for the percentage of distribution lines online (Left) and percentage of loads connected (Right) for varying wind speed intensities (each row). The solid black line is the average performance over the 50 scenarios.

Table 8.1: Power Distribution Network Resilience Metrics

Wind Speed (%)	$R_{\text{load}} (\%)$	$R_{\text{lines}} (\%)$
100	99.58	99.64
125	93.38	92.06
150	79.49	75.80
175	63.83	58.33

Table 8.2: Operational Costs

Control Strategy	Electricity Costs (\$)
(Rule)	10,217
(OWF)	6,665

control strategies ends up varying significantly. In the rule-based control, we see pump 1 switching on and off frequently given the water level of tank 1. The rule-based operation ensures that tank 1's water storage is between 40% and 60% of the total tank capacity. In the optimal control strategies, the pump varies its speed away from the normalized pump speed in order to realize lower costs and/or provide frequency regulation. In the OWF+FR solution, we can observe very frequent pump power changes due to pump speed adjustments as the pumps responds to the historical frequency regulation signal.

Table 8.2 reports the electricity costs, frequency regulation profit, and total costs for the rule-based and OWF control strategy. We can observe that the total costs of the optimal control strategy is less expensive than the rule-based control strategy. For instance, the cost of the OWF solution is a 35% decrease from the rule-based cost. This is because the optimal water pumping strategies minimize the electricity cost associated with pump and, in the OWF+FR problem, maximizes the profits associated with frequency regulation. It should be noted that the OWF+FR iterative solution approach had issues converging to the desired tolerance within the specified number of iterations. The OWF+FR results are taken from the maximum iteration number. When comparing costs, we would expect the water system operation to not want to provide frequency regulation if the cost of adjusting pump operation is more than the profit of providing frequency regulation. However, we found that the cost of the OWF+FR solution was more expensive than the OWF solution. This is likely due to the OWF+FR formulation having issues converging. Additionally, a number of different approximations and relaxations of the pipe head loss and pump head gain equations were tested and some resulted in the tanks being fully depleted by the end of the scheduling horizon under normal operation or WNTR was unable to find a water flow

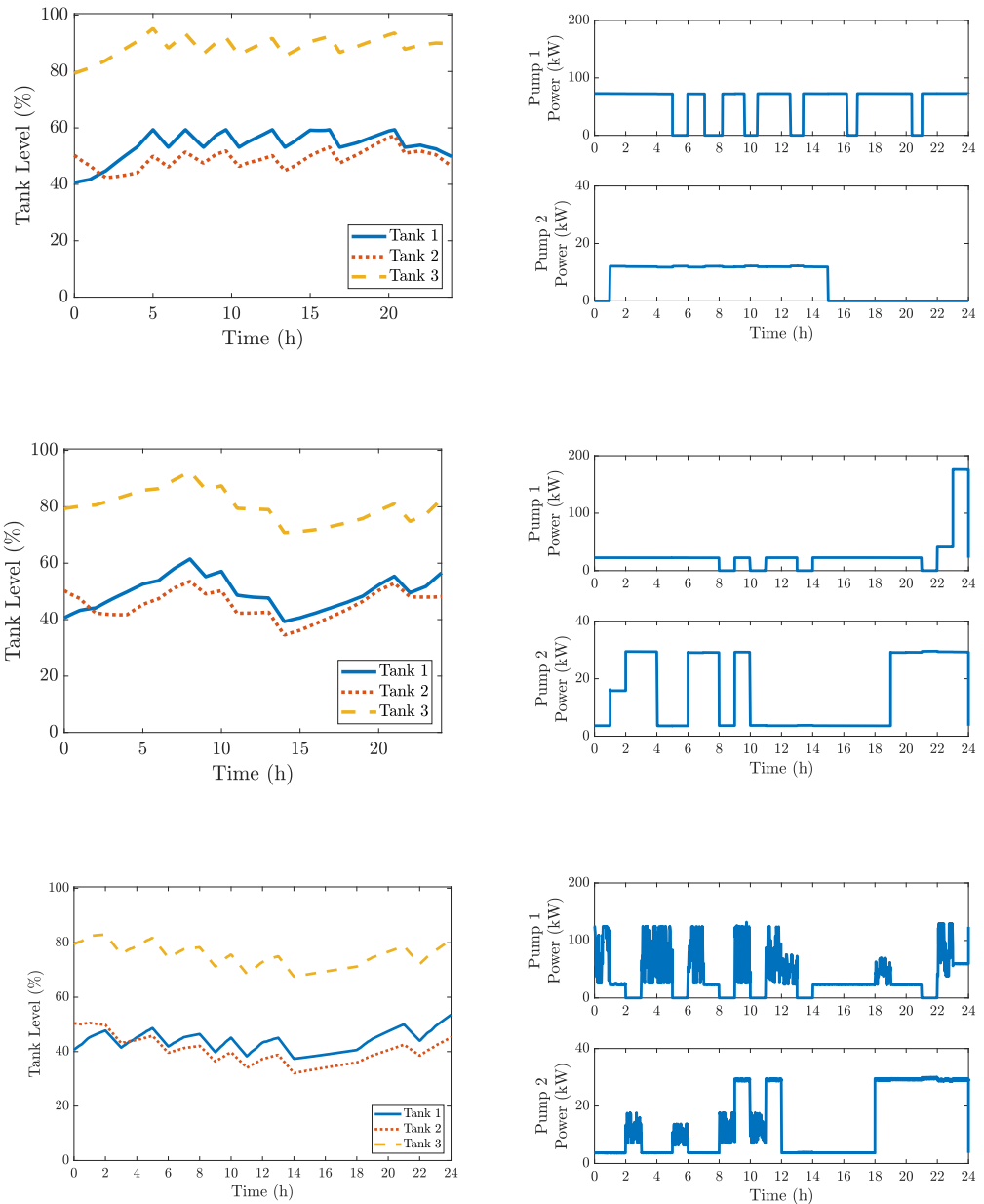


Figure 8.5: (Left) Tank water levels—as percentage of total tank volume—and (Right) pump power consumption in the (Top) Rule-based, (Middle) OWF, and (Bottom) OWF+FR control strategies under normal operating conditions.

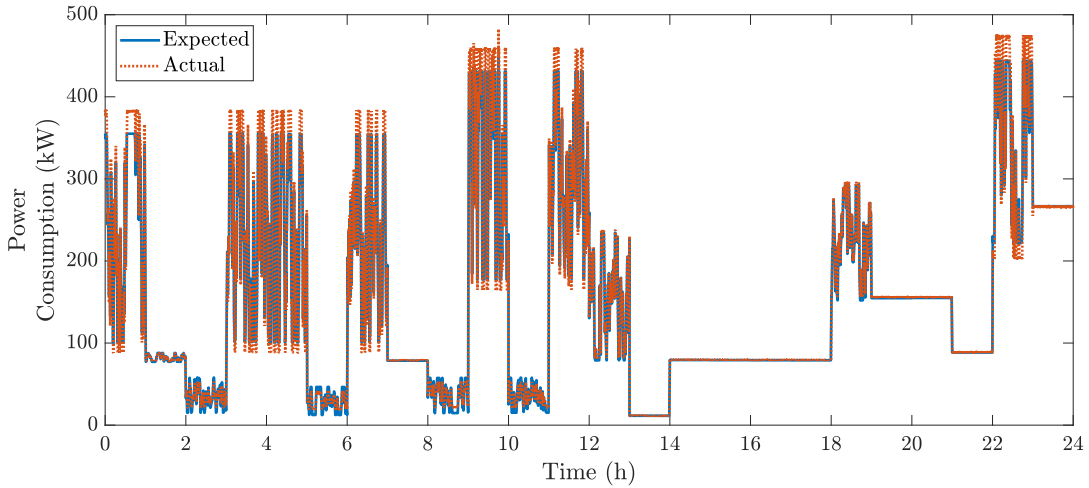


Figure 8.6: Pump power consumption in the OWF+FR problem. The blue solid line is the expected pump power consumption given the frequency regulation signal. The orange dashed line is actual pump power consumption simulated in WNTR.

solution. This motivates future work to evaluate the accuracy and convergence of different water flow models.

Figure 8.6 illustrates the WDN's ability to follow the frequency regulation signal with the OWF+FR control strategy. Given the frequency regulation capacity, we used the affinity laws (8.15) to adjust the pump speed given the historical signal, the scheduled pump speed, and the scheduled pump power consumption. Overall, the WDN is able to follow the frequency signal. In certain cases, we can observe over- and under-estimations of the amount of pump adjustments needed to follow the signal. This is likely due to the linear pump power consumption approximation. To address this, we can improve the water flow approximations in the OWF+FR problem. Alternatively, we could use real-time feedback of the pump power consumption to adjust the pump speed instead of using the affinity laws (e.g., with a proportional-integral controller).

Comparison of Water Network Operation Strategies under Extreme Operation

We next consider the performance of the rule-based, OWF, and OWF+FR control strategies when the WDN is experiencing pump outages due to a wind hazard. Table 8.3 presents the resilience of the rule-based, OWF, and OWF+FR control strategies for varying wind speed intensities. We calculate resilience metrics using (8.4), (8.7)-(8.8) for the junctions that meet

Table 8.3: Water Distribution Network Resilience Metrics

Wind Speed	Rule	$R_{\text{pressure}} (\%)$		$R_{\text{tank}} (\%)$		
		OWF	OWF+FR	Rule	OWF	OWF+FR
100	100.00	100.00	100.00	100.00	100.00	100.00
125	100.00	100.00	100.00	91.14	91.95	91.74
150	99.98	99.88	99.98	39.74	41.96	40.99
175	99.95	99.86	99.92	17.61	16.19	17.13

the minimum water pressure requirement R_{pressure} and the available water capacity in the tank at the end of the scheduling horizon R_{tank} (as compared to the normal operation case). As expected, the resilience of the WDN decreases as the wind hazard intensity increases. Within the WNTR simulation, all cases run found that the expected water demand is always met. As a result, we did not include the water service availability resilience metric in the table. For longer outages, we expect that the water service availability would decrease under the pressure driven demand simulation in WNTR. Generally, we found that the tank capacity and the water pressure violations were comparable between control strategies. One thing to note is that the controls in the rule-based strategy keeps the tank levels within a smaller range of possible tank levels. For instance, in the rule-based operation, pump 1 is turned on whenever tank 1's water level goes below 40% and is turned off whenever tank 1's water level goes above 60% of its total available capacity. Alternatively, the optimal pumping problems do not place further limits on the tank levels throughout the scheduling horizon. Since the optimal pumping strategies choose less expensive operating points, there is a chance that the operational set points may end up being more risky for the WDN. To address this, we can incorporate more constraints within the optimal pumping problem to help improve the resiliency of the operation. For example, we could strictly limit the normal tank level operation to be within a restricted range of values or penalize deviations outside of a certain range of tank levels. Additionally, in the case where the water system operator is aware of an upcoming hazard event, pre-filling tank constraints can be incorporated into the optimal pumping problem. Additional methods to add constraints to ensure resiliency is left to future work.

Fig. 8.7 compares the tank levels for the rule-based and optimal control strategies at 175% wind speed intensity over fifty scenarios. In all cases, we can observe that the tanks are depleted when there is a pump outage (generally starting around hour 10-15). This is because the tanks provide more water to meet demand when the pumps cannot. For short periods, tanks can be used to hedge against outages and water demand uncertainty. Overall,

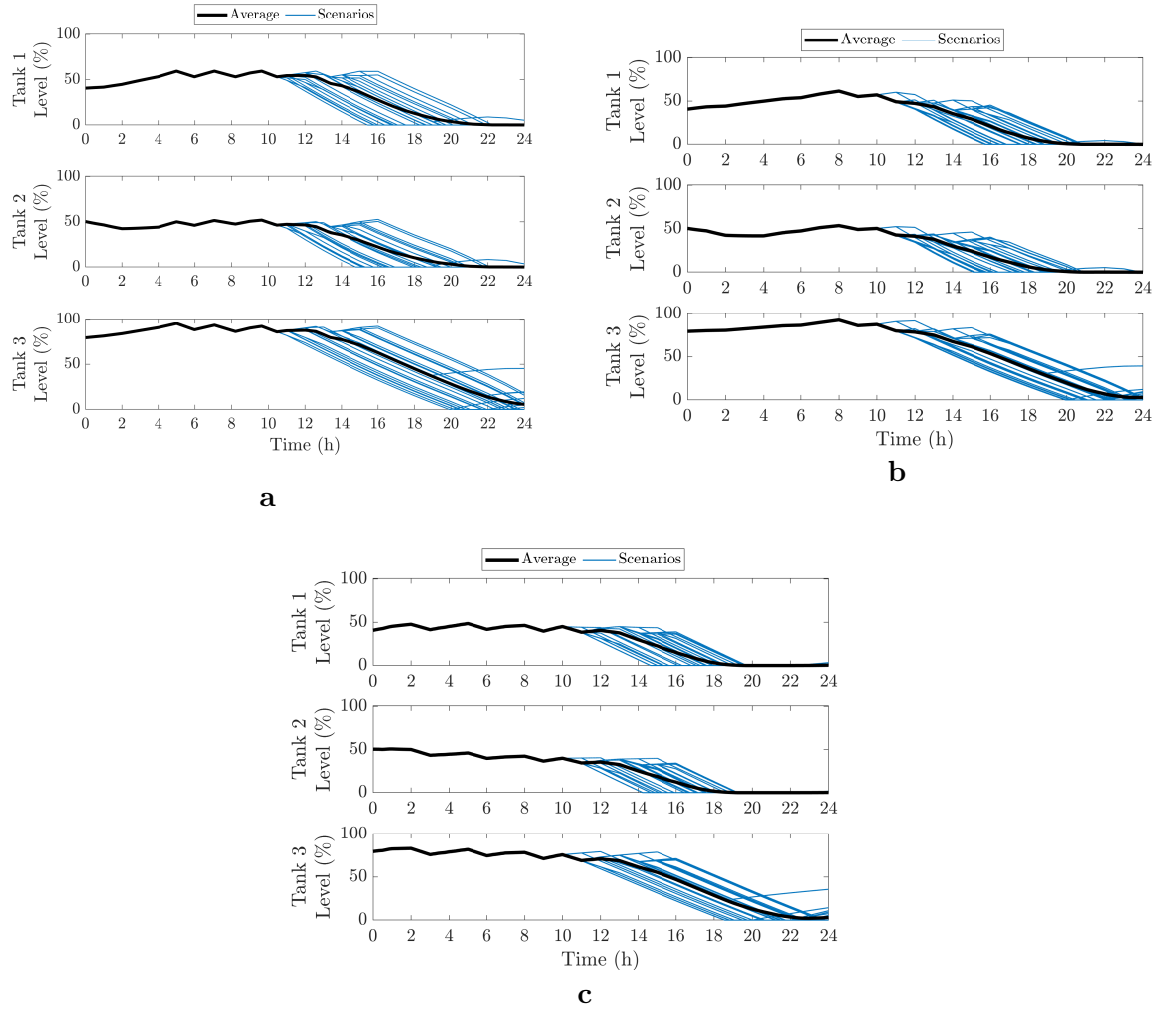


Figure 8.7: Time-varying tank levels (as a percentage of available tank volume) simulated in WNTR with a 175% wind intensity for a) the rule-based control, b) OWF, and c) OWF+FR control strategies. The blue lines are the tank levels for each scenario. The solid black lines are the average tank levels over all scenarios.

the operation via the rule-based and optimal control strategies are similar.

8.7. Chapter Conclusion

In this chapter, we compared the performance and operational resiliency of the water network to a wind-based event under different control strategies. The wind event caused power outages in the PDN which then caused pump outages in the WDN. We found that the performance of the rule-based control strategy and the optimal pumping strategy to be similar, except the cost of the optimal strategy is significantly less expensive. When simulating the wind-based hazards, we found that the optimal strategy performed slightly worse since it needed to draw more water from the tanks than the rule-based control. This is due to the fact that the rule-based control strategy had stricter tank limits than what was included in the optimal water flow problem. However, we can incorporate constraints that can improve the system resiliency (e.g., tank limits throughout the scheduling horizon or tank pre-filling requirements before a big storm).

Chapter 9.

Conclusion

During the transition to low carbon energy systems, leveraging flexible loads is increasingly important. In this dissertation, we optimized and controlled supply pumps in the drinking water distribution network (WDN) to support the power network subject to the power and water network constraints and sources of uncertainty. In this chapter, we summarize the dissertation’s main findings, discuss the current barriers to implementation, and highlight potential directions for future research.

9.1. Summary of Key Results

The research in Chapters 2-8 demonstrated the potential of using water pumps in the WDN as flexible loads, developed computational tractable optimization frameworks for the integrated power-water network problem, and evaluated the network performance and value proposition under this framework.

Chapter 2 provides a rough estimate of the flexibility potential of drinking water distribution networks in the United States. We characterize the flexibility potential in terms of energy capacity and power capacity, similar to a battery. Through municipal water utility reports from Wisconsin, we estimate the power and energy capacity in Wisconsin and extrapolate the measure to the United States by pulling nationwide statistics on water utilities. From this estimate, we found that WDNs in the United States appear to have a sizeable flexibility potential. This work provides motivation for the rest of the dissertation.

Chapter 3 formulates a chance-constrained water pumping optimization problem subject to water and power constraints while managing water demand uncertainty. We reformulated this problem by heuristically applying a scenario-based approach. The chance constraint

helps ensure that the voltages in the power distribution network are within a safe operating range. While using the pumps in the water network seems promising, the formulation did not provide any probabilistic guarantees and we needed to solve the problem multiple times with different warm starts.

Chapter 4 proposes a chance-constrained optimization framework that considered the power demand uncertainty. We employed convex relaxations and approximation techniques to reformulate the problem using the scenario approach for convex problems. We were able to successfully adjust the pumps to respond to voltage violations in the PDN. Here, we were able to provide probabilistic guarantees on the convex problem. A challenge that we observed with the scenario approach is scaling to large networks and long optimization horizons.

Chapter 5 formulates a chance-constrained optimization problem subject to both power and water demand uncertainty. We developed corrective and balancing control policies to adjust the real-time pump set points given the uncertainty realizations. We evaluated the impact of the approximations and relaxations in our case study and found that the approximations for the WDN were reasonable and the PDN ‘Lin3DistFlow’ model overestimated the voltage magnitudes, leading to small voltage deviations. We considered an approach to simplify the power control policy. Overall, we found the solution approach to be conservative and memory intensive.

Chapter 6 proves that the monotonicity properties apply to the WDN and identified the necessary assumptions on tank operation. We proposed a robust formulation that controls water pumping in the WDN to provide voltage support to the PDN given power demand uncertainty. Using the monotonicity properties, we can reformulate the robust problem into a tractable affinely adjustable robust counterpart. As an alternative formulation that is less conservative, we proposed a probabilistic water pumping problem to provide voltage support to the PDN given power demand uncertainty. The problem is subject to a chance-constrained power flow model given power demand uncertainty and a probabilistically robust water flow model given the impact of the power demand uncertainty on the real-time pump power adjustments (i.e., via the voltage support control policy). When comparing the probabilistic approach to the robust approach, we found that the probabilistic approach is significantly less conservative than the robust approach and has a comparable computational performance. The results in the case study indicated that the probabilistic approach can be applied to large networks.

Chapter 7 develops a robust water pumping problem subject to WDN and PDN constraints that provides multiple grid services. We considered providing voltage support and

frequency regulation concurrently. In this formulation, we ensured that providing multiple services simultaneously do not counteract each other (e.g., responding to a minimum voltage limit violation in the power distribution network and providing down frequency regulation). The resulting problem is a mixed-integer nonconvex problem. We reformulated the problem as three sequential sub-problems that are convex. Results indicate that the WDN is capable of providing multiple services at the same time.

Chapter 8 evaluates the performance of optimal control policies within a water distribution network that is experiencing power outages due to a wind-based hazard. We compared the optimal pumping problem that minimizes electricity costs and provides frequency regulation with a traditional rule-based control strategy. We analyzed the control strategies in a hydraulic simulator for 50 pump outage scenarios. The scenarios are generated from the probabilistic fragility curves of wooden utility poles in the power distribution network. Overall, we found that the optimal control strategy was significantly less expensive. We observed that the resilience metrics for the rule-based and optimal control strategies were comparable. The rule-based control strategy had stricter tank limits than what was included in the optimal water flow problem. The optimal control strategies seek to minimize costs and do not explicitly consider network reliability and resiliency. However, we can incorporate constraints into the optimal pumping problems which can further ensure the system resiliency.

9.2. Synthesis of Approaches

Multiple formulation and solution approaches are developed and assessed for leveraging WDN pumps as flexible loads. In this section, we discuss some of the chapters' key modeling differences as well as compare the performance of the solution approaches.

We first discuss the assumptions and approximations used when modeling the WDN's water flow constraints. The water flow constraints are nonconvex due to the head difference equations over the pipes and pumps as well as the pump power consumption equation.

- *Bidirectional water flow in pipes:* WDNs, with the exception of rural networks, are usually mesh networks. Because of this, the direction of water flowing along a pipe can change direction over time. The direction of the water flow is an input in the pipe head loss equations. In Chapters 3-5, we assume that the water flow direction is fixed and known in advance. This allows us to reformulate the now quadratic constraint as a convex hull where the lower bound of the pipe head loss equation is exact. In

Chapters 6-8, we do not make this assumption. Given this, we can either reformulate the pipe head loss equation as a quasi-convex hull (i.e., Chapters 6-7) or linearize the head loss equation with a first-order Taylor series approximation and solve the linearized problem iteratively (i.e., Chapter 8). Using a formulation that allows bi-directional flow in pipes is more realistic; future work will consider the impact of head loss approximations on the pump scheduling operation.

- *Tank Formulation:* In this dissertation, we consider multiple tank formulations. In Chapters 4-5, we consider a separate inlet and outlet pipe. In Chapters 6-7, we make physical and operational tank assumptions in order to apply the monotonicity properties. Specifically, the physical tank assumptions require that there is a pump and/or valve connected to the tank. This assumption is most likely to hold in the case that the tank is located at ground level (i.e., it is not elevated). The implication of these assumptions are further detailed in Chapter 6. In Chapter 8, we use the same tank formulation as EPANET, where there is one inlet/outlet pipe located at the bottom of the tank. All three tank assumptions are used in the literature; however, the most typical tank configuration appears to be the EPANET formulation.
- *Fixed Speed and Variable Speed Pumps:* In this work, we consider both fixed speed and variable speed pumps. Variable speed pumps are pumps that have a variable frequency drive. Variable speed pumps can be operated more efficiently and consume less energy than fixed speed pumps [120]. As a result, variable speed pumps have proven to be beneficial in water and waste water applications and are likely to be used more in future water systems [79].

Second, we discuss the performance of solution approaches proposed in Chapters 3-7. Chapters 3-5 employ scenario-based approaches to solve the chance-constrained optimization problem. Overall, we found this approach to be excessively conservative and memory-intensive. However, scenario generation and reduction techniques could reduce the conservativeness and memory requirements. Chapters 6-7 employ the monotonicity properties which allows us to the tractably reformulate the water flow constraints subject to uncertainty without relying on the scenario approach. Within this work, we found that the probabilistic approach in Chapter 6 was significantly less costly than a robust approach while still maintaining its computational tractability. Lastly, the findings in this dissertation focuses on the power network's interaction with the drinking water distribution network; however, related

systems such as agricultural irrigation, wastewater treatment, and district heating can adopt and modify the proposed formulations and solution approaches.

9.3. Barriers to Implementation

In this dissertation, we demonstrate the feasibility and potential of using the WDN as a flexible load to provide services to the power grid. However, there are several challenges and obstacles that need to be considered. These are detailed below:

- *Communication and Control Infrastructure:* In [28], the authors report that most large water utilities have SCADA systems, which can allow WDNs to have fast, operational control of the pumps and valves within the network. However, real-time operational control is significantly more challenging for utilities that do not have SCADA systems. Historically, there has been governmental funding sources for the installation of SCADA systems or other energy efficiency measures, e.g., the Environmental Protection Agency's Drinking Water State Revolving Fund [80]. Additionally, when co-ordinating the operation between two traditionally independently operated systems, the communication and measurement needs between the networks need to be assessed. Several approaches, such as a distributed formulation, can help reduce these communication needs.
- *Regulatory and Water Quality Constraints:* The operation of the water network needs to meet regulatory constraints on the active control of tank storage and water quality. First, tanks are important for providing equalizing pressure support as well as contingency water for fire fighting needs. As a result, the amount of water in the tanks that can be used for normal operational control (i.e., operational storage) is less than the physical tank volume. The operational limits on the tank level vary by state. For example, in the state of Washington, the minimum equalizing storage capacity is a function of the peak hourly demand and information on the water sources, the minimum fire suppression and standby capacity is determined by the fire flow rate and duration set by the fire authority and the typical water consumed by a household in the network, and the operational storage should be large enough to prevent excessive cycling of the pumps [2]. Second, treated water entering the drinking water distribution network contains a minimal residual disinfectant concentration (e.g., chlorine) to prevent bacterial regrowth [6]. The disinfectant ages, or decays, the longer the water remains in the

distribution network. Storing more water in tanks can reduce water turnover which can lead to disinfection byproduct formation and biological regrowth [6]. EPANET models the water quality in a distribution network; however, it may not be reflective of the chlorine residual throughout the WDN in some cases [6, 102].

- *Scaling to Large Networks:* Chapter 6 in this dissertation focuses on reducing the computational tractability of the optimal pumping problem. However, it remains to be seen how well the approach scales to actual very large networks. Additional solution approaches may be needed to maintain computational tractability for very large networks, e.g., by decoupling the problem by WDN pressure zones.

Additionally, water and power utilities tend to be risk-adverse and hesitant to change. Therefore, it is important to provide clear benefits to both network operators (e.g., financial incentives) and provide a high-level of certainty that new operational strategies maintain or improve upon network reliability and resiliency.

9.4. Future Research

In this dissertation, we have demonstrated how the water distribution networks can be optimized and controlled to provide grid services, examined the impact of uncertainty on the optimal pumping problem, and evaluated the trade-offs of performance and computational tractability. This work has motivated several areas of future research. Below, we outline these research topics.

- *Analyzing the performance of convex approximations and relaxations in the coupled power-water problem:* In this dissertation, we considered several relaxation and approximation techniques. Additionally, a large number of approximations and relaxations have been proposed in the literature. We would like to gain a better understanding of these approaches' feasibility and optimality.
- *Developing solution algorithms to reduce information sharing:* Traditionally, the water network and power network are independently operated. Posing the coupled power-water problem as a centralized optimization problem could cause privacy and information sharing concerns. We could consider solution approaches that minimize information sharing, for example, by considering a distributed optimization approach.

- *Coordination of multiple flexible resources in the coupled WDN-PDN:* In this dissertation, we considered the WDN's flexibility from the water system operator's perspective. We could also consider how to optimize the WDN with other flexible resources in the PDN, such as energy storage or distribution energy resources. This would bring in additional sources of uncertainty into the problem and increase complexity. However, considering how to coordinate the WDN as a part of a larger array of flexible assets is critical for understanding how they complement and compete with each other.

Appendix A.

General Convex Relaxation for Head Loss Formulas

In general, the frictional head loss equations for pipes are nonconvex. In [61], the authors present a quasi-convex hull relaxation for the Darcy-Weisbach head loss formula⁵. Here, we generalize the relaxation so that it also applies to the Hazen-Williams head loss formula. We drop the time superscript t for simplicity. We consider the generic frictional head loss model for a pipe ij

$$\hat{h}(x_{ij}) = k_{ij} \cdot x_{ij} \cdot |x_{ij}|^{n-1}, \quad (\text{A.1})$$

where the function $\hat{h}(x_{ij})$ returns the head loss along pipe ij , i.e., $H_i - H_j$. In the Darcy-Weisbach head loss formula, n is 2 and k is dependent on the pipe's length and diameter as well as the Reynolds number. In the empirically derived Hazen-Williams formula, n is 1.852 and k is a function of the pipe's length, diameter, and roughness coefficient. We create a convex relaxation, similar to [61], in terms of n , k , and the minimum and maximum volumetric flow rates through the pipe. We denote the feasible range of pipe flow rates as $(\underline{x}_{ij}, \bar{x}_{ij})$ where $\underline{x}_{ij} < 0$ and $\bar{x}_{ij} > 0$ are the minimum and maximum flow rates⁶. Fig. A.1 illustrates the convex relaxation given a set of linear inequalities.

For each pipe, the head loss relaxation is a set of four linear inequalities. The linear functions are tangent to the head loss function at \bar{x}_{ij} , \underline{x}_{ij} , x_1 , and x_2 , where x_1 and x_2

⁵It should be noted that the second and fourth linear inequalities in the quasi-convex hull equations (8) in [61] have errors in the signs. This can be confirmed when plotting the quasi-convex hull.

⁶If the minimum and maximum flow rates are the same sign, then we can form the convex hull, e.g., see [61, 111]. Instead, in this work, we consider the case where the volumetric flow rate through the pipe can be bidirectional.

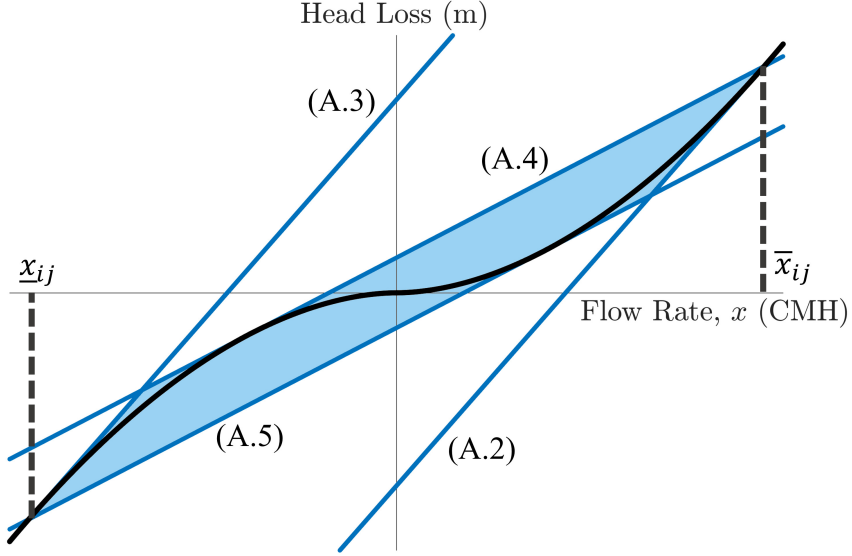


Figure A.1: Convex relaxation (shaded blue area) of a generic pipe head loss formula (black line). The quasi-convex hull is made from a set of linear functions (A.2)-(A.5), shown with blue lines.

are flow rate values on the head loss curve where its tangent intersects with \bar{x}_{ij} and \underline{x}_{ij} , respectively. The tangent line of $\hat{h}(x_{ij})$ evaluated at flow rate x_a is

$$f_{x_a}(x_{ij}) = \hat{h}'(x_a) \cdot (x_{ij} - x_a) + \hat{h}(x_a)$$

for $x_a \neq 0$. Accordingly, we want to solve for

$$\hat{h}(x_{ij}) \geq f_{\bar{x}_{ij}}(x_{ij}), \quad (\text{A.2})$$

$$\hat{h}(x_{ij}) \leq f_{\underline{x}_{ij}}(x_{ij}), \quad (\text{A.3})$$

$$\hat{h}(x_{ij}) \leq f_{x_1}(x_{ij}) \quad \text{where } x_1 \text{ satisfies } f_{x_1}(\bar{x}_{ij}) = \hat{h}(\bar{x}_{ij}), \quad (\text{A.4})$$

$$\hat{h}(x_{ij}) \geq f_{x_2}(x_{ij}) \quad \text{where } x_2 \text{ satisfies } f_{x_2}(\underline{x}_{ij}) = \hat{h}(\underline{x}_{ij}). \quad (\text{A.5})$$

For ease of notation, let's assume $\underline{x}_{ij} = -\bar{x}_{ij}$. Note that this can also be written for the case where $\underline{x}_{ij} \neq -\bar{x}$. Given that $\underline{x}_{ij} = -\bar{x}_{ij}$, $x_1 = -x_2$, and $\bar{x}_{ij} > 0$, the resulting inequalities simplify to

$$\hat{h}(x_{ij}) \geq n \cdot k_{ij} \cdot \bar{x}_{ij}^{(n-1)} \cdot x_{ij} + (1-n) \cdot k_{ij} \cdot \bar{x}_{ij}^n, \quad (\text{A.6})$$

$$\hat{h}(x_{ij}) \leq n \cdot k_{ij} \cdot \underline{x}_{ij}^{(n-1)} \cdot x_{ij} + (n-1) \cdot k_{ij} \cdot \bar{x}_{ij}^n, \quad (\text{A.7})$$

$$\hat{h}(x_{ij}) \leq n \cdot k_{ij} \cdot x_1^{(n-1)} \cdot x_{ij} + (n-1) \cdot k_{ij} \cdot x_1^n, \quad (\text{A.8})$$

$$\hat{h}(x_{ij}) \geq n \cdot k_{ij} \cdot x_2^{(n-1)} \cdot x_{ij} + (1-n) \cdot k_{ij} \cdot x_1^n, \quad (\text{A.9})$$

where x_1 (and correspondingly x_2) can be solved for with the nonlinear equation

$$(n-1) \cdot x_1^n + (n \cdot \bar{x}_{ij}) \cdot x_1^{(n-1)} - \bar{x}_{ij}^n = 0, \quad (\text{A.10})$$

We can solve for x_1 and x_2 in advance (e.g., with a nonlinear solver like ‘fsolve’ in Matlab or ‘nlsolve’ in Julia) before including (A.6)-(A.9) into a optimal water flow problem. It is worth noting that x_1 and x_2 are not dependent on the resistance coefficient k_{ij} , therefore only one value needs to be found for each unique minimum and maximum flow rate magnitude.

Last, we can validate that we get the same relaxation as [61] when we set $n = 2$ (i.e., we consider the Darcy-Weisbach head loss formula). Equation (A.10) is then a quadratic polynomial which we can solve using the quadratic equation (e.g., $x_1 = (1 - \sqrt{2})\bar{x}_{ij}$). When plugging x_1 , x_2 , and n into (A.6)-(A.9), we get

$$\hat{h}(x_{ij}) \geq 2k_{ij}\bar{x}_{ij}x_{ij} - k_{ij}\bar{x}_{ij}^2, \quad (\text{A.11})$$

$$\hat{h}(x_{ij}) \leq 2k_{ij}\bar{x}_{ij}x_{ij} + k_{ij}\bar{x}_{ij}^2, \quad (\text{A.12})$$

$$\hat{h}(x_{ij}) \leq (2 - 2\sqrt{2}) \cdot k_{ij}\bar{x}_{ij}x_{ij} + (3 - 2\sqrt{2}) \cdot k_{ij}\bar{x}_{ij}^2, \quad (\text{A.13})$$

$$\hat{h}(x_{ij}) \geq (2 - 2\sqrt{2}) \cdot k_{ij}\bar{x}_{ij}x_{ij} - (3 - 2\sqrt{2}) \cdot k_{ij}\bar{x}_{ij}^2, \quad (\text{A.14})$$

which is the same result⁷ as [61] when $\underline{x}_{ij} = -\bar{x}_{ij}$.

⁷ Accounting for the sign error typos in the manuscript of [61]

Bibliography

- [1] P. Alstone, J. Potter, M. A. Piette, P. Schwartz, M. A. Berger, L. N. Dunn, S. J. Smith, M. D. Sohn, A. Aghajanzadeh, S. Stensson, et al. *2025 California demand response potential study—Charting California’s demand response future. Final report on phase 2 results*. Tech. rep. 2001113. Lawrence Berkeley National Lab, 2017.
- [2] A. Anderson, J. Johnson, N. Feagin, S. Mallory, D. Pell, S. Perry, S. Torpie, and L. Waring. *Water System Design Manual*. Tech. rep. 331-123. Washington State Department of Health, 2020.
- [3] D. B. Arnold, M. Sankur, R. Dobbe, K. Brady, D. S. Callaway, and A. Von Meier. “Optimal dispatch of reactive power for voltage regulation and balancing in unbalanced distribution systems”. In: *IEEE Power and Energy Society General Meeting* (2016).
- [4] K. S. Ayyagari, S. Wang, N. Gatsis, A. F. Taha, and M. Giacomoni. “Co-optimization of interdependent water and power distribution networks”. In: *Proceedings of the IEEE Power & Energy Society Innovative Smart Grid Technologies Conference (ISGT)* (2021), pp. 1–5.
- [5] A. Babayan, Z. Kapelan, D. Savic, and G. Walters. “Least-cost design of water distribution networks under demand uncertainty”. In: *Journal of Water Resources Planning and Management* 131.5 (2005), pp. 375–382.
- [6] M. Badruzzaman, C. Cherchi, J. Oppenheimer, C. Bros, J. Jacangelo, S. Bunn, M. Gordon, V. Pencheva, C. Jay, and I. Darcazallie. *Optimization of energy and water quality management systems for drinking water utilities*. Tech. rep. CEC-500-2015-088. Water Research Foundation and California Energy Commission, 2015.
- [7] M. E. Baran and F. F. Wu. “Optimal capacitor placement on radial distribution systems”. In: *IEEE Transactions on Power Delivery* 4.1 (1989), pp. 725–734.
- [8] A. Ben-Tal, L. El Ghaoui, and A. Nemirovski. *Robust optimization*. Vol. 28. Princeton University Press, 2009.
- [9] A. Bernstein, C. Wang, E. Dall’Anese, J. Le Boudec, and C. Zhao. “Load flow in multiphase distribution networks: Existence, uniqueness, non-singularity and linear models”. In: *IEEE Transactions on Power Systems* 33.6 (2018), pp. 5832–5843.
- [10] P. R. Bhave and R. Gupta. *Analysis of water distribution networks*. Oxford, U.K.: Alpha Science International Ltd., 2006.

- [11] G. Bonvin, S. Demassey, and A. Lodi. “Pump scheduling in drinking water distribution networks with an LP/NLP-based branch and bound”. In: *Optimization and Engineering* (2021).
- [12] S. Boyd and L. Vandenberghe. *Convex optimization*. Cambridge University Press, 2004.
- [13] J. Burgschweiger, B. Gnädig, and M. C. Steinbach. “Optimization models for operative planning in drinking water networks”. In: *Optimization and Engineering* 10.1 (2009), pp. 43–73.
- [14] J. Burkardt. “The truncated normal distribution”. In: (2014), pp. 1–35. URL: <http://people.sc.fsu.edu/~jburkardt/presentations/truncated>.
- [15] D. S. Callaway and I. A. Hiskens. “Achieving controllability of electric loads”. In: *Proceedings of the IEEE* 99.1 (2011), pp. 184–199.
- [16] M. C. Campi, S. Garatti, and F. A. Ramponi. “A general scenario theory for nonconvex optimization and decision making”. In: *IEEE Transactions on Automatic Control* 63.12 (2018), pp. 4067–4078.
- [17] M. C. Campi, S. Garatti, and M. Prandini. “The scenario approach for systems and control design”. In: *Annual Reviews in Control* 33.2 (2009), pp. 149–157.
- [18] S. W. Carlson and A. Walburger. *Energy index development for benchmarking water and wastewater utilities*. Tech. rep. 3009. Awwa Research Foundation, 2007.
- [19] S. Chanda, A. K. Srivastava, M. U. Mohanpurkar, and R. Hovsapian. “Quantifying power distribution system resiliency using code-based metric”. In: *IEEE Transactions on Industry Applications* 54.4 (2018), pp. 3676–3686.
- [20] C. M. Chini and A. S. Stillwell. “The state of U.S. urban water: Data and the energy-water nexus”. In: *Water Resources Research* 54.3 (2018), pp. 1796–1811.
- [21] D. Cohen, U. Shamir, and G. Sinai. “Optimal operation of multi-quality water supply systems-II: the Q-H model”. In: *Engineering Optimization* 32.6 (2000), pp. 687–719.
- [22] M. Collins, L. Cooper, R. Helgason, J. Kennington, and L. LeBlanc. “Solving the pipe network analysis problem using optimization techniques”. In: *Management science* 24.7 (1978), pp. 747–760.
- [23] C. Copeland and N. T. Carter. *Energy water nexus: The water sector’s energy use*. Congressional Research Service. 2017.
- [24] C. D’Ambrosio, A. Lodi, S. Wiese, and C. Bragalli. “Mathematical programming techniques in water network optimization”. In: *European Journal of Operational Research* 243.3 (2015), pp. 774–788.
- [25] E. Dall’Anese, P. Mancarella, and A. Monti. “Unlocking flexibility: integrated optimization and control of multienergy systems”. In: *IEEE Power Energy Magazine* 15.1 (2017), pp. 43–52.

- [26] E. Dall'Anese, K. Baker, and T. Summers. “Chance-constrained ac optimal power flow for distribution systems with renewables”. In: *IEEE Transactions on Power Systems* 32.5 (2017), pp. 3427–3438.
- [27] Y. M. Darestani and A. Shafieezadeh. “Multi-dimensional wind fragility functions for wood utility poles”. In: *Engineering Structures* 183 (2019), pp. 937–948.
- [28] D. Denig-Chakroff. *Reducing electricity used for water production: questions state commissions should ask regulated utilities*. Tech. rep. Water Research and Policy, 2008.
- [29] C. Dieter, M. Maupin, R. Caldwell, M. Harris, T. Ivahnenko, J. Lovelace, N. Barber, and K. Linsey. *Estimated use of water in the United States in 2015: U.S. Geological Survey Circular 1441*. 2018.
- [30] J. H. Eto, K. H. LaCommare, P. Larsen, A. Todd, and E. Fisher. *An examination of temporal trends in electricity reliability based on reports from U.S. electric utilities*. Tech. rep. LBNL-5268E. Lawrence Berkeley National Laboratory, 2012.
- [31] D. Fooladivanda, A. D. Dominguez-Garcia, and P. Sauer. “Utilization of water supply networks for harvesting renewable energy”. In: *IEEE Transactions on Control of Networked Systems* 6.2 (2019), pp. 763–774.
- [32] D. Fooladivanda and J. A. Taylor. “Energy-optimal pump scheduling and water flow”. In: *IEEE Transactions on Control Network Systems* 5.3 (2018), pp. 1016–1026.
- [33] G. Gamrath, D. Anderson, K. Bestuzheva, W.-K. Chen, L. Eifler, M. Gasse, P. Gemander, A. Gleixner, L. Gottwald, K. Halbig, et al. *The SCIP optimization suite 7.0*. 2020.
- [34] L. Gan and S. H. Low. “Convex relaxations and linear approximation for optimal power flow in multiphase radial networks”. In: *Proceedings of the Power Systems Computation Conference (PSCC)* (2014).
- [35] M. Geidl and G. Andersson. “A modeling and optimization approach for multiple energy carrier power flow”. In: *IEEE Russia Power Tech* (2005).
- [36] S. Geng, M. Vrakopoulou, and I. A. Hiskens. “Optimal capacity design and operation of energy hub systems”. In: *Proceedings of the IEEE* 108.9 (2020), pp. 1475–1495.
- [37] B. Ghaddar, J. Naoum-Sawaya, A. Kishimoto, N. Taheri, and B. Eck. “A Lagrangian decomposition approach for the pump scheduling problem in water networks”. In: *European Journal of Operational Research* 241 (2015), pp. 490–501.
- [38] R. Goldstein and W. Smith. *Water and sustainability (Volume 4): U.S. electricity consumption for water supply and treatment-The next half century*. Tech. rep. 1006787. EPRI, 2002.
- [39] A. P. Goryashko and A. S. Nemirovski. “Robust energy cost optimization of water distribution system with uncertain demand”. In: *Automation and Remote Control* 75.10 (2014), pp. 1754–1769.

- [40] I. Goulter. “Analytical and simulation models for reliability analysis in water distribution systems”. In: *Improving efficiency and reliability in water distribution systems*. Ed. by E. Cabrera and A. F. Vela. Dordrecht: Springer Netherlands, 1995, pp. 235–266.
- [41] S. Grammatico, X. Zhang, K. Margellos, P. Gouliart, and J. Lygeros. “A scenario approach for non-convex control design”. In: *IEEE Transactions on Automatic Control* 61.2 (2016), pp. 334–345.
- [42] Gurobi Optimization, ed. *Gurobi optimizer 8.1*. URL: <http://www.gurobi.com>.
- [43] L. Halilbašić, P. Pinson, and S. Chatzivasileiadis. “Convex relaxations and approximations of chance-constrained AC-OPF problems”. In: *IEEE Transactions on Power Systems* 34.2 (2019), pp. 1459–1470.
- [44] G. S. Hawker and K. R. W. Bell. “Making energy system models useful: Good practice in the modelling of multiple vectors”. In: *WIREs Energy and Environment* 9.1 (2020).
- [45] L. Herre, J. L. Mathieu, and L. Söder. “Impact of market timing on the profit of a risk-averse load aggregator”. In: *IEEE Transactions on Power Systems* 35.5 (2020), pp. 3970–3980.
- [46] G. J. Holland, J. I. Belanger, and A. Fritz. “A revised model for radial profiles of hurricane winds”. In: *Monthly weather review* 138.12 (2010), pp. 4393–4401.
- [47] International Energy Agency. *World energy outlook 2016*. Paris, 2016, pp. 1–684.
- [48] G. V. Iswaran, R. Vakili, and M. Khorsand. “A comprehensive framework based on dynamic and steady state analysis to evaluate power system resiliency to extreme weather conditions”. In: *Proceedings of IREP Bulk Power Systems Dynamics and Controls Symposium* (2022).
- [49] P. W. Jowitt and G. Germanopoulos. “Optimal pump scheduling in water-supply networks”. In: *Journal of Water Resources Planning and Management* 118.4 (1992), pp. 406–422.
- [50] D. Jung, D. Kang, J. H. Kim, and K. Lansey. “Robustness-based design of water distribution systems”. In: *Journal of Water Resources Planning and Management* 140.11 (2014).
- [51] E. Karangelos and L. Wehenkel. “Towards leveraging discrete grid flexibility in chance-constrained power system operation planning”. In: *Electric Power Systems Research* 188 (2020), p. 106571.
- [52] W. H. Kersting. “Radial distribution test feeders”. In: *IEEE Transactions on Power Systems* 6.3 (1991), pp. 975–985.
- [53] P. Khatavkar and L. W. Mays. “Model for optimal operation of water distribution pumps with uncertain demand patterns”. In: *Water Resources Management* 31.12 (2017), pp. 3867–3880.

- [54] G. Klein, M. Krebs, V. Hall, T. O'Brien, and B. B. Blevins. *California's water-energy relationship, final staff report*. Tech. rep. CEC-700-2005-011-SF. California Energy Commission, 2005.
- [55] K. A. Klise, D. Hart, D. M. Moriarty, M. L. Bynum, R. Murray, J. Burkhardt, and T. Haxton. *Water network tool for resilience (WNTR) user manual*. Tech. rep. Sandia National Lab, 2017.
- [56] K. A. Klise, R. Murray, and L. T. N. Walker. *Systems measures of water distribution system resilience*. Tech. rep. EPA/600/R-14/383. Sandia National Lab, 2015.
- [57] S. Koch, J. L. Mathieu, and D. S. Callaway. "Modeling and control of aggregated heterogeneous thermostatically controlled loads for ancillary services". In: *Proceedings of the Power Systems Computation Conference (PSCC)* (2011).
- [58] K. E. Lansey, N. Duan, L. W. Mays, and Y.-K. Tung. "Water distribution system design under uncertainties". In: *Journal of Water Resources Planning and Management* 115.5 (1989), pp. 630–645.
- [59] K. E. Lansey and K. Awumah. "Optimal pump operations considering pump switches". In: *Journal of Water Resources Planning and Management* 120.1 (1994), pp. 17–35.
- [60] Y. Lee and R. Baldick. "A frequency-constrained stochastic economic dispatch model". In: *IEEE Transactions on Power Systems* 28.3 (2013), pp. 2301–2312.
- [61] Q. Li, S. Yu, A. Al-Sumaiti, and K. Turitsyn. "Micro water-energy nexus: optimal demand-side management and quasi-convex hull relaxation". In: *IEEE Transactions on Control Network Systems* (2018).
- [62] Q. Li, S. Yu, A. Al-Sumaiti, and K. Turitsyn. "Modeling and co-optimization of a micro water-energy nexus for smart communities". In: *Proceedings of the IEEE PES Innovative Smart Grid Technologies Conference Europe (ISGT-Europe)* (2018), pp. 1–5.
- [63] Y. Liu, C. Barrows, J. Macknick, and M. Mauter. "Optimization framework to assess the demand response capacity of a water distribution system". In: *Journal of Water Resources Planning and Management* 146.8 (2020), pp. 1–13.
- [64] Y. Liu and M. S. Mauter. "Assessing the demand response capacity of U.S. drinking water treatment plants". In: *Applied Energy* 267 (2020), p. 114899.
- [65] J. Löfberg. "Automatic robust convex programming". In: *Optimization methods and software* 27.1 (2012), pp. 115–129.
- [66] O. Ma, N. Alkadi, P. Cappers, P. Denholm, J. Dudley, S. Goli, M. Hummon, S. Kiliccote, J. MacDonald, N. Matson, D. Olsen, C. Rose, M. D. Sohn, M. Starke, B. Kirby, and M. O'Malley. "Demand response for ancillary services". In: *IEEE Transactions on Smart Grid* 4.4 (2013), pp. 1988–1995.

- [67] Z. Ma, D. Callaway, and I. Hiskens. “Decentralized charging control for large populations of plug-in electric vehicles”. In: *Proceedings of the IEEE Conference on Decision and Control (CDC)* (2010), pp. 206–212.
- [68] J. MacDonald, P. Cappers, D. Callaway, and S. Kiliccote. “Demand response providing ancillary services: A comparison of opportunities and challenges in US wholesale markets”. In: (2020).
- [69] H. Mala-Jetmarova, N. Sultanova, and D. Savic. “Lost in optimisation of water distribution systems? A literature review of system operation”. In: *Environmental Modelling and Software* 93 (2017), pp. 209–254.
- [70] P. Mancarella, G. Andersson, J. A. Peças-Lopes, and K. R. W. Bell. “Modelling of integrated multi-energy systems: drivers, requirements, and opportunities”. In: *Proceedings of the Power Systems Computation Conference (PSCC)* (2016).
- [71] A. Marchi, A. R. Simpson, and N. Ertugrul. “Assessing variable speed pump efficiency in water distribution systems”. In: *Drinking Water Engineering and Science* 5.1 (2012), pp. 15–21.
- [72] K. Margellos, P. Goulart, and J. Lygeros. “On the road between robust optimization and the scenario approach for chance constrained optimization problems”. In: *IEEE Transactions on Automatic Control* 59.8 (2014), pp. 2258–2263.
- [73] O. Mégel, J. L. Mathieu, and G. Andersson. “Scheduling distributed energy storage units to provide multiple services under forecast error”. In: *International Journal of Electrical Power & Energy Systems* 72 (2015), pp. 48–57.
- [74] R. Menke, E. Abraham, P. Parpas, and I. Stoianov. “Demonstrating demand response from water distribution system through pump scheduling”. In: *Applied Energy* 170 (2016), pp. 377–387.
- [75] *MISO Actual Energy Price*. <http://www.energyonline.com/Data/Default.aspx>. Accessed: 2022-02-25.
- [76] S. Misra, M. Vuffray, and A. Zlotnik. “Monotonicity properties of physical network flows and application to robust optimal allocation”. In: *Proceedings of the IEEE* 108.9 (2020), pp. 1558–1579.
- [77] D. K. Molzahn and I. A. Hiskens. “A survey of relaxations and approximations of the power flow equations”. In: *Foundations and Trends in Electric Energy Systems* (2019).
- [78] N. Motegi, M. A. Piette, D. S. Watson, S. Kiliccote, and P. Xu. *Introduction to commercial building control strategies and techniques for demand response-appendices*. Tech. rep. Lawrence Berkeley National Lab (LBNL), Berkeley, CA (United States), 2007.
- [79] New York State Energy Research and Development Authority (NYSERDA). *Water and Wastewater Energy Management: Best Practices Handbook*. Tech. rep. 2010.

- [80] Office of Water. *Strategies for Saving Energy at Public Water Systems*. Tech. rep. EPA 816-F-13-004. U.S. Environmental Protection Agency, 2015.
- [81] K. Oikonomou and M. Parvania. “Optimal coordination of water distribution energy flexibility with power systems operation”. In: *IEEE Transactions on Smart Grid* 10.1 (2019), pp. 1101–1110.
- [82] K. Oikonomou, M. Parvania, and R. Khatami. “Optimal demand response scheduling for water distribution systems”. In: *IEEE Transactions on Industrial Electronics* 14.11 (2018), pp. 5112–5122.
- [83] D. Olsen, A. Aghajanzadeh, and A. McKane. *Opportunities for automated demand response in California agricultural irrigation*. Tech. rep. LBNL-1003786. Lawrence Berkeley National Laboratory, 2015.
- [84] C. Ordoudis, S. Delikaraoglou, J. Kazempour, and P. Pinson. “Market-based coordination of integrated electricity and natural gas systems under uncertain supply”. In: *European Journal of Operational Research* 287.3 (2020), pp. 1105–1119.
- [85] L. E. Ormsbee and K. E. Lansey. “Optimal control of water supply system pumping systems”. In: *Journal of Water Resources Planning and Management* 120.2 (1994), pp. 237–252.
- [86] M. Ouyang and L. Dueñas-Osorio. “Multi-dimensional hurricane resilience assessment of electric power systems”. In: *Structural Safety* 48 (2014), pp. 15–24.
- [87] OWA-EPA. *EPANET*. <http://github.com/OpenWaterAnalytics/EPANET>. 2018.
- [88] S. Pabi, A. Amarnath, R. Goldstein, and L. Reekie. *Electricity use and management in the municipal water supply and wastewater industries*. Tech. rep. 3002001433. Electric Power Research Institute, 2013.
- [89] M. Panteli, P. Mancarella, D. N. Trakas, E. Kyriakides, and N. D. Hatziargyriou. “Metrics and quantification of operational and infrastructure resilience in power systems”. In: *IEEE Transactions on Power Systems* 32.6 (2017), pp. 4732–4742.
- [90] A. Papavasiliou and S. Oren. “A stochastic unit commitment model for integrating renewable supply and demand response”. In: *Proceedings of the IEEE Power and Energy Society General Meeting* (2012).
- [91] C. Peterman. “Decision adopting energy storage procurement framework and design program”. In: *California Public Utilities Commiss.(CPUC), San Francisco, CA, USA, Tech. Rep* (2013).
- [92] PJM. *Ancillary Services: RTO Regulation Signal Data*. <https://www.pjm.com/markets-and-operations/ancillary-services>. Accessed: 2022-12-13.
- [93] Public Service Commission (PSC) of Wisconsin. *Municipal Annual Report Data*. data retrieved from PSC E-Portal, <https://apps.psc.wi.gov/ARS/WEGSqueries/default.aspx>.

- [94] L. Roald and G. Andersson. “Chance-constrained ac optimal power flow: reformulations and efficient algorithms”. In: *IEEE Transactions on Power Systems* 33.3 (2018), pp. 2906–2918.
- [95] L. Roald, G. Andersson, S. Misra, M. Chertkov, and S. Backhaus. “Optimal power flow with wind power control and limited expected risk of overloads”. In: *Proceedings of the Power Systems Computation Conference (PSCC)* (2016).
- [96] L. Roald, S. Misra, T. Krause, and G. Andersson. “Corrective control to handle forecast uncertainty: a chance constrained optimal power flow”. In: *IEEE Transactions on Power Systems* 32.2 (2017), pp. 1626–1637.
- [97] L. A. Roald, K. Sundar, A. Zlotnik, S. Misra, and G. Andersson. “An uncertainty management framework for integrated gas-electric energy systems”. In: *Proceedings of the IEEE* 108.9 (2020), pp. 1518–1540.
- [98] L. A. Roald, K. Sundar, A. Zlotnik, S. Misra, and G. Andersson. “An uncertainty management framework for integrated gas-electric energy systems”. In: *Proceedings of the IEEE* 108.9 (2020), pp. 1518–1540.
- [99] L. Roald, F. Oldewurtel, B. Van Parys, and G. Andersson. “Security constrained optimal power flow with distributionally robust chance constraints”. In: *arXiv:1508.06061* (2015).
- [100] B. A. Robbins and A. D. Domínguez-García. “Optimal reactive power dispatch for voltage regulation in unbalanced distribution systems”. In: *IEEE Transactions on Power Systems* 31.4 (2016), pp. 2903–2913.
- [101] L. Rodriguez-Garcia, M. M. Hosseini, T. M. Mosier, and M. Parvania. “Resilience analytics for interdependent power and water distribution systems”. In: *IEEE Transactions on Power Systems* 37.6 (2022), pp. 4244–4257.
- [102] L. A. Rossman. *EPANET 2: User’s Manual*. Washington, D.C., 2000.
- [103] R. Salgado, E. Todini, and P. O’Connell. “Comparison of the gradient method with some traditional methods for the analysis of water supply distribution networks”. In: *Computer application in water supply: vol. 1-systems analysis and simulation*. Ed. by B. Coulbeck and O. Chun-Hou. Taunton, UK: Research Studies Press Ltd., 1987, pp. 38–62.
- [104] I. Sárba and I. Borza. “Energetic optimization of water pumping in distribution systems”. In: *Periodica Polytechnica Mechanical Engineering* 42.2 (1998), pp. 141–152.
- [105] A. Schewe, A. Arrigo, C. Vervaejen, J. Kazempour, and F. Vallée. “Coordination of electricity, heat, and natural gas systems accounting for network flexibility”. In: *Electric Power Systems Research* 189 (2020), p. 106776.
- [106] A. Shabanpour-Haghghi and A. R. Seifi. “An integrated steady-state operation assessment of electrical, natural gas, and district heating networks”. In: *IEEE Transactions on Power Systems* 31.5 (2016), pp. 3636–3647.

- [107] M. Singh and V. Kekatos. “On the flow problem in water distribution networks: Uniqueness and solvers”. In: *IEEE Transactions on Control of Network Systems* 8.1 (2020), pp. 462–474.
- [108] M. K. Singh and V. Kekatos. “Optimal scheduling of water distribution systems”. In: *IEEE Transactions on Control Network Systems* 7.2 (2020), pp. 711–723.
- [109] B. Sparn and R. Hunsberger. *Opportunities and challenges for water and wastewater industries to provide exchangeable services*. Tech. rep. NREL/TP-5500-63931. NREL, 2015.
- [110] A. Stuhlmacher and J. Mathieu. “Uncertainty-aware methods for leveraging water pumping flexibility for power networks”. In: *Proceedings of IREP Bulk Power Systems Dynamics and Controls Symposium* (2022).
- [111] A. Stuhlmacher and J. L. Mathieu. “Chance-constrained water pumping to manage water and power demand uncertainty in distribution networks”. In: *Proceedings of the IEEE* 108.9 (2020), pp. 1640–1655.
- [112] A. Stuhlmacher and J. L. Mathieu. “Chance-constrained water pumping to support the power distribution network”. In: *Proceedings of the North American Power Symposium (NAPS)* (2019), pp. 1–6.
- [113] A. Stuhlmacher and J. L. Mathieu. “Flexible drinking water pumping to provide multiple grid services”. In: *Electric Power Systems Research* 212 (2022), p. 108491.
- [114] A. Stuhlmacher and J. L. Mathieu. “Water distribution networks as flexible loads: a chance-constrained programming approach”. In: *Electric Power Systems Research* 188 (2020), p. 106570.
- [115] A. Stuhlmacher, L. A. Roald, and J. L. Mathieu. “Tractable robust drinking water pumping to provide power network voltage support”. In: *Proceedings of the IEEE Conference on Decision and Control (CDC)* (2021).
- [116] E. Todini and S. Pilati. “A gradient method for the analysis of pipe networks”. In: *Proceedings of the International Conference on Computer Applications for Water Supply and Distribution* (1988).
- [117] K. M. Twomey and M. E. Webber. “Evaluating the energy intensity of the US public water system”. In: *Proceedings of Energy Sustainability* (2011), pp. 1735–1748.
- [118] U.S. Environmental Protection Agency. *Safe Drinking Water Information System (SDWIS) Federal Reporting Services*. data retrieved from SDWIS Search, <https://www.epa.gov/enviro/sdwis-search>. (Visited on 12/02/2020).
- [119] B. Ulanicki, J. Kahler, and B. Coulbeck. “Modeling the efficiency and power characteristics of a pump group”. In: *Journal of water resources planning and management* 134.1 (2008), pp. 88–93.
- [120] US Department of Energy’s Office of Industrial Technologies. *Pump life cycle costs: A guide to LCC analysis for pumping systems*. Tech. rep. DOE/GO-102001-1190. 2001.

- [121] M. Vanin, H. Ergun, R. D'kulst, and D. Van Hertem. "Comparison of linear and conic power flow formulations for unbalanced low voltage network optimization". In: *Electric Power Systems Research* 189 (2020), p. 106699.
- [122] D. Verleye and E.-H. Aghezzaf. "Optimising production and distribution operations in large water supply networks: A piecewise linear optimisation approach". In: *International Journal of Production Research* 51.23-24 (2013), pp. 7170–7189.
- [123] I. Vijay, A. Aghajanzadeh, and O. Schetrit. *Low-cost, scalable, fast demand response for municipal wastewater and recycling facilities*. Tech. rep. CEC-500-2015-086. California Energy Commission, 2015.
- [124] M. Vrakopoulou, B. Li, and J. L. Mathieu. "Chance constrained reserve scheduling using uncertain controllable loads part I: formulation and scenario-based analysis". In: *IEEE Transactions on Smart Grid* 10.2 (2019), pp. 1608–1617.
- [125] M. Vrakopoulou, K. Margellos, J. Lygeros, and G. Andersson. "A probabilistic framework for reserve scheduling and N–1 security assessment of systems with high wind power penetration". In: *IEEE Transactions on Power Systems* 28.4 (2013), pp. 3885–3896.
- [126] M. Vuffray, S. Misra, and M. Chertkov. "Monotonicity of dissipative flow networks renders robust maximum profit problem tractable: General analysis and application to natural gas flows". In: *Proceedings of the IEEE Conference on Decision and Control*. 2015, pp. 4571–4578.
- [127] A. Wächter and L. T. Biegler. "On the implementation of an interior-point filter line-search algorithm for large-scale nonlinear programming". In: *Mathematical Programming* 106.1 (2006), pp. 25–57.
- [128] S. Wang, A. F. Taha, L. Sela, M. H. Giacomoni, and N. Gatsis. "A new derivative-free linear approximation for solving the network water flow problem with convergence guarantees". In: *Water Resources Research* 56.3 (2020).
- [129] H. E. Willoughby, R. Darling, and M. Rahn. "Parametric representation of the primary hurricane vortex. Part II: A new family of sectionally continuous profiles". In: *Monthly weather review* 134.4 (2006), pp. 1102–1120.
- [130] A. Zamzam, E. Dall'Anese, C. Zhao, J. Taylor, and N. Sidiropoulos. "Optimal water-power flow problem: formulation and distributed optimal solution". In: *IEEE Transactions on Control Network Systems* 6.1 (2019), pp. 37–47.
- [131] C. Zhai, T. Y.-j. Chen, A. G. White, and S. D. Guikema. "Power outage prediction for natural hazards using synthetic power distribution systems". In: *Reliability Engineering & System Safety* 208 (2021), p. 107348.
- [132] A. Zlotnik, L. Roald, S. Backhaus, M. Chertkov, and G. Andersson. "Coordinated scheduling for interdependent electric power and natural gas infrastructures". In: *IEEE Transactions on Power Systems* 32.1 (2017), pp. 600–610.

- [133] S. Zuloaga, P. Khatakar, L. Mays, and V. Vittal. “Resilience of cyber-enabled electrical energy and water distribution systems considering infrastructural robustness under conditions of limited water and/or energy availability”. In: *IEEE Transactions on Engineering Management* 69.3 (2019).
- [134] S. Zuloaga, P. Khatakar, V. Vittal, and L. W. Mays. “Interdependent electric and water infrastructure modelling, optimisation and control”. In: *IET Energy Systems Integration* 2.1 (2020), pp. 9–21.
- [135] S. Zuloaga and V. Vittal. “Quantifying power system operational and infrastructural resilience under extreme conditions within a water-energy nexus framework”. In: *IEEE Open Access Journal of Power and Energy* 8 (2021), pp. 229–238.
- [136] J. E. van Zyl, D. A. Savic, and G. A. Walters. “Operational optimization of water distribution systems using a hybrid genetic algorithm”. In: *Journal of Water Resources Planning and Management* 130.2 (2004), pp. 160–170.